

Spring 5-8-2021

Design, Synthesis and Antineoplastic Evaluation of a Variety of Small Molecule Scaffolds

Bader Huwaimel
University of Nebraska Medical Center

Tell us how you used this information in this [short survey](#).

Follow this and additional works at: <https://digitalcommons.unmc.edu/etd>

 Part of the [Medicinal and Pharmaceutical Chemistry Commons](#)

Recommended Citation

Huwaimel, Bader, "Design, Synthesis and Antineoplastic Evaluation of a Variety of Small Molecule Scaffolds" (2021). *Theses & Dissertations*. 509.
<https://digitalcommons.unmc.edu/etd/509>

This Dissertation is brought to you for free and open access by the Graduate Studies at DigitalCommons@UNMC. It has been accepted for inclusion in Theses & Dissertations by an authorized administrator of DigitalCommons@UNMC. For more information, please contact digitalcommons@unmc.edu.

**Design, Synthesis and Antineoplastic Evaluation of a Variety of Small Molecule
Scaffolds**

by

Bader Huwaimel

A DISSERTATION

Presented to the Faculty of
the University of Nebraska Graduate College
in Partial Fulfillment of the Requirements
for the Degree of Doctor of Philosophy

Pharmaceutical Sciences
Graduate Program

Under the Supervision of Professor Paul Trippier

University of Nebraska Medical Center
Omaha, Nebraska

January, 2021

Supervisory Committee:

Dr. Jonathan L. Vennerstrom, Ph.D.

Dr. Corey Hopkins, Ph.D.

Dr. Joseph A. Vetro, Ph.D.

ACKNOWLEDGEMENT

First and foremost, I would like to express my deepest gratitude to my mentor Dr. Paul Trippier for giving me the opportunity and unwavering support of my Ph.D. study and research. Also, I would like to thank him a lot for his patience, motivation, enthusiasm, and immense knowledge and providing me invaluable guidance throughout my research and writing of this thesis. I never imagined having a better advisor for my Ph.D. study. Actually, without his support, this and assist this dissertation would not have been complete and succeed. I wish to be a teacher and scientist like him in my future career.

Besides my mentor, I would like to extend my gratitude towards all the rest of my advisory committee members: Dr. Jonathan L. Vennerstrom, Dr. Corey Hopkins, and Dr. Joseph A. Vetro for their assistance, encouragement, and suggestions that have improved the quality of my doctoral project.

This work could not be completed without contributions and support from our collaborators Dr. Paul S. Brookes (University of Rochester Medical Center) and Dr. Constantinos Mikelis (Texas Tech University Health Sciences Center).

I address my special thanks to my sponsor University of Hail, Hail, Saudi Arabia, for a full Ph.D. scholarship, being aware that without their support, I would not be able to come to the United States for this Ph.D. program. I would also like to thank all previous supervisory committees at Texas Tech University Health Sciences Center for assistance and encouragement in the first three and a half years of my Ph.D., which I spent there.

I want to thank my fellow lab mates: a special thanks to Dr. Sravan Jonnalagadda, who always supported and helped me whenever I needed him. Also, Dr. Shikha Kumari, Dr. Krishnaiah Madeboina, and my colleagues and my lab mates Ahmed Morsy, Angelica Carmona, and Md. Shafikur Rahman- all specially extended their help. I much appreciate

the assistance of Renee Kaszynski, Terri Vadovsky, and Cody Phillips after I joined to University of Nebraska Medical Center.

Last but not least, I am incredibly grateful to my lovely parents for their prayers, caring, and guidance for educating and preparing me for my future. Also, I am very thankful to my wife and son for their love, understanding, and continuing support to complete this research work.

Abstract

Several appealing strategies emerged for selective anticancer therapy. Mitochondrial respiratory complex II (CII) is a potential target for many human diseases, including cancer. We have designed, synthesized, and characterized a library of potent CII inhibitors atpenin A5 and diazoxide analogues with enhanced 'drug-likeness' and evaluated their antineoplastic activity. Several of these derivatives showed greater activity and selectivity to inhibit the CII. Design aspects of lead derivatives (**16c**) include optimum ligand lipophilicity efficiency of >5, and half-life of >3 hours. This derivative displayed potent and selective inhibition of cell proliferation in both multiple human prostate cancer cell lines and reactive stromal cells in a dose-dependent manner which maybe a novel therapeutic strategy which can confer significant benefit to patients. Also, several of diazoxide derivatives displayed potent and selective inhibition of cell proliferation in triple negative breast cancer MDA-MB-468 cells.

Antiangiogenesis drugs play a beneficial role in cancer treatment. Inhibition of vascular endothelial growth factor (VEGF) is one of the significant targets in tumor angiogenesis. Suppressing vascular permeability in tumor cells leads to inhibition of tumor growth by locking the survival factor that delivers the oxygen and nutrients to the tumors. We have designed and synthesized a library of potent VEGF inhibitors that had potency to inhibit the HUVEC-VEGF treated cells.

Inhibition of specific carbonic anhydrases (CA) enzymes emerged as a new strategy for anticancer therapy. The CA isoforms IX and XII were known to be overexpressed in various human solid tumors and play a critical role in regulating tumor acidification, proliferation, and progression. Series of novel sulfonamides containing coumarin moieties were synthesized as potent CA inhibitors. These compounds would be able to selectively target the tumor-associated CA IX and CA XII with high inhibition

activity. Several of these compounds have anticancer activity against the MDA-MB-468 cells.

The current dissertation emphasizes on the synthesis and evaluation of novel compounds that inhibit CII, VEGF, and CA as anticancer agents. I envision that further studies will lead to the optimization of structure-activity relationship of these new derivatives and recognize molecular and signaling pathways that could further result in the outcome of anticancer therapy.

TABLE OF CONTENTS

ACKNOWLEDGEMENTS	i
ABSTRACT.....	iii
TABLE OF CONTENTS.....	v
LIST OF FIGURES	ix
LIST OF TABLES	xii
LIST OF SCHEMES.....	xv
LIST OF ABBREVIATIONS	xvi
1 CHAPTER 1. Introduction	1
1.1. Overview of cancer and treatment	1
1.2. Targeting of cancer mitochondrial metabolic pathways, specifically mitochondrial respiratory complex II	5
1.3. Targeting of angiogenesis vascular endothelial growth factor	20
1.4. Targeting of carbonic anhydrase enzymes in cancer cells.....	28
2 CHAPTER 2. Design, Synthesis and Antineoplastic Evaluation of Mitochondrial Complex II (Succinate Dehydrogenase) Inhibitors Derived from Atpenin A5	36
2.1. Introduction	36
2.2. Results and Discussion	41
2.2.1. Chemistry	41
2.2.2. Complex II Inhibition Assay	52

2.2.3. Molecular Modeling	60
2.2.4. Cytotoxicity Assay	64
2.3. Conclusions	78
2.4. Experimental Section	79
2.4.1. Chemistry	79
2.4.2. Biology	104
2.4.2.1. Cell Culture and Reagents	104
2.4.2.2. Cytotoxicity Assays	105
2.4.2.3. Complex II Inhibition Assay	106
2.4.2.4. Complex I Inhibition Assay	106
2.4.2.5. Stability Testing of CII Inhibitor 16c	106
2.4.2.6. Assessment of Metabolic Parameters	107
2.4.2.7. Statistical Analysis	107
3 CHAPTER 3. Structure-Activity Relationship Studies of Diazoxide Derivatives as Antineoplastic Agents	108
3.1. Introduction	108
3.2. Results and Discussion	109
3.2.1. Chemistry	109
3.2.2. Complex II Inhibition Assay	126
3.2.3. Cytotoxicity Assay	134
3.3. Conclusions	147

3.4. Experimental Section	147
3.4.1. Biology	147
3.4.1.1. Cell Culture and Reagents	147
3.4.1.2. Cytotoxicity Assays	148
3.4.1.3. Complex II inhibition assay	149
3.4.1.4. Statistical Analysis	149
3.4.2. Chemistry	149
4 CHAPTER 4. Discovery of Halogenated Benzothiadiazine Derivatives as Novel VEGF Inhibitors	208
4.1. Introduction	208
4.2. Results and Discussion	212
4.2.1. Chemistry	212
4.2.2. VEGF Inhibition Assay	212
4.2.3. Cytotoxicity Assay	225
4.3. Conclusions	230
4.4. Experimental Section	232
4.4.1. Biology	232
4.4.1.1. Cell Culture and Reagents	232
4.4.1.2. Cytotoxicity Assays	233
4.4.1.3. VEGF Assay	233
4.4.1.4. Statistical Analysis	234

4.4.2. Chemistry	234
5 CHAPTER 5. Design, Synthesis, and Evaluation of Novel Carbonic Anhydrase Inhibitors as Anticancer Agents	248
5.1. Introduction	248
5.2. Results and Discussion	251
5.2.1. Chemistry	251
5.2.2. Predict Carbonic Anhydrase Inhibition Activity for the synthesized compounds	264
5.2.3. Cytotoxicity Assay	266
5.3. Conclusions	271
5.4. Experimental Section	273
5.4.1. Biology	273
5.4.1.1. Cell Culture and Reagents	273
5.4.1.2. Cytotoxicity Assays	273
5.4.1.4. Statistical Analysis	274
5.4.2. Chemistry	274
6 CHAPTER 6. References	324

List of Figures

Figure 1.1. Three major cancer types for the estimated new cancer cases and deaths by sex, United States, 2020	4
Figure 1.2: The structure of mitochondria respiratory complex II (CII); succinate dehydrogenase (SDH)	11
Figure 1.3. Structures of known mitochondria respiratory complex II inhibitors.....	15
Figure 1.4. Vascular endothelial growth factor (VEGF) ligand and receptor	23
Figure 1.5. Mechanism of action of carbonic anhydrase inhibitor	30
Figure 1.6. Structures of several clinical and preclinical carbonic anhydrase inhibitors.	33
Figure 1.7. Structures of several coumarin derivatives as potent carbonic anhydrase inhibitors	34
Figure 2.1. Mitochondria respiratory complex II; succinate dehydrogenase (SDH)	38
Figure 2.2. Structures of the interesting known mitochondria complex II inhibitors	39
Figure 2.3. Modelling of atpenin A5 and selected derivatives in the ubiquinone binding site of porcine heart complex II (PDB ID: 3AEE)	63
Figure 2.4. Complex II inhibitors are potent antiproliferative agents.	65
Figure 2.5. Complex II inhibitors with greater potency convey greater cytotoxicity	67
Figure 2.6. Inhibition of the stromal cell by complex II inhibitor 16c and 16k	70
Figure 2.7. Metabolic stability of atpenin A5 derivative 16c . Half-life 16c upon incubation with Murine S9 liver fractions.....	73

Figure 2.8. Cytotoxic effect of the clinical chemotherapeutic etoposide, complex II inhibitor 16c and inactive control 18 in PC3 prostate cancer cells under hypoxia	75
Figure 2.9. Complex II inhibitor 16c blocks mitochondrial respiration and function in 22Rv1 prostate cancer cells	77
Figure 3.1. Percentage inhibition of mitochondrial complex II relative to DMSO control at 100 μ M concentration of diazoxide derivatives.....	130
Figure 3.2. Percentage inhibition of mitochondrial complex II relative to DMSO control at 1 mM concentration of diazoxide derivatives.....	131
Figure 3.3. Cytotoxic effect of diazoxide derivatives (100 μ M, 48-hour treatment) in 22Rv1 prostate cancer cells.....	137
Figure 3.4. The cytotoxicity effect of 3.15c a diazoxide derivative in prostate cancer cells.....	138
Figure 3.5. Cytotoxic effect of selected diazoxide derivatives on triple negative breast cancer (TNBC) MDA-MB-468 cells.....	140
Figure 3.6. Cytotoxic effect of diazoxide derivatives (50 μ M, 72-hour treatment) in triple negative breast cancer MDA-MB-468 cells.....	142
Figure 4.1. Structure similarity between diazoxide derivative 3.21b and FDA-approved VEGF inhibitors	211
Figure 4.2. Cytotoxic effect of diazoxide derivatives at 20 μ M concentration in HUVEC cells in the presence of VEGF (10 ng/mL)	216
Figure 4.3. Western blotting demonstrating the effect of selective DZX derivatives on the expression of phosphorylation of vascular endothelial growth factor receptor-2 (VEGFR-2)	217

Figure 4.4. Cytotoxic effect of potent diazoxide derivatives as VEGF inhibitors (50 μ M, 72-hour treatment).....	227
Figure 4.5. Structure activity relationship of the DZX derivative as VEGF inhibitors.....	231
Figure 5.1. Cytotoxic effect of synthesized carbonic anhydrase inhibitors at 50 μ M for 72-hour treatment in triple negative breast cancer MDA-MB-468 cells	269
Figure 5.2. Structure activity relationship of the synthesized carbonic anhydrase inhibitors according to the cytotoxicity on MDA-MB-468 cancer cell line	272

List of Table

Table 1.1. Select agents targeting metabolism that are in clinical trials or FDA-approved for cancer treatment	7
Table 1.2. The FDA-approved antiangiogenic VEGF inhibitors	26
Table 2.1. Complex II inhibition activity, cLogP, Mw, PSA and lipophilic efficiency of atpenin A5 derivatives 16a-16k	54
Table 2.2. Complex II inhibition activity, cLogP, Mw, PSA and lipophilic efficiency of atpenin A5 derivatives 17-24	56
Table 2.3. Activity of CII inhibitors 16c and 16k , the inactive control 24 , and the clinical chemotherapeutic enzalutamide across a panel of human prostate cancer cells and low tumorigenic human endothelial kidney cells	68
Table 2.4. Selectivity of compounds 16c , 16k , and AA5 for the inhibition of mitochondrial complex II over complex I	72
Table 3.1. Structure, molecular weight, calculated logP, and PSA of diazoxide derivatives 3.2a-d and 3.3a-d	114
Table 3.2. Structure, molecular weight, calculated logP, and PSA of diazoxide derivatives with 7-fluoro substitution.	115
Table 3.3. Structure, molecular weight, calculated logP, and PSA of diazoxide derivatives with 6-chloro substitution.	118
Table 3.4. Structure, molecular weight, calculated logP, and PSA of diazoxide derivatives with 7-bromo substitution.	121

Table 3.5. Structure, molecular weight, calculated logP, and PSA of diazoxide derivatives with a non-halogenated ring.	124
Table 3.6. Mitochondrial respiratory complex II IC ₅₀ values of selected diazoxide derivatives	133
Table 3.7. Cytotoxicity of selective diazoxide derivatives and the clinical chemotherapeutic 5-fluorouracil in TNBC MDA-MB-468 cells and low tumorigenic human endothelial kidney (HEK293) cells.	144
Table 4.1. Structure, molecular weight, calculated logP, and polar surface area of diazoxide derivatives with 7-floro, 7-bromo substitution and a non-halogenated ring ...	218
Table 4.2. Structure, molecular weight, calculated logP, polar surface area, and % of proliferation inhibition relative to VEGF treated cells of diazoxide derivatives with 6-chloro substitution.....	220
Table 4.3. Structure, molecular weight, calculated logP, polar surface area, and % of proliferation inhibition relative to VEGF treated cells of diazoxide derivatives with 7-chloro substitution.....	223
Table 4.4. Cytotoxicity of the potent VEGF inhibitors of diazoxide derivatives and the clinical chemotherapeutic sorafenib in triple negative breast cancer MDA-MB-468 cells and low tumorigenic human endothelial kidney (HEK293) cells	228
Table 5.1. Structures, and inhibition value of CA II, IX, and XII for several carbonic anhydrase inhibitors.....	250
Table 5.2. Structure, molecular weight, calculated cLogP and polar surface area of synthesized carbonic anhydrase inhibitors in scheme 5.1	257

Table 5.3. Structure, molecular weight, calculated logP and polar surface area of synthesized carbonic anhydrase inhibitors in schemes 5.2-5.4	258
Table 5.4. Carbonic anhydrase inhibitors sulfonamides containing coumarin moieties, Anticancer activities (IC_{50}) on human breast cancer cell line (MCF-7)	265
Table 5.5. Cytotoxicity of selective synthesized carbonic anhydrase inhibitors and the clinical chemotherapeutic 5-fluorouracil in TNBC MDA-MB-468 cells and low tumorigenic human endothelial kidney (HEK293) cells	270

List of Schemes

Scheme 2.1. Synthesis of hydrocarbon side chain derivatives of atpenin A5	43
Scheme 2.2. Synthesis of oxidation state derivatives of atpenin A5	45
Scheme 2.3. Synthesis of a methyl ether derivative of atpenin A5	45
Scheme 2.4. Synthesis of atpenin A5 derivative 16d	47
Scheme 2.5. Synthesis of atpenin A5 derivative 16e	47
Scheme 2.6. The first method to synthesis of a triphenylphosphine derivative of atpenin A5	49
Scheme 2.7. The second method to synthesis of a triphenylphosphine derivative of atpenin A5.	49
Scheme 2.8. The third method to synthesis of triphenylphosphine derivative of atpenin A5.....	51
Scheme 3.1. Synthesis the derivatives of diazoxide	111
Scheme 3.2. Synthesis of diazoxide derivative with bulky alkyl amino group	113
Scheme 3.3. Synthesis of diazoxide derivative with alkyl group in position 4	113
Scheme 5.1. Synthesis carbonic anhydrase inhibitors 5.5a-d and 5.6a, 5.6d	252
Scheme 5.2. Synthesis carbonic anhydrase inhibitors 5.9a-g	254
Scheme 5.3. Synthesis of carbonic anhydrase inhibitors 5.21	256
Scheme 5.4. Synthesis of carbonic anhydrase inhibitors 5.22	256

List of abbreviations

United States (US)

American Cancer Society (ACS)

Chemotherapy (chemo)

Dihydrofolate reductase enzyme (DHFR)

6-Mercaptopurine (6-MP)

6-Thioguanine (6-TG)

5-phosphoribosyl-1-pyrophosphatase (PRPP)

Thymidine synthesis (TS)

5-Fluorouracil (5-FU)

Mitochondrial complex I (CI)

2-Deoxyglucose (2-DG)

Reactive oxygen species (ROS)

Central carbon metabolism (CCM)

Hydroxyl radical ($\cdot\text{OH}$)

Alkoxy ($\text{RO}\cdot$)

Hydrogen peroxide (H_2O_2)

Oxidative phosphorylation (OXPHOS)

Electron transport chain (ETC)

Tricarboxylic acid cycle (TCA)

Mitochondrial respiratory complex II (CII)

Succinate dehydrogenase (SDH)

Succinate-coenzyme Q reductase (SQR)

Ubiquinone (Q)

Ubiquinol (QH₂)

Hypoxia-inducible factor (HIF)

Myocardial infarction (MI)

Ischemia-reperfusion (IR)

3-Bromopyruvate (3BP)

3-Nitropropionic acid (3NP)

α -Tocopheryl succinate (α -TOS)

Mitochondrially targeted vitamin E succinate (MitoVES)

Cationic triphenylphosphonium (TPP⁺)

Mitochondrial inner membrane (MIM)

Thenoyltrifluoroacetone (TTFA)

Lonidamine (LND)

US Food and Drug Administration (US-FDA)

Diazoxide (DZX)

Triple negative breast cancer (TNBC)

Atpenin A5 (AA5)

Ubiquinone binding site (UQ)

Structure-activity relationship (SAR)

Epidermal growth factor (EGF)

Vascular endothelial growth factor (VEGF)

Tumor necrosis factor- α (TNF- α)

Interleukins (IL-1-7)

Transforming growth factor (TGF)

Vascular endothelial growth factor receptor (VEGFR)

Anti-vascular endothelial growth factor (anti-VEGF)

Receptor tyrosine kinase (RTK).

Carbonic anhydrases (CA)

Carbon dioxide (CO₂)

Bicarbonate (HCO₃)

Zinc ion (Zn²⁺)

N-bromosuccinimide (NBS)

lithium diisopropylamide (LDA)

Trifluoroacetic acid (TFA)

Dess-martin periodinane (DMP)

Diisobutylaluminium hydride (DIBAL-H)

Zinc chloride (ZnCl₂)

Dichlorophenolindophenol (DCPIP)

Polar surface area (PSA)

Ligand-lipophilicity efficiency (LLE)

(3-(4,5-dimethylthiazol-2-yl)-5-(3-carboxymethoxyphenyl)-2-(4-sulfophenyl)-2H-tetrazolium) (MTS)

Enzalutamide (ENZ)

Thin-layer chromatography (TLC)

Parts per million (ppm)

n-butyl lithium (ⁿBuLi)

Trimethyl borate (B(OMe)₃)

Tetrahydrofuran (THF)

Dichloromethane (DCM)

Diethylether (Et₂O)

Ethylacetate (EtOAc)

Chloroform-d (CDCl₃)

Sodium hydride (NaH)

Ethanol (EtOH)

Methanol (MeOH)

Carbon tetrachloride (CCl₄)

Palladium on carbon (Pd/C)

American type culture collection (ATCC)

Dimethyl sulfoxide (DMSO)

Pan-assay interfering compounds (PAINS)

Selectivity Index (SI)

Roswell park memorial institute-1640 medium (RPMI-1640)

Dulbecco's modified eagle medium (DMEM)

Dimethyl sulfoxide- d_6 (dms o - d_6)

Human umbilical vein endothelial cells (HUVECs)

(3-[4, 5-dimethylthiazol-2-yl]-2, 5-dimethyltetrazolium bromide) colorimetric assay (MTT)

1-Ethyl-3-(3-dimethylaminopropyl) carbodiimide hydrochloride (EDC)

1-Hydroxybenzotriazole hydrate (HOBt•H₂O)

Triethylamine (TEA)

N,N-dimethylformamide (DMF)

Chapter 1. Introduction

1.1. Overview of cancer and treatment

Cancer is one of the topmost public health issues worldwide and the second leading cause of death in the United States (US).¹ One-third of the world's population has suffered from some form of cancer in their lifespan. In the US, the American Cancer Society (ACS) estimates more than 1.8 million new cancer cases and 606,520 cancer deaths are projected to occur in 2020.² Cancer is a disease that involves abnormal cell growth with the potential to invade or spread to other parts of the body.³ Most of the cancer cells have the same hallmarks, that include: cell growth and division, avoidance of programmed cell death, promoting blood vessel construction and invasion of tissue and formation of metastases.⁴

There are more than 100 different types of cancer disease. Lung, colorectal, breast, and prostate cancers are the most common cancer types for new cases and number of deaths in the US. Lung and colon cancer types are fatal for both males and females. Prostate cancer is the most frequently diagnosed cancer type in the US and is second only to lung cancer as the most common non-cutaneous cancer diagnosed in men worldwide.⁵ In the US, prostate cancer has 21% of the new cases with 191,930 estimated new cases and with nearly 72,500 related deaths in the year 2020.² Also, it is the third leading cause of cancer deaths.⁶ On the other hand, breast cancer is the most frequently occurring cancer in American woman, with the exception of skin cancers. According to ACS, one in eight women in the US will develop breast cancer in their lifetime with 276,480 estimated new cases in the US with nearly 63,220 related deaths in the year 2020 (**Figure 1.1**).²

Depending on the type, stage of cancer, and how advanced it is, numerous treatment options are available including surgery, chemotherapy, radiation therapy, and

immunotherapy. The old and commonly used cancer treatment is surgery, which is the first choice in the early stage of solid tumors and sometimes used in combination with other types of treatment. It is a procedure to remove the tumor from the origin that depends on the type and the stage of the tumor. The surgery works best if the patients have a localized solid tumor in one area, while this option cannot be used in the case of invasive cancer or metastasized tumor. The next common cancer treatment is radiation therapy, which involves the usage of high doses of radiation to shrink or kill tumor cells. The first type of cancer in which positive results were obtained by using radiation therapy was breast cancer.⁷ Also, one of the common cancer treatments available nowadays is chemotherapy (chemo), which is a type of cancer treatment that uses drugs to kill malignant cells. Chemotherapy drugs could keep cancer from spreading, inhibit the growth of the tumor or even kill cancer cells. However, chemotherapy causes many side effects because it kills cells that grow quickly, including cells in blood, digestive system, and hair follicles. There are over 100 types of chemotherapeutic drugs with different routes of administration including capsule, intravenous, and cream. Chemotherapy is often administered as a single drug or in combination with other drugs because some drugs work better together than alone. With the introduction of adjuvant chemotherapy, the concept of localized treatment changed.⁷ In the last few decades, the immunotherapy was widely used in the treatment of cancer. It is used certain parts person's own immune system to attempts prevent, control, and eliminate cancer. Immunotherapy treatment has many main types of used to treat tumors such as checkpoint inhibitors, cytokines, cancer vaccines, and monoclonal antibodies.⁸ The immunotherapy treatment became a familiar concept in the US; thus, many cancer immunotherapy drugs were approved by the US Food and Drug Administration (FDA).

In this scientific era, scientists are struggling to control this deadly disease because of multifaceted disease progression, including unpredictable mutation, fast metastasis, acquired resistance to chemotherapy, and scarcity of tumor-targeted anticancer agents. In addition to these, severe side effects and the lack of selectivity of anticancer drugs have made the treatment challenging. It is necessary to discover drugs with higher selectivity towards cancer cells and minimal side effects to healthy cells. There are several important targets for cancer therapy and the researchers should focus more on minimizing the side effects of the clinically available anticancer agents or develop new agents that selectively target cancer with reduced side effects.

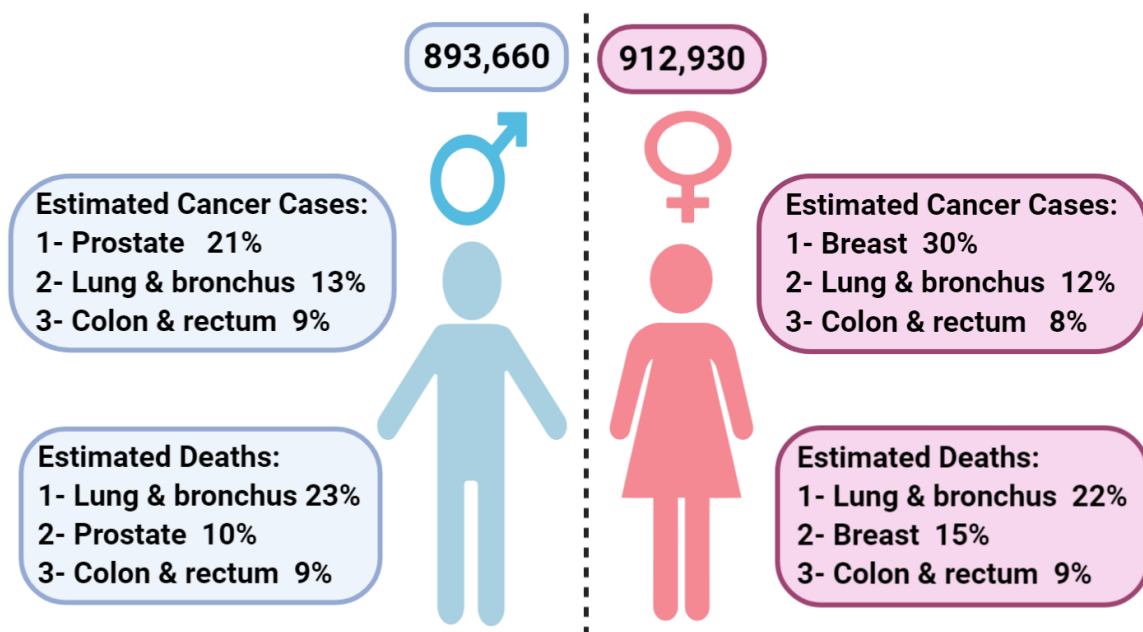


Figure 1.1. Three major cancer types for the estimated new cancer cases and deaths by sex, United States, 2020.

1.2. Targeting of cancer mitochondrial metabolic pathways, specifically mitochondrial respiratory complex II

Proliferating cancer cells are characterized by the ability to rapidly grow and divide uncontrollably that results in the formation of tumor, damage to the immune system, and this impairment can be fatal to cells. Cancer progression requires an increase in the metabolic processes and consumes a high amount of cellular nutrients. During recent years, in cancer drug discovery, the targeting of cancer metabolic pathways has emerged as an appealing strategy to increase the selectivity of anticancer therapy.⁹ The chemotherapies targeting cancer metabolism have been shown effective in the treatment of cancer for decades.¹⁰ While this success of chemotherapies targeting metabolism demonstrates that a novel therapeutic strategy exists to target cancer metabolism. It may provide a therapeutic advantage that can help overcome drug resistance, increase the specificity of drug delivery, enhance the potency of existing treatments, and overcome the side effects.¹¹

Antimetabolites are molecules that often inhibit the activity of enzymes involved in nucleotide base synthesis that leads to inhibition of the metabolism in the cells (**Table 1.1**). Many small molecules have been investigated to inhibit cancer cell metabolism, and one of the notable examples include methotrexate, which targets nucleotide biosynthesis of dihydrofolate reductase enzyme (DHFR).¹² Also, 6-mercaptopurine (6-MP) and 6-thioguanine (6-TG) inhibit the first enzyme in *de novo* purine biosynthesis using 5-phosphoribosyl-1-pyrophosphatase (PRPP) amidotransferase, and these molecules were known to be successful in treating childhood leukemia.¹³ Targeting thymidine synthesis (TS) by an antimetabolite class of nucleoside analogues such as 5-fluorouracil (5-FU) can halt tumor development.¹⁴ 5-Fluorouracil is the primary chemotherapy option for gastrointestinal cancers.^{12,15} Gemcitabine and cytarabine are also antimetabolite

nucleoside analogues that can be incorporated into DNA to result in inhibition of DNA polymerases.

Moreover, metformin has been identified to have an impact on oxidative phosphorylation in cancer cells, as it can inhibit mitochondrial complex I (CI) that leads to a decreased glucose oxidation and increases glutamine dependency in cancer cells.¹⁶⁻¹⁸ Another compound known for its inhibition of glucose metabolism is 2-deoxyglucose (2-DG). 2-Deoxyglucose is phosphorylated by hexokinase to produce 2-deoxyglucose-6-phosphate.¹⁹ Cancer cells that are exposed to high amounts of 2-DG undergo growth arrest and/or apoptosis because 2-DG accumulates intracellularly and competitively inhibits hexokinase to slow glucose uptake.²⁰ According to recent findings, targeting the cellular metabolic process is an attractive choice for bypassing drug resistance and thus providing an alternative strategy for anticancer therapy. The proliferation of normal cells and cancer cells have approximately similar metabolic requirements, thus, finding a therapeutic window between them remains a major challenge in the development of successful cancer therapies targeting metabolic pathways.

Drug	Pathway Target	Effect	Development Status
Methotrexate	Dihydrofolate reductase	Inhibits cell proliferation	FDA-approved
6-Mercaptopurine 6-Thioguanine	PRPP amidotransferase	Inhibits cell proliferation	FDA-approved
5-Flurouracil	Thymidylate synthase	Inhibits cell proliferation	FDA-approved
Metformin	Mitochondrial complex I	Activates AMPK	FDA-approved for diabetes, clinical trials in cancer Phase I/II
Gemcitabine Cytarabine	Nucleotide incorporation (DNA polymerase)	Inhibits cell proliferation	FDA-approved
2-Deoxyglucose	Hexokinase (glycolysis)	Blocks glycolytic flux	Reported in clinical trials

Table 1.1: Select agents targeting metabolism that are in clinical trials or FDA-approved for cancer treatment.

Targeting mitochondrial metabolism has been proposed as a unique approach for the development of anticancer drugs due to the central role that mitochondria play in the life and death of a cell.²¹ Emerging evidence implicates mitochondrial metabolism as vital for tumor growth.^{18, 22} Furthermore, mitochondria are crucial not only for energy production, but also in regulating essential steps for cell apoptosis and reactive oxygen species (ROS) generation.²³ Mitochondria are indispensable for eukaryotes and play many essential roles in the cell, most notably in electron transport-linked phosphorylation, central carbon metabolism (CCM), and the biosynthesis of intermediates for cell growth. Furthermore, the mitochondria is responsible for many other vital processes that determine cell function including cancer, inflammation, metabolic signaling, cell death, and transformation.²¹ Hence, mitochondrial dysfunction and modulating the mitochondrial oxidative metabolism have been found to contribute to many common disorders, including neurodegeneration and is a promising target for cancer therapy. Even though many of the mitochondria-targeted compounds have exhibited potency and selectivity towards cancer cell death in preclinical and early clinical testing, none of these compounds have progressed beyond phase III clinical trials to be used for treatment of human cancers.²⁴ Intensifying research in this area may improve the therapeutic efficacy of these compounds and fulfill the clinical promise of exploiting the mitochondrion as a target for cancer chemotherapy.

Reactive oxygen species are a variety of highly reactive chemicals and free radical oxygen molecules that are able to independently exist with one or more unpaired electrons such as the hydroxyl radical ($\cdot\text{OH}$), alkoxyl ($\text{RO}\cdot$) and hydrogen peroxide (H_2O_2).²⁵ Reactive oxygen species are generated during mitochondrial oxidative metabolism and play an essential role in triggering apoptosis under physiologic and pathologic conditions. In normal physiological conditions, ROS levels in cells are controlled and remain in balance, and also have antiapoptotic effects to drive regulatory pathways but when oxidative stress

occurs, ROS overwhelms the cellular antioxidant defense system and triggers oxidative damage to DNA and proteins.²⁶ Despite the presence of various antioxidant defenses, mitochondria are considered a major source and target of oxidants in most tissues.²⁷ There is evidence showing that ROS can act as cancer suppressents.²⁸ The increased ROS in malignant cells may be a promising approach towards developing a novel anticancer agent.

One of the most important mechanisms in mitochondrial metabolism is oxidative phosphorylation (OXPHOS)/electron transport chain (ETC). Oxidative phosphorylation refers to the generation of ATP from ADP and phosphate by ATP synthase by utilizing the reducing power of NADH and FADH₂ produced by the tricarboxylic acid (TCA) cycle and proton in the inner mitochondrial membrane.²⁹ The ETC (respiratory chain) process releases a huge amount of energy in the form of a proton gradient across the inner membrane of mitochondria, which is then utilized to synthesize ATP via ATP synthase.⁹ The respiratory chain consists of several important parts that include complex I (NADH-ubiquinone reductase), complex II (succinate dehydrogenase), complex III (cytochrome c oxidoreductase), complex IV (cytochrome c oxidase) and ATP synthase (complex V).²⁹ Targeting this type of mitochondrial metabolism has been proposed as a unique approach for the development of anticancer drugs.

Mitochondrial respiratory complex II (CII), also known as succinate dehydrogenase (SDH) or succinate-coenzyme Q reductase (SQR), is a 124 kDa protein complex located in the inner membrane of mitochondria.³⁰ Mitochondrial complex II is an integral membrane protein and contains four nuclear-encoded subunits: SDHA, SDHB, SDHC, and SDHD.³¹ Complex II plays a vital role in mitochondrial metabolism, where it catalyzes the oxidation of succinate to fumarate in the TCA cycle. Also, it reduces ubiquinone (Q) to ubiquinol (QH₂) (**Figure 1.2**).³² It is considered to be a part of the ETC as well as being

implicated in succinate signaling and substantial ROS generation.³¹ Complex II, unlike other mitochondrial complexes, links the two essential energy-producing processes of the cell: the TCA cycle and the ETC, while lacking any contribution to maintaining proton gradient across the mitochondrial inner membrane.³³ Despite the association of some aggressive forms of cancer with CII mutation (probably linked to hypoxia-inducible factor (HIF) activation resulting from inhibition of HIF prolyl-hydroxylases by succinate accumulation), far greater evidence supports an antiproliferative role for CII inhibition.³⁴

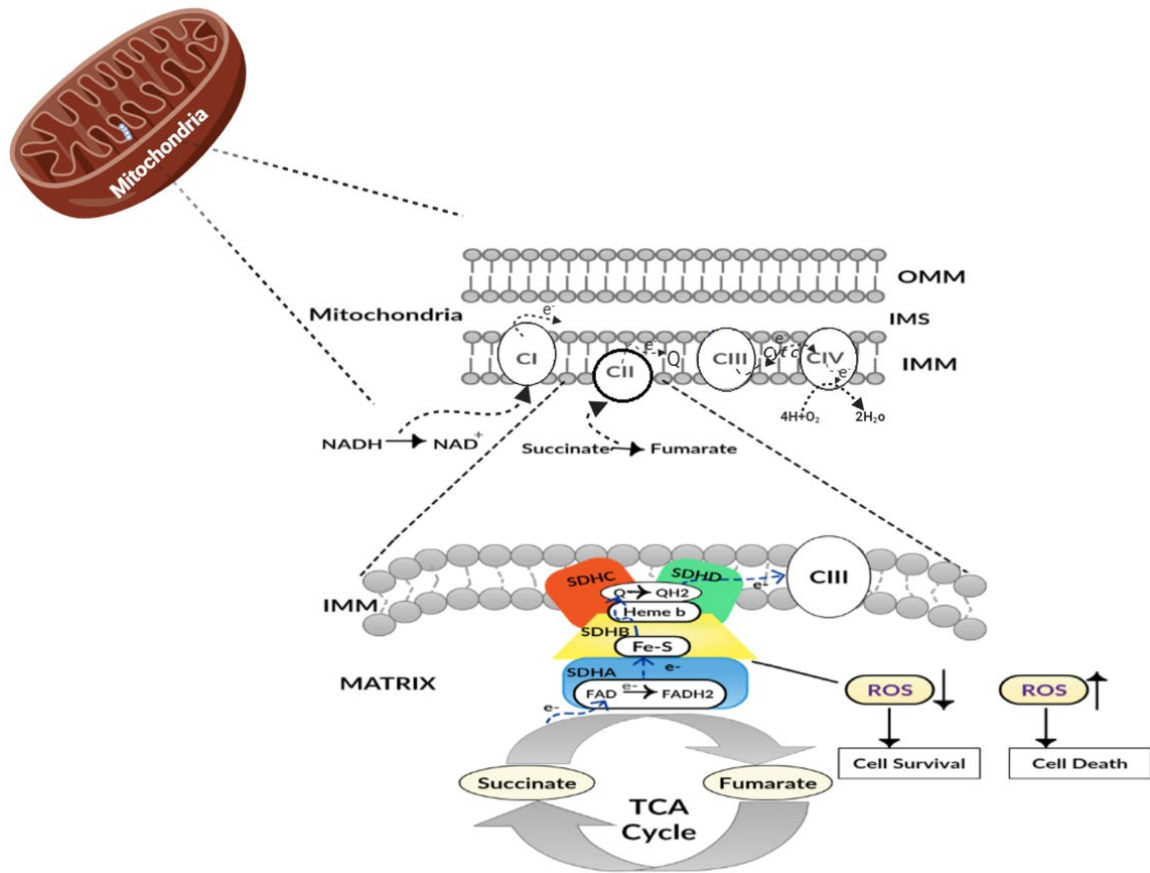


Figure 1.2. The structure of mitochondria respiratory complex II (CII); succinate dehydrogenase (SDH). It is a member of the respiratory chain and TCA cycle, wherein it catalyzes the oxidation of succinate to fumarate. SDHA, B, C, D represent the subunits of SDH.

Many factors make mitochondria an emerging and unique therapeutic target for several human diseases, including myocardial infarction (MI), stroke, and cancer. Complex II activity is responsible for the oxidative stress in stroke and MI due to its role in the generation of pathological ROS.^{23, 35} Several facets of CII inhibition, beyond the generation of ROS, have significant promise for the development of selective small molecule chemotherapeutics. Mutation of CII is rare in individual subunits within cancers, which makes it a unique invariant druggable target for the development of cancer chemotherapy. Complex CII mutations are associated only in infrequent and nonaggressive neoplasia such as pheochromocytomas.^{36, 37} In prostate cancer, which is one of the most common cancer types, the percentage of the patients with mutation in complex II is one in a million.^{36, 38} Inhibiting CII has a significant promise for the development of selective small-molecule chemotherapeutics through inhibiting glutaminolysis, the primary source of energy for cancer cells, at mitochondrial level via inhibition of the TCA cycle.^{33, 39} Along with complex I, complex II (also known as fumarate reductase) is a vital member of the NADH-fumarate reductase system in which amino acids can be used instead of glucose for maintaining mitochondrial energy production in tumor microenvironments under hypoxic conditions.⁴⁰ The inhibition of CII leads to prolonged activation of both autophagy and apoptosis in tumor cells.⁴¹ Malignant cells are known to develop resistance to apoptosis.⁴² Activation of the self-digestion process, autophagy, could therefore be an appropriate strategy for combating drug resistance and enhance cell death.⁴¹ Promisingly, a number of known but low potency CII inhibitors are selectively cytotoxic to cancer cells, albeit with weak effect, while conveying minimal to no toxicity to non-malignant cells.^{43, 44} The mitochondrial inner membrane potential within cancer cells is posited to be greater than their non-malignant counterparts.⁴⁵ This observation may account for the selective cytotoxicity of CII inhibitors to neoplastic cells.

The development of potent CII inhibitors would be expected to provide highly selective antineoplastic agents.

Inhibition of CII has also shown promise in the potential treatment of stroke and neurodegenerative diseases. Cardiac mitochondria sustain major damage in ischemia-reperfusion (IR) injury, tissue damage caused when blood supply returns after a period of ischemia. Recovery of mitochondrial function after IR insult is highly predictive of cardiac contractile recovery⁴⁶ and the preservation of mitochondrial function has become a popular strategy for cardioprotection.⁴⁷ Accumulation of succinate is a universal metabolic signature of ischemia and is responsible for mitochondrial ROS production during reperfusion. Inhibition of CII blocks both succinate accumulation during ischemia and its oxidation upon reperfusion, resulting in decreased volume of infarcted brain tissue caused by IR injury.⁴⁸ As such, it has been shown that inhibiting complex II with low potency compounds can protect the heart against ischemia-reperfusion IR injury, thereby ascribing CII as a potential target for drug development in stroke.^{48, 49}

Several CII inhibitors are known in the literature; however, all have low potency towards CII inhibition, and hence low cytotoxicity. 3-Bromopyruvate (3BP, **Figure 1.3**) was the first identified CII inhibitor, however no IC₅₀ has been reported to the best of our knowledge. This compound is known to be an alkylating agent⁵⁰ and is also an anti-glycolytic agent as hexokinase inhibitor, which strongly inhibits glycolysis,⁵¹ and these mechanisms of action will certainly contribute to antineoplastic activity, yet does not explain the observed selectivity between cancerous and non-malignant cells.⁵² Perhaps this selectivity is a tantalizing glimpse of the utility of CII as a chemotherapeutic target. On the other hand, a new study proved 3BP has high efficacy for anticancer therapy with no apparent side effects in the animal study.⁵³

The three carbon dicarboxylic acid (malonate) was one of the first identified competitive succinate dehydrogenase inhibitors with an IC_{50} of approximately $40\ \mu M$ ⁵⁴ and is often used as a tool compound. It has a significant role in symbiotic nitrogen metabolism and brain development.⁵⁵ It has also been shown to regulate the activity of mitochondrial ATP-sensitive potassium channels.⁵⁶ The competitive inhibitor malonate is also cardioprotective, mimic ischemic preconditioning, and can modulate ROS production in isolated mitochondria.⁵⁷ No high antineoplastic activity associated with malonate has been reported.

3-Nitropropionic acid (3NP) is a mitochondrial toxin, able to impair cellular energy metabolism via inhibition of CII, which induces a reduction in ATP production that leads to oxidative stress and generation of ROS.⁴⁰ According to the best of our knowledge, no IC_{50} has been reported for 3NP. 3-Nitropropionic acid also has the same effect as malonate, including cardioprotective, mimic ischemic preconditioning, and decrease oxygen radical production.⁵⁶ However, the irreversible inhibitor of mitochondrial complex II 3NP has a limited anticancer effect.⁵⁶

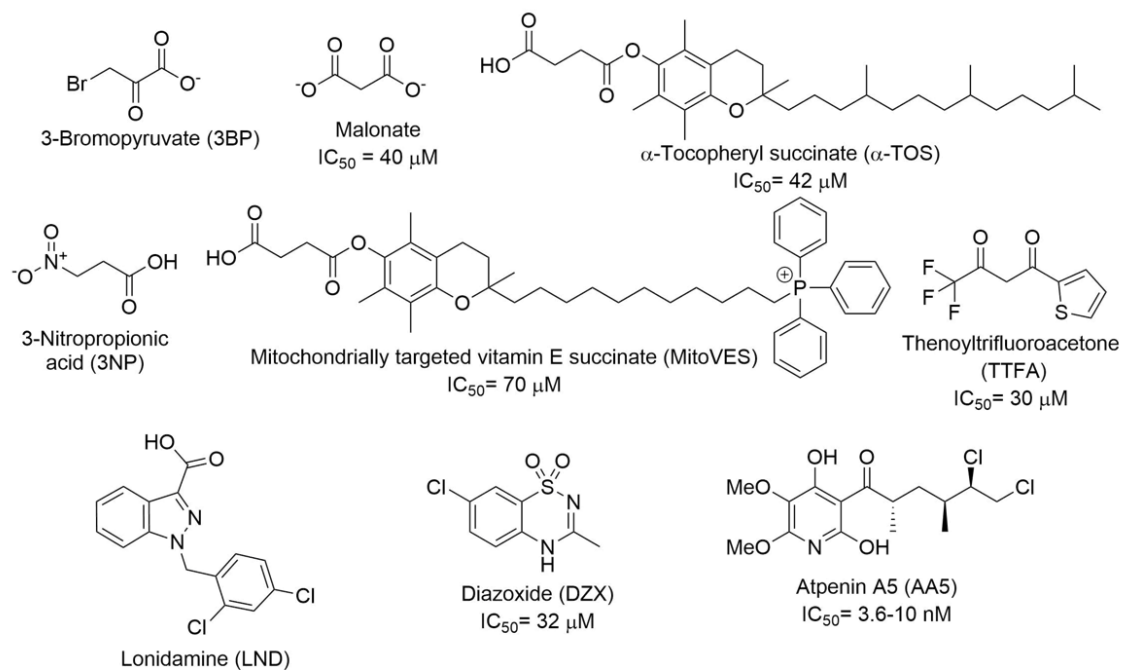


Figure 1.3. Structures of known mitochondria respiratory complex II inhibitors.

Vitamin E analogue α -Tocopheryl succinate (α -TOS) has a CII inhibition $IC_{50} = 42$ μ M was shown to have improved biological activity.⁵⁸ It can inhibit the proliferation and induce apoptosis in cancer cells by rapid generation of ROS.³¹ This compound is selective for cancer cells due to their characteristically diminished antioxidant defenses and low esterase activity, thereby lessening the toxicity on non-malignant cells.⁵⁹ Mechanism of action studies suggest α -TOS can cause membrane damage and induce ceramide-mediated apoptosis.⁶⁰ Several animal data studies of α -TOS have been shown to suppress growth effects for many cancers including prostate, lung, melanoma, and breast.⁶¹⁻⁶⁴

Mitochondrially targeted vitamin E succinate (MitoVES) (**Figure 1.3**) has a lower potency for CII than the parent compound α -TOS with an $IC_{50} = 70$ μ M.⁶⁵ However, MitoVES was found to be 20-50 times more effective in inducing apoptosis in cancer cells than α -TOS.⁶⁶ This is attributed to the introduction of a lipophilic cationic triphenylphosphonium (TPP⁺) group which allows it to permeate throughout phospholipid bilayers, targets and accumulates within mitochondria. The delocalized charge on the quaternary phosphorus atom is known to cause up to 1000-fold greater accumulation in the mitochondria.⁶⁷ This places the pharmacophore of the compound inside the mitochondrial inner membrane (MIM) where CII is located. Thus, the addition of the cationic TPP group serves as a targeted delivery method to enhance the concentration of the compound within the mitochondria and provides enhanced antineoplastic properties.³¹ Again, inhibition of CII has been shown to be selective to cancerous cells with MitoVES possessing an IC_{50} of 0.5-3 μ M for apoptosis induction in cancer cells, which is more cytotoxic than non-malignant cells with approximately 20-60 μ M.⁶⁶

Thenoyltrifluoroacetone (TTFA), is a chelating agent, and potent inhibitor of cellular respiration by inhibition of CII. It is widely used as a control compound to study the

structure and function of CII with an $IC_{50} = 30 \mu M$.⁶⁸ Thenoyltrifluoroacetone induces apoptosis and results in the generation of ROS. However, high toxicity to non-cancerous cells limits TTFA investigation as a CII inhibitor.⁶⁹ Also, TTFA has been shown to potently inhibit carboxylesterase activity.⁷⁰

Lonidamine (LND) has been known to be an anticancer agent that can selectively act on the mitochondrial metabolic pathways of neoplastic cells.⁷¹ Early studies demonstrated that LND can inhibit aerobic glycolysis in cancer cells through its inhibitory effect on mitochondrial bound hexokinase while enhancing aerobic glycolysis in healthy cells.⁷¹ It has limited anticancer activity as a single agent, while having a high potential impact in modulating the activities of conventional antitumor therapies.^{72, 73} It has been used in many clinical trials and can effectively sensitize tumors to chemotherapy, hyperthermia, photodynamic therapy, and radiotherapy selectively.⁷⁴ A recent finding indicates that LND can inhibit CII by interfering with the ubiquinone site and preventing the reduction of ubiquinone, which leads to the alteration of several essential metabolic pathways in cancer cells.⁷⁵ Lonidamine treatment results in mitochondrial dysfunction, mitochondrial mass change, loss of mitochondrial membrane potential, and reduction of cellular ATP levels.⁷¹ Lonidamine also enhances the generation of a large number of ROS through the inhibition of CII, which significantly contributes to halting tumor development.⁷⁵

Several other small molecules with low potency CII inhibition activity are also known. However, their potency precludes them from detailed evaluation as antitumor agents. While many of the above-mentioned known CII inhibitors demonstrate anticancer activity, they all exhibit low potency CII inhibition ability ($IC_{50} = 30-70 \mu M$). Indeed, almost all these inhibitors have been shown to have alternative or complementary mechanisms to CII inhibition that may account for the observed anticancer activity. Reactive oxygen species induction is essential for all the CII inhibitors with proven anticancer activity;

however, the precise sequence of events leading up to and following ROS production are poorly understood. A potent CII inhibitor would be expected to elicit far greater anticancer efficacy and would be an excellent candidate for development as a chemotherapeutic agent, as a probe compound for further elucidation of this promising mechanism and further study of the role of mitochondria in cancer and other diseases.²³

The accumulation of metabolite succinate in the TCA cycle is an essential pathologic event in tissue ischemia, and this is thought to occur by reverse operation of CII.⁴⁸ As such, it has been shown that inhibiting complex II with low potency compounds can protect the heart against ischemia-reperfusion IR injury, thereby ascribing CII as a potential target for drug development in stroke.^{48, 49}

The clinical vasodilator and FDA approved drug diazoxide (DZX) is the second most potent CII inhibitor with an IC_{50} value of 32 μ M disclosed in rat heart mitochondria.⁷⁶ It is known to regulate ROS production, protecting normal cells from ischemic damage but also inducing specific cancer cell death.⁷⁷ Benefits, as well as drawbacks and a narrow therapeutic window, have been observed from DZX administration across different tissues and organelles. In pancreatic β -cells, DZX is known to activate K_{ATP} channels that leads to a suppression of glucose-induced insulin release.⁷⁸ Several studies have shown that DZX reduces glucose-induced insulin secretion in healthy individuals and prevents hyperinsulinemia in patients suffering from insulinoma.^{79, 80} Small doses of DZX regulates ROS production and induces protection from IR injury and elicits cardioprotection.⁸¹ However, the high doses of DZX (more than 750 μ M) is shown to increase the generation of ROS.^{82, 83} In cortical neuron mitochondria, <200 μ M of DZX had no effect, but results in depolarization with more than 300 μ M dose.⁸² Further, a 100 μ M concentration of DZX was reported to inhibit CII in mouse heart mitochondria but IC_{50} was not reached.⁵⁶ Diazoxide has been shown to be neuroprotective in animal models of alzheimer's

disease,^{84, 85} protect neurons from a range of neurotoxic insults, including exposure to amyloid- β peptide (25-35),⁸⁶ and was reported to reduce proliferation in both acute leukemic T cells,⁸⁷ and triple negative breast cancer (TNBC) MDA-MB-468 cells.⁸⁵ The cytotoxicity of DZX on cancer cells was attributed to the downregulation of beta-catenin-mediated cyclin D1 transcription as this mechanism of action is detected for the inhibition of growth in the human lung cancer (H1299) cells.⁸⁸ Despite the low potency of DZX as anticancer agent, it may have a promising approach towards development as a novel anticancer agent.

One of the most interesting compounds acting via targeting and inhibiting CII is the natural product atpenin A5 (AA5, **Figure 1.3**). It is a specific CII inhibitor at the ubiquinone binding site (IIQ) and the most potent inhibitor known to date with $IC_{50} = 3.3\text{-}10\text{ nM}$.⁸⁹ Atpenin A5 is able to generate high ROS levels that leads to the inhibition of CII (75% hydrogen peroxide and 25% superoxide).⁹⁰ Atpenin A5 and its analogs have been shown to demonstrate anticancer activity *in vitro* in DU-145 prostate cancer cells.⁹¹ However, atpenin B which was reported by Quéguiner and co-workers, a close analogue of atpenin A5, was found to have limited anticancer effect in *in vivo* studies which could be attributed to its poor absorption, distribution, metabolism and excretion (ADME) properties.⁹² Among atpenin analogues, atpenin A5 may be a useful tool for CII inhibition and antineoplastic agent in mammalian tissues. Also, CII inhibitor AA5 has been reported to have protective effects against IR injury through mitochondrial K_{ATP} channels activation.⁹³ Atpenin A5 is the most potent K_{ATP} activator discovered to the best of our knowledge.

In this research, we will focus on the most potent CII inhibitors known in the literature. The structure-activity relationship (SAR) of AA5 and DZX will be determined; also, their antineoplastic activity will be evaluated. To the best of our knowledge, no

studies have been reported attempting to optimize the potency of these two compounds as a CII inhibitor and as chemotherapeutic agents.

1.3. Targeting of angiogenesis vascular endothelial growth factor

The human cells always need a constant source of oxygen and nutrients under normal conditions. Most of the nutrients are delivered to cells via the blood vessels in the circulatory system, which have a crucial role in the life of the cells such as proliferation and growth. Considering this vital phenomenon, the researchers are concerned to study this important aspect of the blood vessels. Angiogenesis is an essential process of forming new blood vessels in tissues and organs in the body under physiological and pathological conditions and is regulated by the balance of angiogenic and antiangiogenic molecules.⁹⁴ It is a critical process of growth and development during embryogenesis as well as in wound healing in the body from pre-existing vessels. The primary vessels form and develop through vasculogenesis; after that, any new blood vessel formation will be under the control of angiogenesis during body development or disease.⁹⁵ Most of the normal cells are involved in the formation of new blood vessels. However, angiogenesis also plays a critical role in cancers and also in non-cancerous diseases such as psoriasis, arthritis, and endometriosis.⁹⁴ The essential role of angiogenesis depends on growth factors, which are considered a subset of cytokine ligands that bind to the receptor and activate the growth factor receptors and stimulate cell growth, survival, inflammation, and tissue repair. Large families of growth factors are known to include: epidermal growth factor (EGF), vascular endothelial growth factor (VEGF), tumor necrosis factor-alpha (TNF- α), interleukins (IL-1-7), and transforming growth factor (TGF).⁹⁶

Cancer cells are abnormal in growth, which means they require a high amount of oxygen and nutrients to continue progression and propagation. Without blood vessels,

these cells will stop growing due to a lack of nutrient suppliers.⁹⁷ The blood vessels in a tumor are different from their regular counterparts. They are not organized and are irregularly shaped, dilated, tortuous, and often leaky that is partly due to the overproduction of VEGF.⁹⁸ Pathological induction of angiogenesis is one of the hallmarks of cancer.⁹⁹ Results of many studies have shown that hypoxia is a key driver of the formation of new capillaries to produce signaling and growth factors from tumor cells.¹⁰⁰ In addition, cancer cells can grow around an existing vessel to form a perivascular cuff, which paves way to potentially identify new targets for therapy.⁹⁵

Antiangiogenic or angiogenesis inhibitors are molecules that are able to block the angiogenesis process. The tumor sends signals that stimulate blood vessel growth.¹⁰¹ Blocking this process leads to the suppression of nutrients and oxygen from cancer cells and allows the cells to starve.⁹⁷ Thus, angiogenesis inhibitors are used to reduce and slow down the spread and growth of many types of cancers by diminishing the tumor's ability to form new blood vessels.⁹⁵ The angiogenesis inhibition process is a fascinating area of research in cancer treatment and drug discovery. This type of cancer treatment should have low toxicity because it is not designed to directly target tumor cells. The high mutation rates of cancer cells will not interfere with antiangiogenic drugs, but chemotherapy often renders it ineffective.

A breakthrough in tumor angiogenesis research became possible through the crucial discovery of the main molecular drivers of VEGF that include VEGF-A, VEGF-B, VEGF-C, VEGF-D, and placental growth factor and their cognate receptors.¹⁰² The major function of VEGF in our body is to modulate vessel permeability, and the remodeling of endothelial cells. It is considered as one of the most significant growth and survival factors for endothelium, which induces angiogenesis and endothelial cell proliferation and plays a vital role in human body. Vascular endothelial growth factor is a heparin-binding

glycoprotein that is secreted as a homodimer of 45 kDa.¹⁰³ In the cardiovascular system, VEGF expression has been demonstrated in cardiac myofibroblasts which have a significant role in the growth, development and repair of normal tissue.¹⁰⁴ It was shown higher excretion rate in most human tumors because the tumor tricks the body into creating new blood vessels by stimulating this type of angiogenesis factor. The VEGF forms ligands via three specific and cognate tyrosine-kinase receptors (VEGFR): VEGFR-1, VEGFR-2, and VEGFR-3.⁹⁹ Vascular endothelial growth factor receptors are responsible for binding with VEGF to initiate signal cascades that act to induce and activate the angiogenesis process.¹⁰⁵ The VEGFR-1 expression has been shown in many cells such as stem cells, monocytes, and vascular endothelial cells and is essential for recruiting hematopoietic stem cells as well as the migration of monocytes and macrophages.¹⁰⁶ The VEGFR-2 is expressed on vascular endothelial cells and lymphatic endothelial cells and regulates vascular endothelial function.¹⁰⁷ The VEGFR-3 is only expressed on lymphatic endothelial cells and regulates its functions.¹⁰⁶ Vascular endothelial growth factor and its receptors are dysregulated upon activation, overexpression, or mutation that could lead to tumorigenesis and metastasis by initiating downstream signaling transduction pathways (Ras/MAPK, PI3K/Akt, and Jak/STAT), and results in angiogenesis, vascular permeability enhancement, and tumor development **(Figure 1.3)**.¹⁰¹ Therefore, VEGF or its receptors represent an important and valuable target in the research, development, and design of anticancer agents.

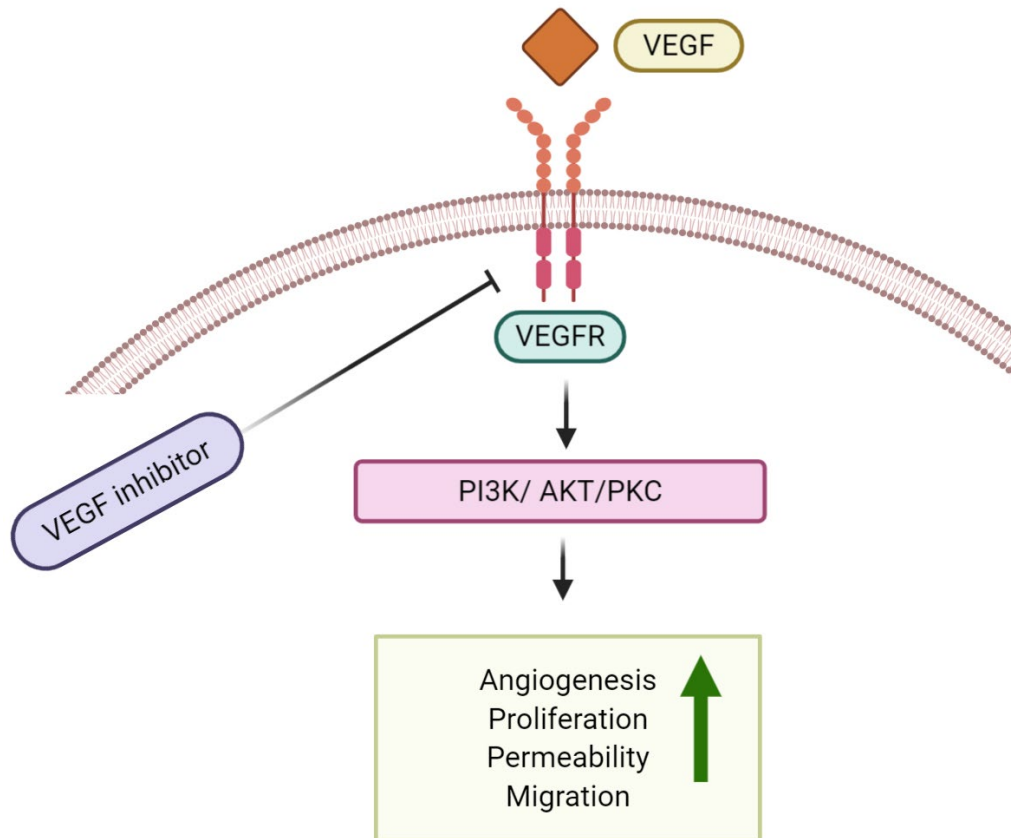


Figure 1.4. Vascular endothelial growth factor (VEGF) ligand and receptor. VEGFs and PlGF (placental growth factor) can interact with a combination of VEGF receptors (VEGFRs), which activate tyrosine kinase proteins (PI3K/ AKT/ PKC) and initiates downstream signaling transduction pathways.

Anti-vascular endothelial growth factor (anti-VEGF) or a VEGF inhibitor is a drug usually used as an antineoplastic agent that functions by blocking VEGF from adhering to the receptors on blood vessels which in turn inhibits the growth and propagation of blood vessels.¹⁰⁸ In the last two decades, a variety of anti-VEGF compounds were discovered and designed to inhibit tumor growth and angiogenesis because of the VEGF's vital role in angiogenesis within tumors (**Table 1.2**). Regorafenib is a multi-kinase inhibitor which targets angiogenic, stromal, and oncogenic receptor tyrosine kinase (RTK). The FDA approved regorafenib for the treatment of refractory metastatic colorectal cancer in 2013. It was also approved by the FDA for the treatment of hepatocellular carcinoma in 2017.¹⁰¹ Sorafenib is an antiangiogenics drug with a similar structure to regorafenib except for one fluorine atom on the phenyl ring. It is a kinase inhibitor approved in 2005 for the treatment of advanced renal cell carcinoma. Also, in 2007, it was approved for advanced primary liver cancer. Recently, this drug was approved for thyroid cancer in 2013.¹⁰⁹ The oral small molecule sunitinib inhibits cellular signaling by targeting multiple receptor tyrosine kinase inhibitors, and was approved by the FDA in 2006 for the treatment of renal cell carcinoma.¹¹⁰ In 2011, the FDA approved sunitinib for treatment of rare cancer pancreatic neuroendocrine tumors which happened in a ratio of two to four people per million annually worldwide.^{101, 111} Another anti-VEGF and anticancer drug is pazopanib which is a potent and selective multi-targeted receptor tyrosine kinase inhibitor. It has been approved by FDA for renal cell carcinoma in 2009 and soft tissue sarcoma in 2012. Some other anti-VEGF agents were discovered and approved by the FDA in the last ten years including axitinib, vandetanib, and lenvatinib, which are used for the treatment of specific types of cancers such as renal cell carcinoma and thyroid cancer (**Table 1.2**).¹⁰¹

Several antibodies and protein-based therapies have also been designed to target angiogenic signaling for cancer therapy. The first and common antiangiogenic agent

discovered and gained FDA approval in 2004 for specific types of cancer is bevacizumab.¹¹² It is a humanized monoclonal IgG antibody (molecular weight, 149 kDa) that suppresses the angiogenesis process by binding and neutralizing VEGF-A.¹¹³ Bevacizumab was approved for the treatment of several types of cancers, such as metastatic colorectal, non-small-cell lung, breast, and renal cell cancers.¹¹⁴ Ramucirumab is also another is a humanized anti-VEGF monoclonal IgG₁ antibody (molecular weight, 147 kDa) developed for the treatment of tumors. In 2014-2015, the FDA approved ramucirumab as a single-agent treatment for advanced gastric cancer or gastro-esophageal junction.¹¹⁵ In addition, ramucirumab was also approved by the FDA for non-small-cell lung cancer and metastatic colorectal cancer.

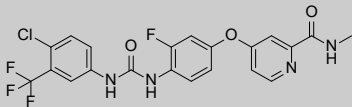
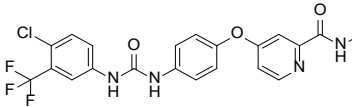
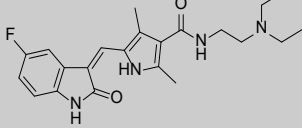
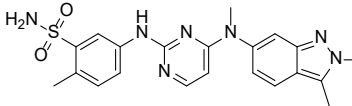
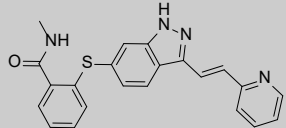
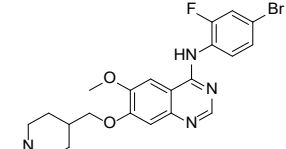
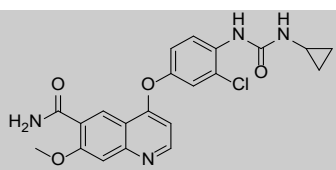
Drug	Structure	Cancer
Regorafenib		Refractory metastatic colorectal cancer and Hepatocellular carcinoma
Sorafenib		Hepatocellular carcinoma, Renal cell carcinoma, and Thyroid cancer
Sunitinib		Renal cell carcinoma, and Pancreatic neuroendocrine tumors
Pazopanib		Renal cell carcinoma, and Soft tissue sarcoma
Axitinib		Renal cell carcinoma
Vandetanib		Medullary carcinoma of the thyroid
Lenvatinib		Thyroid cancer
Bevacizumab	$C_{6538}H_{10034}N_{1716}O_{2033}S_{44}$	Metastatic colorectal cancer, Non-small-cell lung cancer, Renal cell carcinoma, Ovarian cancer, and Breast cancer
Ramucirumab	$C_{6374}H_{9864}N_{1692}O_{1996}S_{46}$	Gastric esophageal junction cancers, Non-small-cell lung cancer, and Metastatic colorectal cancer

Table 1.2: The FDA-approved antiangiogenic VEGF inhibitors.

Despite the number of the antiangiogenic drugs approved by the FDA, the success of antiangiogenic treatment has so far been relatively limited because these drugs provide short-term relief from tumor growth, and upon prolonged treatment, tumors become resistant and typically result in modest survival benefits.¹⁰⁰ Potent and therapeutically significant effects were achieved when combining the antiangiogenics with other treatments such as radiotherapy and chemotherapy, a situation that reflected the earliest clinical experience with these drugs as a novel therapy.¹⁰¹ As an example, the combination of the VEGF inhibitor bevacizumab with carboplatin and paclitaxel is approved for the first-line treatment of advanced cancers. Radiation therapy elevates VEGF levels significantly within malignant tumors after treatment, and anti-VEGF drugs could protect tumor cells from radiation resistance, and have potential to provide higher antitumor efficacy.^{116, 117} In general, combining repurposed pharmaceutical drugs with other chemotherapeutic agents has also shown promising results, which is useful when the anticancer monotherapy is faced with difficulty in providing a safe and effective treatment for cancer patients.¹¹⁸ Using anti-VEGF therapies in combination with chemotherapy or radiotherapy is effective against many types of cancers because the VEGF blockade leads to angiogenesis inhibition and renders tumor cells more susceptible to conventional treatment.¹¹⁹

The significance of targeting angiogenesis growth factors for anticancer research encourages the researchers to discover and develop new agents. Here, we envision to design a potential VEGF inhibitor to improve the applicability and reach of antiangiogenic cancer therapies.

1.4. Targeting of carbonic anhydrase enzymes in cancer cells

Carbonic anhydrases (CA; also known as carbonate dehydratases EC 4.2.1.1) are a superfamily of ubiquitous metalloenzyme which play a catalytic role in the reversible interconversion of carbon dioxide (CO_2) and water to bicarbonate (HCO_3^-) and a proton.¹²⁰ The active site structure of most CAs contains a zinc ion (Zn^{2+}) located at the base, which is essential for catalysis and allows for nucleophilic attack on the carbon dioxide group.¹²¹ Carbonic anhydrases are significant for many physiological processes including pH regulation, CO_2 homeostasis, respiration, bone resorption, fatty acid metabolism, and tumorigenesis.¹²²⁻¹²⁴ The CA family in humans consists of 16 isoforms and their expression is varied by localization and catalytic activity: cytosolic carbonic anhydrases are CA I, CA II, CA III, CA VII, CA XIII; membrane-bound carbonic anhydrases are CA IV, CA IX, CA XII, CA XIV, CA XV; mitochondrial CA Va and CA Vb and CA VI secreted in saliva and colostrum.^{125, 126} These enzymes are found in many tissues in the body, such as the renal cortex, gastric mucosa, red blood cells, lung, pancreas, and central nervous system.^{127, 128} The CA IX and CA XII have been reported to have elevated expression in many types of tumors. They play a significant role in the process of tumorigenesis, cancer cell signaling, tumor progression, acidification, and metastasis.^{129, 130}

In general, the bicarbonate must be transported through the cell membrane because it is poorly soluble in lipid membranes compared to carbon dioxide. Therefore, to facilitate its transport into the cell, the bicarbonate is converted to carbon dioxide and water by producing carbonic anhydrase enzymes to do this conversion. Carbonic anhydrases have essential roles in all kingdoms of life to facilitate the transport of carbon dioxide and protons across biological membranes to the intra and extra-cellular space (**Figure 1.5**).¹²⁶ The carbonic anhydrase enzyme employs a vital role in a two-step mechanism: first, there is a nucleophilic attack on CO_2 by a zinc-bound hydroxide ion. In the second step, the

active site is regenerated by the ionization of the zinc-bound H₂O molecule and removing a proton from the active site.^{125, 131} Through this mechanism, carbonic anhydrases are essential enzymes in cell survival and proliferation by maintaining and regulating the pH of the cells.¹²⁸

Inhibition or prevention of the mechanism of action of the metalloenzyme CA has significant pharmacologic applications in many fields including anticancer,¹²⁰ diuretics,¹³² anticonvulsant,¹³³ and antiglaucoma agents.¹³⁴ Also, CA inhibitors are known as antiinfectives such as antifungal, antibacterial, and antiprotozoal agents.¹³⁵ There are two main categories of CA inhibitors known: the metal-complexing anions and the unsubstituted sulfonamides and their bioisosteres.¹²⁰ A primary sulfonamide group (R-SO₂NH₂) is an important pharmacophore for carbonic anhydrase activity.¹³⁶ Carbonic anhydrase enzyme inhibitors have become an exciting aspect for clinicians when the first drugs were established as a promising group of diuretics. Hypoxia leads to a strong overexpression of CA IX and CA XII in many tumors.¹²⁰ The CA IX and CA XII catalyze the rapid interconversion of CO₂ and water into CO₂, protons, and bicarbonate ions, which contributes to maintain acidification of the tumor microenvironment, which results in resistance to cytotoxic therapy in some hypoxic tumors to several anticancer drugs.^{120, 137} Targeting carbonic anhydrase CA IX and CA XII has been an emerging strategy to combat tumor growth and regulation of tumor pH.¹³⁸ Recently, inhibition of the CA enzymes have been proposed as a potential new class of anticancer agents. Many studies showed that inhibiting CA IX and CA XII with sulfonamide and coumarin-based small-molecules inhibits cancer cell growth both *in vitro* and *in vivo* and effects tumor acidification.^{120, 128, 137} Several of these compounds are in preclinical development, especially for tumors with overexpression of CA IX or CA XII.¹³⁸

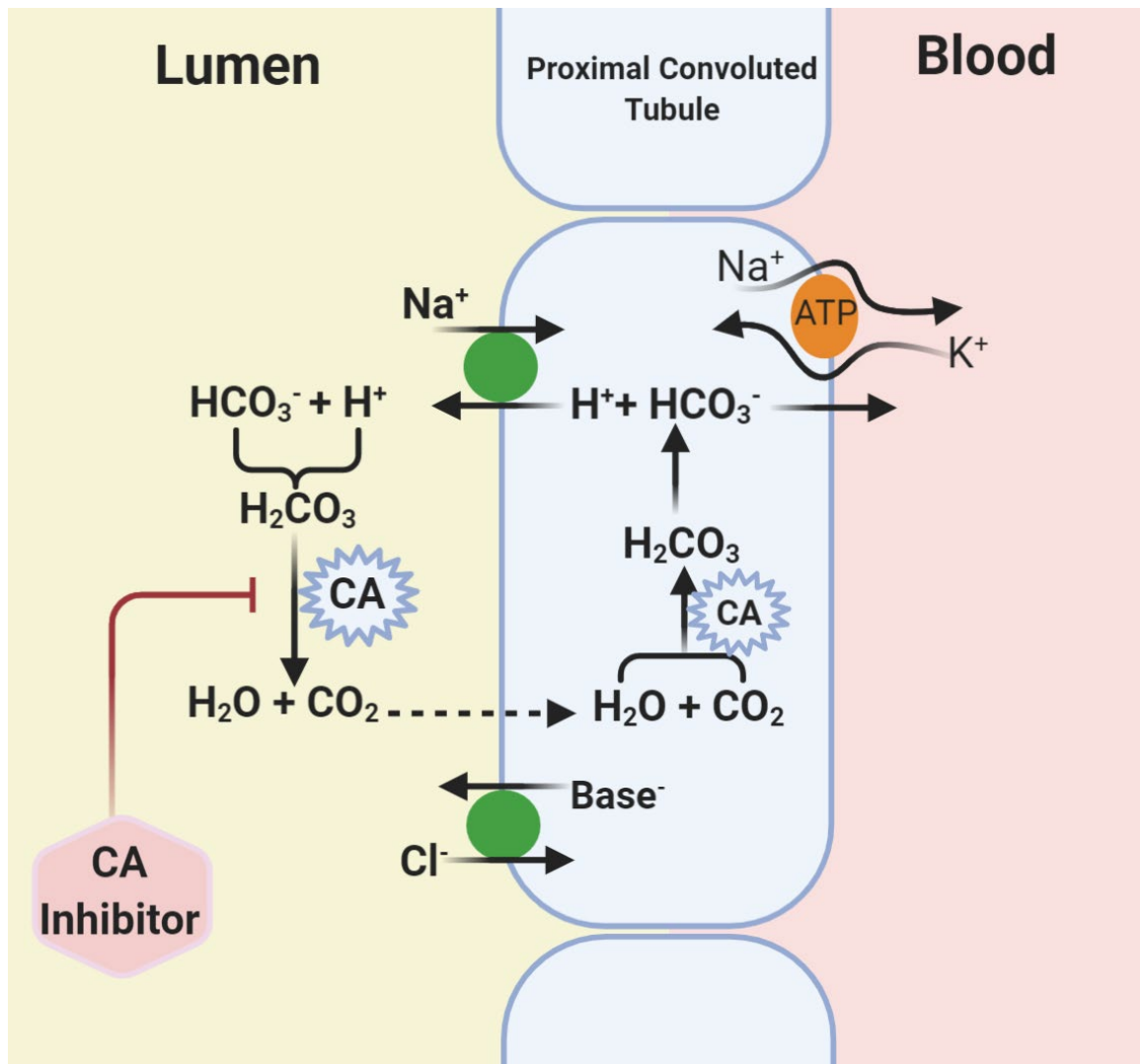


Figure 1.5. Mechanism of action of carbonic anhydrase inhibitor. The absorption of bicarbonate (HCO_3^-) by the proximal convoluted tubule (PCT) happened after converted to carbon dioxide (CO_2) and water (H_2O) by carbonic anhydrase enzyme (CA). The CA inhibitor used to prevent the completion of this mechanism.

The most common and important carbonic anhydrase inhibitors are sulfonamide compounds and their isosteres which strongly inhibit CA belonging to most families. There are many carbonic inhibitor medications currently available with the different formulas administered through topical, oral, or IV route. The first discovered organic inhibitor of these enzymes was sulfanilamide.¹³⁹ The sulfonamide derivative, acetazolamide, was first introduced as an oral potent carbonic anhydrase inhibitor used for diuretic and glaucoma therapy (**Figure 1.6**). Acetazolamide is a beneficial adjunctive agent in the pharmacotherapy of the treatment of certain convulsive disorders (e.g., epilepsy),¹⁴⁰ altitude sickness,¹⁴¹ and periodic paralysis.¹⁴² Also, several studies showed that acetazolamide has an antitumor activity for many types of cancer, including neuroblastoma, colorectal cancer, and bronchial carcinoids.¹⁴³⁻¹⁴⁵ Dichlorphenamide is another FDA approved carbonic anhydrase inhibitor drug used to treat primary periodic paralysis (muscle weakness).¹⁴⁶ It is also used to treat glaucoma by partially reducing the secretion of aqueous humor.¹⁴⁷ Methazolamide is one of the most potent carbonic anhydrase inhibitor drugs approved by the FDA. It is used to treat high pressure inside the eye due to certain types of glaucoma by decreasing the production of fluid inside the eye.¹⁴⁸

The sulfonamide derivative dorzolamide is one of the most potent drugs able to block the carbonic anhydrase enzymes. It is used to treat the elevation in intraocular pressure associated with open-angle glaucoma and ocular hypertension.¹⁴⁹ Also, dorzolamide has been known to inhibit solid tumor growth *in vivo*.¹⁵⁰ Ethoxzolamide is another sulfonamide drug used in the treatment of glaucoma which inhibits carbonic anhydrase activity and decreases reabsorption of water, sodium, potassium, bicarbonate.¹⁵¹ A preclinical carbonic anhydrase inhibitor U-104 has been shown to selectively inhibit CA IX and CA XII with K_i of 45.1 nM and 4.5 nM, respectively.¹⁵² The

carbonic anhydrase inhibitor U-104 has also been reported as a potent anticancer agent *in vitro* and *in vivo* with several tumors because it binds specifically to hypoxic cells, which overexpress CA IX.¹⁵³ These CA inhibitors have been shown to inhibit tumor-associated CA IX, resulting in increased cell death in hypoxic tumors.¹⁵⁴

Coumarins in drug discovery have biological significance and several derivatives have been studied for various ailments. They have various pharmacological activities that depend on the type of coumarin nucleus which includes antimicrobial, antiinflammatory, anticoagulant, and antioxidant effects.¹⁵⁵⁻¹⁵⁷ Also, coumarins possess immeasurable antitumor potential with minimal side effects, depending on their substitutions.¹⁵⁸ Coumarins have been shown to help control the pH balance of cancer cells and reduce the activity of tumor-associated carbonic anhydrases in the management of hypoxic tumors.¹⁵⁹ In the last decades, coumarin (1,2-benzopyrane) and its derivatives were reported as potent non-classical carbonic anhydrase inhibitors that selectively target human CA IX and CA XII carbonic anhydrases over other isoforms.¹⁶⁰ Coumarins, unlike the sulfonamides, directly interact with the CA active site metal ion, and undergoes hydrolysis under the influence of the zinc hydroxide with the generation of substituted 2-hydroxycinnamic acids.¹⁶¹

The glycosyl coumarin GC-204 has been reported as a potent and selective carbonic anhydrase IX and XII inhibitor with K_i 9.2 nM and 43 nM, respectively (**Figure 1.7**).¹⁶¹ Also glycosyl coumarin GC-205 has been shown to selectively inhibit carbonic anhydrase IX and XII with K_i 201 nM and 1.8 nM, respectively.¹⁶² GC-205 was recently shown to strongly attenuate the growth of primary tumors and metastases in an animal model of breast cancer and is in advanced preclinical evaluation as an anticancer agent.¹⁵² The coumarin derivatives 8-hydroxy-6,7-dimethoxy-2H-chromen-2-one (**1.1**) and 7,8-dihydroxy-6-methoxy-2H-chromen-2-one (**1.2**) showed potent CA IX inhibition with K_i 0.85

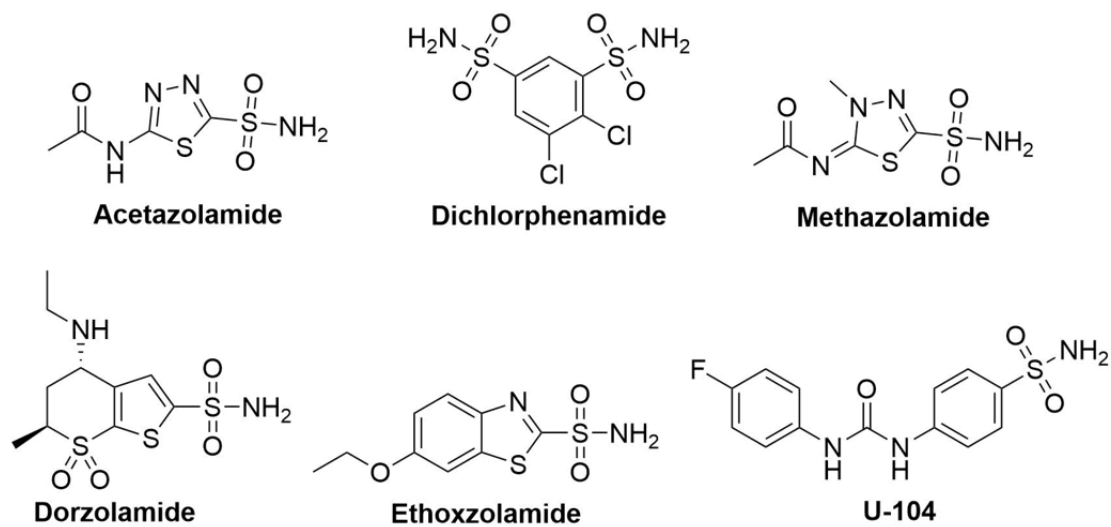


Figure 1.6. Structures of several clinical and preclinical sulfonamide derivative carbonic anhydrase inhibitors.

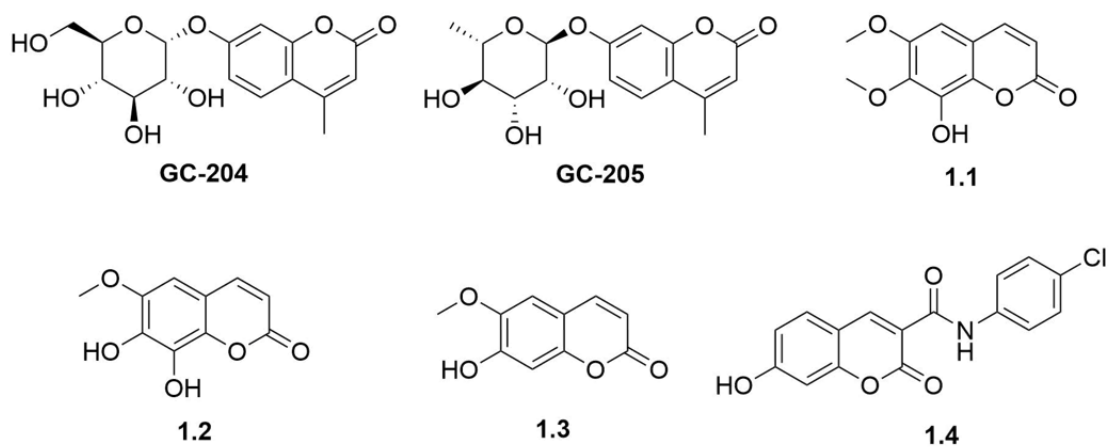


Figure 1.7. Structures of several coumarin derivatives as potent carbonic anhydrase inhibitors.

μM and $0.61 \mu\text{M}$, respectively.¹⁶³ In addition, they are able to inhibit CA XII with K_i $7.84 \mu\text{M}$ and $7.70 \mu\text{M}$ respectively.¹⁶⁴ The coumarin derivative 7-hydroxy-6-methoxy-2H-chromen-2-one (**1.3**) also evaluated as a potent CA IX and XII inhibitor with K_i $0.96 \mu\text{M}$ and $4.05 \mu\text{M}$, respectively. Literature reports show that *N*-(4-chlorophenyl)-7-hydroxy-2-oxo-2H-chromene-3-carboxamide (**1.4**) is a highly effective inhibitor against both CA IX and CA XII with a K_i of $0.2 \mu\text{M}$ (**Figure 1.7**).¹⁶⁵ Several carbonic anhydrase inhibitors with sulfonamides containing coumarin moiety have been previously reported. Some of these derivatives have high efficacy for inhibiting the enzymatic activity of the physiologically dominant tumor-associated isoenzyme human CA IX with IC_{50} in the range of 0.024 - $0.188 \mu\text{M}$.^{159, 166} The results indicate that the higher binding affinity of the sulfonamide-containing coumarin moieties to the cancer-associated CA IX have a potent anticancer activity. Dr. Zhu group shows that several coumarin containing sulfonamide moieties moiety compounds have anticancer activity more than the chemotherapeutic agent doxorubicin to inhibit *in vitro* the growth of breast carcinoma cell lines (MCF-7).¹⁶⁶

By using a coumarin's containing sulfonamide moiety, I envisioned to synthesize a carbonic anhydrase inhibitor that could potentially improve both enzymatic inhibition and physical properties for CA inhibitors. I focused to synthesize compounds that target the cancer associated CA IX and XII and evaluated the anticancer activity of these compounds.

Chapter 2. Design, Synthesis and Antineoplastic Evaluation of Mitochondrial Complex II (Succinate Dehydrogenase) Inhibitors Derived from Atpenin A5

2.1. Introduction

In cancers, metabolic pathways have emerged as an appealing target for selective antineoplastic therapy.⁹ The metabolic pathways can provide a therapeutic advantage that can help overcome drug resistance, increase the specificity of drug delivery, enhance the potency and overcome the side effects of existing therapies.¹¹ Emerging evidence implicate the role of mitochondrial metabolism in tumor growth progression.^{18, 21} Mitochondrial complex II plays an essential role in mitochondrial metabolism, where it catalyzes the oxidation of succinate to fumarate in the tricarboxylic acid cycle, and the reduction of ubiquinone to ubiquinol in the electron transport chain (**Figure 2.1**). Inhibition of the ETC induces cell death through generation of reactive oxygen species.³³

There are several known CII inhibitors presented in the literature; however, most of them have low potency for this target and meager anticancer activity. Mitochondrially targeted vitamin E succinate (MitoVES, **1**) (**Figure 2.2**) has an IC₅₀ of 70 µM, which has lower potency for CII than the parent compound α-TOS.⁶⁵ However, MitoVES was found to be 20-50 times more effective in inducing apoptosis in cancer cells than α-TOS.⁶⁶ This efficacy is attributed to the introduction of a cationic triphenylphosphonium group which acts to target the compound to the mitochondria and provides enhanced antineoplastic properties. Inhibition of CII has been shown to be selective to cancerous cells with MitoVES possessing an IC₅₀ of 0.5-3 µM for apoptosis induction in cancer cells and approximately 20-60 µM for non-malignant cells.⁶⁶ Thenoyltrifluoroacetone (**2**), a widely employed control compound in CII assay kits has an IC₅₀ of 30 µM. There has been limited investigation of this compound as a CII inhibitor because of its highly toxic to non-

cancerous cells.⁶⁸ The clinical vasodilator diazoxide (**3**) inhibits CII which has an IC_{50} of 32 μ M.⁷⁶ Diazoxide is known to regulate ROS production and induce specific cancer cell death.⁷⁷

As described above, CII inhibitors are known to exhibit anticancer activity; however, these inhibitors show mediocre CII inhibition with IC_{50} values ranging from ~30-70 μ M. Almost all of these inhibitors are known to have alternative or complementary mechanisms to CII inhibition that may account for the observed anticancer activity. Reactive oxygen species induction is important for all the CII inhibitors with proven anticancer activity. However, the precise sequence of events leading up to and following ROS production are poorly understood. A potent CII inhibitor would be expected to elicit far greater anticancer efficacy and would be an excellent candidate for development as a chemotherapeutic agent, as a probe compound for further elucidation of this promising mechanism and further study of the role of mitochondria in cancer.

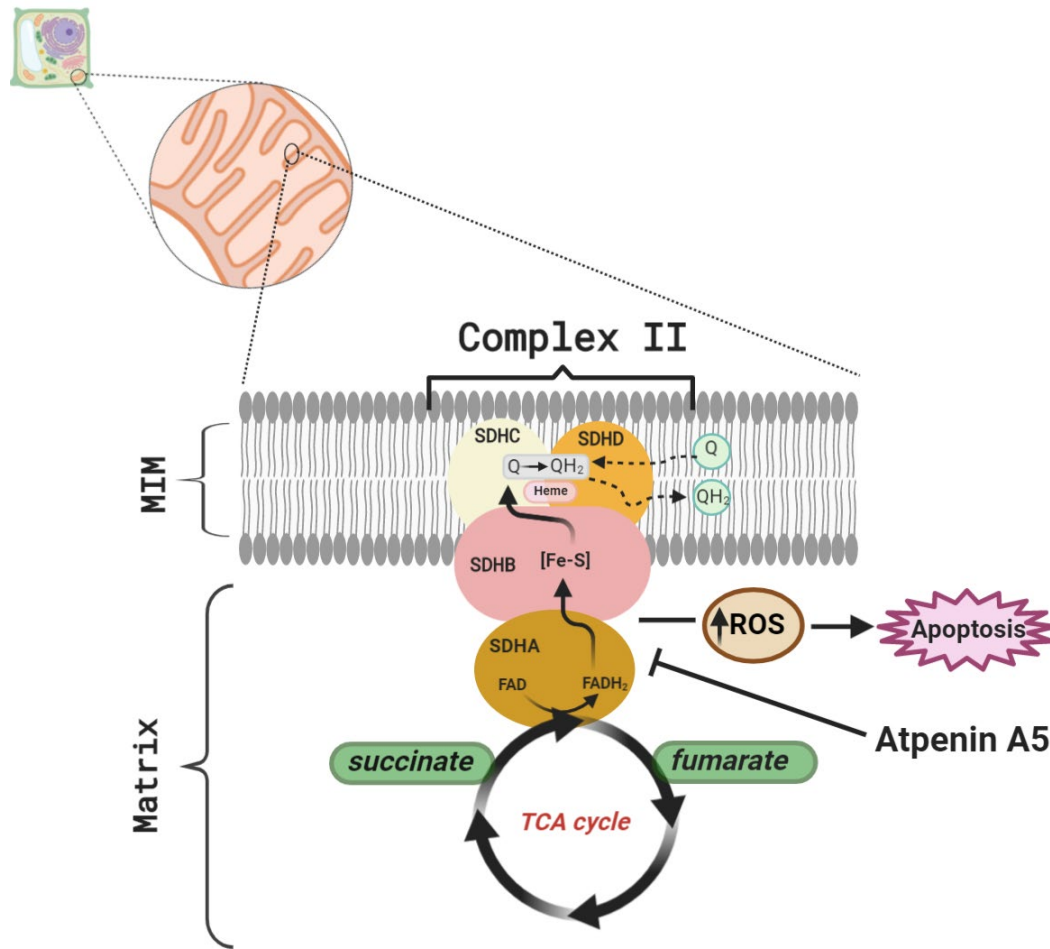


Figure 2.1. Mitochondria respiratory complex II; succinate dehydrogenase (SDH). It is a member of the respiratory chain and tricarboxylic acid cycle (TCA). It catalyzes the oxidation of succinate to fumarate in the TCA cycle and transports the electron generated by this oxidation to ubiquinone (Q) in the respiratory chain to ubiquinol (QH₂). Generally, mitochondria complex II consists of four subunits SDHA, B, C, D, and these subunits include redox-active coenzyme flavin adenine dinucleotide (FAD) and FADH₂, Iron–sulfur clusters (Fe-S).

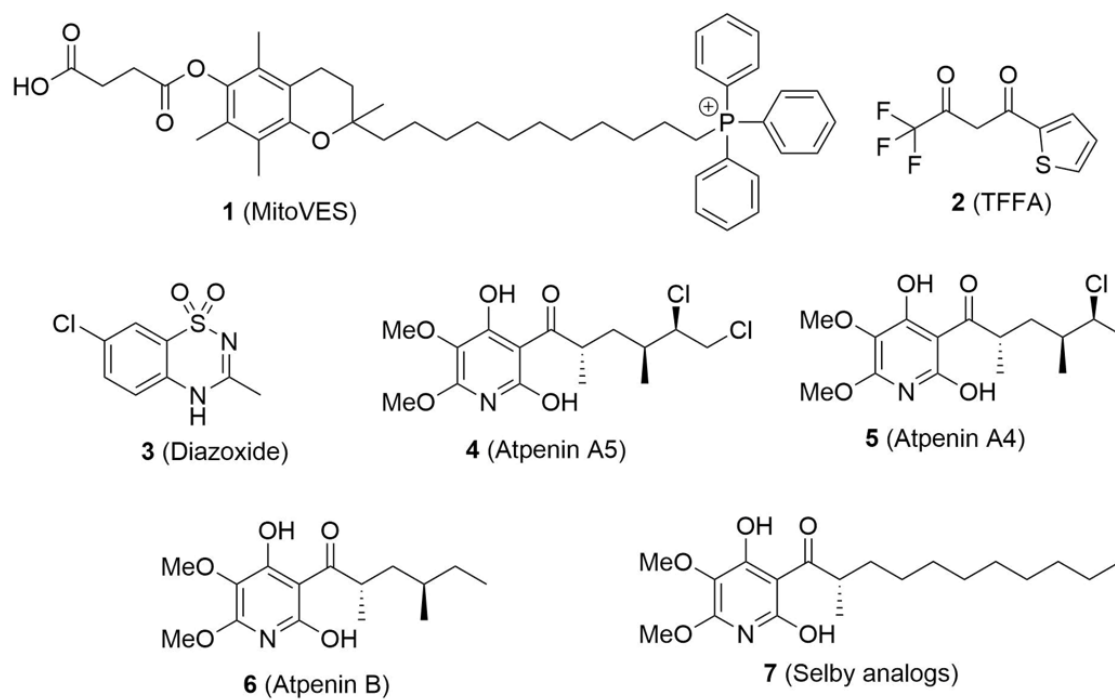


Figure 2.2. Structures of the interesting known mitochondria complex II inhibitors.

The potent and specific succinate-ubiquinone oxidoreductase inhibitor atpenin A5 (AA5, **4**, **Figure 2.2**) has an IC_{50} of 3.6-10 nM, and acts on the ubiquinone binding site (IIQ). It has traditionally been used as an antifungal. Atpenin A5 is known to be the most potent CII inhibitor to date.⁸⁹ Inhibition of CII by AA5 results in production of ROS (75% hydrogen peroxide and 25% superoxide).⁹⁰ Atpenin A4 (**5**), with two chlorine atoms on vicinal carbons in the side chain, has CII inhibition activity with an IC_{50} of 24 nM as compared to a mono chloro substituted AA5 which has an IC_{50} of 3.7 nM in rat liver mitochondria.⁸⁹ A recent report showed that the chloro methyl or methyl substituents in the atpenin side-chains have approximately similar biological activity which suggests that chloro methyl or methyl substituents can be used interchangeably as bioisosteres.¹⁶⁷ Atpenin A5 and its analogues have been reported to have antineoplastic activity by targeting the prostate stromal cells by reducing the expression of insulin-like growth factor-I in DU-145 prostate cancer cells.^{77, 91} However, atpenin B (**6**), a similar structure to atpenin A5 but without chlorine atoms on the hydrocarbon side chain, was found to have limited anticancer efficacy in *in vivo* studies attributable to poor absorption, distribution, metabolism and excretion (ADME) properties.⁹² In addition, atpenin B has been shown to inhibit ATP-generation. An atpenin A5 derivative (**7**), synthesized by Selby et al. as part of an antifungal library, showed bovine CII inhibition with an IC_{50} of 3 nM.¹⁶⁸ However, the compound retains a stereocenter on the side chain alpha to the ketone. This moiety is present in all the most active CII inhibitors described in the Selby library. Excision of the methyl group resulted in significant amelioration of CII inhibition, suggesting a pharmacophoric role and complicating the generation of synthetic derivatives. The inhibitory potency for CII and the observed anticancer effects in prostate cancer cell models make AA5 an excellent hit compound for further drug discovery efforts. However, its suitability as a chemotherapeutic or chemical probe is hindered by low abundance, complex structure leading to lower synthetic yields, 50-fold reduction in *in vivo* activity and

lack of structural diversity for better lead optimization. To the best of our knowledge, no studies have been reported that attempt to optimize the potency of atpenin A5 as a CII inhibitor and chemotherapeutic.

2.2. Results and Discussion

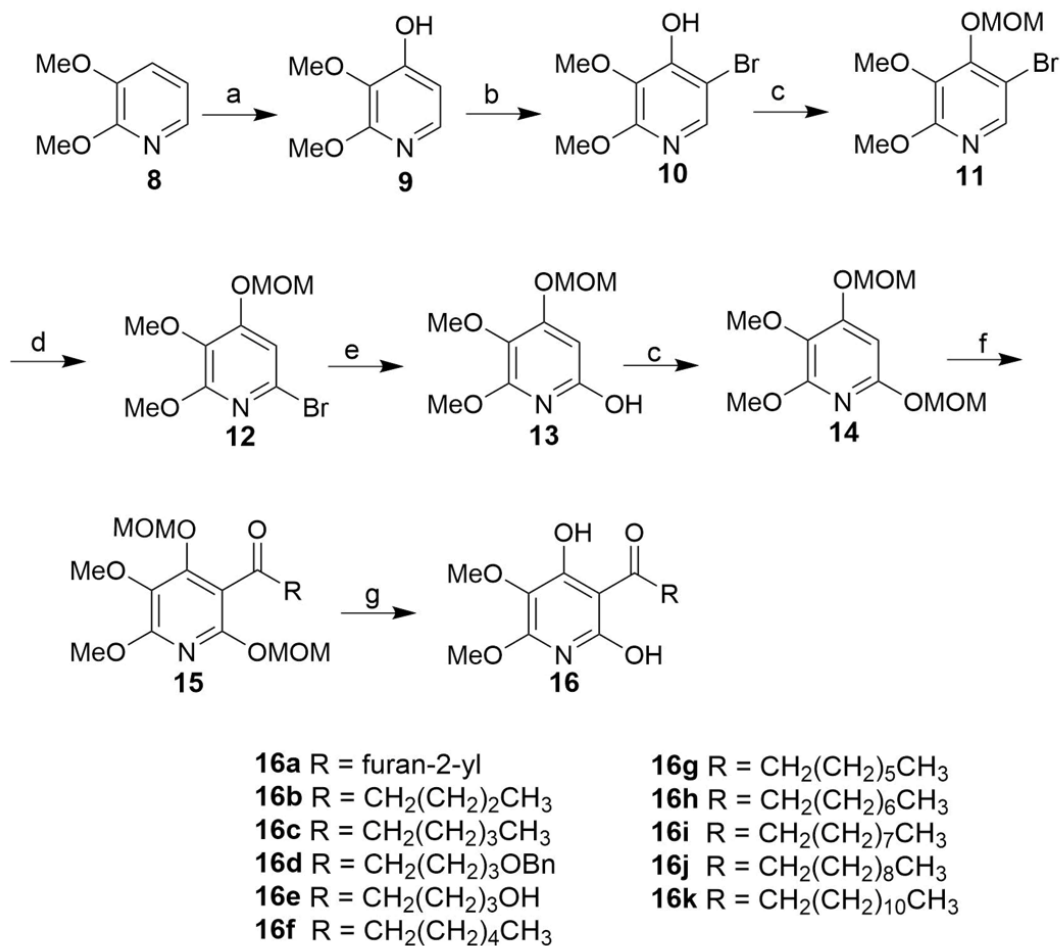
2.2.1 Chemistry

The known crystal structure of *E.coli* CII with AA5,¹⁶⁹ and porcine CII (PDB ID: 3AEE) indicates a role for the highly substituted pyridine ring in active site recognition and hence in our first series of designed analogues, this moiety remained unchanged. The hydrocarbon side chain of AA5 contains three stereocenters that hinder large scale preparation, similarly AA5 derivative **7** (**Figure 2.2**), while simplified, still contained a stereocenter alpha to the side chain ketone. Colleagues in the Trippier lab sought to simplify the side chain through the generation of unfunctionalized and non-chiral hydrocarbon chain derivatives.

To date several hydrocarbon side chain derivatives of atpenin A5 have been synthesized to determine CII inhibition activity as a mechanism of action to achieve antifungal activity. However, only one has shown enhanced activity. Three routes of total synthesis of the atpenin A5 scaffold and its derivatives have been reported in the literature to date from the groups of Omura,¹⁷⁰ Selby,¹⁶⁸ and Carreira¹⁶⁷ as well as one report of racemic atpenin B by Quéguiner et. al.¹⁷¹ Our synthetic route to access atpenin A5 derivatives for structure-activity relationship (SAR) study is based on modification of all four routes.

We started the synthesis with the commercially available 2,3-dimethoxypyridine (**8**) which was lithiated with ⁿButyl lithium (1.5 equivalents of base to overcome potential

chelation with the methoxy groups)¹⁷¹ and exposed to trimethylborate followed by oxidation with peracetic acid to provide 2,3-dimethoxy-4-hydroxypyridine (**9**) in moderate yield (**Scheme 2.1**). Regioselective addition of bromine was achieved at the 5-position by exposure to *N*-bromosuccinimide (NBS) and purification by column chromatography to afford 5-bromo-2,3-dimethoxypyridin-4-ol (**10**) as the major product in 83% yield. Subsequent protection of bromide (**10**) as the methoxymethyl ether (**11**) was achieved in excellent yield. Rearrangement of the bromine of pyridine **11** from the 5-position to the 6-position was accomplished by a 'halogen dance' reaction¹⁷² upon treatment with lithium diisopropylamide (LDA) and catalytic bromine provided the desired 6-bromo-2,3-dimethoxy-4-(methoxymethoxy)pyridine (**12**) in excellent yield. Metal-halogen exchange of bromide (**12**) with ⁿButyl lithium, critically with just one minute of stirring at -78 °C, followed by trapping with trimethylborate and subsequent oxidation with peracetic acid provided 5,6-dimethoxy-4-(methoxymethoxy) pyridin-2-ol (**13**) in moderate yield. Protection of the hydroxy functionality of **13** as the methoxymethyl ether afforded the critical intermediate 2,3-dimethoxy-4,6-bis(methoxymethoxy)pyridine (**14**) in excellent yield. Subsequent exposure of tetra-substituted pyridine (**14**) to ⁿButyl lithium and a suitably functionalized aldehyde provided the respective alcohol which was oxidized to the ketone with DMP to afford a series of MOM-protected atpenin A5 derivatives of type **15**. Deprotection of the MOM ether moieties by exposure to trifluoroacetic acid (TFA) resulted in a variety of hydrocarbon chain atpenin A5 derivatives (**16a-k**) in moderate to good yield.²³



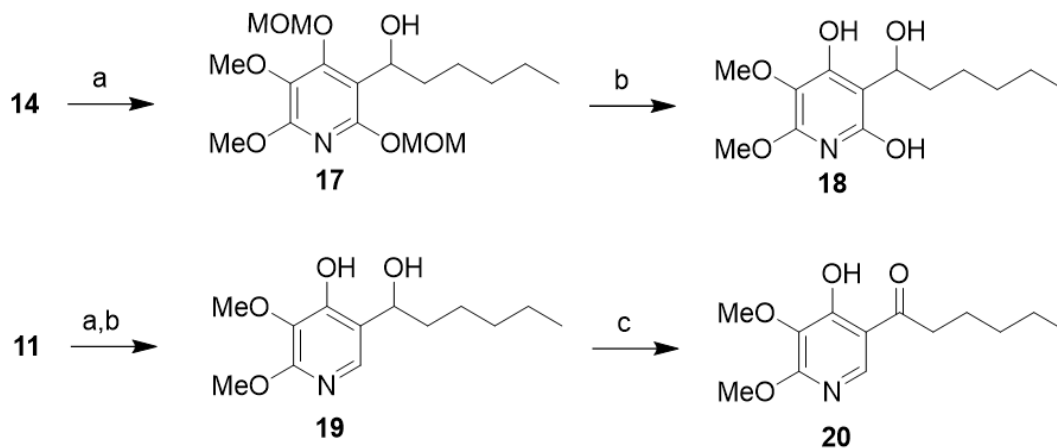
Scheme 2.1. Synthesis of hydrocarbon side chain derivatives of atpenin A5.

Reagents and Conditions: **a)** i) ⁿBuLi, THF, -78 °C, 1 h, ii) (MeO)₃B, -78 °C, 2 h, iii) MeCO₃H, RT, 1 h, 63% over three steps, **b)** NBS, MeCN, 0 °C, 12 h, 83%; **c)** NaOH, MOMCl, DMF, 1 h, 94%; **d)** i) LDA (3 equiv.) THF, -78 °C, 1 h, ii) Br₂ (cat.) -40 °C, 1 h, 89% over two steps ; **e)** i) ⁿBuLi, THF, -78 °C, 1 minute, ii) (MeO)₃B, -78 °C, 2 h, iii) MeCO₃H, 0 °C, 2 h, 63% over three steps; **f)** i) ⁿBuLi, RCHO, -78 °C, 1 h, ii) DMP, DCM, RT, 30 minutes, **g)** TFA, DCM, RT, 30 minutes.

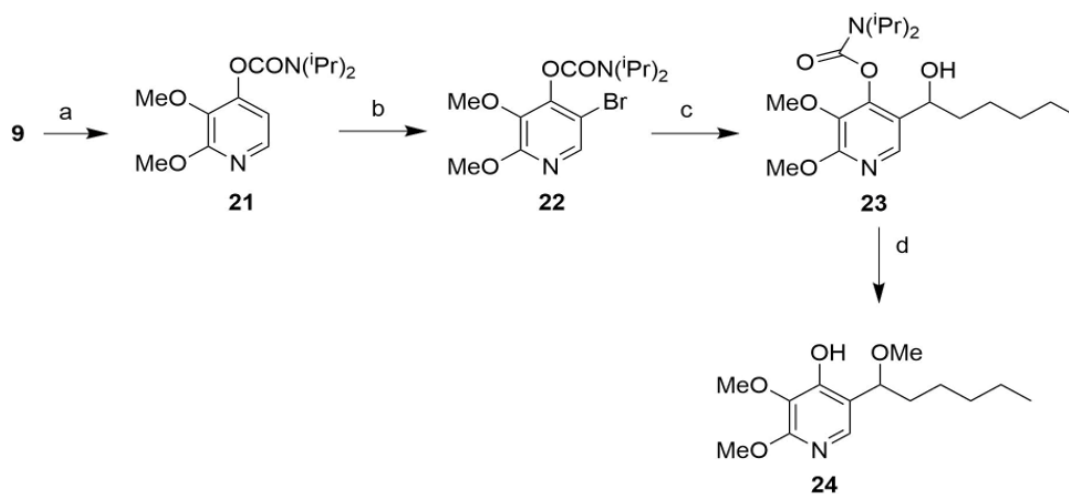
To determine the effect of the oxidation state of the first position of the hydrocarbon chain derivatives on complex II inhibition, we isolated triol (**18**) (**Scheme 2.4**) from the methoxymethyl ether intermediate (**17**) by omitting the oxidation step from our developed synthetic route.²³

Previous antifungal structure activity studies of atpenin A5 have focused solely on generating analogues of the hydrocarbon side chain with little or no focus on the pyridine ring system. Given the structural similarity between atpenin A5 and the natural complex II substrate Coenzyme Q₁₀ (ubiquinone), we hypothesized that the 2,3-dimethoxy and 4-hydroxy substituents on the atpenin A5 pyridine ring would be essential for CII binding site recognition. However, as the 6-hydroxy substituent of atpenin A5 is not present in ubiquinone we sought to determine the effects of removing this group. To this end colleagues in the Trippier lab synthesized the 6-hydroxy excised derivative (**20**) by direct addition of a suitably functionalized aldehyde to bromide intermediate (**11**), lacking the 6-hydroxy functionality (**Scheme 2.4**). This route provided diol intermediate (**19**) in good yield which was selectively oxidized with DMP to provide the desired 1-(4-hydroxy-5,6-dimethoxypyridin-3-yl)hexan-1-one (**20**) in moderate yield.²³

During the course of our investigation into the synthesis of atpenin A5 derivatives we partially adopted the route of Quéguiner et. al. to atpenin B.¹⁷¹ Protection of alcohol (**9**) as the *N,N*-diisopropyl carbamate (**21**) followed by addition of Br₂ provided access to bromide (**22**) in excellent yield (**Scheme 2.5**). Subsequent transmetallation and trapping with hexanal provide alcohol (**23**) in good overall yield. However, deprotection of the *N,N*-diisopropyl carbamate by exposure to methanolic potassium hydroxide in this system failed to yield the desired compound, with the respective methyl ether derivative (**24**) obtained in 50% yield.

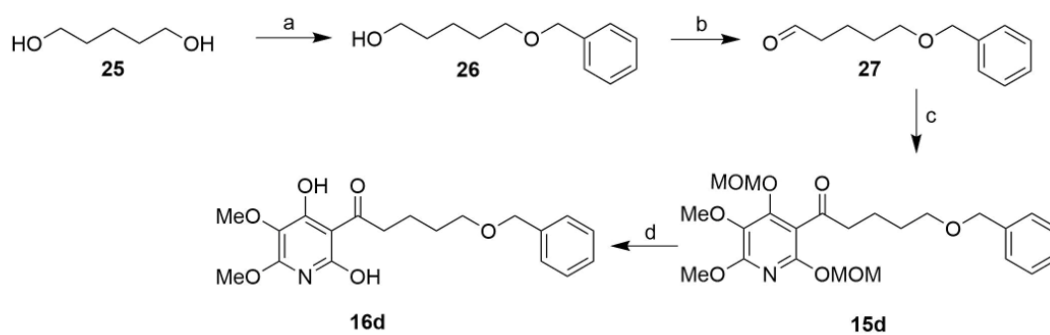


Scheme 2.2. Synthesis of oxidation state derivatives of atpenin A5. *Reagents and conditions:* **a)** $n\text{BuLi}$, hexanal, $-78\text{ }^{\circ}\text{C}$, 80%; **b)** TFA, CH_2Cl_2 , RT, 63%; **c)** DMP, CH_2Cl_2 , RT, 51%.

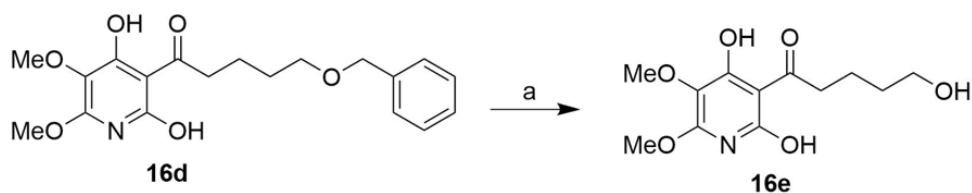


Scheme 2.3. Synthesis of a methyl ether derivative of atpenin A5. *Reagents and conditions:* **a)** Ag_2CO_3 , $(i\text{Pr})_2\text{NCOCl}$, toluene, $110\text{ }^{\circ}\text{C}$, 73%; **b)** Br_2 , CCl_4 , RT, 90%; **c)** $n\text{BuLi}$, hexanal, THF, $-78\text{ }^{\circ}\text{C}$, 84%; **d)** KOH, MeOH, $65\text{ }^{\circ}\text{C}$, 50%.

To synthesize the atpenin A5 derivative **16d** with the carbon side chain 5-benzyloxy pentyl, we started the synthesis with commercially available pentane-1,5-diol (**25**) which was reacted with benzyl bromide in the presence of sodium hydride to form 5-(benzyloxy)pentane-1-ol (**26**). The swern oxidation was used to convert **26** to 5-(benzyloxy)pentanal (**27**) in a good yield. After that, the **27** was reacted with the compound **14** to yield 6-(benzyloxy)-1-(5,6-dimethoxy-2,4-bis(methoxymethoxy)pyridin-3-yl)hexan-1-one (**15d**) which followed by of the MOM ether moieties by exposure to TFA to provide **16d** in moderate yield (**Scheme 2.4**). The 1-(2,4-dihydroxy-5,6-dimethoxypyridin-3-yl)-5-hydroxypentan-1-one (**16e**) was synthesized by hydration of **16d** using palladium on carbon and acetic acid under hydrogen (H₂) atmosphere (**Scheme 2.5**).



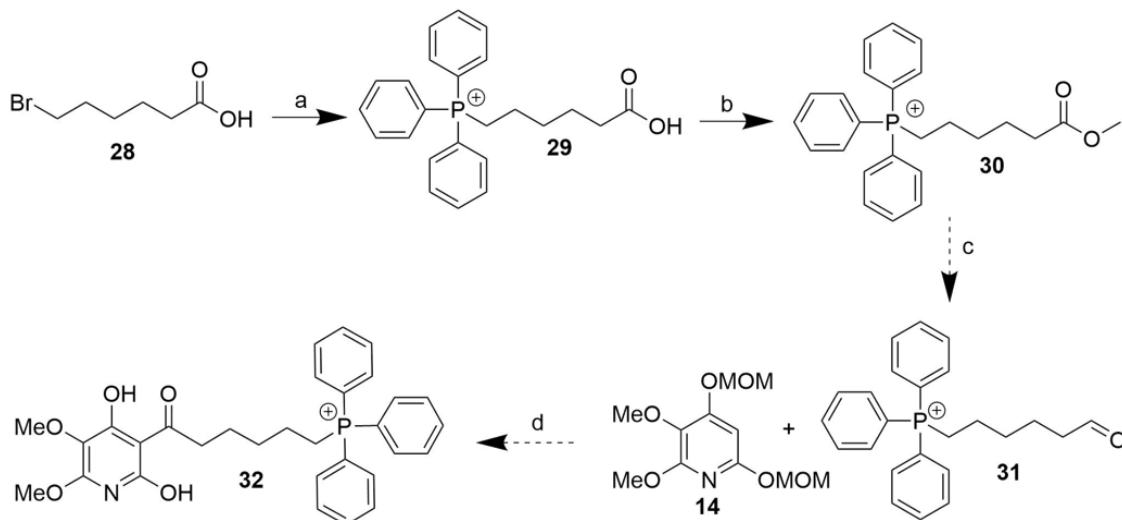
Scheme 2.4. Synthesis of atpenin A5 derivative 16d. *Reagents and Conditions:* **a)** NaH, benzyl bromide, THF, 70 °C, 12 h, 65%; **b)** i) (COCl)₂, DMSO, ii) Et₃N, CH₂Cl₂, -78 °C to RT; 83% **c)** **14**, BuLi, -78 °C, ii) DMP, CH₂Cl₂, RT, **d)** TFA, CH₂Cl₂, RT, 58%.



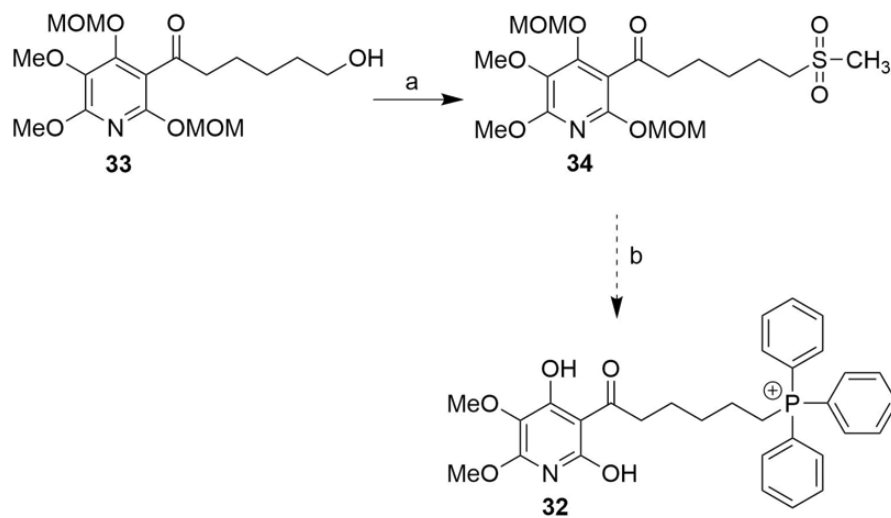
Scheme 2.5. Synthesis of atpenin A5 derivative 16e. *Reagents and Conditions:* **a)** Pd/c, MeOH, AcOH, RT under H₂, 12 h, 86%.

To achieve greater delivery to the mitochondria, we envision the appendage of a mitochondrial targeting TPP group to **16c**.¹⁷³ The first method was used to achieve **16c** with TPP in the terminal carbon by forming (6-oxohexyl)- triphenylphosphonium (**31**) followed by reaction with **14** to obtained the target compound. I started synthesis by treating the commercially available 6-bromohexanoic acid (**28**) with triphenylphosphine to afford the (5-carboxypentyl)triphenylphosphonium (**29**). Esterification of the carboxylic acid by exposure to H₂SO₄ with methanol to achieved (6-methoxy-6-oxohexyl) triphenylphosphonium (**30**). Afterward, partial reduction of an ester to an aldehyde using diisobutylaluminium hydride (DIBAL-H), but unfortunately, the TPP group lost because the instability for this group in the reduction reaction (**Scheme 2.6**). Also, the TPP group was lost after using the reduction agent lithium aluminum hydride (LiAlH₄).

Therefore, a new reaction method was established to achieve the target compound by starting with atpenin A5 derivative with terminal OH in the hydrocarbon side chain **33**. The terminal alcohol functions of the derivative were further activated with a leaving group (-OSO₂CH₃) to obtain **34**. The terminal group was afterward displaced via a nucleophilic substitution reaction with triphenylphosphine (TPP) to attain the triphenylphosphonium cations.¹⁷⁴ However, The TPP group was hydrolysis after deprotection of the MOM groups with TFA (**Scheme 2.7**). I hypothesize that the deprotection of two MOM groups with strong acid was an effect on the stability of the TPP on the compound. Therefore, another method was established to solve this issue. We learn from this adding the TPP group should be the last step in the reaction to avoid any alternative reaction.

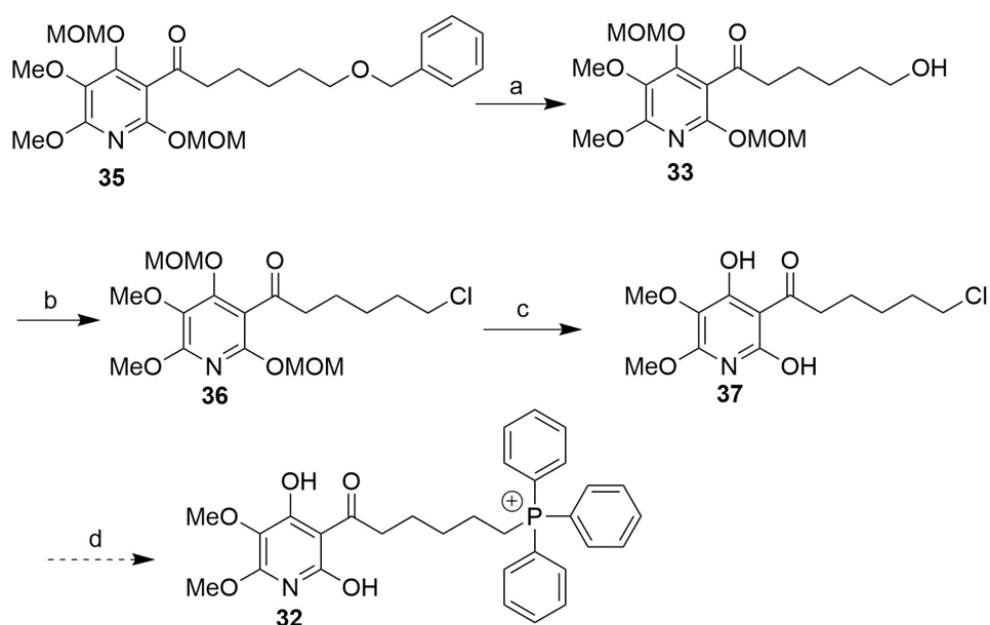


Scheme 2.6. The first method to synthesis of a triphenylphosphine derivative of atpenin **A5**. *Reagents and Conditions:* **a)** TPP, toluene, 110 °C, 4 h, 87%; **b)** H₂SO₄, MeOH, 65 °C, 12 h; **c)** DIBAL-H, Toluene, 0 °C, 2 h; **d)** i) ⁿBuLi, THF, -78 °C, ii) DMP, DCM, RT, iii) TFA, DCM, RT.



Scheme 2.7. The second method to synthesis of a triphenylphosphine derivative of atpenin **A5**. *Reagents and Conditions:* **a)** CH₃SO₂Cl, DCM, TEA, 0 °C, 30 min, RT, 2 h, 53%; **b)** i) TPP, toluene, 110 °C, 2 h. ii) TFA, DCM, RT, 30 mins.

Continuing to find an appropriate method to get the target compound, I started the synthesis with debenzylation of the **35** to effort the hydroxyl group in the terminal carbon **33** by using palladium on carbon under hydrogen (H₂) atmosphere. Afterwards, replacing the hydroxyl group in **33** to chloride was achieved by exposure to thionyl chloride to afford 6-chloro-1- (5,6-dimethoxy-2,4-bis(methoxymethoxy) pyridin-3-yl)hexan-1-one (**35**), followed by deprotection of MOM by trifluoroacetic acid to achieve 6-chloro-1-(2,4-dihydroxy-5,6-dimethoxypyridin-3-yl)hexan-1-one (**37**). The final step involves the addition of triphenylphosphine under reflux conditions in the presence of sodium iodide (NaI) to obtain (6-(2,4-dihydroxy-5,6-dimethoxypyridin-3-yl) -6 oxohexyl) triphenylphosphonium (**32**) as described in (**Scheme 2.8**).¹⁷⁵ I faced difficulty with the purification of the final compound (**32**); which I lost the compound after the silica column purification. Furthermore, another way was used to purify the product by adding zinc chloride to the product in acetone to form the complexes ZnCl(TPP),¹⁷⁶ which should allow the product to be crystallized. However, we still face the problem of the impurity of the product. Attempts to access the TPP-containing compound will continue.



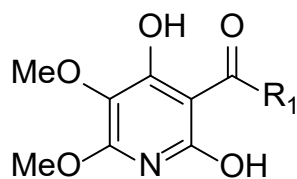
Scheme 2.8. The third method to synthesis of triphenylphosphine derivative of atpenin A5. *Reagents and Conditions:* **a)** Pd/C, MeOH, AcOH, H_2 , RT, 12 h, 86%; **b)** SOCl_2 , DCM, 75 °C, 1 h, 86%; **c)** TFA, DCM, RT, 30 mins, 69%; **d)** TPP, toluene, NaI, 110 °C, 2 h.

2.2.2. Complex II inhibition assay

Complex II activity was measured spectrophotometrically according to the literature method using isolated rat mitochondria,⁵⁴ based on the thenoyltrifluoroacetone-sensitive rate of succinate-driven, co-enzyme Q₂-linked reduction of dichlorophenolindophenol (DCPIP) which was performed by our collaborators at the University of Rochester Medical Center. Mitochondria are isolated from fresh rat hearts by differential centrifugation in sucrose-based buffer as described in the literature,^{177, 178} with suitable modifications to ensure rapid isolation.⁵⁴ The complex II inhibition activity of each newly synthesized atpenin A5 derivative is reported in **Tables 2.1** and **2.2**.

The CII inhibition of the control compounds atpenin A5 and diazoxide were reported to have IC₅₀ values of 3.6-10 nM^{89, 93} and 32 μM,⁷⁶ respectively. The inhibitory concentration value for CII of atpenin A5 was determined to follow in accordance with the literature value IC₅₀ of 3.3 ±2 nM (**Table 2.1**). The known crystal structure of complex II with atpenin A5 indicated a potential role for the highly substituted pyridine ring in active site recognition. Hence, in our first series of designed analogues, this moiety remained unchanged. The hydrocarbon side chain of atpenin A5 contains three stereocenters that hinder large scale preparation, naturally occurring analogues of atpenin A5 at the side chain are known to retain cytotoxic activity. We sought to simplify the side chain through the generation of simple unfunctionalized hydrocarbon chain derivatives. With the sole exception of the furan-2-yl moiety, all the synthesized side chain derivatives displayed CII inhibition activity ranging from 3.3 nM to 3.7 μM, all of which are more potent than any reported CII inhibitor except atpenin A5. Two of the most potent inhibitors ever, compounds **16j** and **16k** displayed CII inhibition with IC₅₀ of 8.6 ±2.9 nM and 3.3 ±2.4 nM respectively (**Table 2.1**). In order to compare CII activity in different sources of mitochondria, two known derivatives (**16b** and **16f**) that were also reported to have

antifungal activity were synthesized.¹⁶⁸ These derivatives in literature have bovine CII IC₅₀ values of 96 nM and 20 nM, respectively. In rat heart CII, activity is substantially attenuated with IC₅₀ of 346 nM and 282 nM, respectively, suggesting that compound **16k** described herein may represent the most potent CII inhibitor yet described.



Comp.	R_1	Mw	cLogP ^a	PSA ^b	LLE ^c	CII IC ₅₀ (nM) ^d
16a	2-furan	265.22	-0.02	102.02	n/a	0% ^e
16b	butyl	255.27	1.09	88.88	5.37	345.5 ±7.6
16c	pentyl	269.29	1.53	88.88	5.62	64.0 ±4.3
16d	5-OBn butyl	361.39	2.02	98.11	3.41	280.8 ±88.7
16e	5-hydroxybutyl	271.27	-0.35	109.11	6.90	3730.2 ±1021.1
16f	hexyl	283.32	1.98	88.88	4.57	282.4 ±135.5
16g	heptyl	297.35	2.42	88.88	4.89	49.1 ±22.1
16h	octyl	311.37	2.87	88.88	4.93	15.7 ± 3.5
16i	nonyl	325.40	3.31	88.88	4.69	9.9 ±1.9
16j	decyl	339.43	3.75	88.88	4.32	8.6 ±2.9
16k	dodecyl	367.48	4.64	88.88	3.76	3.3 ±2.4

AA5	n/a	366.24	2.64	88.88	5.36	3.3 ±2.0
DZX	n/a	230.67	1.0	58.53	1.85	32,000 ⁷⁶

^a Calculated by MarvinSketch 5.10.3.

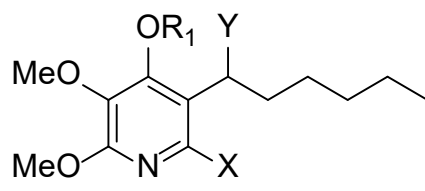
^b Polar Surface Area (PSA, pH = 7.4), calculated by MarvinSketch 5.10.3.

^c Ligand-Lipophilicity Efficiency (LLE = pIC₅₀-cLogP).

^d Mean value of four experiments.

^e 0% inhibition of CII at 100 nM.

Table 2.1. Complex II inhibition activity, cLogP, Mw, PSA and ligand lipophilic efficiency of atpenin A5 derivatives **16a-16k**.

								
Comp.	R ₁	X	Y	Mw	cLogP ^a	PSA ^b	LLE ^c	CII IC ₅₀ (nM) ^d
17	MOM	OMOM	OH	359.42	2.95	88.50	n/a	0% ^[e]
18	H	OH	OH	271.31	0.97	92.04	n/a	0% ^[e]
19	H	H	OH	255.31	2.24	71.81	n/a	0% ^[e]
20	H	H	O	253.29	2.97	68.65	n/a	0% ^[e]
24	H	H	OMe	269.34	2.88	60.81	n/a	0% ^[e]

^a Calculated by MarvinSketch 5.10.3

^b Polar Surface Area (pH = 7.4), calculated by MarvinSketch 5.10.3

^c Ligand-Lipophilicity Efficiency (LLE = pIC₅₀-cLogP)

^d Mean value of four experiments

^e 0% inhibition of CII at 100 nM.

Table 2.2. Complex II inhibition activity, cLogP, Mw, PSA and ligand lipophilic efficiency of atpenin A5 derivatives **17-24**.

Addition of an aromatic furan-2-yl moiety (**16a**) to the 5-position of the atpenin A5 pyridine ring side chain abrogates activity, with no inhibition of CII at 100 nM concentration. This may be due to the extended conjugated system present in the derivative. The enol tautomer would be expected to be inactive based on subsequent data that shows a pharmacophoric role for the keto functionality. Shortening the side chain to a simple butane chain provided a compound with an IC_{50} of 345.5 ± 7.6 nM and a 1.5-fold lower logP (1.09) (**16b**). Retaining the length of the natural atpenin A5 hydrocarbon chain but with no substituents resulted in compound **16c** which displays an IC_{50} of 64.0 ± 4.3 nM, lower lipophilicity, but identical PSA to **16b**. The ligand-lipophilicity efficiency (LLP) of **16c**, a measure of potency and lipophilicity, was calculated to be 5.62, the optimum value calculated across all of the derivatives herein. A LLE greater than 5 combined with a lipophilic cLogP is often considered desirable for a lead or clinical compound,¹⁷⁹ parameters of which compound **16c** meets, combined with significant potency.

Interestingly, retaining the length of the natural product side chain but replacing the terminal methyl with a benzyl ether (**16d**) reduced activity ($IC_{50} = 280.8 \pm 88.7$ nM) compared to AA5. Removal of the benzyl protecting group to provide alcohol (**16e**) further decreased activity with CII IC_{50} value of $3.7 \mu M$, but still provided a compound of 10-fold greater activity than diazoxide. This observation suggests the alcohol moiety of **16e** is not engaging in hydrogen bonding within the complex II protein given its lower potency compared with the identical side chain length derivative **16c**.

Addition of a methyl group to the pentane side chain of **16c** provided hexyl derivative **16f** which displayed equipotent activity with the benzyl ether derivative (**16d**) with an IC_{50} of 280.8 ± 88.7 nM, further suggesting that the oxygen of **16d** and **16e** is not involved in intermolecular interactions with CII. Again, a difference in activity between species of CII is observed, when derivative **16f** is assayed in bovine CII, an IC_{50} of 20 nM

is obtained.¹⁶⁸ This suggests that the CII inhibitors detailed herein may possess much greater activity when assayed in bovine CII.

Progressive homologation of the 5-position side chain from hexane to dodecane resulted in a progressive increase in CII inhibition, resulting in the identification of one compound (**16i**) which displays equipotent activity to atpenin A5 with an IC_{50} of 9.9 ± 1.9 nM and two compounds with greater potency: decane (**16j**) with an IC_{50} of 8.6 ± 2.9 nM and dodecane (**16k**) with an IC_{50} of 3.3 ± 2.4 nM. Homologation was stopped at the dodecane chain as this compound represents comparable molecular weight and PSA to the atpenin A5 natural product, albeit with increased logP. In general, increasing lipophilicity increases activity, a common phenomenon in medicinal chemistry. However, this pattern may not fully explain the observed activity in this series of compounds, as hexane derivative (**16f**) retains equipotency with terminal alcohol **16e** despite contrasting lipophilicity properties: cLogP and PSA of 1.98 and 88.88 for **16f** and -0.35 and 109.11 for **16e**. The length of the hydrocarbon chain is identical in both compounds and may excerpt a significant influence on CII inhibition activity. Additionally, compound **16e** does not fit this trend when transitioning from pentane (**16c**) to heptane (**16g**), wherein the activity of hexane side chain derivate **16e** displays significantly attenuated CII inhibition.

A similar trend is observed in the MitoVES (**4**) series of compounds (**Figure 2.2**) wherein shortening the alkyl chain results in progressive loss of complex II inhibition activity.⁶⁶ Penetration of the mitochondrial inner membrane to access the CII target is necessary for inhibitory activity, with lipophilicity a key determinant in this process along with cationic charge.¹⁸⁰ To achieve greater delivery to the mitochondria we envision the appendage of a mitochondrial targeting TPP group. The delocalized charge on the quaternary phosphorus atom is known to result in up to 1000-fold greater accumulation in the mitochondria.⁶⁷ However, an optimum hydrocarbon linker length between the activity

CII inhibitor 'warhead' and the TPP group has been shown to be essential to have activity.⁶⁶ This series of atpenin A5 derivatives provide significant foundation for further studies to append a mitochondria targeting delivery moiety.

Computational analysis of the crystal structure of the complex II quinone binding site with bound atpenin A5 predicts a pharmacophoric role for the highly substituted pyridine moiety, but no role for the 5-position carbonyl in intermolecular binding.¹⁶⁹ Colleagues in the Trippier lab next sought to generate bioisosteres of our atpenin A5 derivatives about the pyridine ring to confirm this model. The intermediate bismethoxymethyl protected hexanol derivative **17** does not inhibit complex II at 100 nM concentration, suggesting that both pyridine alcohols are required for intermolecular binding to the complex II quinone site, or alternatively, the additional steric bulk of the MOM groups preclude access of the compound to the CII binding site (**Table 2.2**). Interestingly, alcohol **18**, an oxidation state analogue of the active complex II inhibitor **16c** displayed no CII inhibition activity. The only structural difference between these compounds and thus the only difference between a 70 nM CII inhibitor and an inactive compound is the oxidation state of the alpha position of the pyridine 5-position hydrocarbon chain. A carbonyl at this position confers activity while an alcohol completely abrogates CII inhibition activity. Excision of the pyridine 6-position alcohol (**19**), a close structural analogue of compound **18** also resulted in an inactive compound. Oxidation of alcohol **19** to the respective carbonyl (**20**) and thus a direct bioisostere of **16c** wherein the pyridine 6-position alcohol is excised, displayed no CII inhibitory activity at 100 nM concentration. An alternative synthetic route to access hydrocarbon chain derivatives of atpenin A5 resulted in the isolation of the methyl ether substituted hydrocarbon chain compound **24**. This ether, like its alcohol counterpart, showed no activity to inhibit CII at

100 nM (**Table 2.2**). These collections of derivatives confirm the pharmacophoric role of the pyridine substituents in binding the quinone site of complex II.

Together these observations suggest a pharmacophoric role for the carbonyl of the side chain in the design of atpenin A5 derivatives. When replacement of the carbonyl with an alcohol or methyl ether is performed, CII inhibition activity is abrogated. While the possibility that the inactivity of these derivatives may indicate a failure of the compounds to penetrate into the mitochondria, analysis of their physicochemical properties disputes this hypothesis. Polar surface area values of **18** and **24** (71.81 and 60.81) calculated at pH 7.4 are significantly lower than active inhibitor **16c** and the atpenin A5 natural product (both 88.88) indicating lower lipophilicity, however they are higher than the active, albeit low potency, complex II inhibitor diazoxide (58.83). The cLogP values, a more direct measure of lipophilicity of **18** and **24** (2.24 and 2.88) are actually higher than the active and structurally similar inhibitor **16c** (1.53) and in the case of compound **24**, higher than the atpenin A5 scaffold (2.64) itself, although shape, size and charge requirements also play a role in mitochondrial penetration.

2.2.3. Molecular modeling

Enabled by the synthesis of a unique library of structural analogues of the hit compound (**Tables 2.1 and 2.2**), aimed at fully exploring the pharmacophore of atpenin A5 and its derivatives, it was evident that reduction of the side chain ketone to an alcohol or conversion to an ether results in complete amelioration of CII inhibition activity. A correction to the reported pharmacophore of atpenin A5 is thus proposed. Through detailed structure-activity relationship studies we have shown that the side chain ketone is critical for CII inhibition activity and thus forms part of the pharmacophore of this class of inhibitor. Quantitative structure-activity relationship prediction was employed to

understand the SAR of our compound series. The known crystal structure of AA5 bound in the ubiquinone binding site of porcine heart mitochondria complex II (PDB ID: 3AEE) provided the basis of our analysis. The AA5 binding site was defined and the ligand replaced with compounds **16c**, **18**, or **24** using SeeSAR 5.5 (BioSolveIT GmbH) performed by Dr. Trippier. Binding poses for each ligand were generated and scoring performed by HYDE.¹⁸¹

The active CII inhibitor **16c** is predicted to form hydrogen bonding between the pyridine 4-OH of **16c** to the amine of TrpB173 amino acid residue, between the 3-OMe and the hydroxyl moiety of TyrD91, between the pyridine nitrogen (amine tautomer) and SerC42 and between the pyridine 6-OH and the hydroxy moiety of MetC39 (**Figure 2.3A**). This is in agreement with the observed inactivity of the 6-OH excised or protected analogues **17**, **19**, **20** and **24**. These predicted active site interactions match those obtained from the crystal structure of atpenin A5 with porcine heart complex II,¹⁶⁹ when **16c** is overlaid with atpenin A (**Figure 2.3B**).

Modelling of the inactive alcohol derivative **18** into the complex II active site shows a significant change of binding pose, which is sufficient to prevent formation of, or reduce the strength of, hydrogen bonds between the pyridine 3-OMe and TyrD91 and between the pyridine 6-OH and MetC39. The 6-OH hydrogen is predicted instead to partake in intramolecular hydrogen bonding to the side chain alcohol, forming a thermodynamically stable six-membered ring (**Figure 2.3C**). The methyl ether derivative **24** also suffers a significant change in binding pose sufficient to reduce the predicted strength of the hydrogen bond between the pyridine 3-OMe and TyrD91 and to preclude hydrogen bond formation between the pyridine 6-OH and MetC39, instead of forming an intramolecular hydrogen bond between the 6-OH and the methyl ether oxygen atom on the C5-position chain resulting in a stable six-membered ring (**Figure 2.3D**).

The QSAR ligand-protein interaction predictions show excellent correlation with the determined SAR. The molecular modelling studies and SAR data reveal a pharmacophoric role for the side chain ketone moiety, not as might be expected by participating in hydrogen bonding to complex II binding site residues, but by conferring an optimal binding pose to active inhibitors. Indeed, in all three compound interaction models (**16c**, **18** and **24**, **Figure 2.3**) and in the original crystal structure of AA5 bound with porcine heart mitochondria CII, the ketone oxygen is not predicted to be involved in intermolecular hydrogen bonding. Excision of the carbonyl moiety leads to conformational changes that reduces distance between hydrogen bond donors and receptors and lead to suboptimal bonding angles, thus either preventing formation of hydrogen bonds between ligands and complex II amino acid residues or significantly reducing their strength resulting in inactive complex II inhibitors.

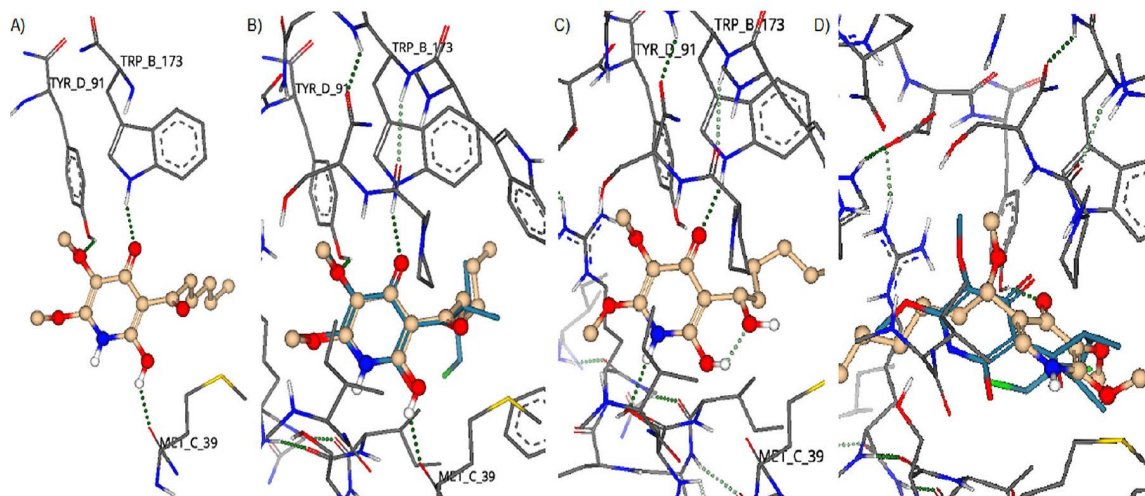


Figure 2.3. Modelling of atpenin A5 and selected derivatives in the ubiquinone binding site of porcine heart complex II (PDB ID: 3AEE); **A)** Hypothetical binding interactions of CII inhibitor **16c**. **B)** Overlay of AA5 (**7**) (turquoise) and **16c** (gold) in the active site of porcine heart mitochondria complex II. **C)** Hypothetical binding interactions of inactive compound **18**. **D)** Hypothetical binding interactions of inactive compound **24** (gold), overlaid with AA5 (**7**) (turquoise). Red: oxygen, blue: nitrogen, white: hydrogen, gold: carbon. Green dotted lines represent hydrogen bonds (greater opacity represents a stronger bond).

2.2.4. Cytotoxicity assay

Atpenin A5 derivative **16c** was taken forward for cytotoxicity evaluation to provide proof-of-concept that CII inhibition by compounds of this structural scaffold provide antineoplastic effect. This derivative was chosen for further study due to its high structural resemblance to natural atpenin A5; the same hydrocarbon chain length, same PSA, yet lower lipophilicity engendering greater solubility, structural simplicity thus high yields of synthetic material and favorable LLE value (5.62), combined with high CII inhibition potency ($IC_{50} = 64.0 \text{ nM}$, $17.23 \times 10^{-3} \text{ } \mu\text{g/mL}$). Four human prostate cancer cell lines and HEK293 cells were exposed to compound **16c** and cytotoxicity was measured by (3-(4,5-dimethylthiazol-2-yl)-5-(3-carboxymethoxyphenyl)-2-(4-sulfophenyl)-2H-tetrazolium) (MTS) assay after 48 hours (**Figure 2.4**).

Treatment of DU-145 prostate cancer cells with CII inhibitor **16c** provided a great significant inhibitory effect on cell growth in a dose-dependent manner, resulting in an IC_{50} of $13 \text{ } \mu\text{g/mL}$ (**Figure 2.4A**). Also, with the exposure of the CII inhibitor **16c** to PC3 prostate cancer cells, a much lower inhibitory effect was observed, resulting in an IC_{50} of $55 \text{ } \mu\text{g/mL}$ (**Figure 2.4B**). In 22Rv1 prostate cancer cells, inhibitor **16c** demonstrated an IC_{50} of $11 \text{ } \mu\text{g/mL}$ (**Figure 2.4C**). Also, In LNCap prostate cancer cells, inhibitor **16c** exhibited an IC_{50} of $8.8 \text{ } \mu\text{g/mL}$ (**Figure 2.4D**). The variation in the cytotoxicity results between the prostate cancer cell lines refers to the stage of the metastatic potential, in which the PC3 cells have high metastatic potential compared to the other cells, whereas DU145 cells have a moderate metastatic potential, and LNCaP and 22Rv1 cells have low metastatic potential.¹⁸² On the other hand, selectivity to cancerous cells over low tumorigenic cells, was confirmed by the use of human embryonic kidney cells (HEK293) where **16c** demonstrated an IC_{50} of $71 \text{ } \mu\text{g/mL}$, an approximate 7-fold selectivity for DU-145, 22Rv1 and LNCap prostate cancer cells over this transformed cell line (**Figure 2.4E**). The inactive

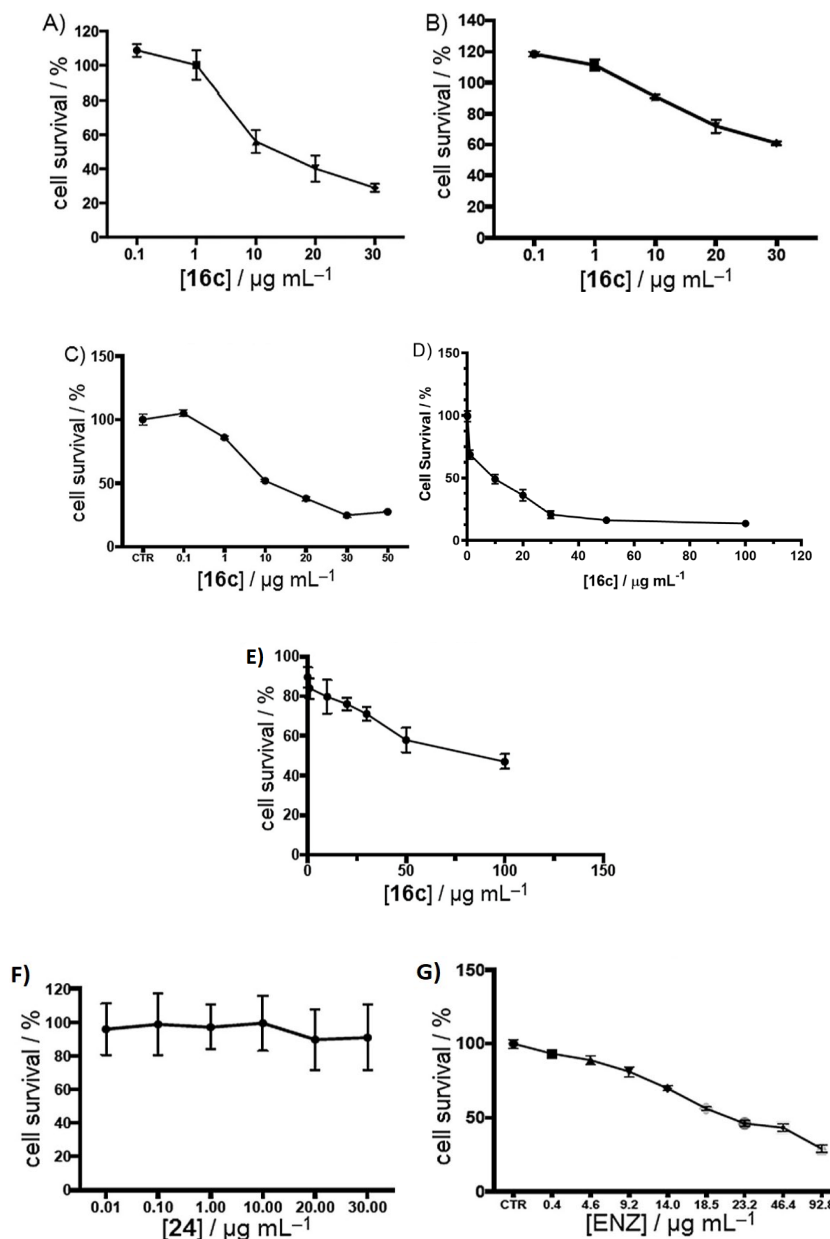


Figure 2.4. Complex II inhibitors are potent antiproliferative agents. Dose–response curves of the effect of complex II inhibitor **16c** (48 h treatment) on the cell viability of: **A)** DU-145 prostate cancer cells, **B)** PC3 prostate cancer cells, **C)** 22Rv1 prostate cancer cells, **D)** LNCap prostate cancer cells, and **E)** low tumorigenic HEK293 cells. **F)** Dose–response curve of the effect of structurally similar but inactive complex II inhibitor **24** on the viability of DU-145 prostate cancer cells. **G)** Dose–response curve of the effect of the clinical chemotherapeutic enzalutamide (ENZ) on the viability of 22Rv1 prostate cancer cells after 72 hours incubation. Values are the mean \pm SD of triplicate experiments.

control compound **24** displayed no growth inhibition effect upon treatment of DU-145 cells up to 30 $\mu\text{g/mL}$ (**Figure 2.4F**), implicating CII inhibition as a primary mechanism of action to inhibit prostate cancer cell growth. The clinically available prostate cancer drug enzalutamide (ENZ) displayed an IC_{50} of 29 $\mu\text{g/mL}$ after 72 hours treatment in 22Rv1 prostate cancer cells (**Figure 2.4G**), a cell line known to be resistant to this chemotherapeutic agent.¹⁸³ CII inhibitor **16c** displayed an IC_{50} of 11 $\mu\text{g/mL}$ after just 48 hours, which our compound **16c** exhibited 3-fold potency than clinically available prostate cancer drug enzalutamide. This observed cytotoxicity, along with that of CII inhibitor **16k** (**Figure 2.5**), suggests that CII inhibition may be a novel target for the treatment of advanced drug-resistant prostate cancer.

Further, when the more potent CII inhibitor **16k** ($\text{IC}_{50} = 3.3 \text{ nM}$, $1.21 \times 10^{-3} \mu\text{g/mL}$) was exposed to 22Rv1 prostate cancer cells, an even greater reduction of cell viability was observed with an IC_{50} of just 2 $\mu\text{g/mL}$ (**Figure 2.5A**). This shows that CII inhibition potency is directly proportional to antiproliferative effect. However, maximal cytotoxicity is reached at 10 $\mu\text{g/mL}$, beyond which a plateau is observed. Selectivity over the low tumorigenic HEK 293 cell line was again observed with **16k** providing an IC_{50} of 28 $\mu\text{g/mL}$, conferring 14-fold selectivity (**Figure 2.5B**). A summary of the IC_{50} values for compounds **16c** and **16k** across prostate cancer cell lines and HEK293 cells compared with enzalutamide positive control is depicted in **Table 2.3**.

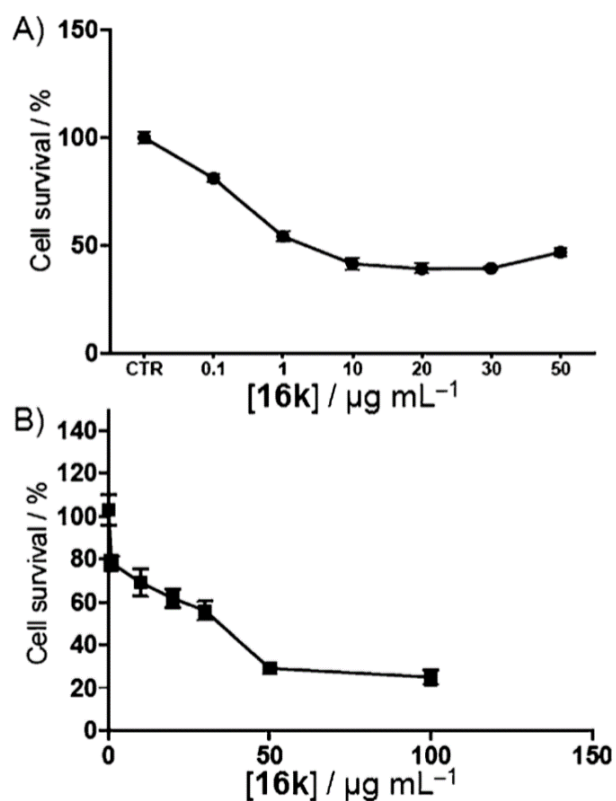


Figure 2.5. Complex II inhibitors with greater potency convey greater cytotoxicity.

Dose–response curves of the effect of complex II inhibitor **16k** (48-hour treatment) on the cell viability of **A)** 22Rv1 prostate cancer cells and **B)** low tumorigenic HEK293 cells.

Values are the mean \pm SD of triplicate experiments.

Compound	CII IC ₅₀ (nM) ^a	IC ₅₀ [μg mL ⁻¹] ^b				
		DU-145	PC3	22Rv1	LNCap	HEK293
16c	64.0 ±4.3	13.0 ±1.6	55.2 ±9.4	11.4 ±1	8.8 ±1.8	70.5 ±5.2
16k	3.3 ±2.4	N.D. ^c	N.D.	2.1 ±0.5	N.D.	28.1 ±2.0
24	0% ^d	>30 ^e	N.D.	N.D.	N.D.	N.D.
Enzalutamide	N.D.	N.D.	N.D.	29.3 ±2.4	N.D.	N.D.

^aMean value of four experiments

^bValues are the mean ±SD of n = 3 experiments.

^cNot determined.

^d0% inhibition of CII at 100 nM.

^eNo cell death at 30 mg mL⁻¹.

Table 2.3. Activity of CII inhibitors **16c** and **16k**, the inactive control **24**, and the clinical chemotherapeutic enzalutamide across a panel of human prostate cancer cells and low tumorigenic human endothelial kidney cells.

Treatment of prostate stromal cells (WPMY-1) with CII inhibitors **16c** and **16k** provided a significant inhibitory effect on cell growth in a dose-dependent manner, resulting in an IC_{50} of $18.06 \pm 2.5 \mu\text{g/mL}$ and $13.47 \pm 2.2 \mu\text{g/mL}$, respectively, after 48 h (**Figure 2.6 A,C**). Also, treatment of NIH 3t3 mouse fibroblast cell line with CII inhibitor **16c** provided a significant inhibitory effect on cell growth in a dose-dependent manner, resulting in an IC_{50} of $35.4 \pm 3 \mu\text{g/mL}$ after 48 h (**Figure 2.6 B**). The tumor-stromal interaction is a developing area of interest for anticancer therapeutics. Reactive stromal cells such as WPMY-1 cells assist the metastatic process through extensive cross-talk in the tumor microenvironment.¹⁸⁴ Targeting the selective death of both cancer cells and reactive stromal cells may be a novel therapeutic strategy with significant benefit to patients.

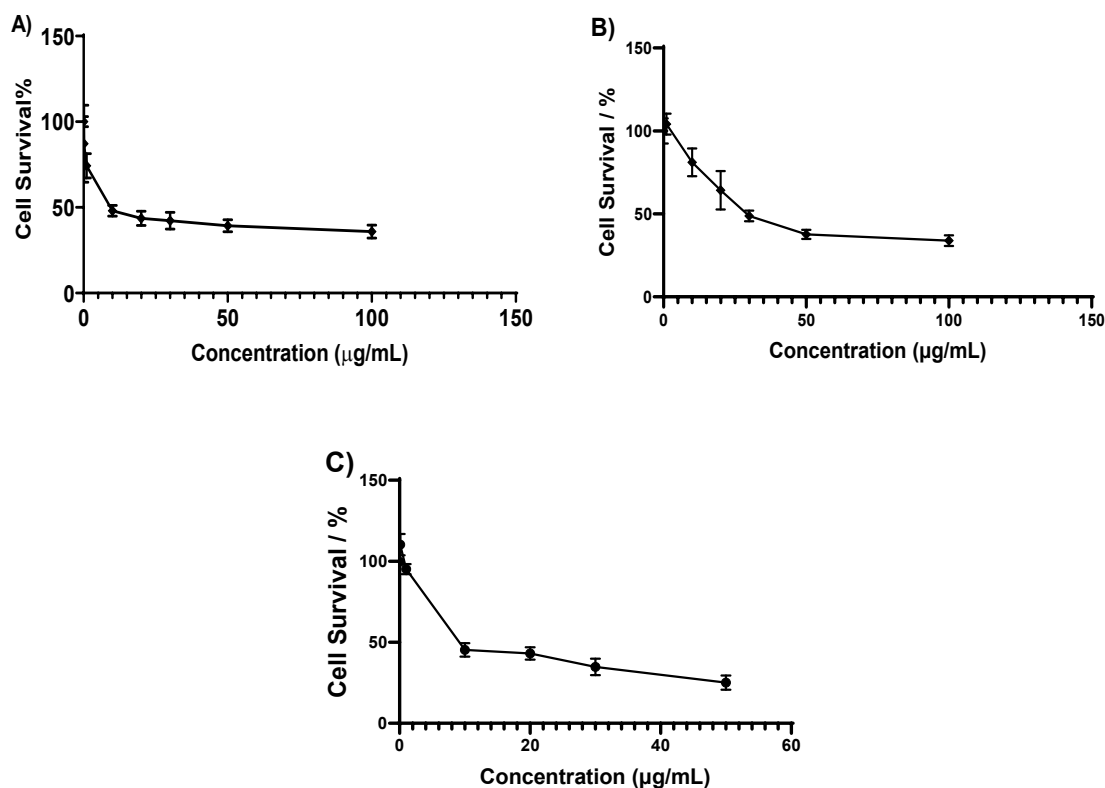


Figure 2.6. Inhibition of the stromal cell by complex II inhibitor 16c and 16k. **A)** Dose–response curves of the effect of complex II inhibitor **16c** (48 h treatment) on the cell viability of WPMY-1 A human prostatic stromal myofibroblast cell line. **B)** Dose–response curves of the effect of complex II inhibitor **16c** (48 h treatment) on the cell viability of NIH 3T3 mouse fibroblast cell line. **C)** Dose–response curves of the effect of complex II inhibitor **16k** (48 h treatment) on the cell viability of WPMY-1 A human prostatic stromal myofibroblast cell line. Values are the mean \pm SD of triplicate experiments.

To determine if our synthetic CII inhibitors retain the selectivity of the parent compound for CII over other constituent members of the electron transport chain, our collaborators at the University of Rochester Medical Center assayed **16c** and **16K** for mitochondrial complex I (CI) inhibition activity. Both compounds were found to be inactive up to 10 μ M leading to a selectivity ratio for CII:CI of >156-fold for **16c** and >3030-fold for **16k** (**Table 2.4**). This data highlights these compounds as promising chemical probes for further interrogation of the NADH-fumarate reductase system, specifically targeting complex II.

To understand the stability of the atpenin A5 derivatives our collaborators at the University of Texas Southwestern Medical Center carried out metabolic stability studies. The mitochondria complex II inhibitor AA5 derivative **16c** was subjected to incubation with mouse liver S9 fractions in the presence of NADPH (NADPH regenerating system) co-factors at 6 different time points between 0-240 min. Aliquots were taken from various fractions and analyzed by LC-MS at various time points. The atpenin A5 derivative **16c** displayed remarkable stability and half-life of > 190 min (**Figure 2.7**).

Compound	IC ₅₀ (nM) ^a		Selectivity Ratio
	Complex II	Complex I	CII:CI
16c	64 ±4.3	> 10000	> 156
16k	3.3 ±2.4	> 10000	> 3030
AA5	3.3 ±2.0	> 10000	> 3030

^a Values are the mean ± SD of n = 3 experiments

Table 2.4. Selectivity of compounds **16c**, **16k**, and AA5 for the inhibition of mitochondrial complex II over complex I.

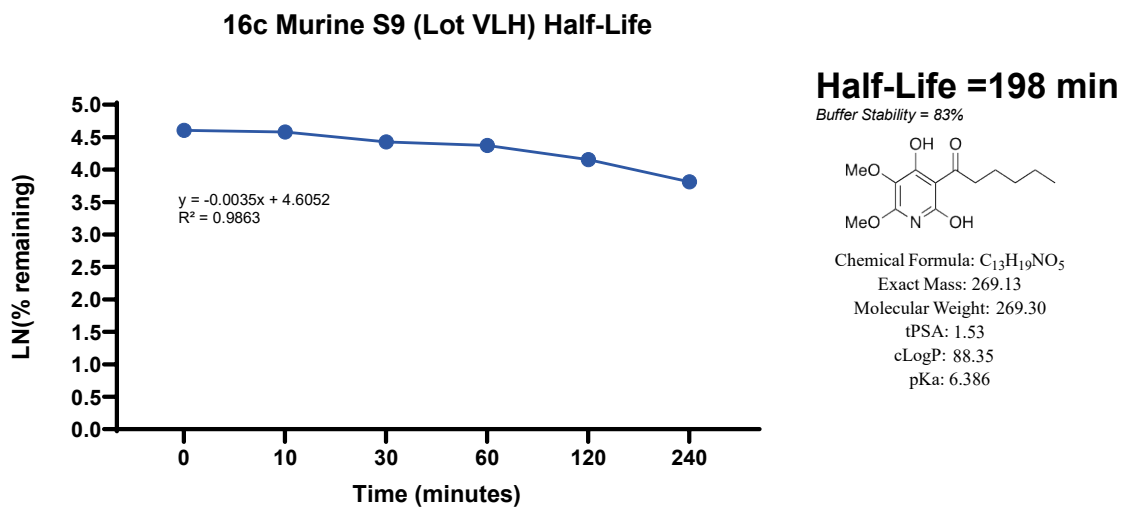


Figure 2.7. Metabolic stability of atpenin A5 derivative **16c**. Half-life **16c** upon incubation with Murine S9 liver fractions.

A recent report identified atpenin A5 as an active hit in a screen for the identification of compounds that target cells in dormant tumor spheroid regions.¹⁸⁵ Cancer cells in poorly vascularized tumor regions react to diminished nutrients by stopping cell cycle progression and becoming dormant. Hence those cells in hypoxic regions of the tumor are usually dormant and more likely to be resistant to chemotherapeutics. As cytostatic drugs target proliferating cells, dormancy is a major resistance mechanism to these antineoplastics.¹⁸⁶ Small molecules that target cancer cells in poorly vascularized (hypoxic) regions have the potential to enhance cytotoxicity and reduce resistance mechanisms.¹⁸⁷

Utilizing a microfluidic culture system,¹⁸⁸ our collaborators at Texas Tech University exposed PC3 prostate cancer cells under hypoxic conditions to the clinical chemotherapeutic drug etoposide,¹⁸⁹ CII inhibitor **16c** and inactive control **18** (**Figure 2.8**). As expected, the inactive compound **18** demonstrated no cytotoxic effect at 1 μ M and no effect at 10 μ M concentration within experimental error, further supporting the antineoplastic role of the CII inhibition mechanism. Complex II inhibitor **16c** provided 12% cell death at 1 μ M concentration and 20% cell death at 10 μ M concentration. On the other hand, etoposide is known to have poor cytotoxicity in hypoxic environments,¹⁸⁹ displaying only 7% cell death at 10 μ M concentration in hypoxic assay. Our designed CII inhibitor (**16c**), at 10-fold lower concentration (1 μ M), provides superior cytotoxicity in PC3 cells under hypoxia than the clinical chemotherapeutic drug etoposide. This data suggests that CII inhibition provides a potential mechanism for targeting cytotoxicity to dormant tumor cells and may be able to counter this resistance mechanism of tumor cells.

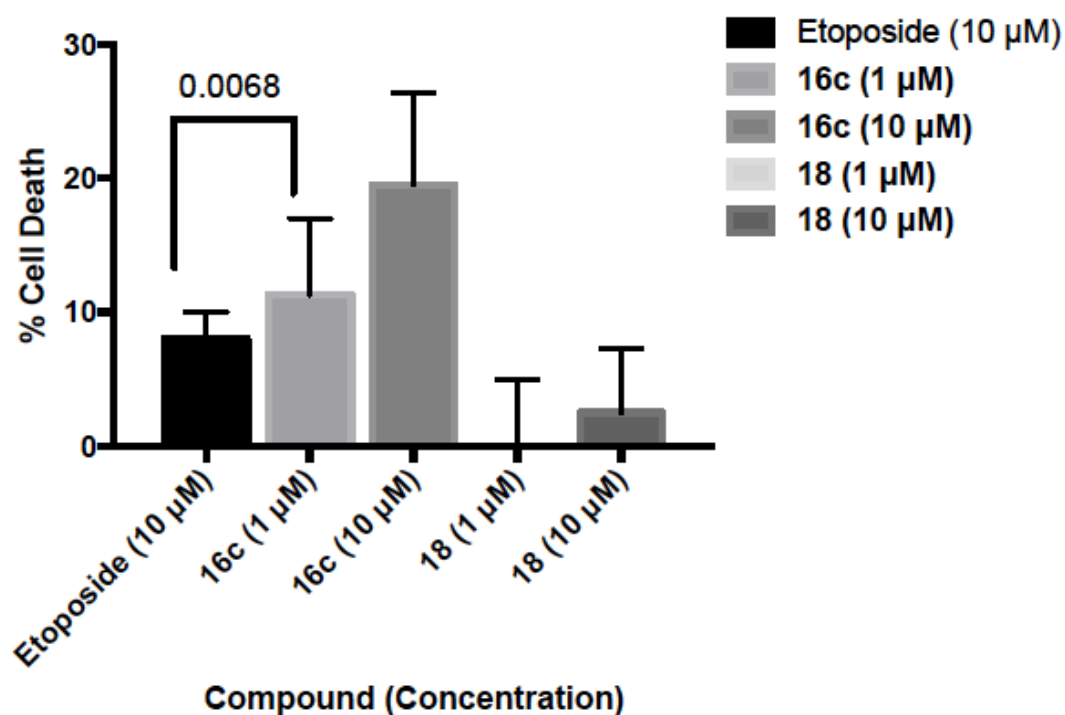


Figure 2.8. Cytotoxic effect of the clinical chemotherapeutic etoposide, complex II inhibitor 16c and inactive control 18 in PC3 prostate cancer cells under hypoxia. Cell death was measured with Annexin V and Sytox Green. Values are the mean \pm SD for triplicate experiments. A one-way ANOVA analysis was used to compare statistical difference between etoposide and **16c** at 1 μ M concentrations, * $p = 0.0068$.

We next sought to determine the effect of complex II inhibition by our developed inhibitors on mitochondrial metabolic processes. The effect of **16c** on electron transport parameters of 22Rv1 cells after 48-hour incubation was studied using a Seahorse XF Extracellular Flux Analyzer. The oxygen consumption rate of 22Rv1 cells is substantially reduced in a dose-dependent manner upon exposure to **16c** (**Figure 2.9A**). Mitochondria complex II inhibitor **16c** significantly inhibited mitochondrial function in 22Rv1 prostate cancer cells in a dose-dependent manner, including reducing basal respiration (**Figure 2.9B**), inhibition of ATP production (**Figure 2.9C**) and reduction of maximal respiration (**Figure 2.9D**) compared with no treatment control. This suggests the CII inhibitor **16c** targeting mitochondrial metabolism in cancer cells and may have the potential for the treatment of this disease.

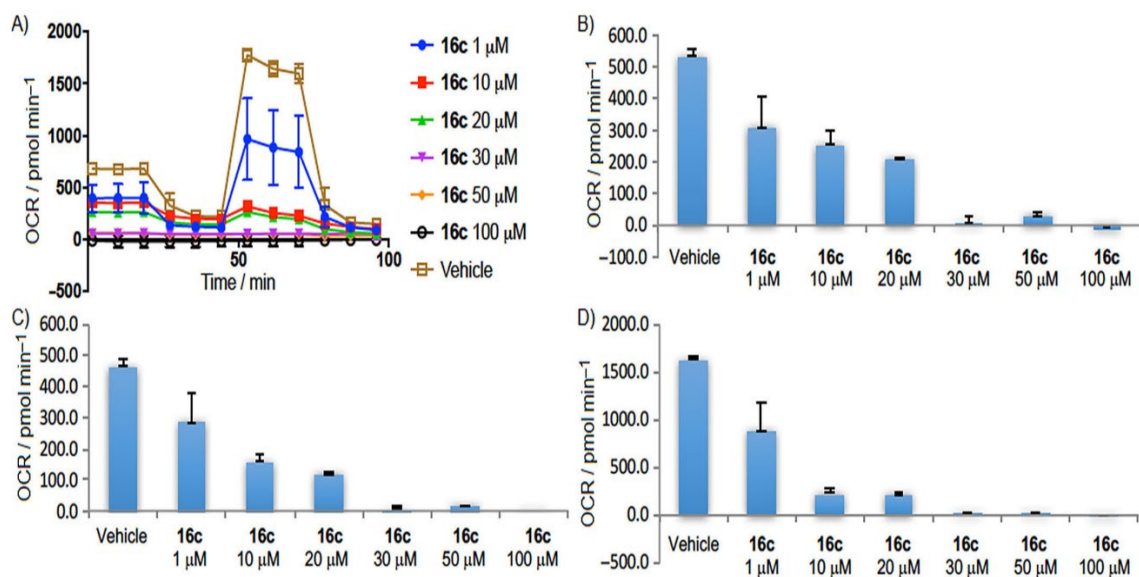


Figure 2.9. Complex II inhibitor 16c blocks mitochondrial respiration and function in 22Rv1 prostate cancer cells. **A)** Oxygen consumption rate (OCR), **B)** basal respiration, **C)** ATP production, and **D)** maximal respiration are decreased in a dose-dependent manner. Error bars: mean \pm SD, $n = 3$.

2.3.Conclusions

We disclose the design, synthesis, and evaluation of ten highly potent CII inhibitors, the most potent CII inhibitors disclosed to date. Modelling studies reveal the role of the side chain carbonyl functionality to ensure a bioactive conformation of the inhibitor within CII. Thus, expansion of the pharmacophore of the atpenin A5 natural product to include the functionalized pyridine ring and side chain carbonyl is proposed. Analysis of physicochemical properties indicated compound **16c** as the most 'drug-like' molecule for further study, while the potency of **16c** is reduced (CII IC₅₀ = 64 nM) over **16k** (CII IC₅₀ = 3.3 nM) the ligand-lipophilicity efficiency of **16c** is the most optimal of the CII inhibitors synthesized and represents far greater potency than existing inhibitors. The CII inhibitors **16c** has low clearance, a half-life of >3 hours, and >150-fold selective towards CII over mitochondrial complex I.

Significant antiproliferative activity was demonstrated by **16c** in DU-145 and 22Rv1 human prostate cancer cell lines. This effect was shown to be selective to cancer cells with a 7.4-fold greater antiproliferative activity over low tumorigenic human embryonic kidney cells for **16c** which increased to 17.5-fold for the highly potent CII inhibitor **16k**. Both compounds showed superior antiproliferative activity to the clinical chemotherapeutic enzalutamide. Further, this effect is retained under hypoxic conditions providing greater than double the antiproliferative activity of the clinical chemotherapeutic etoposide. Compounds with no CII inhibition activity provided no antiproliferative effect in normoxic or hypoxic environments. Mitochondria complex II inhibitor **16c** significantly inhibited mitochondrial function, reducing oxygen consumption rate, basal respiration, ATP production and maximal respiration.

In summary, for the first time, truly potent CII inhibitors with nanomolar activity are shown to elicit significant and selective anticancer activity. Mitochondrial complex II

inhibitors **16c**, **16j** and **16k** represent valuable molecular tools to study the effect of CII in cancer and other diseases.

2.4. Experimental Section

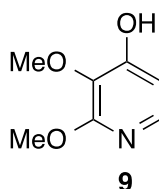
2.4.1. Chemistry

General

All reactions were carried out in oven- or flame-dried glassware under positive nitrogen pressure unless otherwise noted. Reaction progress was monitored by thin-layer chromatography (TLC) carried out on silica gel plates (2.5 cm x 7.5 cm, 200 μ m thick, 60 F254) and visualized by using UV (254 nm) or by potassium permanganate and/or phosphomolybdic acid solution as indicator. Flash column chromatography was performed with silica gel (40-63 μ m, 60 Å) or on a Teledyne Isco (CombiFlash R_f 200 UV/Vis). Commercial grade solvents and reagents were purchased from Fisher Scientific (Houston, TX) or Sigma Aldrich (Milwaukee, WI) and were used without further purification except as indicated. Anhydrous solvents were purchased from Acros Organics and stored under an atmosphere of dry nitrogen over molecular sieves.

¹H, ¹³C, COSY, HMQC and DEPT NMR spectra were recorded in the indicated solvent on a Bruker 400 MHz Advance III HD spectrometer at 400 and 100 MHz for ¹H and ¹³C respectively, with TMS as an internal standard. Multiplicities are indicated by s (single), d (doublet), dd (doublet of doublets), t (triplet), q (quartet), m (multiplet), and br (broad). Chemical shifts (δ) are reported in parts per million (ppm), and coupling constants (J), in Hertz. High-resolution mass spectroscopy was performed on a LC/MS IT-TOF (Shimadzu) using an ESI source conducted at the University of Texas at Arlington, Shimadzu Center for Advanced Analytical Chemistry. High-pressure liquid

chromatography was performed on a Gilson HPLC system with 321 pumps and 155 UV/Vis detector using trilution software v2.1 with an ACE Equivalence 3 (C18, 3 μ M, 4.6 x 150 mm) column. All samples were determined to possess >95% purity.

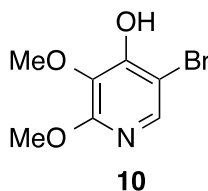


2,3-Dimethoxypyridin-4-ol (**9**).¹⁷⁰

To a solution of 2,3-dimethoxypyridine (0.30 g, 2.16 mmol) in tetrahydrofuran (THF, 15 mL) at -78 °C was added n-butyl lithium (ⁿBuLi, 1.3 mL, of a 2.5 M solution in hexanes, 3.24 mmol) dropwise. The mixture was stirred for 1 h at 0 °C in an ice water bath. The reaction mixture was cooled to -78 °C, trimethyl borate (B(OMe)₃, 0.62 mL, 5.4 mmol) was added and the mixture was stirred at -78 °C for 2 h. A solution of peracetic acid (32 wt % in dilute acetic acid, 1.02 mL, 4.32 mmol) was added and the mixture was slowly warmed to room temperature over one hour. To the reaction solution was added an aqueous solution of sodium bisulfite. The solution was extracted with ethyl acetate, washed with brine and dried over anhydrous sodium sulfate, the solvent was removed in vacuo and purification by flash column chromatography [dichloromethane (DCM): diethylether (Et₂O) 94:6] afforded the title compound as a colorless oil (211 mg, 63% yield):

¹H NMR (400 MHz, CDCl₃): δ = 3.71 (s, 3H), 3.90 (s, 3H), 6.48 (d, 1H, J =5.7 Hz), 7.61 (d, 1H, J =5.7 Hz), 7.99 ppm (s, 1H).

¹³CNMR (100 MHz, CDCl₃): δ = 53.30, 60.20, 107.30, 130.40, 140.70, 156.60, 157.80 ppm.



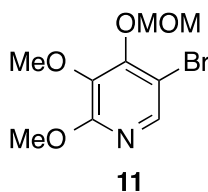
5-Bromo-2,3-dimethoxypyridin-4-ol (10).

To a solution of 2,3-dimethoxypyridin-4-ol (0.106 g, 0.68 mmol) in acetonitrile (5 mL) at 0 °C was added *N*-bromosuccinamide (0.134 g, 0.75 mmol). The reaction mixture was allowed to warm to room temperature and stirred overnight. The reaction mixture was extracted with ethyl acetate, the organic layer washed with brine and dried over anhydrous sodium sulfate, the solvent was removed in vacuo and purification by flash column chromatography [Hexanes: ethylacetate (EtOAc) 20:1] afforded the title compound as a yellow powder (0.132 g, 83% yield):

¹H NMR (400 MHz, CDCl₃): δ= 3.91 (s, 3H), 3.99 (s, 3H), 6.77 (s, 1H), 7.90 ppm (s, 1H).

¹³C NMR (100 MHz, CDCl₃): δ= 53.76, 60.99, 100.88, 130.63, 141.98, 152.60, 156.59 ppm.

HRMS (ESI): *m/z* calcd for C₇H₈BrNO₃ (*M*+Na⁺): 255.9580, found: 255.9574.



5-Bromo-2,3-dimethoxy-4-(methoxymethoxy)pyridine (11).

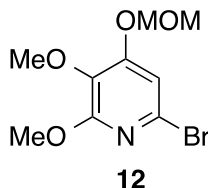
To a solution of 5-bromo-2,3-dimethoxypyridin-4-ol (**10**) (3.68 g, 15.7 mmol) in *N,N*-dimethylformamide (50 mL) as a solvent at 0 °C was added sodium hydride (NaH, 0.943 g, 23.6 mmol of a 60% dispersion in mineral oils). The mixture was stirred for 10 minutes

and methoxymethyl chloride (1.79 mL, 23.6 mmol) was added. The reaction mixture was allowed to warm to room temperature and stirred for 1 h. The reaction mixture was extracted with ethyl acetate, the organic layer washed with brine and dried over sodium sulfate, the solvent was removed in vacuo and purification by flash column chromatography (Hexanes: EtOAc 20:1) afforded the title compound as a yellow powder (4.11g, 94% yield):

¹H NMR (400 MHz, CDCl₃): δ= 3.57 (s, 3H), 3.82 (s, 3H), 3.94 (s, 3H), 5.33 (s, 2H), 7.90 ppm (s, 1H).

¹³C NMR (100 MHz, CDCl₃): δ= 53.88, 57.68, 60.51, 98.57, 107.24, 136.29, 142.25, 153.16, 158.56 ppm.

HRMS (ESI): *m/z* calcd for C₉H₁₂NBrO₄ (*M*+Na⁺): 299.9842, found: 299.9835.



6-Bromo-2,3-dimethoxy-4-(methoxymethoxy)pyridine (12).

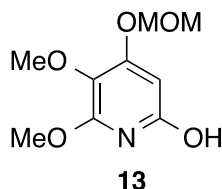
Lithium diisopropylamide (LDA) was prepared by addition of ⁿBuLi (1.41 mL, 1.6 M in hexanes, 2.26 mmol) to diisopropylamine (0.317 mL, 2.26 mmol) in THF (10 mL) at -78 °C and warmed up to 0 °C for 30 min with stirring. Lithium diisopropylamide solution was cooled to -78 °C and a solution of 5-bromo-2,3-dimethoxy-4-(methoxymethoxy)pyridine (**11**, 0.21 g, 0.76 mmol) in THF (10 mL) was added. The solution was warmed to -40 °C in an acetonitrile-dry ice bath and 2 μL of bromine was added. The reaction mixture was stirred for 1 h at -40 °C and then cooled to -78 °C. An excess of ethanol (EtOH, 4 mL) was added and the mixture was warmed up to 23 °C, which was treated with a saturated

aqueous solution of ammonium chloride (NH_4Cl , 5 mL) and then extracted with ethyl acetate. The organic washings were washed with brine and dried over sodium sulfate, the solvent was removed in vacuo and purification by flash column chromatography (Hexanes: EtOAc 10:1) afforded the title compound as a yellow powder (0.187 g with 89% yield):

^1H NMR (400 MHz, CDCl_3): δ = 3.39 (s, 3H), 3.72 (s, 3H), 3.86 (s, 3H), 5.14 (s, 2H), 6.82 ppm (s, 1H).

^{13}C NMR (100 MHz, CDCl_3): δ = 54.06, 56.30, 60.36, 94.42, 108.95, 131.10, 131.69, 158.5, 157.43 ppm.

HRMS (ESI): m/z calcd for $\text{C}_9\text{H}_{12}\text{NBrO}_4$ ($M+\text{Na}^+$): 299.9842, found: 299.9839.



5,6-Dimethoxy-4-(methoxymethoxy)pyridin-2-ol (**13**).

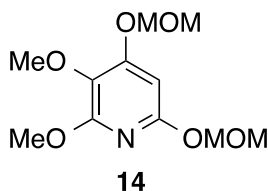
To a solution of 6-bromo-2,3-dimethoxy-4-(methoxymethoxy)pyridine (**12**, 3.79 g, 13.6 mmol) in THF (120 mL) at $-78\text{ }^\circ\text{C}$ was quickly added $n\text{BuLi}$ (18.7 mL, of a 1.6 M solution in hexanes, 40.9 mmol). The mixture was stirred for 1 minute and $\text{B}(\text{MeO})_3$ (4.89 mL, 40.9 mmol) was added with stirring for 2 h at $-78\text{ }^\circ\text{C}$. A solution of peracetic acid (32 wt % in dilute acetic acid, 12.9 mL, 54.5 mmol) was then added and the reaction mixture allowed to warm to $0\text{ }^\circ\text{C}$ under stirring for 2 h. An aqueous solution of sodium bisulfite was added dropwise, and the mixture extracted with ethyl acetate. The organic washings were washed with brine and dried over sodium sulfate, the solvent was removed in vacuo and

purification by flash column chromatography (Hexanes: EtOAc 10:1) afforded the title compound as a yellow powder (1.86 g, 63% yield):

¹H NMR (400 MHz, CDCl₃): δ= 3.41(s, 3H), 3.69 (s, 3H), 3.86 (s, 3H), 5.16 (s, 2H), 6.04 ppm (s, 1H).

¹³C NMR (100 MHz, CDCl₃): δ= 54.90, 56.45, 60.99, 89.02, 94.36, 126.31, 155.69, 158.34, 160.32 ppm.

HRMS (ESI): *m/z* calcd for C₉H₁₃NO₅ (*M*+Na⁺): 238.0686, found: 238.0678.



2,3-Dimethoxy-4,6-bis(methoxymethoxy)pyridine (14).

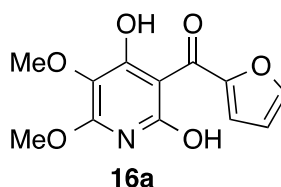
To a solution of 5,6-dimethoxy-4-(methoxymethoxy)pyridin-2-ol (**13**, 1.805 g, 8.38 mmol) in DMF (10 mL) at 0 °C was added NaH (0.537 g, 13.4 mmol, of a 60% dispersion in mineral oils). After 10 minutes, methoxymethyl chloride (0.96 mL, 12.6 mmol) was added. The reaction mixture was allowed to warm to room temperature and stirred for 1h. The reaction mixture was extracted with EtOAc, the organic washings were washed with brine and dried over sodium sulfate, the solvent was removed in vacuo and purification by flash column chromatography (Hexanes: EtOAc 10:1) afforded the title compound as a yellow powder (2.05 g, 94% yield):

¹H NMR (400 MHz, CDCl₃): δ= 3.48 (s, 3H), 3.49 (s, 3H), 3.77 (s, 3H), 3.92 (s, 3H), 5.22 (s, 2H), 5.41 (s, 2H), 6.21 ppm (s, 1H).

^{13}C NMR (100 MHz, CDCl_3): δ = 53.67, 56.47, 56.96, 60.86, 88.99, 91.95, 94.54, 127.50, 156.02, 156.46, 159.21 ppm.

HRMS (ESI): m/z calcd for $\text{C}_{11}\text{H}_{17}\text{NO}_6$ ($M+\text{Na}^+$): 282.0948, found: 282.0940.

General method for the synthesis of compounds 16a-16k.



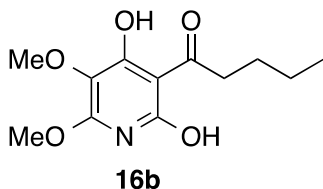
(2,4-dihydroxy-5,6-dimethoxypyridin-3-yl)(furan-2-yl)methanone (16a).

To a solution of 2,3-dimethoxy-4,6-bis(methoxymethoxy)pyridine (**14**, 0.029 g, 0.11 mmol) in THF (5 mL) at $-78\text{ }^{\circ}\text{C}$ was added $n\text{BuLi}$ (0.09 mL, 2.5 M, 0.22 mmol) and the reaction mixture stirred for 1 h. Furan-2-carbaldehyde (10.6 mg, 0.11 mmol) was added and the mixture stirred for 1 h. The reaction was quenched by addition of ethanol and extracted with ethyl acetate, the organic washings were washed with brine and dried over sodium sulfate, the solvent was removed in vacuo and the crude product used for the next step without further purification. To a solution of the crude material in DCM (5 mL) at room temperature was added Dess-Martin Periodinane (0.071 g, 0.17 mmol), and the reaction mixture stirred for 30 minutes. The reaction was quenched by addition of saturated sodium thiosulfate and extracted with ethyl acetate, the organic washings were washed with brine and dried over sodium sulfate, the solvent was removed in vacuo and the crude product used for the next step without further purification. To a solution of the crude material in DCM (2 mL) at $0\text{ }^{\circ}\text{C}$ was added trifluoroacetic acid (TFA, 0.5 mL) and the reaction mixture stirred for 30 minutes. The solvent was removed in vacuo and the residue purified by

flash column chromatography (Hexanes: EtOAc 4:1) to afford the title compound as a colorless oil (0.014 g, 48% yield):

¹H NMR (400 MHz, CDCl₃): δ = 3.84 (s, 3H), 4.11 (s, 3H), 6.57 (s, 1H), 7.68 ppm (m, 2H).

¹³C NMR (100 MHz, CDCl₃): δ = 57.31, 61.54, 111.97, 120.97, 122.16, 146.87, 151.46, 156.19, 160.53, 182.98 ppm.



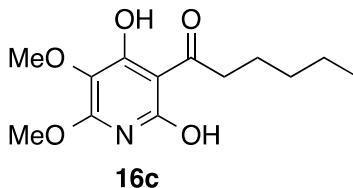
1-(2,4-dihydroxy-5,6-dimethoxypyridin-3-yl)pentan-1-one (16b).

The colorless oil compound was obtained from **15** by following the experimental conditions described for **16a**. (0.015 g, 53% yield):

¹H NMR (400 MHz, CDCl₃): δ = 0.96 (3H, t, J =7.0 Hz), 1.33 (m, 2H), 1.66 (m, 2H), 3.05 (2H, t, J =7.0 Hz), 3.79 (s, 3H), 4.16 ppm (s, 3H).

¹³C NMR (100 MHz, CDCl₃): δ = 13.94, 22.51, 26.32, 42.25, 61.51, 101.04, 121.05, 155.56, 162.07, 205.93 ppm.

HRMS (ESI): m/z calcd for C₁₂H₁₇NO₅ (M +Na⁺): 278.0999, found: 278.1005.



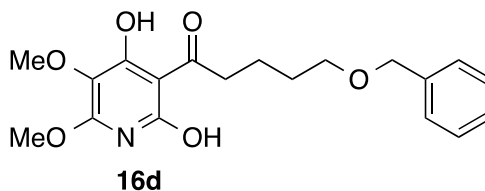
1-(2,4-dihydroxy-5,6-dimethoxypyridin-3-yl)hexan-1-one (16c).

The colorless oil compound was obtained from **15** by following the experimental conditions described for **16a**. (0.037 g, 51% yield):

¹H NMR (400 MHz, CDCl₃): δ = 0.89 (3H, t, J =7.0 Hz), 1.30 (m, 4H), 1.65 (m, 2H), 3.04 (2H, t, J =7.0 Hz), 3.80 (s, 3H), 4.16 ppm (s, 3H).

¹³C NMR (100 MHz, CDCl₃): δ = 14.01, 22.40, 24.07, 31.82, 42.50, 57.78, 60.61, 101.55, 121.06, 155.08, 161.82, 206.60 ppm.

HRMS (ESI): m/z calcd for C₁₃H₁₉NO₅ (M +Na⁺): 292.1161, found: 292.1155.



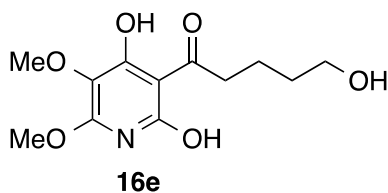
5-(benzyloxy)-1-(2,4-dihydroxy-5,6-dimethoxypyridin-3-yl)pentan-1-one (16d).

The colorless oil compound was obtained from **15** by following the experimental conditions described for **16a** with the slight modification that the crude material was purified by flash column chromatography (Hexanes: EtOAc 4:1) after oxidation with DMP and after deprotection with TFA. (0.098 g, 58% yield):

¹H NMR (400 MHz, CDCl₃): δ = 1.17 (m, 4H), 1.25 (m, 18 H), 3.09 (2H, t, J =6.3 Hz), 3.51 (2H, t, J =6.3 Hz), 3.78 (s, 3H), 4.15 (s, 3H), 4.50 (s, 2H), 7.32 ppm (m, 5H).

¹³C NMR (100 MHz, CDCl₃): δ = 20.94, 29.37, 42.26, 57.94, 61.49, 70.16, 72.92, 100.67, 121.49, 127.49, 127.60, 128.34, 138.55, 155.94, 161.82, 205.74 ppm.

HRMS (ESI): m/z calcd for C₁₉H₂₃NO₆ (M +Na⁺): 384.1423, found: 384.1417.



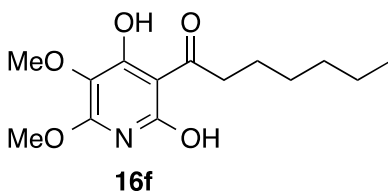
1-(2,4-dihydroxy-5,6-dimethoxypyridin-3-yl)-5-hydroxypentan-1-one (16e).

The colorless oil compound was obtained from **15** by following the experimental conditions described for **16a**. (0.045 g, 86% yield):

¹H NMR (400 MHz, CD₃OD): δ = 1.60 (m, 2H), 1.73 (m, 2 H), 3.10 (2H, t, J =7.4 Hz), 3.59 (2H, t, J =7.4 Hz), 3.71 (s, 3H), 4.99 ppm (s, 3H).

¹³C NMR (100 MHz, CD₃OD): δ = 21.86, 33.26, 43.84, 61.19, 62.75, 101.06, 124.70, 160.08, 162.86, 207.51 ppm.

HRMS (ESI): m/z calcd for C₁₂H₁₇NO₆ (M +Na⁺): 294.0948, found: 294.0954.



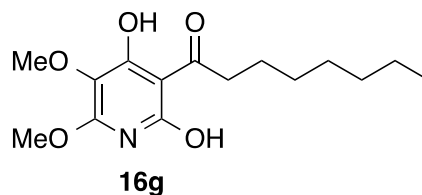
1-(2,4-dihydroxy-5,6-dimethoxypyridin-3-yl)heptan-1-one (16f).

The colorless oil compound was obtained from **15** by following the experimental conditions described for **16a** (0.025 g, 52% yield):

¹H NMR (400 MHz, CDCl₃): δ = 0.89 (3H, t, J =7.0 Hz), 1.31 (m, 6H), 1.66 (m, 2H), 3.03 (2H, t, J =7.0 Hz), 3.79 (s, 3H), 4.16 ppm (s, 3H).

¹³C NMR (100 MHz, CDCl₃): δ = 13.94, 22.51, 26.32, 42.25, 57.63, 61.51, 101.04, 121.05, 155.56, 162.07, 205.93 ppm.

HRMS (ESI): m/z calcd for $C_{14}H_{21}NO_5$ ($M+Na^+$): 306.1312, found: 306.1308.



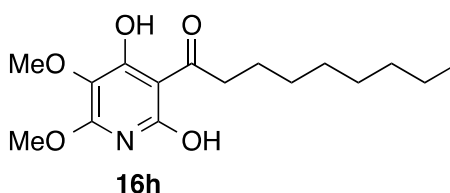
1-(2,4-dihydroxy-5,6-dimethoxypyridin-3-yl)octan-1-one (16g).

The colorless oil compound was obtained from **15** by following the experimental conditions described for **16a** (0.017 g, 51% yield):

1H NMR (400 MHz, $CDCl_3$): δ = 0.88 (3H, t, J =7.0 Hz), 1.31 (m, 8H), 1.64 (m, 2H), 3.06 (2H, t, J =7.0 Hz), 3.79 (s, 3H), 4.17 ppm (s, 3H).

^{13}C NMR (100 MHz, $CDCl_3$): δ = 14.08, 22.64, 24.21, 29.17, 29.39, 31.75, 42.56, 57.63, 61.50, 100.99, 121.25, 155.95, 161.82, 206.33 ppm.

HRMS (ESI): m/z calcd for $C_{15}H_{23}NO_5$ ($M+Na^+$): 320.1468, found: 320.1463.



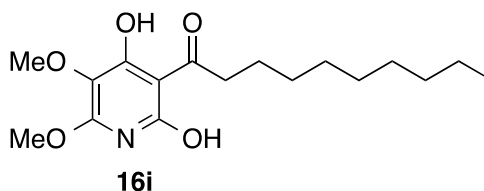
1-(2,4-dihydroxy-5,6-dimethoxypyridin-3-yl)nonan-1-one (16h).

The colorless oil compound was obtained from **15** by following the experimental conditions described for **16a** (0.019 g, 55% yield):

1H NMR (400 MHz, $CDCl_3$): δ = 0.89 (3H, t, J =7.0 Hz), 1.29 (m, 10H), 1.69 (m, 2H), 3.10 (2H, t, J =7.0 Hz), 3.82 (s, 3H), 4.21 ppm (s, 3H).

^{13}C NMR (100 MHz, CDCl_3): δ = 14.10, 22.67, 24.15, 29.19, 29.34, 29.44, 31.85, 42.77, 58.33, 61.68, 100.48, 121.96, 154.84, 161.67, 206.41 ppm.

HRMS (ESI): m/z calcd for $\text{C}_{16}\text{H}_{25}\text{NO}_5$ ($M+\text{Na}^+$): 334.1625, found 334.1626.



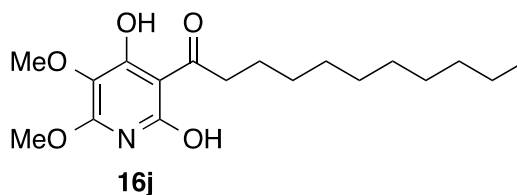
1-(2,4-dihydroxy-5,6-dimethoxypyridin-3-yl)decan-1-one (16i).

The colorless oil compound was obtained from **15** by following the experimental conditions described for **16a** (0.018 g, 52% yield):

^1H NMR (400 MHz, CDCl_3): δ = 0.87 (3H, t, J =7.0 Hz), 1.26 (m, 12 H), 1.65 (m, 2H), 3.06 (2H, t, J =7 Hz), 3.78 (s, 3H), 4.17 ppm (s, 3H).

^{13}C NMR (100 MHz, CDCl_3): δ = 14.10, 22.65, 24.19, 29.29, 29.42, 29.51, 31.87, 42.56, 57.63, 61.52, 100.05, 121.10, 155.19, 161.65, 206.76 ppm.

HRMS (ESI): m/z calcd for $\text{C}_{17}\text{H}_{27}\text{NO}_5$ ($M+\text{Na}^+$): 348.1781, found: 348.1778.



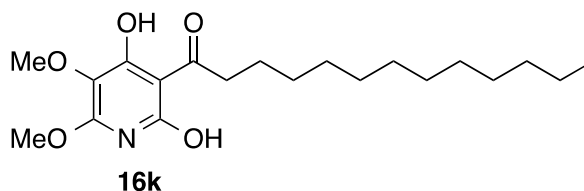
1-(2,4-dihydroxy-5,6-dimethoxypyridin-3-yl)undecan-1-one (16j).

The colorless oil compound was obtained from **15** by following the experimental conditions described for **16a** (0.028 g, 55% yield):

¹H NMR (400 MHz, CDCl₃): δ = 0.87 (3H, t, J =7.0 Hz), 1.26 (m, 14 H), 1.65 (m, 2H), 3.04 (2H, t, J =7.0 Hz), 3.78 (s, 3H), 4.17 ppm (s, 3H).

¹³C NMR (100 MHz, CDCl₃): δ = 14.09, 22.66, 24.20, 29.32, 29.43, 29.51, 29.55, 29.59, 31.88, 42.57, 57.25, 61.50, 100.69, 121.26, 155.67, 160.99, 206.08 ppm.

HRMS (ESI): m/z calcd for C₁₈H₂₉NO₅ (M +Na⁺): 362.1938, found: 362.1937.



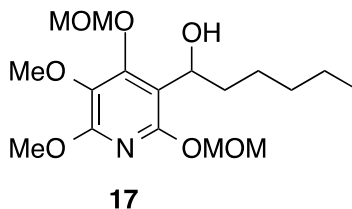
1-(2,4-dihydroxy-5,6-dimethoxypyridin-3-yl)tridecan-1-one (16k).

The colorless oil compound was obtained from **15** by following the experimental conditions described for **16a** (0.035 g, 56% yield):

¹H NMR (400 MHz, CDCl₃): δ = 0.89 (3H, t, J =7.0 Hz), 1.25 (m, 18 H), 1.68 (m, 2H), 3.07 (2H, t, J =7.0 Hz), 3.79 (s, 3H), 4.15 ppm (s, 3H).

¹³C NMR (100 MHz, CDCl₃): δ = 14.10, 22.67, 24.20, 29.34, 29.42, 29.51, 29.55, 29.64, 29.67, 31.90, 42.55, 57.63, 61.51, 101.07, 121.25, 155.19, 161.80, 206.42 ppm.

HRMS (ESI): m/z calcd for C₁₈H₂₉NO₅ (M +Na⁺): 390.2251, found: 390.2256.

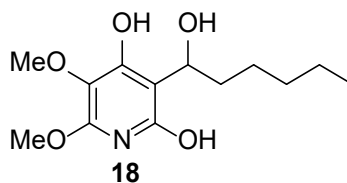


1-(5,6-dimethoxy-2,4-bis(methoxymethoxy)pyridin-3-yl)hexan-1-ol (17).

To a solution of 2,3-dimethoxy-4,6-bis(methoxymethoxy)pyridine (**14**, 0.030 g, 0.116 mmol) in THF (3 mL) at -78 °C was added ⁿBuLi (0.19 mL, of a 2.5 M solution in hexanes, 0.35 mmol), which was stirred for 1 h. Hexanal (0.074 mL, 0.58 mmol) was added and the reaction was stirred for 1 h. The reaction was quenched with ethanol and extracted with ethyl acetate, the organic washings were washed with brine and dried over anhydrous sodium sulfate, the solvent was removed in vacuo and the residue was purified by column chromatography (Hexanes: EtOAc 4:1) to afford the title compound as a colorless oil (33.3 mg, 80% yield):

¹H NMR (400 MHz, CDCl₃): δ= 0.89 (t, 3H, *J*=7.0 Hz), 1.30 (m, 4H), 1.52 (m, 2H), 1.74 (m, 1H), 1.91 (m, 1H), 3.22 (s, 1H), 3.53 (s, 3H), 3.56 (s, 3H), 3.75 (s, 3H), 3.93 (s, 3H), 4.95 (1H, t, *J*=6.7 Hz), 5.29 (1H, d, *J*=5.0 Hz), 5.32 (1H, d, *J*=5.0 Hz), 5.49 (1H, d, *J*=5.0 Hz), 5.60 ppm (1H, d, *J*=5.0 Hz).

¹³C NMR (100 MHz, CDCl₃): δ= 13.9, 22.2, 25.9, 31.8, 37.5, 53.6, 57.3, 57.8, 60.6, 67.3, 91.8, 99.2, 112.0, 129.0, 153.0, 154.9, 156.8 ppm.



(rac)-3-(1-hydroxyhexyl)-5,6-dimethoxypyridine-2,4-diol (18**).**

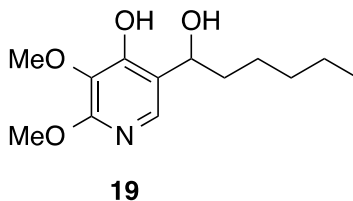
To a solution of 2,3-dimethoxy-4,6-bis(methoxymethoxy)pyridine (**14**, 0.020 g, 0.077 mmol) in THF (5 mL) at -78 °C was added ⁿBuLi (0.068 mL, of a 2.5 M solution in hexanes, 0.17 mmol), which was stirred for 1 h. Hexanal (0.010 mL, 0.077 mmol) was added and the reaction was stirred for 1 h. The reaction was quenched with ethanol and extracted with ethyl acetate, the organic washings were washed with brine and dried over anhydrous

sodium sulfate, the solvent was removed in vacuo and the crude product used for the next step without further purification. To a solution of the crude material in DCM (4 mL) at 0 °C was added TFA (1 mL) and the reaction stirred for 30 minutes. The solvent was removed in vacuo and the residue purified by flash column chromatography (Hexanes: EtOAc 4:1) to afford the title compound as a racemic mixture as a colorless oil (0.061 g, 63% yield):

¹H NMR (400 MHz, CDCl₃): δ= 0.87 (m, 4H), 1.29 (m, 6H), 3.81 (m, 4H), 3.93 (s, 3H), 5.55 (1H, d, *J*=7.0 Hz), 7.71 ppm (br. s, 1H).

¹³C NMR (100 MHz, CDCl₃): δ= 13.89, 22.63, 25.17, 31.79, 36.94, 72.83, 80.03, 157.16, 163.58 ppm.

HRMS (ESI): *m/z* calcd for C₁₃H₂₁NO₅ (*M*+H-H₂O⁺): 254.1387 found 254.1366.



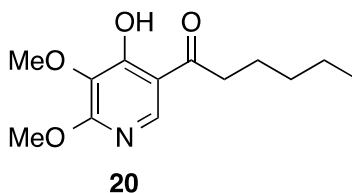
(rac)-5-(1-hydroxyhexyl)-2,3-dimethoxypyridin-4-ol (19).

To a solution of 5-bromo-2,3-dimethoxy-4-(methoxymethoxy)pyridine (**11**, 0.032 g, 0.115 mmol) in THF (5 mL) at -78 °C was added ⁿBuLi (0.10 mL, of a 2.5 M solution in hexanes, 0.25 mmol), which was stirred for one minute. Hexanal (0.012 g, 0.15 mmol) was added and stirring was continued for 1 h. The reaction was quenched by ethanol and extracted with ethyl acetate, the organic washings were washed with brine and dried over anhydrous sodium sulfate, the solvent was removed in vacuo and the residue purified by flash

column chromatography (Hexanes: EtOAc 4:1) to afford the title compound as a colorless oil (25 mg, 85%):

¹H NMR (400 MHz, CDCl₃): δ = 0.89 (m, 2H), 1.30 (m, 6H), 1.73 (q, J =5.5 Hz), 3.90 (s, 3H), 4.27 (s, 3H), 4.86 (1H, t, J =5.5 Hz), 7.76 (s, 1H), 10.59 ppm (br, 2H).

¹³C NMR (100 MHz, CDCl₃): δ = 13.90, 22.45, 25.0, 31.37, 37.0, 58.58, 61.40, 69.54, 114.39, 117.28, 124.97, 130.53, 132.05, 155.08, 162.0 ppm.



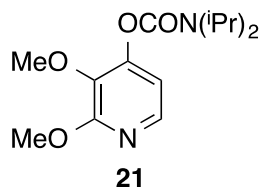
1-(4-hydroxy-5,6-dimethoxypyridin-3-yl)hexan-1-one (20).

To a solution of 5-(1-hydroxyhexyl)-2,3-dimethoxypyridin-4-ol (**19**, 28 mg, 0.11 mmol) in DCM (5 mL) at room temperature was added Dess-Martin Periodinane (0.073 g, 0.17 mmol) and the reaction stirred for 30 minutes. The reaction was quenched by the addition of saturated sodium thiosulfate and extracted with ethyl acetate, the organic washings were washed with brine and dried over anhydrous sodium sulfate, the solvent was removed in vacuo and the crude product used for the next step without further purification. To a solution of the crude material in DCM (4 mL) at 0 °C was added TFA (1 mL) and the reaction stirred for 30 minutes. The solvent was removed in vacuo and the residue purified by flash column chromatography (Hexanes: EtOAc 4:1) to afford the title compound as a colorless oil (0.015 g, 51% yield):

¹H NMR (400 MHz, CDCl₃): δ = 0.91 (3H, t, J =7.0 Hz), 1.37 (m, 6H), 1.75 (m, 2H), 2.93 (2H, t, J =7.0 Hz), 3.89 (s, 3H), 4.05 (s, 3H), 8.44 (s, 1H), 12.63 ppm (s, 1H).

^{13}C NMR (100 MHz, CDCl_3): δ = 13.88, 22.43, 24.44, 31.41, 38.19, 54.40, 60.57, 114.55, 130.525, 145.07, 160.81, 161.39, 206.02 ppm.

HRMS (ESI): m/z calcd for $\text{C}_{13}\text{H}_{19}\text{NO}_4$ ($M+\text{Na}^+$): 276.1206, found: 276.1207.

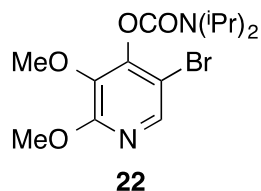


2,3-Dimethoxypyridin-4-yl diisopropylcarbamate (21).¹⁷¹

To a solution of 2,3-dimethoxypyridin-4-ol (**9**, 0.30 g, 1.93mmol) in toluene (10 mL) was added silver carbonate (0.80 g, 2.9 mmol) and diisopropylcarbamyl chloride (0.484 g, 2.9 mmol) and the reaction mixture was refluxed for 3 h. The suspension was allowed to cool and passed through celite washing with methanol (MeOH), removal of the solvent in vacuo and purification by chromatography (DCM: Et₂O 96:4) provided the title compound as a colorless oil with yield (398 mg, 73%):

^1H NMR (400 MHz, CDCl_3): δ = 1.26 (d, 12H, J =6.8 Hz), 3.81 (s, 3H), 3.95 (s, 3H), 3.99 (m, 2H), 6.68 (d, 1H, J =5.6 Hz), 7.77 ppm (1H, d, J =5.6 Hz).

^{13}C NMR (100 MHz, CDCl_3): δ = 20.2, 21.0, 46.6, 53.5, 60, 112.7, 135.70, 140.4, 150.80, 152.1, 158.8 ppm.

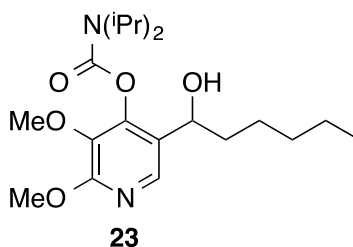


5-Bromo-2,3-dimethoxypyridin-4-yl diisopropylcarbamate (22).¹⁷¹

To a solution of 2,3-dimethoxypyridin-4-yl diisopropylcarbamate (**21**, 0.60 g, 2.12 mmol) in carbon tetrachloride (CCl₄, 20 mL) was added bromine (0.273 mL, 5.31 mmol) and the reaction mixture was stirred at room temperature for 48 h, which was shielded from light with aluminum foil. To the reaction mixture was added a solution of saturated aqueous sodium bicarbonate (5 mL) and sodium thiosulfate (5 mL) and extracted with ethyl acetate. The organic phase was washed with brine and dried over sodium sulfate, the solvent was removed in vacuo and the residue purified by column chromatography (DCM:Et₂O 98:2) to afford the title compound as a yellow solid (383 mg, 50% yield):

¹H NMR (400 MHz, CDCl₃): δ = 1.29 and 1.34 (12H, 2d, J = 6.8 Hz), 3.86 (s, 3H), 3.97 (s, 3H), 4.01-4.04 (m, 2 H), 7.99 ppm (s, 1H).

¹³C NMR (100 MHz, CDCl₃): δ = 19.9, 20.8, 46.6, 46.9, 53.4, 58.9, 107.5, 137.1, 141.1, 148.3, 150.5, 157.5 ppm.



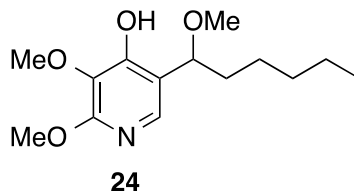
5-(1-hydroxyhexyl)-2,3-dimethoxypyridin-4-yl diisopropylcarbamate (23).

To a solution of 5-bromo-2,3-dimethoxypyridin-4-yl diisopropylcarbamate (**22**, 0.12 g, 0.33 mmol) in THF (3 mL) at -78 °C was added ⁿBuLi (0.45 mL, of a 2.5 M solution in hexanes, 1.1 mmol) which was stirred for 1 minute. Hexanal (0.24 mL, 1.66 mmol) was added and the reaction mixture stirred for 1 h. The reaction was quenched by addition of ethanol and extracted with ethyl acetate, the organic washings were washed with brine and dried over

sodium sulfate, the solvent was removed in vacuo and the residue purified by column chromatography (Hexanes: EtOAc 4:1) to afford the title compound as a colorless oil (104.7 mg, 83% yield):

¹H NMR (400 MHz, CDCl₃): δ = 0.86 (3H, t, J =7.0 Hz), 1.1-1.5 (m, 18H), 1.70-2.00 (m, 2H), 3.82 (s, 3H), 4.00 (s, 3H), 3.98-4.12 (m, 2H), 4.69 (1H, t, J =6.7 Hz), 7.97 ppm (s, 1H).

¹³C NMR (100 MHz, CDCl₃): δ = 14.1, 20.4, 21.3, 22.6, 25.7, 31.6, 36.7, 47, 47.1, 53.8, 60.1, 60.3, 128.1, 135.6, 138.2, 148.9, 153.1, 158.0 ppm.



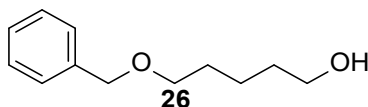
2,3-Dimethoxy-5-(1-methoxyhexyl)pyridin-4-ol (24).

5-(1-hydroxyhexyl)-2,3-dimethoxypyridin-4-yl diisopropylcarbamate (**23**, 0.090 g, 0.23 mmol) was refluxed in potassium hydroxide solution (5 M, in methanol, 10 mL) for 20 h. The solvent was removed in vacuo and diluted acetic acid added. The reaction mixture was neutralized by addition of saturated aqueous NaHCO₃, extracted with ethyl acetate. The organic washings were washed with brine and dried over anhydrous sodium sulfate, the solvent was removed in vacuo and purification by column chromatography afforded the title compound as a colorless oil (50% yield):

¹H NMR (400 MHz, CDCl₃): δ = 0.85 (3H, t, J =7.0 Hz), 1.26 (m, 6H), 1.68-1.83 (m, 2H), 3.34 (s, 3H), 3.90 (s, 3H), 3.98 (s, 3H), 4.28 (1H, t, J =6.7 Hz), 7.55 (s, 1H), 7.68 ppm (s, 1H).

^{13}C NMR (100 MHz, CDCl_3): δ = 13.9, 22.2, 25.0, 31.5, 35.7, 53.6, 57.1, 60.7, 80.7, 117.9, 130.4, 139.8, 154.8, 157.1 ppm.

HRMS (ESI): m/z calcd for $\text{C}_{14}\text{H}_{23}\text{NO}_4$ ($M+\text{Na}^+$): 292.1525, found: 292.1517.

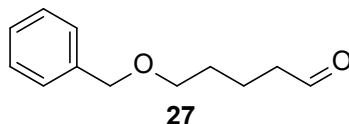


5-(Benzyloxy)pentan-1-ol (26).

A solution of pentane-1,5-diol (**25**, 5 mL, 48.01 mmol) in THF (20 mL) was added dropwise to a suspension of NaH (1.15 g, 60 % dispersion in mineral oil, 48.01 mmol) in THF (5 mL) under argon atmosphere. The reaction mixture was heated under reflux for 4 h, cooled to room temperature and benzyl bromide (5.7 mL, 48.01 mmol) was added to it drop wise. The reaction mixture was heated under reflux overnight. After that, the reaction mixture was cooled to room temperature and the solvent was removed in vacuo. Reaction mixture was extracted with ethyl acetate, the organic layer washed with brine and dried over anhydrous sodium sulfate, the solvent was concentrated under reduced pressure and purification by flash column chromatography afforded the title compound as a yellow oil (Hexanes: EtOAc 20:1) (65% yield):

^1H NMR (400 MHz, CDCl_3): δ = 1.44 (m, 2H), 1.55 (m, 2H), 1.66 (m, 2H), 2.67 (s, 1H), 3.49 (2H, t, $J=6.5$ Hz), 3.59 (2H, t, $J=6.5$ Hz), 4.51 (s, 1H), 7.30 (m, 1H), 7.35 ppm (4H, d, $J=4.3$ Hz).

^{13}C NMR (100 MHz, CDCl_3): δ = 24.4, 25.6, 29.9, 32.2, 62.1, 69.7, 72.9, 127.5, 127.6, 127.8, 128.4, 128.4, 137.4 ppm.

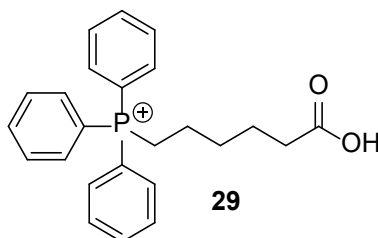


5-(Benzyloxy)pentanal (**27**).

A solution of dimethyl sulfoxide (3.66 mL, 51.5 mmol) in dimethyl chloride (3 mL) was added dropwise to a solution of oxalyl chloride (2.2 mL, 25.7 mmol) dimethyl chloride (1 mL). After stirring 15-minute a solution of 5-(benzyloxy)pentan-1-ol (**26**, 1 g, 5.15 mmol) in DCM (3 mL) was adding dropwise. After 30-minute, the triethylamine was added dropwise, the reaction was stirring for 1 h at -78 C. After that, reaction was slowly cooled to room temperature, the solvent was removed in vacuo and purification by flash column chromatography (Hexanes: EtOAc 20:1) resulted in the title compound as a yellow color liquid (56% yield):

¹H NMR (400 MHz, CDCl₃): δ = 1.69 (m, 3 H), 1.74 (m, 2H), 2.48 (2H, t, J =7.0 Hz), 3.51 (2H, t, J =6.2 Hz), 4.51 (s, 2H), 7.3 (m, 1H), 7.35 (m, 4H), 9.77 ppm (1H, t, J =2.0 Hz).

¹³C NMR (100 MHz, CDCl₃): δ = 18.9, 29.6, 43.5, 69.7, 72.9, 127.5, 127.6, 127.6, 128.3, 128.6, 138.4, 202.5 ppm.

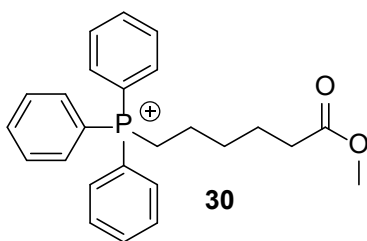


(5-Carboxypentyl)triphenylphosphonium (**29**).

A solution of 6-bromohexanoic acid (**28**, 1 g, 5.1 mmol) in dry acetonitrile the triphenylphosphine (1.34 g, 5.1 mmol) and reacted at 80 °C under inert N₂ gas for 16 h.

After cooling of the reaction solution to room temperature, a white precipitate was obtained in a crystallized form. (1.8, 95% yield).

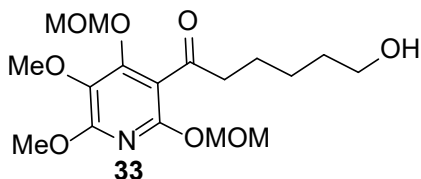
¹H NMR (400 MHz, CDCl₃): δ= 1.43 (m, 1H), 1.63 (m, 4H), 2.31 (m, 2H), 3.40 (1H, t, *J*=6.1 Hz), 3.54 (m, 1H), 7.31 (s, 6H), 7.72 (m, 9H), 8.16 ppm (br, 1H).



(6-Methoxy-6-oxohexyl)triphenylphosphonium (30).

A solution of (5-carboxypentyl)triphenylphosphonium (**29**, 1 g, 2.65 mmol) in methanol (50 mL) was added a catalytic amount of H₂SO₄ (5 drops). The mixture was refluxed overnight, after which time the solvent was removed in vacuo. The reaction mixture was extracted with EtOAc, the organic washings were washed with brine and dried over sodium sulfate, the solvent was removed in vacuo to provide the product as a yellow oil. (0.87 g, 84%).

¹H NMR (400 MHz, CDCl₃): δ= 1.42 (m, 1H), 1.63 (m, 4 H), 2.30 (m, 2H), 3.40 (1H, t, *J*=6.1 Hz), 3.53 (m, 1H), 3.92 (s, 3H), 7.31 (s, 6H), 7.70 (m, 9H), 8.22 ppm (br, 1H).

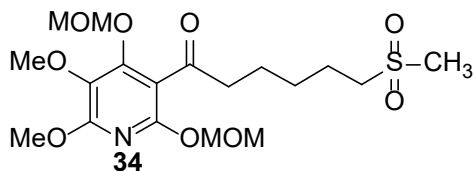


1-(5,6-Dimethoxy-2,4-bis(methoxymethoxy)pyridin-3-yl)-6-hydroxyhexan-1-one (33).

To a solution of 6-(benzyloxy)-1-(5,6-dimethoxy-2,4-bis(methoxymethoxy)pyridin-3-yl)hexan-1-one (**35**, 0.07 g, 0.19 mmol) in methanol (2 mL) and acetic acid (1 mL) at room temperature was added palladium on carbon (Pd/C, 0.227 g, 0.21 mmol), which was stirred for overnight under H₂. After celite filtration, the solvent was removed in vacuo and the residue purified by flash column chromatography (Hexane: EtOAc 4:1) to afford the title compound as a colorless oil (0.045 g, 86% yield):

¹H NMR (400 MHz, CDCl₃): δ = 1.32 (m, 2H), 1.57 (m, 2H), 1.63 (m, 2H), 3.10 (2H, t, J =7.4 Hz), 3.32 (s, 3H), 3.59 (2H, t, J =7.4 Hz), 3.71 (s, 3H), 4.99 (s, 3H) 6.13 (s, 2H), 6.24 ppm (s, 2H).

¹³C NMR (100 MHz, CDCl₃): δ = 21.8, 25.2, 33.2, 43.8, 54.5, 56.7, 56.7, 61.1, 62.7, 94.4, 95.7, 101.1, 124.7, 159.7, 160.2, 162.7, 203.7 ppm.

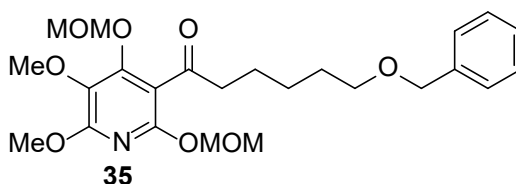


1-(5,6-Dimethoxy-2,4-bis(methoxymethoxy)pyridin-3-yl)-6-(methylsulfonyl)hexan-1-one (34**).**

To a solution of 1-(5,6-dimethoxy-2,4-bis(methoxymethoxy)pyridin-3-yl)-6-hydroxyhexan-1-one (**33**, 0.09 g, 0.24 mmol) in tetrahydrofuran (5 mL) the triethylamine (0.1 mL, 0.48 mmol) was added. The mixture was stirred at room temperature over a period of 30 min. A solution of methanesulfonyl chloride (0.024 mL, 0.312 mmol) in tetrahydrofuran (3 mL) was then added dropwise to the mixture. The reaction mixture stirred at room temperature for overnight. The mixture was neutralized, and solvent was removed in vacuo. The reaction was extracted with dichloromethane, the organics phases were washed with

water and brine and dried over sodium sulfate. The crude product was used without further purification in the next step. The title compound as a yellow oil (0.056 g, 53% yield):

¹H NMR (400 MHz, CDCl₃): δ = 1.49 (m, 2H), 1.69 (m, 4H), 2.67 (s, 3H), 2.84 (m, 2H), 3.34 (s, 6H), 3.57 (2H, t, J =7.2 Hz), 3.86 (s, 3H), 4.03 (s, 3H), 6.03 (s, 2 H), 6.24 ppm (s, 2H).

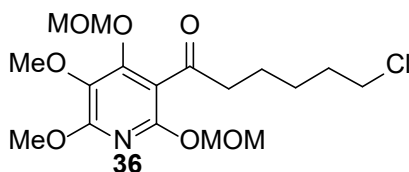


5-(benzyloxy)-1-(5,6-dimethoxy-2,4-bis(methoxymethoxy)pyridin-3-yl)hexan-1-one (35).

To a solution of 2,3-dimethoxy-4,6-bis(methoxymethoxy)pyridine (**14**, 0.121 g, 0.47 mmol) in THF (5 mL) at -78 °C was added ⁿBuLi (0.4 mL, 2.5 M, 1.02 mmol) and the reaction mixture stirred for 1 h. 5-(benzyloxy)hexanal (0.096 mg, 0.47 mmol) was added and the mixture stirred for 1 h. The reaction was quenched by addition of ethanol and extracted with ethyl acetate, the organic washings were washed with brine and dried over sodium sulfate, the solvent was removed in vacuo and the crude product used for the next step without further purification. To a solution of the crude material in DCM (5 mL) at room temperature was added DMP (0.297 g, 0.7 mmol), and the reaction mixture stirred for 30 minutes. The reaction was quenched by addition of saturated sodium thiosulfate and extracted with ethyl acetate, the organic washings were washed with brine and dried over sodium sulfate, the solvent was removed in vacuo and the residue purified by flash column chromatography (Hexanes: EtOAc 4:1) to afford the title compound as a colorless oil (0.098 g, 58% yield):

¹H NMR (400 MHz, CDCl₃): δ= 1.27 (m, 2H), 1.52 (m, 4 H), 3.09 (2H, t, *J*=6.3 Hz), 3.51 (2H, t, *J*=6.3 Hz), 3.78 (s, 6H), 4.05 (s, 3H), 4.15 (s, 3H), 4.81 (2H, t, *J*=6.3 Hz), 6.23 (m, 4H), 7.32 ppm (m, 5H).

¹³C NMR (100 MHz, CDCl₃): δ= 24.9, 28.3, 29.8, 39.2, 55.3, 56.9, 61.4, 70.1, 72.9, 100.6, 106.3, 119.5, 127.4, 127.4, 127.6, 128.5, 138.5, 152.8, 153.5, 156.7, 203.5 ppm.

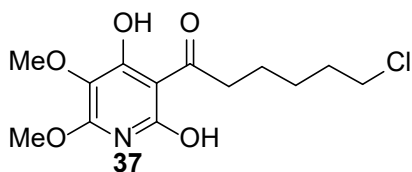


6-Chloro-1-(5,6-dimethoxy-2,4-bis(methoxymethoxy)pyridin-3-yl)hexan-1-one (36).

The 1-(5,6-dimethoxy-2,4-bis(methoxymethoxy)pyridin-3-yl)-6-hydroxyhexan-1-one (**33**, 0.2 g, 0.51 mmol) was dissolved in thionyl chloride (0.69 mL, 5.10 mmol) in DCM (2 mL) and refluxed for 3 h. the solvent was removed in vacuo and the residue purified by flash column chromatography (Hexanes: EtOAc 4:1) to afford the title compound as a yellow oil (0.173 g, 86% yield):

¹H NMR (400 MHz, CDCl₃): δ= 1.29 (m, 2H), 1.57 (m, 2H), 1.72 (m, 2 H), 3.04 (2H, t, *J*=7.4 Hz), 3.34 (s, 6H), 3.73 (2H, t, *J*=7.4 Hz), 3.79 (s, 3H), 5.08 (s, 3H), 6.03 (s, 2H), 6.24 ppm (s, 2H).

¹³C NMR (100 MHz, CDCl₃): δ= 24.7, 25.1, 34.5, 42.9, 54.5, 56.7, 56.7, 61.1, 62.7, 94.7, 95.8, 101.1, 124.7, 158.5, 161.7, 162.7, 200.0 ppm.



6-Chloro-1-(2,4-dihydroxy-5,6-dimethoxypyridin-3-yl)hexan-1-one (37).

To a solution of 6-chloro-1-(5,6-dimethoxy-2,4-bis(methoxymethoxy)pyridin-3-yl) hexan-1-one (**36**, 0.07 g, 0.18 mmol) in DCM (2 mL) at 0 °C was added TFA (0.5 mL) and the reaction mixture stirred for 30 minutes. The solvent was removed in vacuo and the residue purified by flash column chromatography (Hexanes: EtOAc 4:1) to afford the title compound as a yellow oil (0.038 g, 69% yield):

¹H NMR (400 MHz, CDCl₃): δ= 1.27 (m, 2H), 1.59 (m, 4H), 2.97 (m, 2H), 3.34 (m, 2H), 3.93 (s, 3H), 4.23 (s, 3H), 14.88 ppm (s, 1H).

¹³C NMR (100 MHz, CDCl₃): δ= 24.7, 25.1, 34.5, 42.9, 54.5, 56.7, 56.7, 101.1, 101.2, 124.7, 158.4, 161.6, 203.2 ppm.

2.4.2. Biology

2.4.2.1. Cell culture and Reagents

Cell lines (DU-145 a human prostate carcinoma cell line, 22Rv1 a human prostate carcinoma epithelial cell line, LNCap prostate cancer, PC3 prostate cancer cell lines, WPMY-1 prostate stromal cells, HEK293 human embryonic kidney cells, and NIH 3t3 mouse fibroblast cell line) were obtained from the American Type culture Collection (ATCC). The cells were cultured in Roswell Park Memorial Institute-1640 medium (RPMI-1640) (ATCC® 30-2001™) for DU-145, 22Rv1 and LNCap cells and in F-12K Medium (Kaighn's Modification of Ham's F-12 Medium) (ATCC® 30-2004™) for PC3 prostate cancer cell lines and in Eagle's Minimum Essential Medium (ATCC® 30-2003™) for

HEK293 human embryonic kidney cells and Dulbecco's Modified Eagle's Medium (ATCC® 30-2002™) for WPMY-1 prostate stromal cells and NIH 3t3 mouse fibroblast cell line with fetal bovine serum (ATCC 30-2020) to a final concentration of 10% and Corning™ Penicillin-Streptomycin Solution (Catalog No. MT30001CI) according to the supplier's recommended protocol. Enzalutamide (ENZ) (catalog no. 50-101-3979) and Etoposide (catalog no. AAJ63651MC) were purchased from Fisher Scientific. Atpenin A5 (catalog no. 10189-198) was purchased from VWR. Stock solutions of AA5 were prepared in DMSO and were serially diluted for cell culture treatment maintaining the final DMSO concentration at less than 1%. CellTiter 96 AQueous One Solution Cell Proliferation Assay (3-(4,5-dimethylthiazol-2-yl)-5-(3-carboxymethoxyphenyl)-2-(4-sulfophenyl)-2H-tetrazolium) (MTS) assay (catalog no. G3580) was purchased from Promega.

2.4.2.2. Cytotoxicity Assays

To determine the cell growth inhibition ability of the synthesized compounds, cells were seeded at a density of 0.1×10^6 cells per mL in 96-well plates containing 100 μ L cell suspension per well. Stock solutions of the synthesized compounds were prepared in DMSO. Cells were treated at the indicated concentrations of test compounds, limiting the final DMSO concentration to less than 1%. After incubation at 37°C, 5% CO₂ for 48 h, 20 μ L of MTS reagent (CellTiter 96® AQueous One Solution Reagent) was added to each well and incubated at the above-mentioned conditions for 3–4 h. Absorbance was recorded at 490 nm on a BioTek Synergy Mx multimode plate reader and the viability of cells were plotted as percentage of controls. Human PC3 prostate cancer cells were cultured in a microfluidic chip for 16 h and the chip was placed in a hypoxia chamber and pre-conditioned at <1% oxygen before treating the cells with various concentrations of

synthesized compounds. Apoptosis was assayed using Annexin V and Sytox Green dye as previously reported.¹⁹⁰

2.4.2.3. Complex II Inhibition Assay

Mitochondria were isolated from fresh rat hearts by differential centrifugation in sucrose-based buffer as previously described.⁵⁴ Complex II enzymatic activity was determined spectrophotometrically as the rate of succinate-driven, coenzyme Q2-linked reduction of dichlorophenolindophenol (DCPIP).¹⁹¹ Mitochondria or sub-mitochondrial particles were incubated in phosphate buffer (pH 7.4) containing 40 μM DCPIP, 1 mM KCN, 10 μM rotenone, and 50 μM coenzyme Q2. The rate of reduction of DCPIP to DCPIPH₂ was followed at 600 nm ($\epsilon = 21 \text{ mM}^{-1}\text{cm}^{-1}$). The reaction was initiated by addition of succinate (10 mM), and varying amounts of inhibitors were used to determine an IC₅₀ value. At the end of each run thenoyltrifluoroacetone (1 mM) was added and the residual TTFA-insensitive rate subtracted.

3.4.2.4. Complex I Inhibition Assay

Complex I (NADH ubiquinone-oxidoreductase) was measured spectrophotometrically (340 nm) in frozen/ thawed mouse cardiac mitochondria, as the rotenone-sensitive oxidation of NADH (40 μM) in the presence of coenzyme Q1 (10 μM), in phosphate buffer at pH 7.2, according to literature procedures.¹⁹²

2.4.2.5. Stability Testing of CII Inhibitor 16c

The CII inhibitor **16c** (2 mM in DMSO, final concentration 2 μM) was incubated with Murine Liver S9 fraction (Lot VLH) and Phase I (NADPH Regenerating System) cofactors

for 0-240 minutes. Reactions were quenched with a 500 μ L (1:1) of a MeOH/(+)-IS, vortexed for 15 seconds, incubated at RT for 10 minutes and spun for 5 minutes at 2400 rpms. Supernatant (1 mL) was then transferred to an eppendorf tube and spun in a tabletop, chilled centrifuge for 5 minutes at 13.2 K rpms. Supernatant (800 μ L) was transferred to an HPLC vial (w/out insert) and analyzed by HPLC/MS by using the following parameters: Ion Source/Gas Parameters: CUR = 50, CAD = low, IS = 4500, TEM = 700, GS1 = 70, GS2 = 70. Buffer A: Water + 0.1% formic acid; Buffer B: MeOH + 0.1% formic acid; flow rate 1.5 mL/min; column Agilent C18 XDB column, 5 micron packing 50 X 4.6 mm size ; 0-1.5 min 97% A, 1.5-2.0 min gradient to 100% B, 2.0 - 3.5 min 100% B, 3.5-3.6 min gradient to 97% A, 3.6-4.5 97% A; IS: tolbutamide (transition 271.2 to 91.2); **16c** transition 270.089 to 151.2.

2.4.2.6. Assessment of Metabolic Parameters

Changes in oxygen consumption rate were measured using a XF24 Extracellular Flux Analyzer (Seahorse Bioscience, Billerica, MA). The human prostate carcinoma cells (22Rv1) were plated in XF24 well plates (40000 cells per well) and allowed to adapt overnight. Treatments were performed with **16c** at concentrations of 1, 10, 20, 30, 50 and 100 μ M and incubated for 48 h. Mitochondrial Stress test was performed using oligomycin (10 μ M), FCCP (5 μ M) and rotenone/antimycin A (5 μ M) based on the manufacturer's recommended protocol.¹⁹³

2.4.2.7. Statistical Analysis

Experiments were repeated at least thrice, and the statistical significance was calculated using the one-way ANOVA. A p value of <0.05 was considered statistically significant. IC₅₀ values were calculated by GraphPad prism software.

Chapter 3. Structure-Activity Relationship Studies of Diazoxide Derivatives as Antineoplastic Agents

3.1. Introduction

In drug discovery, targeting metabolic pathways of cancer has emerged as an appealing strategy for the development of selective antineoplastic agents.⁹ The mitochondrial respiratory complex II plays a vital role in mitochondrial metabolism, where it catalyzes the oxidation of succinate to fumarate and the reduction of ubiquinone to ubiquinol. The Food and Drug Administration approved clinical vasodilator drug diazoxide (DZX) has a reported mitochondrial complex II inhibition IC_{50} value of 32 μM in rat heart mitochondria,⁷⁶ and is known to regulate reactive oxygen species production, protecting normal cells from ischemic damage and also inducing specific cancer cell death.⁷⁷ Benefits, as well as drawbacks and a narrow therapeutic window have been observed from DZX administration across different tissues and organelles. In the pancreas, DZX opens K_{ATP} channels, the closing of which is required for glucose-induced insulin secretion (GSIS) in pancreatic beta cells, thus insulin secretion is blocked, and hypoglycemia prevented.¹⁹⁴ In the context of ischemia, DZX can regulate ROS production and confer protection.⁸¹ However, further reports found that high doses of DZX (750 μM) led to increased levels of ROS.^{82, 83} In cortical neuron mitochondria <200 μM of DZX had no effect on mitochondria, but a 300 μM dose did result in depolarization.⁸² Further, a 100 μM concentration of DZX was reported to inhibit CII in mouse heart mitochondrial but IC_{50} was not reached.⁵⁶ Diazoxide has been shown to have neuroprotective properties in animal models of Alzheimer's disease,^{84, 85} protect neurons from a range of neurotoxic insults, including exposure to amyloid- β peptide (25-35),⁸⁶ and was reported to reduce proliferation in both acute leukemic T cells,⁸⁷ and triple negative breast cancer (TNBC)

MDA-MB-468 cells.⁸⁵ One mechanism of action of this observed cytotoxicity was attributed to the downregulation of beta-catenin-mediated cyclin D1 transcription.⁸⁸ A new study shows that some benzothiadiazine derivatives are potent and selective PI3K δ inhibitors for treating β -cell-mediated malignancies.¹⁹⁵ No studies have been reported, to the best of our knowledge, to probe the structure-activity relationship of DZX for either CII inhibition or antineoplastic activity.¹⁹⁶

Herein, we report the synthesis of a library of novel DZX derivatives to understand structural effect on CII inhibition activity and antineoplastic effect in 22Rv1 prostate cancer cells and the TNBC MDA-MB-468 cell line. In the current project, the DZX parent compound exhibited no CII inhibition activity at 100 μ M (IC_{50} was found to be 1236 μ M) which corresponded to no effect to reduce cell viability of either prostate or breast cancer cells at 100 μ M up to 72 hours. Several derivatives were identified that possessed enhanced CII inhibition (IC_{50} values 11.88 - 89 μ M) over DZX but which did not significantly reduce cell viability in either cancer cell line. Importantly, many DZX derivatives were identified that possessed potent and selective activity to reduce TNBC cell viability more than the clinical agent 5-fluorouracil, representing novel hit compounds for further optimization as potential chemotherapeutics for this difficult to treat cancer.

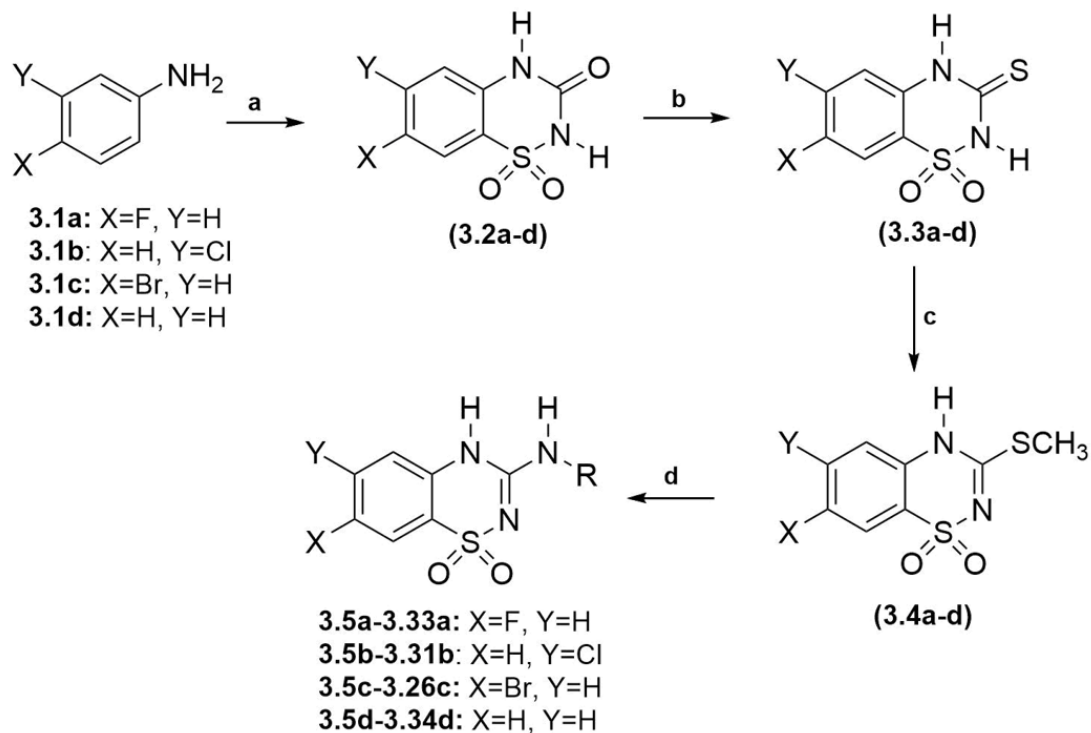
3.2. Results and Discussion

3.2.1. Chemistry

The parent compound diazoxide (7-chloro-3-methyl-2H-1,2,4-benzothiadiazine 1,1-dioxide) (**3**) can be accessed by a number of reported syntheses, our adopted route blends elements of several.^{194, 197-200} Additionally, a number of alkyl chain derivatives of **3** have been synthesized as K_{ATP} channel activators that are selective to pancreatic β -cells,

although no determination of antineoplastic effects of these compounds have been reported.¹⁹⁷ We sought to modify the side chain through different primary amine also through different halogen substitutes in the phenyl ring of the DZX structure.

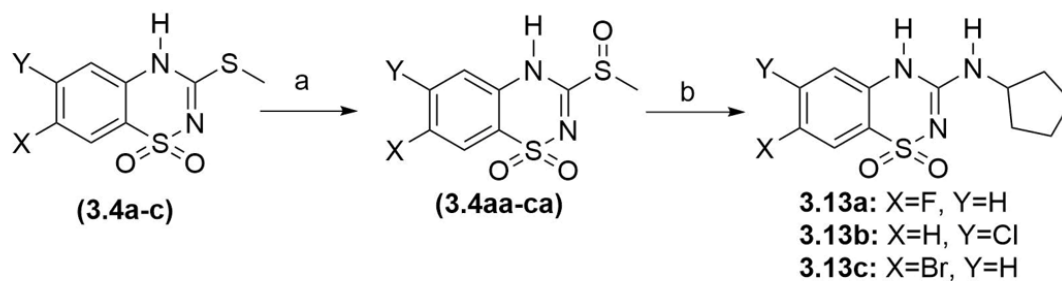
Halogen substituted DZX analogues at the 4- or 5- position of the phenyl ring were accessed in good yield over four steps (**Scheme 3.1**) starting from commercially available substituted aniline (**3.1a-d**). Electrophilic substitution of the appropriate aniline with chlorosulfonyl isocyanate in the presence of anhydrous aluminum chloride and nitromethane resulted in ring closure to yield 6- and 7-halo-3-oxo-3,4-dihydro-2H-1,2,4-benzothiadiazine-1,1-dioxides (**3.2a-c**), or 3-oxo-3,4-dihydro-2H-1,2,4-benzothiadiazine-1,1-dioxides (**3.2d**) in moderate yield.¹⁹⁷ Subsequently, the 3-oxo compounds (**3.2a-d**) were converted into the corresponding 3-thioxo derivatives (**3.3a-d**) by reacting with phosphorus pentasulfide in anhydrous pyridine under reflux (**Table 3.1**).¹⁹⁴ Methylation of **3.3a-d** was accomplished with methyl iodide in 1:1 hydromethanolic solution of sodium bicarbonate to yield the desired 3-methylsulfide intermediates (**3.4a-d**) in good yield.¹⁹⁸ Nucleophilic substitution of these intermediates with the corresponding primary amine was accomplished with overnight heating at 130 °C in a sealed vessel to afford the desired DZX derivatives (**Tables 3.2-3.5**).²⁰¹ Several synthesis analogues with secondary amines and aniline was failed to react with 3-methylsulfide intermediates (**3.4a-d**). The reason of that could refer to the high resonance in these amines which prevents the reaction.¹⁹⁶



Scheme 3.1. Synthesis of diazoxide derivatives. *Reagents and Conditions:* **a)** chlorosulfonyl isocyanate, CH_3NO_2 , $-5\text{ }^\circ\text{C}$, AlCl_3 , $100\text{ }^\circ\text{C}$, 1 h, 53-64%; **b)** P_2S_5 , anhydrous pyridine, $115\text{ }^\circ\text{C}$, 12 h, 50-58%; **c)** NaHCO_3 , CH_3I , $\text{CH}_3\text{OH}/\text{H}_2\text{O}$, RT, 81-90%; **d)** RNH_2 , sealed tube, $130\text{ }^\circ\text{C}$, 42-88%.

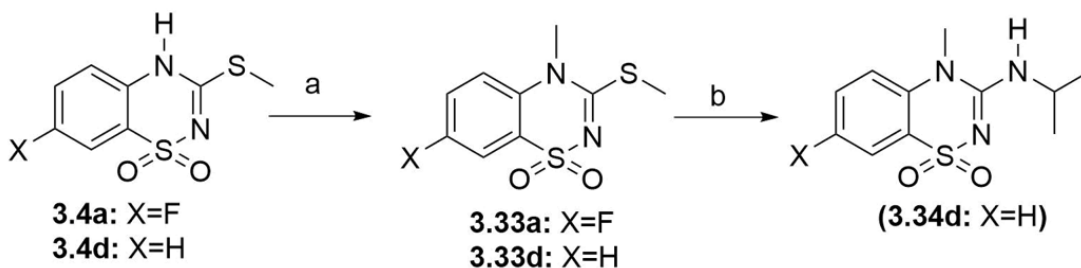
Derivatives possessing a cyclopentyl substituted amine could not be obtained in sufficient yield from the methylsulfide intermediates **3.4a-c** due to the increased steric bulk. To increase the reactivity of **3.4a-c** to nucleophilic substitution, the methylsulfides were oxidized to the corresponding 3-methylsulfinyl intermediates (**3.4aa-ca**) (**Scheme 3.2**). Subsequently these intermediates were reacted with cyclopentamine to yield DZX derivatives **3.13a-c**.¹⁹⁹

Access to the *N*-methylated DZX derivative (**3.34d**) was achieved (**Scheme 3.3**) by exposing methylsulfides **3.4a** and **3.4d** to methyl iodide in the presence of base to provide corresponding intermediates 7-fluoro-4-methyl-3-(methylthio)-4*H*-benzo[e][1,2,4]thiadiazine 1,1-dioxide (**3.33a**) and 4-methyl-3-(methylthio)-4*H*-benzo[e][1,2,4]thiadiazine 1,1-dioxide (**3.33d**), respectively. Subsequent nucleophilic substitution with isopropylamine yield 3-(isopropylamino)-4-methyl-4*H*-1,2,4benzothiadiazine 1,1-dioxide (**3.34d**).²⁰²



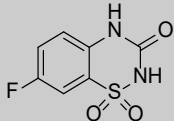
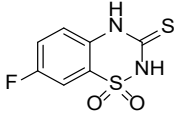
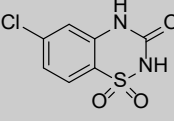
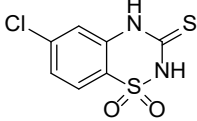
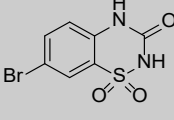
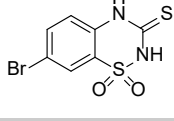
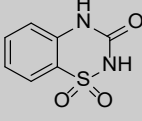
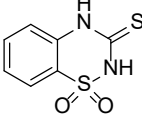
Scheme 3.2. Synthesis of diazoxide derivative with bulky alkyl amino group.

Reagents and Conditions: **a)** Na_2CO_3 , Br_2 , H_2O , RT, 75-91%; **b)** cyclopentamine, 1,4-dioxane, sealed tube, 130°C , 49-68%.



Scheme 3.3. Synthesis of diazoxide derivative with alkyl group in position 4.

Reagents and Conditions: **a)** K_2CO_3 , CH_3I , $\text{CH}_3\text{CN}/\text{DMF}$, RT, 76-89%; **b)** isopropylamine, 1,4-dioxane, sealed tube, 130°C , 55%.

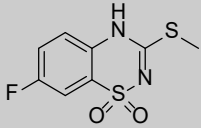
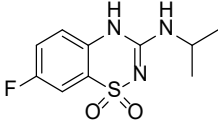
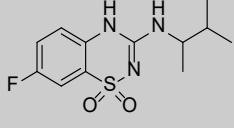
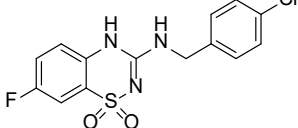
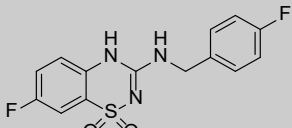
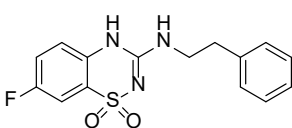
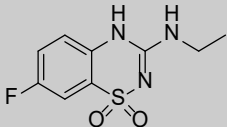
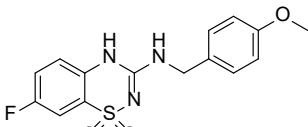
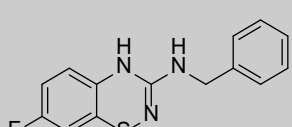
Compound	Structure	Mw	cLogP ^a	PSA ^b	% CII activity (100 μ M) ^c
3.2a		216.19	0.95	75.27	6 \pm 1.5
3.3a		232.25	0.76	58.20	0
3.2b		232.64	1.52	75.27	0
3.3b		248.70	1.33	58.20	81 \pm 6.9
3.2c		277.09	1.67	75.27	0
3.3c		293.15	1.48	58.20	55 \pm 15.2
3.2d		198.20	0.49	75.27	0
3.3d		214.26	0.36	58.20	2 \pm 5.8

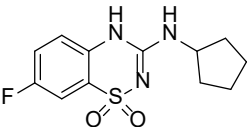
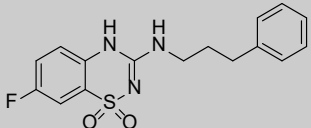
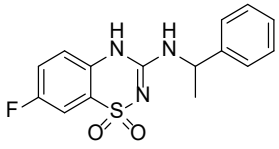
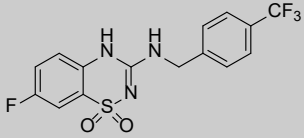
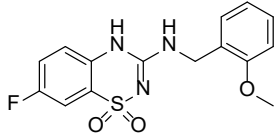
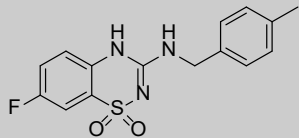
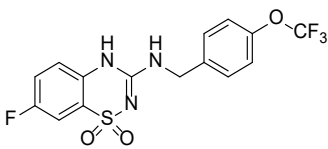
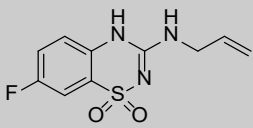
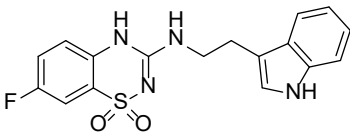
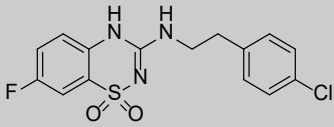
^a Calculated by ChemDraw Professional 16.0.

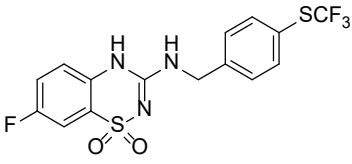
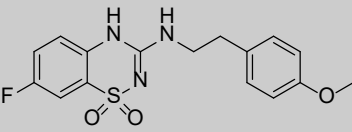
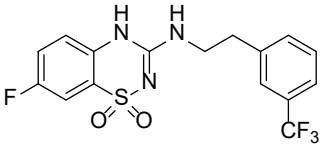
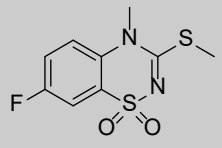
^b Polar surface area (pH 7.4), calculated by ChemDraw Professional 16.0.

^c Values represent the mean \pm SD of n = 4 experiments.

Table 3.1. Structure, molecular weight, calculated logP, and PSA of diazoxide derivatives **3.2a-d** and **3.3a-d**.

Compound	Structure	Mw	cLogP ^a	PSA ^b	% CII activity (100 μ M) ^c
3.4a		246.27	0.97	58.53	0
3.5a		257.28	0.73	70.56	4 \pm 6.9
3.6a		285.34	1.66	70.56	5 \pm 4.5
3.7a		339.77	2.37	70.56	30 \pm 6.5
3.8a		323.32	1.80	70.56	1 \pm 6.2
3.9a		319.35	1.99	70.56	4 \pm 15.5
3.10a		243.26	0.42	70.56	0
3.11a		335.35	1.58	79.79	0
3.12a		305.33	1.66	70.56	0

3.13a		283.32	1.36	70.56	1 ±4.7
3.14a		333.38	2.37	70.56	14 ±10.4
3.15a		319.35	1.97	70.56	22 ±9.9
3.16a		373.33	2.54	70.56	6 ±15.7
3.17a		335.35	1.58	79.79	27 ±5.6
3.18a		319.35	2.16	70.56	23 ±9.9
3.21a		389.32	2.69	79.79	2 ±6.9
3.23a		255.27	0.67	70.56	38 ±7.8
3.27a		358.39	1.98	82.59	17 ±8.2
3.28a		353.80	2.70	70.56	34 ±18.4

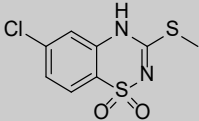
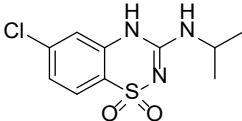
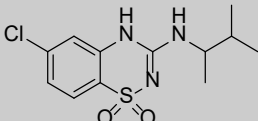
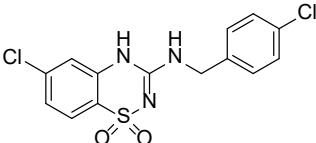
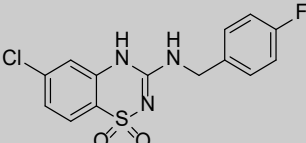
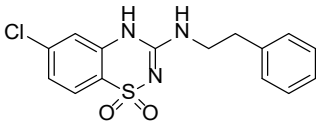
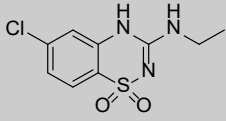
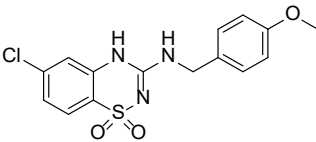
3.29a		405.39	3.33	70.56	23 ±12.3
3.30a		349.38	1.91	79.79	18 ±6.2
3.32a		387.35	2.87	70.56	20 ±5.2
3.33a		290.30	1.84	49.74	6 ±13.4

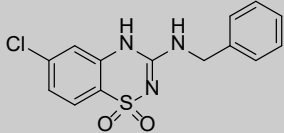
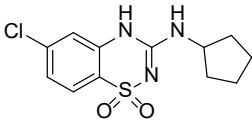
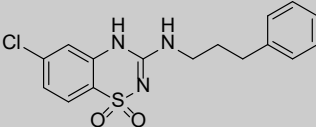
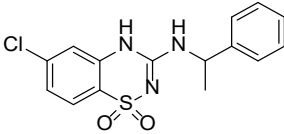
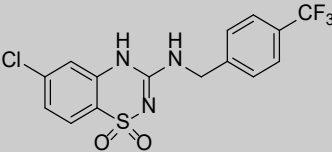
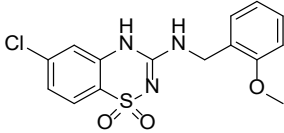
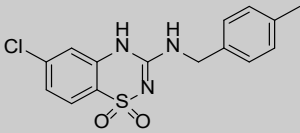
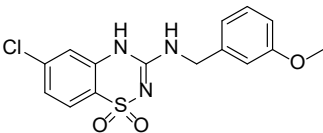
^a Calculated by ChemDraw Professional 16.0.

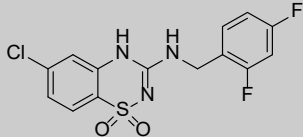
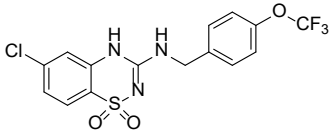
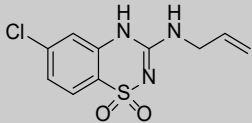
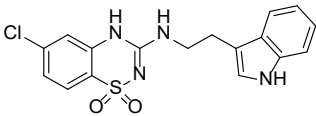
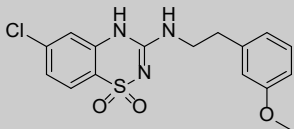
^b Polar surface area (pH 7.4), calculated by ChemDraw Professional 16.0.

^c Values represent the mean ±SD of n = 4 experiments.

Table 3.2. Structure, molecular weight, calculated logP, and PSA of diazoxide derivatives with 7-fluoro substitution.

Compound	Structure	Mw	cLogP ^a	PSA ^b	% CII activity (100 μ M) ^c
3.4b		262.73	1.54	58.53	24 \pm 0.7
3.5b		273.74	1.30	70.56	0
3.6b		301.79	2.23	70.56	0
3.7b		356.22	2.94	70.56	34 \pm 1.2
3.8b		339.77	2.37	70.56	0
3.9b		335.81	2.56	70.56	19 \pm 22.6
3.10b		259.71	0.99	70.56	0
3.11b		351.81	2.15	79.79	17 \pm 4.2

3.12b		321.78	2.23	70.56	0
3.13b		299.77	1.93	70.56	27 ±19.8
3.14b		349.83	2.94	70.56	30 ±14.0
3.15b		335.81	2.54	70.56	51 ±13.9
3.16b		389.28	3.11	70.56	19 ±10.1
3.17b		351.81	2.15	79.79	0
3.18b		335.81	2.73	70.56	17 ±8.9
3.19b		351.81	2.15	79.79	24 ±19.2

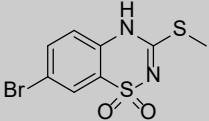
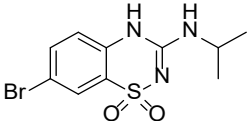
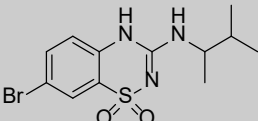
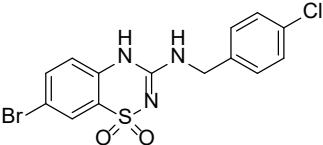
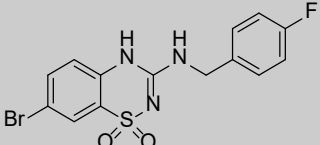
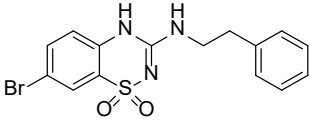
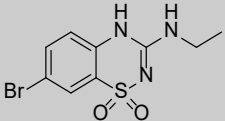
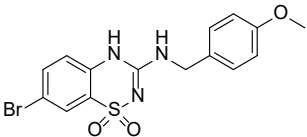
3.20b		357.76	2.52	70.56	15 ±2.8
3.21b		405.78	3.36	79.79	0
3.23b		271.72	1.24	70.56	0
3.27b		374.84	1.98	82.59	25 ±19
3.31b		365.83	2.48	79.79	24 ±14.1

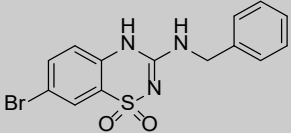
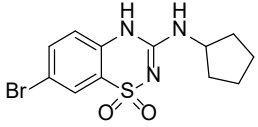
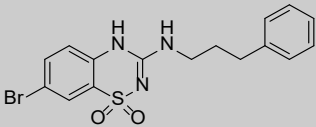
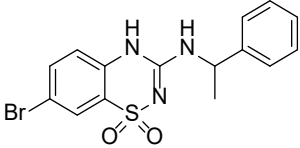
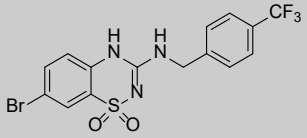
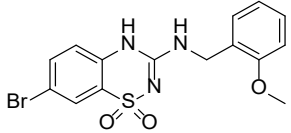
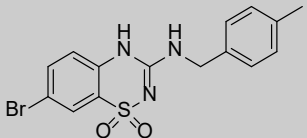
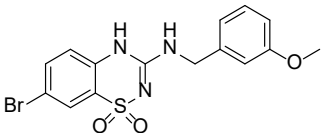
^a Calculated by ChemDraw Professional 16.0.

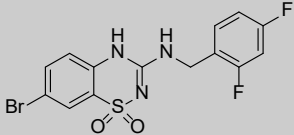
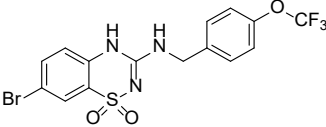
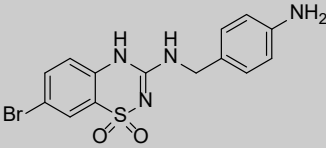
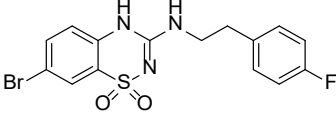
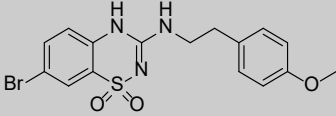
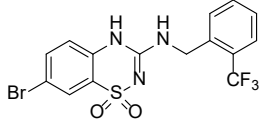
^b Polar surface area (pH 7.4), calculated by ChemDraw Professional 16.0.

^c Values represent the mean ±SD of n = 4 experiments.

Table 3.3. Structure, molecular weight, calculated logP, and PSA of diazoxide derivatives with 6-chloro substitution.

Compound	Structure	Mw	cLogP ^a	PSA ^b	% CII activity (100 μ M) ^c
3.4c		307.18	1.69	58.53	10 \pm 2.7
3.5c		318.19	1.45	70.56	0
3.6c		346.24	2.38	70.56	19 \pm 10.4
3.7c		400.68	3.09	70.56	45 \pm 5.6
3.8c		384.22	2.52	70.56	35 \pm 9.9
3.9c		380.26	2.71	70.56	37 \pm 4.7
3.10c		304.16	1.14	70.56	11 \pm 6.9
3.11c		396.26	2.30	79.79	64 \pm 15.3

3.12c		366.23	2.38	70.56	36 ±9
3.13c		344.23	2.08	70.56	25 ±7.8
3.14c		394.29	3.09	70.56	46 ±13.4
3.15c		380.26	2.69	70.56	55 ±8.2
3.16c		434.23	3.26	70.56	0
3.17c		396.26	2.30	79.79	44 ±12.3
3.18c		380.26	2.88	70.56	29 ±6.2
3.19c		396.26	2.30	79.79	24 ±5.2

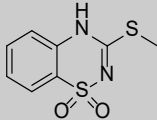
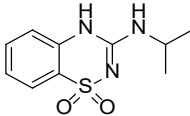
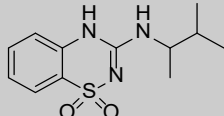
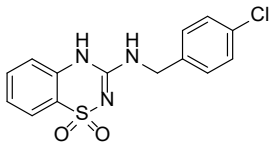
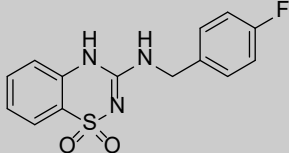
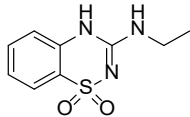
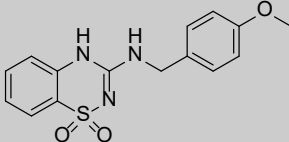
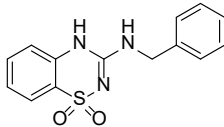
3.20c		402.21	2.67	70.56	38 ±4.5
3.21c		450.23	3.41	79.79	22 ±21.1
3.22c		381.25	1.15	96.58	9 ±6
3.24c		398.25	2.85	70.56	45 ±17.1
3.25c		410.29	2.63	79.79	17 ±3.3
3.26c		434.23	3.26	70.56	29 ±5.9

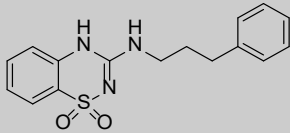
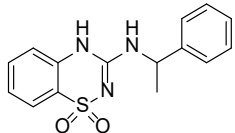
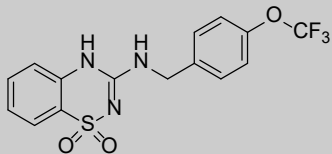
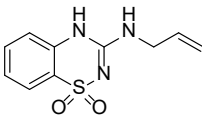
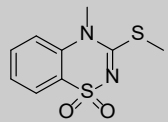
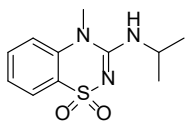
^a Calculated by ChemDraw Professional 16.0.

^b Polar surface area (pH 7.4), calculated by ChemDraw Professional 16.0.

^c Values represent the mean ±SD of n = 4 experiments

Table 3.4. Structure, molecular weight, calculated logP, and PSA of diazoxide derivatives with 7-bromo substitution.

Compound	Structure	Mw	cLogP ^a	PSA ^b	% CII activity (100 μ M) ^c
3.4d		228.28	1.69	58.53	4 \pm 5.5
3.5d		239.29	0.59	70.56	0
3.6d		267.35	1.51	70.56	0
3.7d		321.78	2.23	70.56	0
3.8d		305.33	1.66	70.56	7 \pm 9.9
3.10d		225.27	0.28	70.56	0
3.11d		317.36	1.44	79.79	0
3.12d		287.34	1.51	70.56	0

3.14d		315.39	2.22	70.56	0
3.15d		301.36	1.83	70.56	0
3.21d		371.33	2.54	79.79	7 ±6.2
3.23d		237.28	0.52	70.56	2 ±12.3
3.33d		242.31	1.69	49.74	0
3.34d		253.32	1.46	61.77	0

^a Calculated by ChemDraw Professional 16.0.

^b Polar surface area (pH 7.4), calculated by ChemDraw Professional 16.0.

^c Values represent the mean ±SD of n = 4 experiments.

Table 3.5. Structure, molecular weight, calculated logP, and PSA of diazoxide derivatives with a non-halogenated ring.

3.2.2. Complex II Inhibition Assay

Mitochondrial respiratory complex II activity was measured spectrophotometrically by our collaborators at the University of Rochester Medical Center using isolated mouse liver mitochondria, with suitable modifications to ensure rapid isolation as previously described.²⁰³ The natural product, and potent CII inhibitor, Atpenin A5 with $IC_{50} = 3.3$ nM,^{54, 89} was employed as a positive control with dimethyl sulfoxide (DMSO) as a negative control. The parent compound DZX was found to be inactive in our assay with no inhibition activity at 100 μ M and has a calculated IC_{50} of >1000 μ M (**Table 3.6**) compared with the value of 32 μ M reported in the literature.⁷⁶ It should be noted that the literature CII IC_{50} was determined in rat heart mitochondria while in this study, we employed mouse liver mitochondria, which may account for this apparent discrepancy. The positive control compound AA5 induced 93% inhibition at 0.1 μ M, validating the assay protocol. To unequivocally associate this activity to the parent compound, we employed both synthesized and commercially acquired samples of DZX. The inactivity was confirmed in the prostate and breast cancer cell lines wherein DZX had no effect on cell viability (see below). Literature studies employing DZX mostly employ a concentration much greater than the reported 32 μ M IC_{50} value, with some experiments performed at concentrations up to 750 μ M.^{76, 82, 83}

Undeterred by the apparent lack of CII inhibition activity of the parent compound ($IC_{50} = 1236$ μ M), we continued to screen derivatives of DZX for CII inhibition. All the synthesized derivatives were initially screened at 100 μ M. Halogen substitution on the benzothiadiazine ring provided increased CII inhibition activity over saturated counterparts. Among 7-fluorobenzothiadiazine substituted derivatives (**Figure 3.1A**), 4-chlorobenzylamine (**3.7a**) provided 30% inhibition whereas 2-phenylpropylamine (**3.9a**) provided 5% inhibition. When the chain length was extended, the 3-phenylpropylamine

(**3.14a**) induced 14% inhibition. When the chain length was extended, the 4-chlorophenethylamine derivative (**3.28a**) induced 34% inhibition. Replacement of the electron-withdrawing chlorine on the side chain benzylamine with an electron-donating methyl substituent to afford 4-methylbenzylamine derivative **3.18a** decreased inhibition to 23%. Replacement with a highly electron withdrawing trifluoromethyl substituent (**3.16a**) afforded an inactive compound (7% inhibition at 100 μ M) while the 2-methoxybenzylamine (**3.17a**) induced 37% inhibition. The most active derivative of the 7-fluoro series was allylamine **3.23a**, inducing 38% inhibition, equipotent with **3.17a**, indicating that a side chain containing an aromatic ring is not required for activity.

When the 7-fluoro substituent on the benzothiadiazine ring was switched to a 6-chloro substituent (**Figure 3.1B**) the unfunctionalized thiourea derivative (**3.3b**) exhibited startlingly potent inhibition activity (81% inhibition at 100 μ M). However, the chromophoric nature of the compound was determined to interfere with the assay readout, leading to what we postulate to be a false positive. An in silico pan-assay interfering compounds (PAINS)²⁰⁴ filter did not predict this scaffold to be a PAINS. The 4-chlorobenzylamine derivative (**3.7b**) induced 34% inhibition, equipotent with its 7-fluoro benzothiadiazine substituted counterpart **3.7a**. Cyclopentamine derivative **3.13b** induced 27% inhibition, substantially more active than the respective 7-fluoro benzothiadiazine substituted compound **3.13a** (inactive). The *H*-Indole-3-ethylamine side chain substituted compound (**3.27b**) induced 25% inhibition. The 7-fluoro benzothiadiazine substituted derivatives with the same side chain; 3-phenylpropylamine (**3.14a**) induces just 14% inhibition while *H*-Indole-3-ethylamine (**3.27a**) is equipotent. The most active derivative from the 6-chloro series possessed a 1-phenylethylamine side chain (**3.15b**) inducing 51% CII inhibition at 100 μ M, possibly indicating a role for the phenyl ring in pi-pi stacking at this position of the

molecule. Overall, the 6-chloro substitution pattern on the benzothiadiazine ring provided no appreciable increase in CII inhibition activity compared to 7-fluoro substitution.

When the 7-fluoro substituent on the benzothiadiazine ring was interchanged with 7-bromo substitution the inhibitory activity of the derivatives notably increased (**Figure 3.1C**). The unfunctionalized thiourea derivative **3.3c** was active, inducing 55% inhibition of CII at 100 μ M, compared with 81% with the 6-chloro substituted benzothiadiazine. However, the chromophore of the compound was again found to interfere with the assay read out. The 4-chlorobenzylamine derivative (**3.7c**) induced 45% CII inhibition at 100 μ M with the 7-bromo substituted benzothiadiazine ring, conferring increased activity over its 7-fluoro (**3.7b**) and 6-chloro (**3.7a**) counterparts and in contrast to the inactive unsubstituted derivative **3.7d**. Equipotent inhibition to **3.7c** was noted with 3-phenylpropylamine (**3.14c**), which induced 46% inhibition. Again the 7-bromo substituted benzothiadiazine ring was more active than the 6-chloro substituted 3-phenylpropylamine (**3.14a**) and the unsubstituted derivative **3.14d**, which induced 14% and 0% inhibition, respectively. The 1-phenylethylamine derivative (**3.15c**) induced 55% inhibition of CII at 100 μ M, equipotent with its 6-chloro counterpart (**3.15b**). On the other hand, 1-phenylethylamine (**3.15a**) as a side chain will have CII inhibition by 24%. The most active compound identified in this study outside of the chromophoric false positives, 4-methoxybenzylamine (**3.11c**), induced 64% inhibition at 100 μ M. Derivatives possessing an unsubstituted benzothiadiazine ring (**Figure 3.1D**), exhibited no inhibition of CII at 100 μ M. Increasing the treatment doses to 1mM for some DZX derivatives, the CII inhibition increased significantly. 7-Fluoro-3-thioxo-3,4-dihydro-2*H*-1,2,4-benzothiadiazine 1,1-dioxide (**3.3a**) and 6-chloro-3-thioxo-3,4-dihydro-2*H*-1,2,4-benzothiadiazine 1,1-dioxide (**3.3b**) have CII inhibition 97.4%, 91.5%, respectively. Also, the inhibition of CII for 7-bromo-3-thioxo-3,4-dihydro-2*H*-1,2,4-benzothiadiazine 1,1-dioxide (**3.3c**) increased by

96.8%. 7-Fluoro-3-methylsulfanyl-4*H*-1,2,4-benzothiadiazine 1,1-Dioxide (**3.4a**) and 6-chloro-3-((3-methylbutan-2-yl)amino)-4*H*-benzo[e][1,2,4]thia-diazine 1,1-dioxide (**3.6b**) inhibit the CII by 44% and 42%, respectively (**Figure 3.2**).

A preliminary structure-activity relationship can be derived for CII inhibition activity of this scaffold. Halogen substitution at the 6- or 7- position of the benzothiadiazine ring affords for inhibition activity which is completely absent from the respective non-halogenated derivatives. Of all halogen substituents evaluated herein, 7-bromo represents the most active inhibitors. The side chain derivatives require either aromatic or possibly allyl (in the case of a 7-F substituted benzothiadiazine ring, but interestingly not when combined with 6-Cl substitution) moieties to confer CII inhibition activity. However, no clear chain substituent pattern can be derived beyond 4-CF₃ is deleterious to activity (**3.16a** and **3.16c** confer 0% inhibition while **3.16b** induces only 19% inhibition). Alkyl side chains yield inactive compounds; however, a cyclopentane ring does provide some activity (approximately 25% inhibition).¹⁹⁶

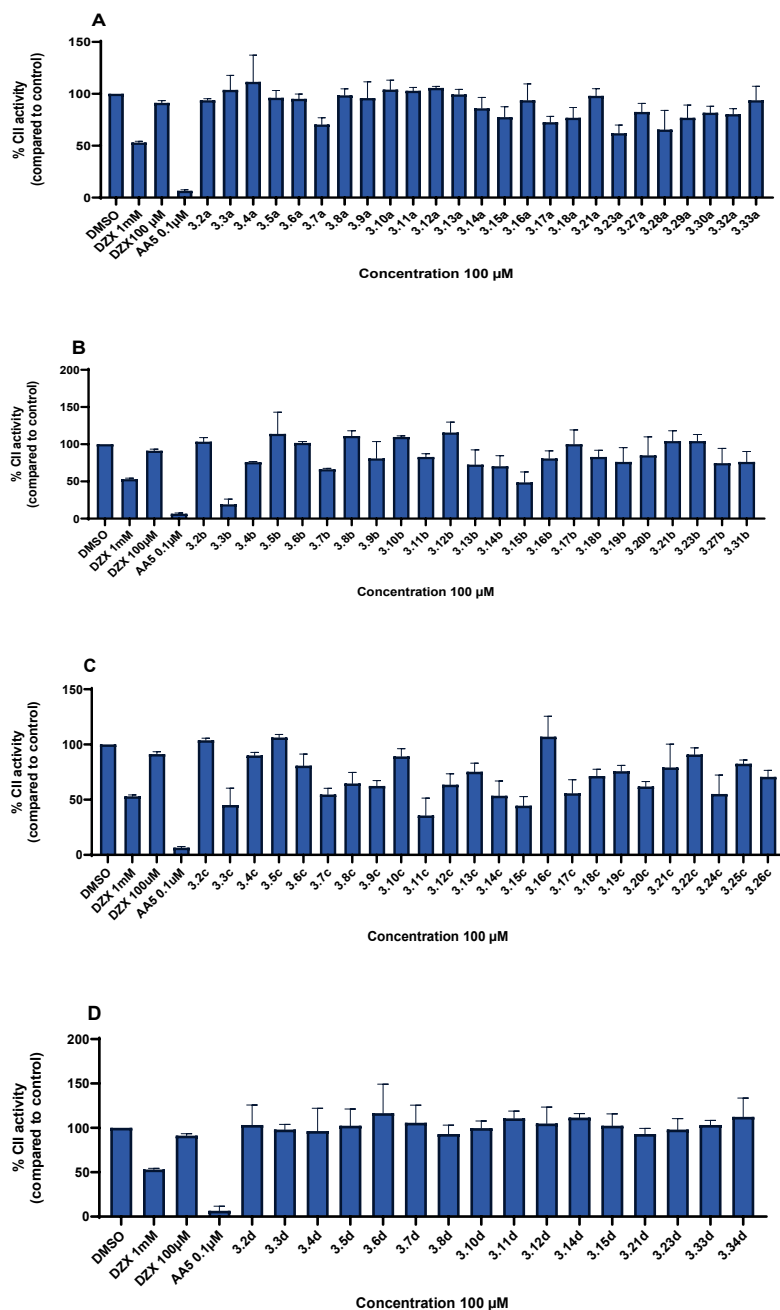


Figure 3.1. Percentage inhibition of mitochondrial complex II relative to DMSO control at 100 μ M concentration of diazoxide derivatives. A) Complex II inhibitory activity for diazoxide derivatives with 7-fluoro substitution. **B)** Complex II inhibitory activity for diazoxide derivatives with 6-chloro substitution. **C)** Complex II inhibitory activity for diazoxide derivatives with 7-bromo substitution. **D)** Complex II inhibitory activity for diazoxide derivatives with a non-halogenated ring. Values represent the mean \pm SD of n = 4 experiments.

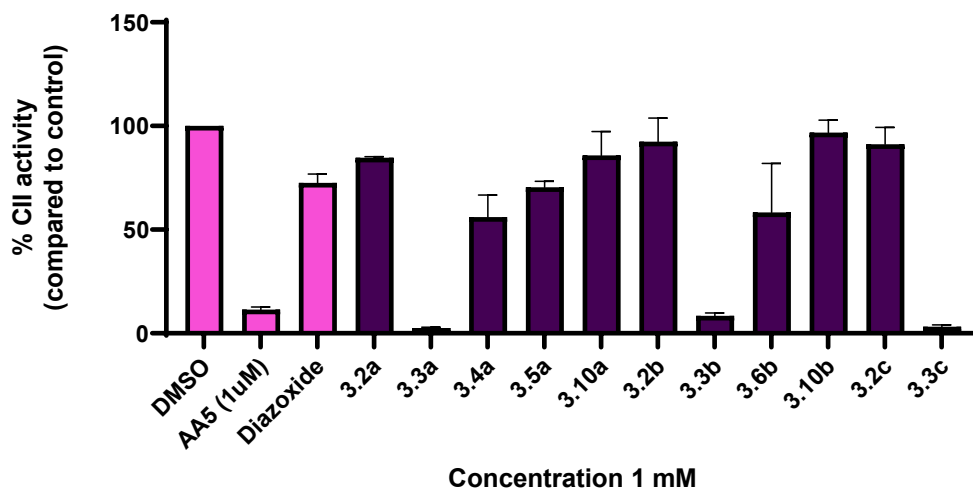


Figure 3.2. Percentage inhibition of mitochondrial complex II relative to DMSO control at 1 mM concentration of diazoxide derivatives. Values represent the mean of three separate experiments performed in triplicate.

The five most active CII inhibitors at 100 μM (**3.3b**, 81% inhibition; **3.3c**, 55%; **3.11c**, 64%; **3.15b**, 51% and **3.15c**, 55%), the parent compound DZX (9% inhibition at 100 μM) and positive control atpenin A5 (93% inhibition at 0.1 μM) were selected for IC_{50} determination (**Table 3.6**). The parent compound **DZX** possessed an $\text{IC}_{50} = 1236 \mu\text{M}$ in our CII inhibition assay, greatly reduced over the 32 μM IC_{50} reported in the literature.⁷⁶ Positive control compound **AA5** possessed an $\text{IC}_{50} = 3.3 \text{ nM}$, in accordance with literature values.²⁰⁴ The two unfunctionalized sulfonylureas **3.3b** and **3.3c** displayed the most potent IC_{50} values of 11.88 and 36.98 μM respectively, as expected from the initial compound screen at 100 μM . However, it should again be noted we expect these compounds to be false positives. The most active compound identified in the initial screen **3.11c**, possessed an $\text{IC}_{50} = 79.68 \mu\text{M}$. The 6-chloro substituted 1-phenylethylamine side chain derivative **3.15b** possessed an $\text{IC}_{50} = 89.01 \mu\text{M}$ and its 7-bromo counterpart (**3.15c**) an $\text{IC}_{50} = 79.82 \mu\text{M}$. The 6-chloro substituted 2,4-difluorobenzylamine side chain derivative **3.20b** possessed an $\text{IC}_{50} = 1100 \mu\text{M}$. The obtained IC_{50} values directly correlate with the activity pattern obtained in the initial screen conducted at 100 μM . Several novel DZX derivatives have been identified with significantly increased activity to inhibit CII, with the most active compounds conferring >15-fold increased potency over the parent compound.

Compound	Structure	CII IC ₅₀ (μM) ^a
Diazoxide		1236.0 ±2.5
Atpenin A5		0.0033 ±2.0
3.3b		11.88* ±3.3
3.3c		36.98* ±2.4
3.11c		79.68 ±4
3.15c		79.82 ±4.1
3.15b		89.01 ±10.4
3.20b		1100.0 ±6.7

^aValues are the mean ±SD of n = 4 experiments.

*Probable interference.

Table 3.6. Mitochondrial respiratory complex II IC₅₀ values of selected diazoxide derivatives.

3.2.3. Cytotoxicity Assay

The cytotoxicity of DZX and its derivatives at 100 μ M concentration was determined in 22Rv1 human prostate cancer cell line after 48 hours treatment employing the MTS assay as previously reported.^{205, 206} Atpenin A5 derivative **16c** which possesses a CII IC_{50} = 64 nM and a 'drug-like' ligand-lipophilicity efficiency of 5.62 was employed as a positive control with dimethyl sulfoxide (DMSO) as negative control. This compound has been previously reported by our lab to reduce cell viability of 22Rv1 cells.²³ In this assay, compound AA5 analogue **16c** provided a significant inhibitory effect at 20 μ M concentration, reducing cell viability by 60%. The parent compound DZX, despite lacking any CII inhibition activity at 100 μ M, reduced 22Rv1 prostate cancer cell survival by 12% (**Figure 3.3**), possibly due to the aforementioned ability of the compound to down regulate beta-catenin-mediated cyclin D1 transcription.⁸⁸

The 7-fluorobenzothiadiazine substituted derivatives generally conferred the least effect on 22Rv1 prostate cancer cell viability at 100 μ M of all the halogen substituted derivatives. The most potent CII inhibitor from this series, allylamine (**3.23a**) displaying 38% CII inhibition, afforded 24% reduction of cell viability (**Figure 3.3A**). However, this derivative was not the most cytotoxic in the 22Rv1 cells; 1-phenylethylamine (**3.15a**) which possess 22% CII inhibition affords 34% reduction in cell viability while the 3-indoleethylamine derivative (**3.27a**) which possesses 17% CII inhibition activity induces 30% reduction of cell viability in 22Rv1 cells. The 4-chlorobenzylamine **3.7a** (30% CII inhibition) and 4-chlorophenethylamine homologue **3.28a** (34% CII inhibition) both proved inactive in 22Rv1 cells. The cyclopentylamine side chain (**3.13a**) (0% CII inhibition), 3-phenylpropylamine (**3.14a**) (14% CII inhibition) and 2-Methoxybenzylamine (**3.17a**) (28% CII inhibition) reduces cell survival of 22Rv1 cells by approximately 27%.

From the 6-chlorobenzothiadiazine substituted derivatives, the most active compound 1-phenylethylamine (**3.15b**) (51% CII inhibition at 100 μ M, IC_{50} = 89.0 \pm 10.4 μ M) afforded a 50% reduction in 22Rv1 cell viability (**Figure 3.3B**). The cyclopentamine derivative (**3.13b**) which afforded a 34% reduction in cell viability was the next most active of this class. However, 4-chlorobenzylamine **3.7b**, which was equipotent with **3.13b** in CII inhibition, afforded just 10% reduction of 22Rv1 cell viability. The 2,4-difluorobenzylamine derivative **3.20b** which possessed an CII IC_{50} = 1100 μ M afforded a 28% reduction in 22Rv1 cell viability. Unfunctionalized thiourea compound **3.3b** (CII Inhibition IC_{50} = 11.88 \pm 3.3 μ M) afforded just 12% reduction in 22Rv1 cell viability at 100 μ M.

The most active 7-bromobenzothiadiazine substituted derivative, 1-phenylethylamine **3.15c** (55% CII inhibition at 100 μ M, IC_{50} = 79.8 \pm 4.1 μ M) significantly reduced 22Rv1 cell survival by 70% at the same concentration after 48 hrs incubation and is the most potent derivative in the 22Rv1 cell line (IC_{50} = 38.9 \pm 3.2 μ M). To confirm the effect of **3.15c** on prostate cancer cells, the effect of **3.15c** on LNCap cell line was tested. The **3.15c** suppress the LNCap cell lines with IC_{50} = 44.58 \pm 3.3 μ M (**Figure 3.4**). Derivatives **3.21c**, the 4-(trifluoromethoxy)benzylamine (21% CII inhibition) and **3.14c**, the 3-Phenylpropylamine (47% CII inhibition) reduced cell survival of 22Rv1 cells by 45% and 42% respectively, while the 4-methoxybenzylamine (**3.11c**) (64% CII inhibition) and 4-(trifluoromethyl)benzylamine (**3.16c**) (0% CII inhibition) derivatives resulted in 41% and 34% reduced cell viability, respectively. Unfunctionalized thiourea **3.3c** (55% CII Inhibition) afforded just 16% reduction in 22Rv1 cell viability (**Figure 3.3C**).

The unsubstituted benzothiadiazine derivatives that possess no significant CII inhibition activity generally afforded no reduction of 22Rv1 cell viability. However, 1-phenylethylamine (**3.15d**) and 4-(trifluoromethoxy) benzylamine (**3.21d**) were both equipotent to reduce cell survival of 22Rv1 cells by approximately 30%. These two side

chain derivatives display the greatest reduction in 22Rv1 cell viability across all benzothiadiazine derivative classes tested, suggesting the 1-phenethylamine and 4-(trifluoromethoxy)benzylamine contribute to a common pharmacophore. Furthermore, greater cytotoxicity was correlated with increased cLogP, possibly due to increased cell penetration. While several novel benzothiadiazine derivatives have been identified that possess significant activity to suppress prostate cancer cell viability, potency to inhibit CII does not correlate to antineoplastic effect. Indeed, the derivatives with the greatest effect to reduce cell viability in 22Rv1 cells (**Figure 3.3**) possess a range of CII inhibition activity from 0% to 64%. Derivative **3.15c** possessing an $IC_{50} = 38.9 \pm 3.2 \mu M$ in 22Rv1 prostate cancer cells and $IC_{50} = 44.58 \pm 3.3 \mu M$ in LNCap prostate cancer cells is more potent in this cell line than the clinical agents a prostate cancer drugs, apalutamide ($IC_{50} = 77.0 \pm 17 \mu M$) and darolutamide ($IC_{50} = 46.0 \pm 10 \mu M$),⁴⁷ identifying this scaffold as a hit for further studies (**Figure 3.4**).¹⁹⁶

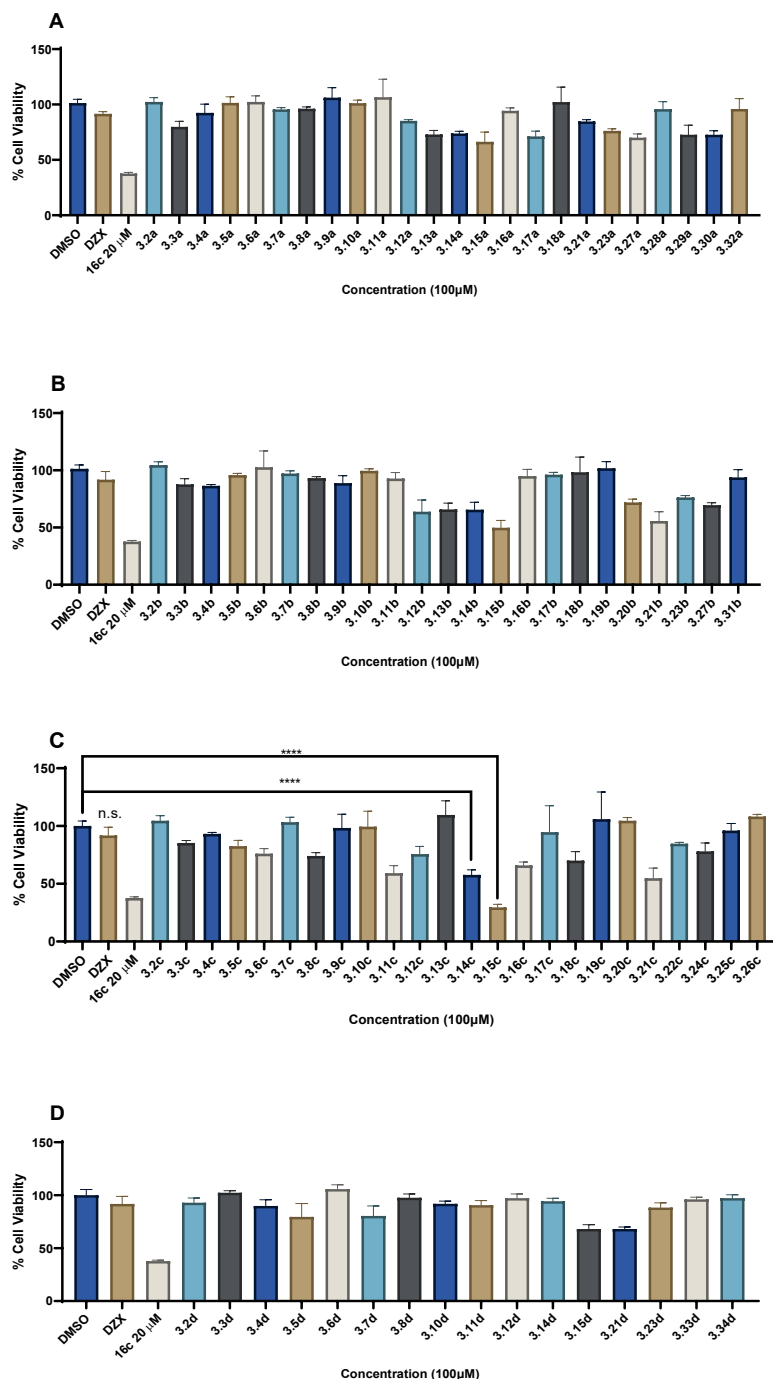


Figure 3.3. Cytotoxic effect of diazoxide derivatives (100 μ M, 48 h treatment) in 22Rv1 prostate cancer cells. A) Cytotoxic effect of diazoxide derivatives with 7-fluoro substitution. B) Cytotoxic effect of diazoxide derivatives with 6-chloro substitution. C) Cytotoxic effect of diazoxide derivatives with 7-bromo substitution. D) Cytotoxic effect of diazoxide derivatives with a non-halogenated ring. Values represent the mean \pm SD of n = 3 experiments. Unpaired t test; n.s.= not significant, ** p < 0.0001.**

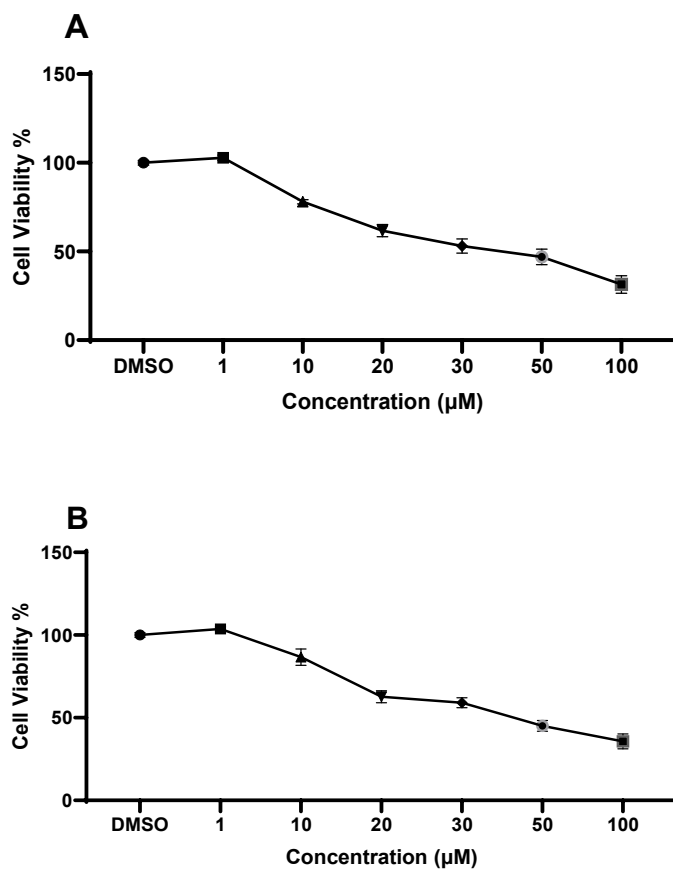


Figure 3.4. The cytotoxic effect of 3.15c, a diazoxide derivative, in prostate cancer cells. A) Cytotoxicity effect of **3.15c** diazoxide derivative in 22Rv1 prostate cancer cells. **B)** Cytotoxicity effect of **3.15c** diazoxide derivative in LNCap prostate cancer cells. Values represent the mean \pm SD of n = 3 experiments.

Administration of 300 mg/kg of DZX to rats bearing hormone-dependent mammary carcinomas was reported to result in 90% inhibition of tumor growth but induced mild reversible diabetes.²⁰⁷ Additionally, DZX has been reported to be cytotoxic in TNBC cells.⁸⁵ Based on these studies, The cytotoxic effect of the DZX derivatives were initially studied by our collaborator at the University of Nebraska Medical Center in the TNBC MDA-MB-468 cell line. Some derivatives were dosed at 10, 50 and 100 μ M for different period of times 24, 48 and 72 hours and viable cells were counted using a hemocytometer (**Figure 3.5**). We found the best cytotoxicity time to inhibit the proliferation of this type of cell line is over 72 hr. After that, all the derivatives were initially screened for cytotoxic effect at 50 μ M over 72 hours (**Figure 3.6**). Those derivatives that reduced cell viability measured by MTS assay by 50% or more at this concentration underwent an IC₅₀ determination (**Table 3.7**).

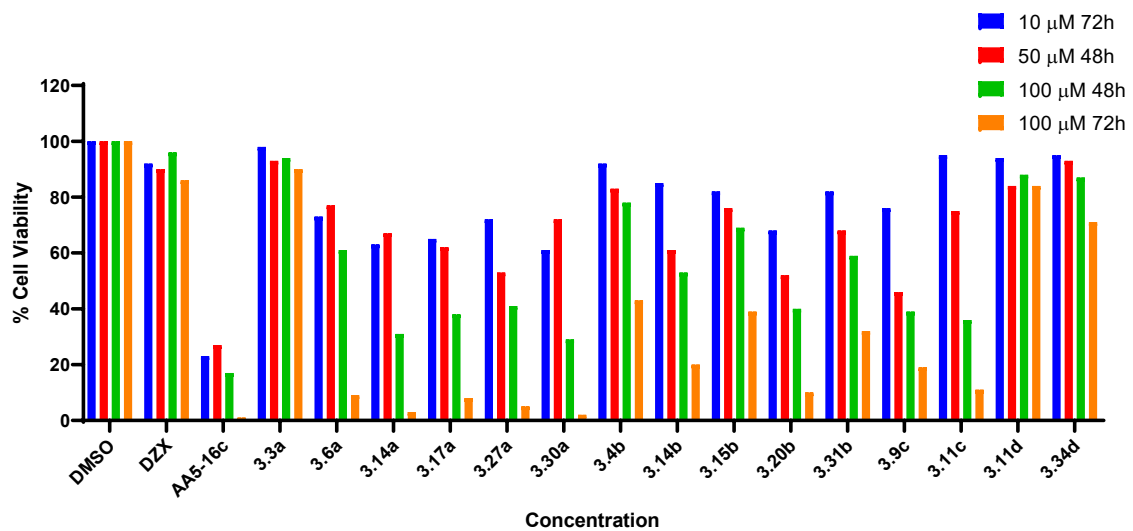


Figure 3.5. Cytotoxic effect of selected diazoxide derivatives on triple negative breast cancer (TNBC) MDA-MB-468 cells.

The parent compound DZX afforded no activity to reduce TNBC cells viability ($IC_{50} > 400 \mu M$) in our hands. Gratifyingly, several derivatives demonstrated marked dose and time-dependant reduction of cell viability with greater effect than the clinical agent 5-fluorouracil. The 7-fluoro and 7-bromo substituted benzothiadiazine derivatives in particular exhibited potent reduction in TNBC cell viability. Within the 7-fluorobenzothiadiazine derivatives, the aliphatic amine substitution have been shown no activity at $> 50 \mu M$ concentration, but aromatic substitution to the amine was required for activity. In general, functionalized benzyl amine substituents exhibited greater reduction of cell viability than the ethyl (**3.9a**, $IC_{50} > 50 \mu M$) and propyl (**3.14a**, $IC_{50} = 57.85 \mu M$) homologation series. Addition of an electron withdrawing 4-SCF₃ group to the phenyl ring of the benzyl amine (**3.29a**, $IC_{50} = 48.70 \mu M$) improved activity over the unfunctionalized benzylamine **3.12a** ($IC_{50} = 57.98 \mu M$). While an electron-donating 4-OMe group reduces activity (**3.11a**, $IC_{50} > 50 \mu M$), positional switching to a 2-OMe further increases activity (**3.17a**, $IC_{50} = 15.71 \mu M$). The most potent compound identified from the 7-fluorobenzothiadiazine derivatives features chain branching alpha to the amine with 1-phenylethan-1-amine (**3.15a**) possessing an $IC_{50} = 4.17 \mu M$ with a selectivity index over low tumorigenic HEK293 cells ($IC_{50} = 42.55 \mu M$) of > 10 -fold. A profile that is superior to the clinical agent 5-fluorouracil in MDA-MB-468 ($IC_{50} = 6.83$), and HEK293 cells ($IC_{50} = 7.06 \mu M$) (**Table 3.7**).

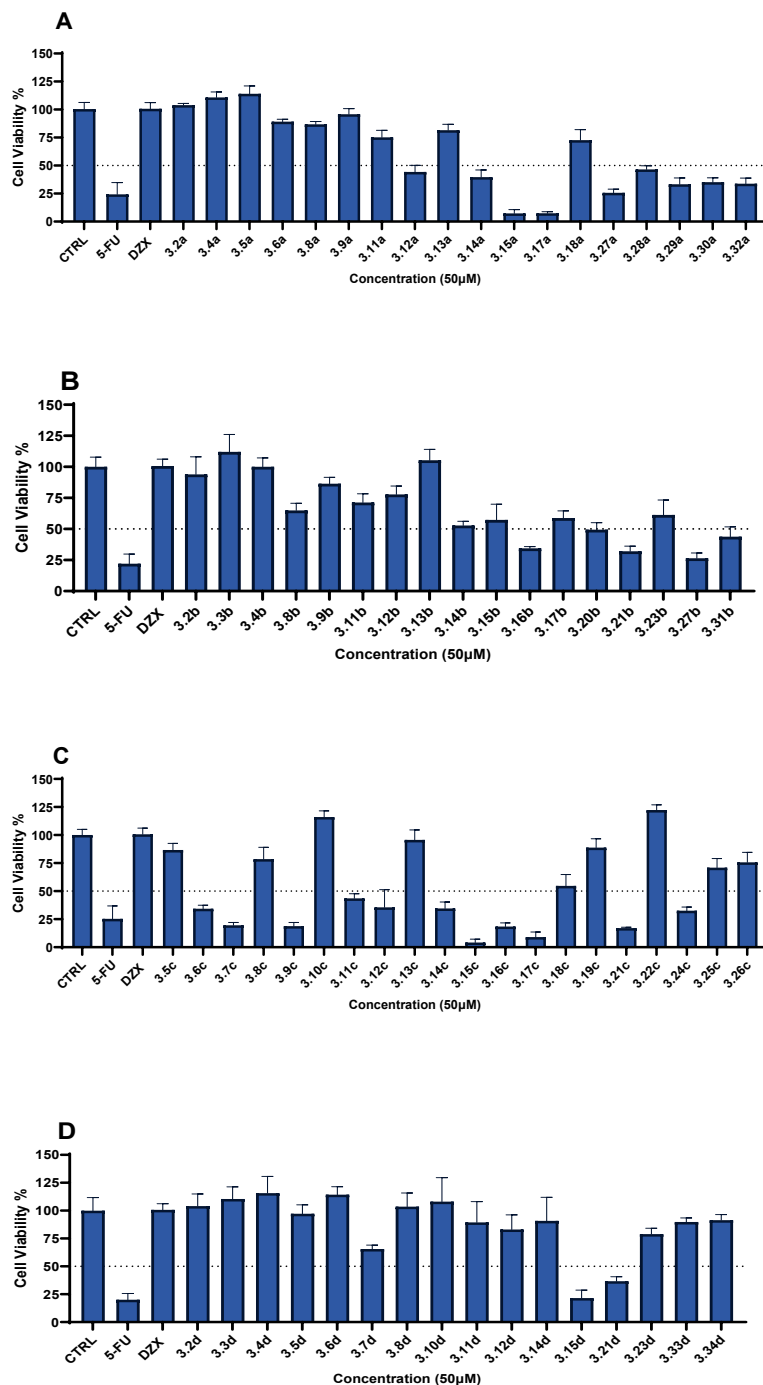


Figure 3.6. Cytotoxic effect of diazoxide derivatives (50 µM, 72 hours treatment) in triple negative breast cancer MDA-MB-468 cells. A) Cytotoxic effect of diazoxide derivatives with 7-fluoro substitution. **B)** Cytotoxic effect of diazoxide derivatives with 6-chloro substitution. **C)** Cytotoxic effect of diazoxide derivatives with 7-bromo substitution. **D)** Cytotoxic effect of diazoxide derivatives with a saturated ring. Values represent the mean \pm SD of n = 3 experiments.

The 7-bromobenzothiadiazine derivatives showed the most potent activity to reduce MDA-MB-468 cell viability. The benzyl amine derivative (**3.12c**, $IC_{50} = 30.8 \mu M$) is less active than the homologation series of phenethyl (**3.9c**, $IC_{50} = 18.6 \mu M$) and phenyl propyl (**3.14c**, $IC_{50} = 9.27 \mu M$), possible due to increased lipophilicity enabling greater cell penetration. Substitution of the benzyl group increases activity with an inverse proportionality to electron-withdrawing effect at the *para* position; 4-OCF₃ (**3.21c**, $IC_{50} = 18 \mu M$), 4-CF₃ (**3.16c**, $IC_{50} = 16.15 \mu M$) and 4-Cl (**3.7c**, $IC_{50} = 12.54 \mu M$). Electron-donating substitution with a methoxy group increases activity dependent on position; 4-OMe (**3.11c**, $IC_{50} = 27.21 \mu M$), 3-OMe (**3.19c**, $IC_{50} = >50 \mu M$), 2-OMe (**3.17c**, $IC_{50} = 13.61 \mu M$). Similar to the 7-fluorobenzothiadiazine derivatives branching at the benzylamine to afford 1-phenylethan-1-amine (**3.15c**) afforded the most active compound ($IC_{50} = 2.93 \mu M$) with 11-fold selectivity towards TNBC cells over low tumorigenic HEK293 cells ($IC_{50} = 32.18 \mu M$) (Table 3.7). The 7-chlorobenzothiadiazine derivative (**3.15e**) is a third potent derivatives possessing an $IC_{50} = 7.14 \mu M$.

The position and type of halogen in DZX derivatives are critical for the activity; for example, 7-fluoro, 7-bromo and 7-chloro are shown to have higher inhibition properties. Switching the 7-halo to 6-halo series diminished the cytotoxicity inhibition. The 1-phenylethan-1-amine (**3.15b**) afforded $IC_{50} = 43.47 \mu M$ which that lower activity more than the **3.15a** and **3.15c**. Also, the substitution of the benzyl group 4-CF₃ (**3.16b**, $IC_{50} = 25.05 \mu M$) and 4-OCF₃ (**3.21b**, $IC_{50} = 48.01 \mu M$) less active than the **3.16c** and **3.21c**. The diazoxide derivatives with a saturated ring have been shown inactive ($>50 \mu M$) except with the 1-phenylethan-1-amine (**3.15d**) and 4-(trifluoromethoxy)benzylamine (**3.21d**) substitutions which they have $IC_{50} = 12.39 \mu M$ and $19.58 \mu M$, respectively.

Compound	Mw	cLogP	MDA-MB-468	HEK293	SI ^b
			IC ₅₀ (μM) ^a	IC ₅₀ (μM) ^a	
5-Fluorouracil	130.08	-0.6	6.83 ±2.9	7.06 ±0.8	1.03
Diazoxide	230.67	1.0	434.31 ±26.2	547.40 ±34.1	1.26
AA5-16c	269.29	1.53	6.71 ±0.8	25.93 ±2.4	3.36
3.12a	305.33	1.66	57.98 ±4.2	N.D. ^c	N.D.
3.14a	333.38	2.37	57.85 ±3.1	181.01 ±7.3	3.12
3.15a	319.35	1.97	4.17 ±0.1	42.55 ±5.9	10.2
3.17a	335.35	1.58	15.71 ±1	47.63 ±2	3.03
3.27a	358.39	1.98	35.95 ±4.2	N.D.	N.D.
3.28a	353.80	2.70	46.38 ±1.9	N.D.	N.D.
3.29a	405.39	3.33	48.70 ±9.8	N.D.	N.D.
3.30a	349.38	1.91	37.54 ±1.0	122.80 ±21.4	3.27
3.32a	387.35	2.87	25.2 ±1.2	N.D.	N.D.
3.15b	376.86	1.85	43.47 ±11.0	118.20 ±22.3	2.72
3.16b	389.28	3.11	25.05 ±3.8	N.D.	N.D.
3.21b	405.78	3.36	48.01 ±14.3	77.16 ±5.2	1.6
3.27b	374.84	1.98	15.53 ±1.2	41.27 ±5.2	2.66

3.6c	346.24	2.38	20.38 ±0.5	35.66 ±1.6	1.75
3.7c	400.68	3.09	12.54 ±0.3	43.07 ±3.2	3.43
3.9c	380.26	2.71	18.60 ±0.8	63.05 ±1.8	3.40
3.11c	396.26	2.30	27.21 ±6.7	88.01 ±12.3	3.23
3.12c	366.23	2.38	30.80 ±5.3	N.D.	N.D.
3.14c	394.29	3.09	9.27 ±1.4	71.81 ±8.2	7.75
3.15c	380.26	2.69	2.93 ±0.07	32.18 ±1.5	11
3.16c	434.23	3.26	16.15 ±1.3	57.54 ±4.7	3.56
3.17c	396.26	2.30	13.61 ±0.9	54.36 ±4.2	4
3.21c	450.23	3.41	18.03 ±1.4	52.89 ±1.8	2.93
3.24c	398.25	2.85	20.08 ±2.5	48.67 ±12.0	2.42
3.15d	301.36	1.83	12.39 ±0.9	48.60 ±1.7	3.92
3.21d	371.33	2.54	19.58 ±2.4	N.D.	N.D.
3.15e	335.81	2.54	7.14 ±0.8	N.D.	N.D.

^aValues are the mean ±SD of n=3 experiments at 72 hours.

^bSelectivity Index.

^cNot Determined

Table 3.7. Cytotoxicity of selective diazoxide derivatives and the clinical chemotherapeutic 5-fluorouracil in TNBC MDA-MB-468 cells and low tumorigenic human endothelial kidney (HEK293) cells.

Clearly the effects of these compounds to inhibit cell viability of TNBC does not correlate to CII inhibition. Exposure of human T leukemic Jurkat cells to 100 μM of DZX resulted in significant inhibition of proliferation; however, upon removal of the compound proliferation resumed.⁸⁷ The study demonstrated that while DZX exposure depolarized the mitochondrial membrane, this was insufficient to modulate cellular energy metabolism. It was found that exposure to DZX resulted in reduction of cellular Ca^{2+} influx.⁸⁷ Diazoxide has further been reported to inhibit lung cancer cell proliferation by downregulating cyclin D1 transcription.⁸⁸

Diazoxide has been investigated in one pilot clinical study in breast cancer patients at a dose of 200-300 mg per day. Treatment of nine patients resulted in a 33% response rate conferring stable disease for between 4-8 months either in combination with tamoxifen (two patients) or monotherapy (one patient).²⁰⁸ The repurposing of DZX as a potential treatment for TNBC has been recently proposed based on a study employing a KinomeScanTM assay of 438 kinases, the three most inhibited at 100 μM were TTK (15%), IRAK1 (9%) and DYRK1A (7%). Dysfunction of all three kinases are known to be associated with various cancers. In this study, as observed herein, the activity of DZX was highly dependent on the cell line employed; no activity was observed in MCF-7 breast cancer cells ($\text{IC}_{50} = 130 \mu\text{M}$) but in MDA-MB-468 TNBC cells an $\text{IC}_{50} = 0.87 \mu\text{M}$ was reported for DZX.⁸⁵ The potential of repurposing DZX in breast cancer has been advanced previously, with the authors suggesting combination treatment to manage the hyperglycemia 'side effect' of DZX in this context.²⁰⁸ Our studies dispute the use of DZX for direct repurposing as in our hands, DZX is inactive in MDA-MB-468 TNBC cells as well as in a prostate cancer cell line. Through the SAR studies initiated herein, medicinal chemistry modulation of the parent compound has been shown to increase antineoplastic effect significantly and presents the possibility of tuning out the known pharmacophore of

K_{ATP} opening activity along with the associated hyperglycemic effect, potentially allowing access to novel treatments for cancer.

3.3. Conclusions

In summary, I identify novel benzothiadiazine derivatives that possess enhanced activity to reduce the cell viability of 22Rv1 prostate cancer cells and potent derivatives that show significant and time-dependent inhibition of MDA-MB-468 triple-negative breast cancer cells suitable for further investigation. The reported derivatives showed higher selectivity to MDA-MB-468 cells over low tumorigenic HEK293 cells and possessed superior potency and selectivity than the clinical agent 5-fluorouracil with compounds **3.15a** and **3.15c**. We demonstrate that the CII inhibition activity of DZX derivatives is not responsible for the observed cytotoxicity in either cancer cell line. To understand the antineoplastic activity and further literature studies on DZX, I extended the research towards other molecular targets. One such mechanism involves targeting angiogenesis via inhibition of VEGF.²⁰⁹

3.4 Experimental Section

3.4.1 Biology

3.4.1.1 Cell Culture and Reagents

Cell lines (22Rv1 prostate cancer, LNCap prostate cancer, HEK293 human embryonic kidney cells and MDA-MB-468 triple-negative breast cancer cells) were purchased from the American Type Culture Collection (ATCC). 22Rv1 and LNCap cells were cultured in Roswell Park Memorial Institute-1640 medium (RPMI-1640) (ATCC® 30-2001™) cells and MDA-MB-468 cells in Dulbecco's Modified Eagle Medium (DMEM)

(Fisher Scientific) (Catalog No. 50-188-267FP), and HEK293 human embryonic kidney cells in Eagle's Minimum Essential Medium (ATCC® 30-2003™) with fetal bovine serum (ATCC 30-2020) to a final concentration of 10% and Corning™ Penicillin-Streptomycin Solution (Catalog No. MT30001CI) according to the supplier's recommended protocol. Atpenin A5 (AA5) (catalog no. 10189-198) was purchased from VWR. Alfa Aesar™ Diazoxide (Catalog No. AAJ66010ME) and 5-Fluorouracil, 99%, ACROS Organics™ (Catalog No. AC228440010) were purchased from Fisher Scientific. Stock solutions of AA5 were prepared in DMSO and were serially diluted for cell culture treatment maintaining the final DMSO concentration at less than 1%. CellTiter 96 AQueous One Solution Cell Proliferation Assay (3-(4,5-dimethylthiazol-2-yl)-5-(3-carboxymethoxy phenyl)-2-(4-sulfophenyl)-2H-tetrazolium) (MTS) assay (Catalog No. G3580) was purchased from Promega.

3.4.1.2 Cytotoxicity Assays

To determine the cell growth inhibition ability of the synthesized compounds the MTS assay used according to the manufacturer's recommended protocol. Stock solutions of the synthesized compounds were prepared in DMSO. Cells were seeded at a density of 1×10^5 cells in 96-well plates. After 24 hours for 22Rv1 and 72 hours for MDA-MB-468 cells, cells were treated at the indicated concentrations of test compounds, limiting the final DMSO concentration to less than 1%. After incubation at 37 °C in an environment of 5% CO₂ for 48-72 hours, 10 µL of MTS reagent (CellTiter 96® AQueous One Solution Reagent) was added to each well and incubated at the above-mentioned conditions for 2-4 hr. Absorbance was recorded at 570 nm on a BioTek Synergy Mx multimode plate reader and the viability of cells were plotted as percentage of controls. Also, MDA-MB-468 cells were seeded at a density of 1×10^5 cells/dish in 12-well plates. After incubation at 37 °C

in an environment of 5% CO₂ for 48-72 hours, the numbers of viable cells were counted using a hemocytometer. The relative cell viability was calculated by normalizing the cell number with drug treatment to that with DMSO.

3.4.1.3 Complex II inhibition assay

Mitochondria were isolated from mouse liver by differential centrifugation in sucrose-based buffer as previously described.²⁰³ Complex II enzymatic activity was determined spectrophotometrically as the rate of succinate-driven, co-enzyme Q2-linked reduction of dichlorophenolindophenol (DCPIP).¹⁹¹ Freeze-thawed mitochondria were incubated in phosphate buffer (pH 7.4) containing 40 μ M DCPIP, 1 mM KCN, 10 μ M rotenone, and 50 μ M co-enzyme Q2. The rate of reduction of DCPIP to DCPIPH₂ was followed at 600 nm (ϵ = 21,000 M⁻¹). At the end of each run thenoyltrifluoroacetone (1 mM) was added and the residual TTFA-insensitive rate subtracted. Varying amounts of benzothiadiazine derivatives were used to determine an IC₅₀ value.

3.4.1.4 Statistical Analysis

Experiments were repeated at least thrice, and the statistical significance was calculated using the unpaired *t* test. A *p* value of <0.05 was considered statistically significant. IC₅₀ values were calculated by GraphPad prism software.

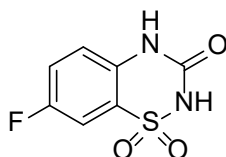
3.4.2 Chemistry

General

All reactions were carried out in oven- or flame-dried glassware under positive nitrogen pressure unless otherwise noted. Reaction progress was monitored by thin-layer

chromatography (TLC) carried out on silica gel plates (2.5 cm x 7.5 cm, 200 μ m thick, 60 F254) and visualized by using UV (254 nm) or by potassium permanganate or phosphomolybdic acid stain as indicator. Flash column chromatography was performed with silica gel (40-63 μ m, 60 Å) or on a Teledyne Isco (CombiFlash R_f 200 UV/Vis). Commercial grade solvents and reagents were purchased from Fisher Scientific (Houston, TX) or Sigma Aldrich (Milwaukee, WI) and were used without further purification except as indicated. Anhydrous solvents were purchased from Across Organics and stored under an atmosphere of dry nitrogen over molecular sieves.

¹H and ¹³C NMR spectra were recorded in the indicated solvent on a Bruker 400 MHz Advance III HD spectrometer at 400 and 100 MHz for ¹H and ¹³C, respectively, with solvent peak as an internal standard. Multiplicities are indicated by s (single), d (doublet), dd (doublet of doublet), t (triplet), q (quartet), m (multiplet), and br (broad). Chemical shifts (δ) are reported in parts per million (ppm), and coupling constants (*J*), in Hertz. High-resolution mass spectroscopy (HRMS) was performed on a TripleTOF 5600 (SCIEX) using an ESI source conducted at the Texas Tech University Health Sciences Center School of Pharmacy in Dallas, TX. The spectral data was extracted from total ion chromatogram (TIC). High-pressure liquid chromatography (HPLC) was performed on a Gilson HPLC system with 321 pumps and 155 UV/Vis detector using trilution software v2.1 with an ACE Equivalence 3 (C18, 3 μ M, 4.6 x 150 mm) column. All samples were determined to possess >95% purity.



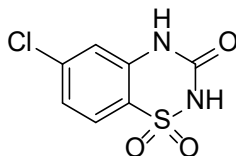
7-Fluoro-3-oxo-3,4-dihydro-2H-1,2,4-benzothiadiazine 1,1-dioxide (3.2a).

A solution of chlorosulfonyl isocyanate (2.82 mL, 32.4 mmol) in nitromethane (30 mL) was mixed in a closed dried vessel under nitrogen pressure and cooled at -5 °C (ice and salt bath). To this mixture 4-fluoroaniline (**3.1a**, 2.6 mL, 27 mmol) was added slowly. The contents were vigorously stirred for 20 mins followed by the addition of anhydrous AlCl_3 (4.7 g, 35.1 mmol) and the mixture was refluxed for 1h. The hot solution was poured onto ice (200 g) and stirred for an additional 30 mins and the resulting precipitate was collected by filtration and washed with water. The crude solid was treated with an aqueous solution of sodium bicarbonate (5 g/100 mL) followed by heating until the solid precipitate was dissolved. The solution was treated with charcoal and was filtered, the filtrate solution was adjusted to pH 1 using 12N HCl. The resulting pure white precipitate was filtered, washed with water, and air dried (3.17 g, 54% yield):

^1H NMR (400 MHz, DMSO-d_6): δ = 7.30 (m, 1H), 7.55 (1H, t, J =8.7 Hz), 7.68 (1H, dd, J =7.5, 2.8 Hz), 11.40 ppm (s, 1H).

^{13}C NMR (100 MHz, DMSO-d_6): δ = 109.27, 119.81, 121.88, 123.58, 132.18, 151.67, 156.58, 159.01 ppm.

HRMS (ESI): m/z calcd for $\text{C}_7\text{H}_5\text{FN}_2\text{O}_3\text{S}$ [$M+\text{Na}$] $^+$: 238.9902, found: 238.9901.



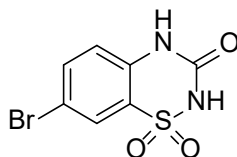
6-Chloro-3-oxo-3,4-dihydro-2H-1,2,4-benzothiadiazine 1,1-dioxide (3.2b).

The white compound was obtained from 3-chloroaniline (**3.1b**, 3.32 mL, 31.35 mmol) by following the experimental conditions described for **3.2a** (4.5 g, 62% yield):

^1H NMR (400 MHz, DMSO- d_6): δ = 7.26 (1H, d, J =2 Hz), 7.32 (1H, dd, J =8.5, 1.8 Hz), 7.80 (1H, d, J =8.5 Hz), 11.39 ppm (s, 1H).

^{13}C NMR (100 MHz, DMSO- d_6): δ = 116.91, 121.73, 123.96, 124.65, 136.97, 138.54, 151.15 ppm.

HRMS (ESI): m/z calcd for $\text{C}_7\text{H}_5\text{ClN}_2\text{O}_3\text{S}$ [$M+\text{Na}$] $^+$: 254.9607, found: 254.9606.



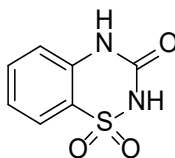
7-Bromo-3-oxo-3,4-dihydro-2H-1,2,4-benzothiadiazine 1,1-dioxide (3.2c).

The white compound was obtained from 4-bromoaniline (**3.1c**, 3 g, 17.44 mmol) by following the experimental conditions described for **3.2a** with the slight modification that the crude material was dissolved in a 1:1 hydromethanolic solution of sodium bicarbonate instead of an aqueous solution of sodium bicarbonate (3.1 g, 64% yield):

^1H NMR (400 MHz, DMSO- d_6): δ = 7.19 (1H, d, J =8.7 Hz), 7.78 (1H, dd, J =8.7, 2.2 Hz), 7.91 (1H, d, J =2.2 Hz), 11.46 ppm (s, 1H).

^{13}C NMR (100 MHz, DMSO- d_6): δ = 115.08, 119.83, 124.34, 124.79, 134.86, 137.00, 151.52 ppm.

HRMS (ESI): m/z calcd for $\text{C}_7\text{H}_5\text{BrN}_2\text{O}_3\text{S}$ [$M+\text{Na}$] $^+$: 298.9101, found: 298.9096.



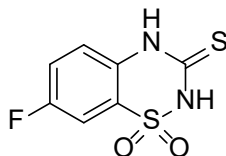
2H-benzo[e][1,2,4]thiadiazin-3(4H)-one 1,1-dioxide (3.2d).

The white compound was obtained from aniline (**3.1d**, 4.86 mL, 53.7 mmol) by following the experimental conditions described for **3.2a** (5.7 g, 53% yield):

¹H NMR (400 MHz, DMSO-*d*₆): δ= 7.27 (m, 2H), 7.63 (1H, t, *J*=7.2 Hz), 7.77 (1H, d, *J*=7.6 Hz), 11.27 ppm (s, 1H).

¹³C NMR (100 MHz, DMSO-*d*₆): δ= 117.47, 122.43, 122.97, 123.89, 134.40, 135.48, 151.08 ppm.

HRMS (ESI): *m/z* calcd for C₇H₆N₂O₃S [*M*+Na]⁺: 220.9996, found: 220.9998.



7-Fluoro-3-thioxo-3,4-dihydro-2H-1,2,4-benzothiadiazine 1,1-dioxide (3.3a).

A mixture of 7-fluoro-3-oxo-3,4-dihydro-2H-1,2,4-benzothiadiazine 1,1-dioxide (**3.2a**, 2.8 g, 12.95 mmol) and phosphorus pentasulfide (5.47 g, 12.95 mmol) was dissolved in anhydrous pyridine (50 mL) and refluxed under nitrogen pressure overnight. The reaction was allowed to cool, and the solvent removed in vacuo, the crude product was dissolved in an aqueous solution of sodium hydroxide (NaOH) (5 g/100 mL). This solution was treated with charcoal and was filtered. The filtrate was acidified to pH 1 using 12N HCl. The precipitated compound was collected by filtration, washed with water, and was allowed to air dry. The dried compound was suspended in an aqueous solution of sodium bicarbonate (NaHCO₃) (10 g/200 mL) and heated until the solid was dissolved. This solution was treated with charcoal and filtered. The filtrate was adjusted to pH 1 using 12N

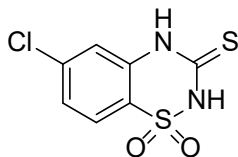
HCl, and the white precipitate was collected by filtration, washed with water, and air dried.

(1.76 g, 58% yield):

¹H NMR (400 MHz, DMSO-*d*₆): δ= 7.29 (m, 1H), 7.56 (m, 1H), 7.68 (1H, dd, *J*=7.5, 2.8 Hz), 11.35 ppm (s, 1H).

¹³C NMR (100 MHz, DMSO-*d*₆): δ= 109.93, 121.01, 122.12, 123.31, 132.56, 158.33, 160.79 ppm.

HRMS (ESI): *m/z* calcd for C₇H₅FN₂O₂S₂ [*M*+Na]⁺: 254.9674, found: 254.9674.



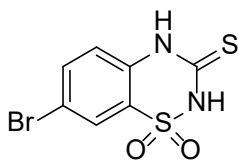
6-Chloro-3-thioxo-3,4-dihydro-2H-1,2,4-benzothiadiazine 1,1-dioxide (3.3b).

The white compound was obtained from **3.2b** (4.5 g, 19.34 mmol) by following the experimental conditions described for **3.3a**. (2.7 g, 56% yield):

¹H NMR (400 MHz, DMSO-*d*₆): δ= 7.26 (1H, d, *J*=2 Hz), 7.34 (1H, dd, *J*=8.4, 2 Hz), 7.80 (1H, d, *J*=8.4 Hz), 11.33 ppm (s, 1H).

¹³C NMR (100 MHz, DMSO-*d*₆): δ= 117.76, 121.21, 126.03, 126.95, 137.55, 137.90, 144.72 ppm.

HRMS (ESI): *m/z* calcd for C₇H₅ClN₂O₂S₂ [*M*+Na]⁺: 270.9378, found: 270.9373.



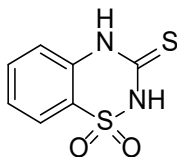
7-Bromo-3-thioxo-3,4-dihydro-2H-1,2,4-benzothiadiazine 1,1-dioxide (3.3c).

The white compound was obtained from **3.2c** (2.4 g, 8.63 mmol) by following the experimental conditions described for **3.3a** with the slight modification that the crude material was dissolved in 1:1 hydromethanolic solution of sodium bicarbonate instead of an aqueous solution of sodium bicarbonate by heating the mixture until most of the insoluble material dissolved. Charcoal was added to the suspension and filtered. The filtrate was adjusted to pH 1 with 12 N HCl, and the white precipitate was collected by filtration, washed with water, and air dried (1.35 g, 53% yield):

¹H NMR (400 MHz, DMSO-*d*₆): δ = 5.08 (br, 1H), 7.32 (1H, d, *J*=8.8 Hz), 7.85 (1H, d, *J*=8.7 Hz), 7.95 (s, 1H), 11.45 ppm (br, 1H).

¹³C NMR (100 MHz, DMSO-*d*₆): δ = 118.22, 120.67, 123.82, 126.08, 135.15, 136.82, 157.57 ppm.

HRMS (ESI): *m/z* calcd for C₇H₅BrN₂O₂S₂ [*M*+Na]⁺: 314.8873, found: 314.8863.



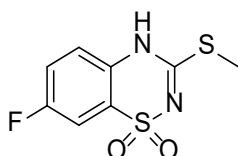
2H-benzo[e][1,2,4]thiadiazine-3(4H)-thione 1,1-dioxide (3.3d).

The white compound was obtained from **3.2d** (4.9 g, 24.72 mmol) by following the experimental conditions described for **3.3a** yield (2.67 g, 50% yield):

¹H NMR (400 MHz, DMSO-*d*₆): δ = 7.38 (m, 2H), 7.70 (1H, t, *J*=7.8 Hz), 7.80 (1H, d, *J*=7.4 Hz), 12.12 ppm (br, 1H).

^{13}C NMR (100 MHz, DMSO- d_6): δ = 115.52, 121.14, 125.21, 126.83, 136.59, 138.94, 144.16, 144.66 ppm.

HRMS (ESI): m/z calcd for $\text{C}_7\text{H}_6\text{N}_2\text{O}_2\text{S}_2$ $[M+\text{Na}]^+$: 236.9768, found: 236.9765.



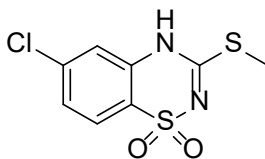
7-Fluoro-3-methylsulfanyl-4H-1,2,4-benzothiadiazine 1,1-dioxide (3.4a).

7-Fluoro-3-thioxo-3,4-dihydro-2H-1,2,4-benzothiadiazine 1,1-dioxide (**3.3a**, 2.8 g, 12.06 mmol) was dissolved in a 1:1 hydromethanolic solution of sodium bicarbonate (5 g/ 200 mL). Methyl iodide was added (1.5 mL, 24.12 mmol) and the solution was stirred for 1h. The resulting suspension was adjusted to pH 5 using 6N HCl. The suspension was concentrated under reduced pressure, and the white precipitate was collected by filtration, washed with water, and air dried (1.67 g, 89% yield):

^1H NMR (400 MHz, DMSO- d_6): δ = 2.53 (s, 2H), 7.33 (m, 1H), 7.58 (1H, t, J =8.8 Hz), 7.55 (1H, dd, J =7.5, 2.8 Hz), 12.61 ppm (br, 1H).

^{13}C NMR (100 MHz, DMSO- d_6): δ = 13.85, 109.80, 120.06, 121.91, 122.83, 132.77, 157.84, 161.61 ppm.

HRMS (ESI): m/z calcd for $\text{C}_8\text{H}_7\text{FN}_2\text{O}_2\text{S}_2$ $[M+\text{Na}]^+$: 268.9831, found: 268.9832.



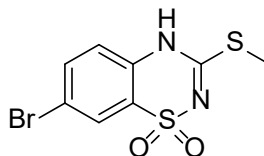
6-Chloro-3-methylsulfanyl-4H-1,2,4-benzothiadiazine 1,1-dioxide (3.4b).

The white compound was obtained from **3.3b** (2.5, 10.05 mmol) by following the experimental conditions described for **3.4a** (2.23 g, 84% yield):

¹H NMR (400 MHz, DMSO-*d*₆): δ= 2.52 (s, 2H), 7.26 (1H, d, *J*=2 Hz), 7.34 (1H, dd, *J*=8.5, 2 Hz), 7.80 (1H, d, *J*=8.5 Hz), 12.61 ppm (s, 1H).

¹³C NMR (100 MHz, DMSO-*d*₆): δ= 13.90, 116.83, 120.76, 126.12, 126.48, 137.20, 137.87, 161.88 ppm.

HRMS (ESI): *m/z* calcd for C₈H₇ClN₂O₂S₂ [*M*+Na]⁺: 284.9535, found: 284.9527.

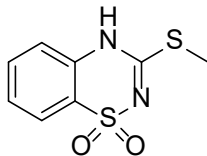
**7-Bromo-3-methylsulfanyl-4H-1,2,4-benzothiadiazine 1,1-dioxide (3.4c).**

The white compound was obtained from **3.3c** (3.73 g, 12.72 mmol) by following the experimental conditions described for **3.4a** (3.19 g, 81% yield):

¹H NMR (400 MHz, DMSO-*d*₆): δ= 2.52 (s, 2H), 7.24 (1H, d, *J*=8.8 Hz), 7.83 (1H, dd, *J*=8.7, 2.2 Hz), 7.93 (1H, d, *J*=2.1 Hz), 12.65 ppm (s, 1H).

¹³C NMR (100 MHz, DMSO-*d*₆): δ= 13.88, 117.22, 119.87, 123.43, 125.97, 135.26, 136.60, 161.75 ppm.

HRMS (ESI): *m/z* calcd for C₈H₇BrN₂O₂S₂ [*M*+Na]⁺: 328.9030, found: 328.9024.



3-(methylthio)-4H-benzo[e][1,2,4]thiadiazine 1,1-dioxide (3.4d).

The white compound was obtained from **3.3d** (1.92 g, 8.96 mmol) by following the experimental conditions described for **3.4a** (1.84 g, 90% yield):

¹H NMR (400 MHz, DMSO-*d*₆): δ = 2.52 (s, 2H), 7.28 (1H, d, *J*=8.7 Hz), 7.41 (1H, t, *J*=7.2 Hz), 7.67 (1H, d, *J*=8.7 Hz), 7.78 (1H, dd, *J*=7.9, 2 Hz), 12.51 ppm (s, 1H).

¹³C NMR (100 MHz, DMSO-*d*₆): δ = 13.98, 117.31, 122.08, 123.85, 126.41, 133.73, 135.99, 161.38 ppm.

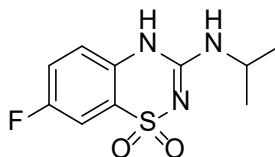
HRMS (ESI): *m/z* calcd for C₈H₈N₂O₂S₂ [*M*+Na]⁺: 250.9924, found: 250.9920.

General Procedures for the Synthesis of 3-(alkylamino)-7-halo-4H-1,2,4-benzothiadiazine 1,1-dioxides (3.5a-3.33a) (3.5b-3.31b) (3.5c-3.26c) (3.5d-3.34d).

Method A: A appropriate 3-methylsulfonyl-4H-1,2,4-benzothiadiazine 1,1-dioxide (**3.4a-d**) (0.25 g) and an appropriate alkylamine (0.7 mL) were dissolved in 1,4-dioxane (8 mL) in a sealed vessel and heated for 24h at 130 °C. The solvent and the excess amine were removed in vacuo, and the residue was dissolved in an aqueous 2% w/v solution of NaOH (7 mL). This solution was treated with charcoal and was filtered. The filtrate was adjusted to pH 1 using 6N HCl. The precipitated compound was collected by filtration, washed with water and air dried. The dried compound was suspended in an aqueous solution of sodium bicarbonate NaHCO₃ (1 g/40 mL). The alkaline solution was treated with charcoal and filtered; the filtrate was adjusted to pH 4-5 with 6N HCl. The white precipitate was collected by filtration, washed twice with water, and air dried.

Method B: A solution of the appropriate 3-methylsulfanyl-4H-1,2,4-benzothiadiazine 1,1-dioxide (**3.4a-d**) (0.25 g) and the appropriate amine (5 mL) was heated in a sealed vessel for 48 h at 120°C. The solvent and excess amine was removed in vacuo, and the residue was dissolved in an aqueous 2% w/v solution of sodium hydroxide (7 mL). This solution was treated with charcoal and was filtered. The filtrate was adjusted to pH 1 using 6N HCl. The precipitated compound was collected by filtration, washed with water and air dried. The dried compound was suspended in an aqueous solution of sodium bicarbonate NaHCO_3 (1 g/40 mL). The alkaline solution was treated with charcoal and filtered, and the filtrate was adjusted to pH 4-5 with 6N HCl. The white precipitate was collected by filtration, washed twice with water, and air dried.

Method C: A appropriate 3-methylsulfanyl-4H-1,2,4-benzothiadiazine 1,1-dioxide (**3.4a-d**) (0.25 g) were dissolved in an appropriate alkylamine (0.7 mL) in a sealed vessel and heated for 96 h at 140 °C. The solvent and the excess amine were removed in vacuo, and the residue was dissolved in an aqueous 2% w/v solution of NaOH (7 mL). This solution was treated with charcoal and was filtered. The filtrate was adjusted to pH 1 using 6N HCl. The precipitated compound was collected by filtration, washed with water and air-dried. The dried compound was suspended in an aqueous solution of sodium bicarbonate NaHCO_3 (1 g/40 mL). The alkaline solution was treated with charcoal and filtered; the filtrate was adjusted to pH 4-5 with 6N HCl. The white precipitate was collected by filtration, washed twice with water, and air dried.



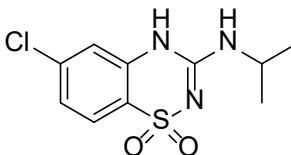
7-Fluoro-3-isopropylamino-4H-1,2,4-benzothiadiazine 1,1-dioxide (3.5a).

The white compound was obtained from **3.4a** by following the experimental conditions described for Method **A** (79% yield):

¹H NMR (400 MHz, DMSO-*d*₆): δ= 1.16 (6H, d, *J*=6.3 Hz), 3.91 (m, 1H), 7.09 (s, 1H), 7.26 (q, 1H), 7.50 (m, 1H), 10.42 ppm (s, 1H).

¹³C NMR (100 MHz, DMSO-*d*₆): δ= 22.66, 43.27, 109.18, 119.50, 120.69, 132.79, 150.96, 156.77, 159.19 ppm.

HRMS (ESI): *m/z* calcd for C₁₀H₁₂FN₃O₂S [*M*+Na]⁺: 280.0532, found: 280.0541.



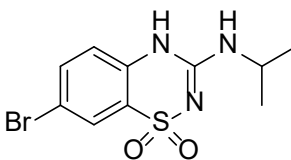
6-Chloro-3-isopropylamino-4H-1,2,4-benzothiadiazine 1,1-dioxide (3.5b).

The white compound was obtained from **3.4b** by following the experimental conditions described for Method **A** (76% yield):

¹H NMR (400 MHz, DMSO-*d*₆): δ= 1.18 (6H, d, *J*=6.4 Hz), 3.93 (m, 1H), 7.09 (br, 1H), 7.27 (m, 1H), 7.47 (m, 1H), 10.40 ppm (s, 1H).

¹³C NMR (100 MHz, DMSO-*d*₆): δ= 22.67, 43.26, 109.18, 119.50, 120.68, 132.79, 150.96, 156.77, 159.19 ppm.

HRMS (ESI): *m/z* calcd for C₁₀H₁₂ClN₃O₂S [*M*+Na]⁺: 296.0236, found: 296.0237.



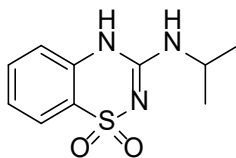
7-Bromo-3-isopropylamino-4*H*-1,2,4-benzothiadiazine 1,1-dioxide (3.5c).

The white compound was obtained from **3.4c** by following the experimental conditions described for Method **A** with the slight modification that the crude material was dissolved in a 1:1 hydromethanolic solution of sodium bicarbonate instead of an aqueous solution of sodium bicarbonate (81% yield):

¹H NMR (400 MHz, DMSO-*d*₆): δ= 1.16 (6H, d, *J*=6.5 Hz), 3.91 (m, 1H), 7.16 (2H, d, *J*=8.3 Hz), 7.70 (1H, dd, *J*=8.7, 2.1 Hz), 7.76 (1H, d, *J*=2.1 Hz), 10.48 ppm (s, 1H).

¹³C NMR (100 MHz, DMSO-*d*₆): δ= 22.62, 43.30, 114.97, 119.59, 124.61, 125.34, 135.42, 145.54, 150.68 ppm.

HRMS (ESI): *m/z* calcd for C₁₀H₁₂BrN₃O₂S [*M*+Na]⁺: 339.9731, found: 339.9716.



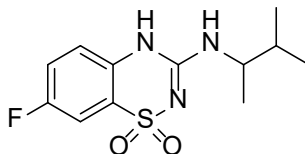
3-(Isopropylamino)-4*H*-benzo[*e*][1,2,4]thiadiazine 1,1-dioxide (3.5d).

The white compound was obtained from **3.4d** by following the experimental conditions described for Method **A** (76%):

¹H NMR (400 MHz, DMSO-*d*₆): δ= 1.16 (6H, d, *J*=6.5 Hz), 3.93 (m, 1H), 6.97 (s, 1H), 7.18 (1H, d, *J*=8.2 Hz), 7.24 (1H, t, *J*=7.8 Hz), 7.54 (1H, t, *J*=8.7 Hz), 7.65 (1H, dd, *J*=7.8, 2 Hz), 10.31 ppm (s, 1H).

¹³C NMR (100 MHz, DMSO-*d*₆): δ= 22.70, 43.13, 116.96, 123.12, 123.24, 124.10, 132.78, 136.10, 150.82 ppm.

HRMS (ESI): *m/z* calcd for C₁₀H₁₃N₃O₂S [*M*+Na]⁺: 262.0626, found: 262.0629.



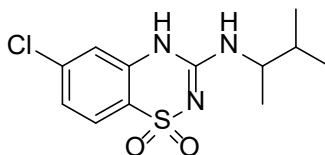
7-Fluoro-3-((3-methylbutan-2-yl)amino)-4H-benzo[e][1,2,4]thiadiazine 1,1-dioxide (3.6a).

The white compound was obtained from **3.4a** by following the experimental conditions described for Method **B** (67% yield):

¹H NMR (400 MHz, DMSO-*d*₆): δ = 0.87 (q, 6H), 1.09 (3H, d, *J*=6.6 Hz), 1.74 (m, 1H), 3.69 (m, 1H), 6.96 (br, 1H), 7.24 (br, 1H), 7.49 (m, 2H), 10.32 ppm (s, 1H).

¹³C NMR (100 MHz, DMSO-*d*₆): δ = 17.47, 18.70, 18.97, 32.70, 52.08, 109.19, 119.39, 120.67, 132.70, 124.10, 151.42, 156.77, 159.19 ppm.

HRMS (ESI): *m/z* calcd for C₁₂H₁₆FN₃O₂S [*M*+Na]⁺: 308.0844, found: 308.0844.



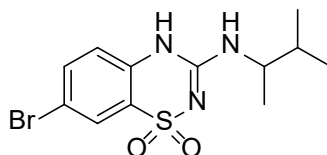
6-Chloro-3-((3-methylbutan-2-yl)amino)-4H-benzo[e][1,2,4]thiadiazine 1,1-dioxide (3.6b).

The white compound was obtained from **3.4b** by following the experimental conditions described for Method **B** (64% yield):

¹H NMR (400 MHz, DMSO-*d*₆): δ = 0.90 (q, 6H), 1.08 (3H, d, *J*=6.6 Hz), 1.74 (m, 1H), 3.69 (m, 1H), 6.96 (br, 1H), 7.24 (br, 1H), 7.50 (m, 2H), 10.31 ppm (s, 1H).

^{13}C NMR (100 MHz, DMSO- d_6): δ = 17.48, 18.70, 18.97, 32.70, 52.08, 109.19, 119.39, 120.43, 132.71, 151.42, 156.77, 159.19 ppm.

HRMS (ESI): m/z calcd for $\text{C}_{12}\text{H}_{16}\text{ClN}_3\text{O}_2\text{S}$ $[\text{M}+\text{Na}]^+$: 324.0550, found: 324.0565.



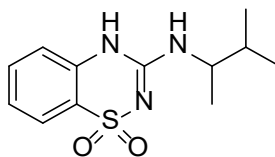
7-Bromo-3-((3-methylbutan-2-yl)amino)-4H-benzo[e][1,2,4]thiadiazine 1,1-dioxide (3.6c).

The white compound was obtained from **3.4c** by following the experimental conditions described for Method **B** with the slight modification that the crude material was dissolved in a 1:1 hydromethanolic solution of sodium bicarbonate instead of an aqueous solution of sodium bicarbonate (71% yield):

^1H NMR (400 MHz, DMSO- d_6): δ = 0.89 (q, 6H), 1.08 (3H, d, J =6.6 Hz), 1.76 (m, 1H), 3.71 (m, 1H), 6.99 (br, 1H), 7.16 (1H, d, J =8.7 Hz), 7.72 (1H, dd, J =8.7, 1.9 Hz), 7.75 (1H, d, J =1.9 Hz), 10.37 ppm (s, 1H).

^{13}C NMR (100 MHz, DMSO- d_6): δ = 17.45, 18.71, 18.97, 32.68, 52.11, 114.95, 119.57, 124.68, 125.35, 135.36, 135.52, 151.16 ppm.

HRMS (ESI): m/z calcd for $\text{C}_{12}\text{H}_{16}\text{BrN}_3\text{O}_2\text{S}$ $[\text{M}+\text{Na}]^+$: 368.0044, found: 368.0040.



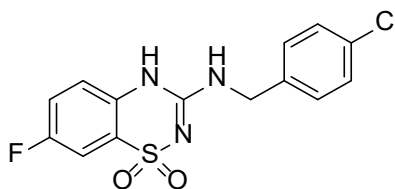
3-((3-Methylbutan-2-yl)amino)-4*H*-benzo[*e*][1,2,4]thiadiazine 1,1-dioxide (3.6d).

The white compound was obtained from **3.4d** by following the experimental conditions described for Method **B** (73% yield):

¹H NMR (400 MHz, DMSO-*d*₆): δ= 0.90 (q, 6H), 1.10 (3H, d, *J*=6.6 Hz), 1.75 (m, 1H), 3.72 (m, 1H), 6.88 (br, 1H), 7.16 (1H, d, *J*=7.4 Hz), 7.24 (1H, t, *J*=8.1 Hz), 7.54 (1H, t, *J*=8.2 Hz), 7.66 (1H, dd, *J*=7.8, 2 Hz), 10.23 ppm (s, 1H).

¹³C NMR (100 MHz, DMSO-*d*₆): δ= 17.47, 18.69, 18.97, 32.68, 51.89, 116.93, 123.17, 123.25, 124.09, 132.78, 136.04, 151.27 ppm.

HRMS (ESI): *m/z* calcd for C₁₂H₁₇N₃O₂S [*M*+Na]⁺: 290.0939, found: 290.0947.



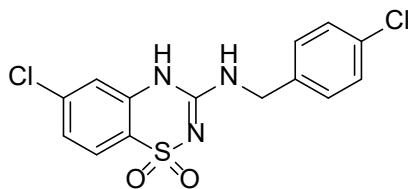
3-((4-Chlorobenzyl)amino)-7-fluoro-4*H*-benzo[*e*][1,2,4]thiadiazine 1,1-dioxide (3.7a).

The white compound was obtained from **3.4a** by following the experimental conditions described for Method **A** (73% yield):

¹H NMR (400 MHz, DMSO-*d*₆): δ= 4.46 (s, 2H), 7.28 (q, 1H), 7.36 (2H, d, *J*=8.5 Hz), 7.41-7.52 (m, 4H), 7.70 (br, 1H), 10.89 ppm (s, 1H).

¹³C NMR (100 MHz, DMSO-*d*₆): δ= 43.67, 109.48, 119.62, 120.80, 123.77, 127.64, 128.78, 129.50, 132.07, 132.94, 138.15, 151.82, 156.83, 159.25 ppm.

HRMS (ESI): *m/z* calcd for C₁₄H₁₁ClFN₃O₂S [*M*+Na]⁺: 362.0142, found: 362.0137.



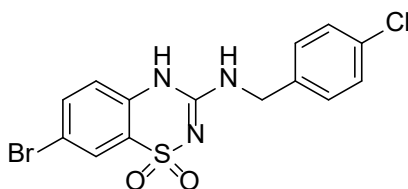
6-Chloro-3-((4-chlorobenzyl)amino)-4H-benzo[e][1,2,4]thiadiazine 1,1-dioxide (3.7b).

The white compound was obtained from **3.4b** by following the experimental conditions described for Method **A** (76% yield):

¹H NMR (400 MHz, DMSO-*d*₆): δ= 4.47 (2H, d, *J*=5.8 Hz), 7.29 (q, 2H), 7.37 (2H, d, *J*=8.5 Hz), 7.41 (2H, d, *J*=8.5 Hz), 7.68 (1H, d, *J*=8.5 Hz), 7.70 (br, 1H) 10.84 ppm (br, 1H).

¹³C NMR (100 MHz, DMSO-*d*₆): δ= 43.67, 116.64, 121.84, 124.34, 125.45, 128.80, 129.54, 131.31, 132.11, 137.01, 137.53, 138.00, 151.47 ppm.

HRMS (ESI): *m/z* calcd for C₁₄H₁₁Cl₂N₃O₂S [*M*+Na]⁺: 377.9846, found: 377.9839.



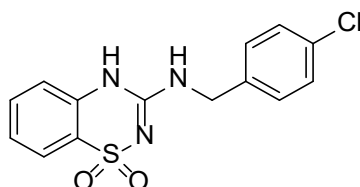
7-Bromo-3-((4-chlorobenzyl)amino)-4H-benzo[e][1,2,4]thiadiazine 1,1-dioxide (3.7c).

The white compound was obtained from **3.4c** by following the experimental conditions described for Method **A** (68% yield):

¹H NMR (400 MHz, DMSO-*d*₆): δ= 4.46 (2H, d, *J*=5.8 Hz), 7.19 (1H, d, *J*=8.7 Hz), 7.36 (2H, d, *J*=8.7 Hz), 7.40 (2H, d, *J*=8.7 Hz), 7.78 (m, 3H), 7.70 (s, 1H), 11.01 ppm (s, 1H).

¹³C NMR (100 MHz, DMSO-*d*₆): δ= 43.68, 115.14, 119.63, 124.53, 125.41, 128.80, 129.52, 132.11, 135.45, 135.66, 138.01, 151.52 ppm.

HRMS (ESI): *m/z* calcd for C₁₄H₁₁ClBrN₃O₂S [*M*+Na]⁺: 421.9341, found: 421.9324.



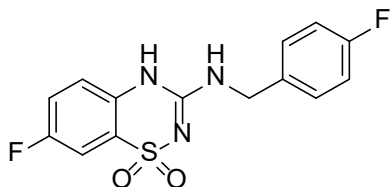
3-((4-Chlorobenzyl)amino)-4*H*-benzo[*e*][1,2,4]thiadiazine 1,1-dioxide (3.7d).

The white compound was obtained from **3.4d** by following the experimental conditions described for Method **A** (67% yield):

¹H NMR (400 MHz, DMSO-*d*₆): δ= 4.47 (2H, d, *J*=5.8 Hz), 7.21 (1H, d, *J*=8.5 Hz), 7.26 (1H, t, *J*=7.8 Hz), 7.37 (2H, d, *J*=8.5 Hz), 7.41 (2H, d, *J*=8.5 Hz), 7.56 (1H, t, *J*=8.3 Hz), 7.61 (br, 1H), 7.65 (1H, dd, *J*=7.8, 2 Hz), 10.85 ppm (s, 1H).

¹³C NMR (100 MHz, DMSO-*d*₆): δ= 43.57, 117.02, 119.63, 123.05, 123.30, 124.26, 128.79, 129.51, 132.05, 132.89, 136.13, 138.22, 151.62 ppm.

HRMS (ESI): *m/z* calcd for C₁₄H₁₁ClN₃O₂S [*M*+Na]⁺: 344.0236, found: 344.0236.



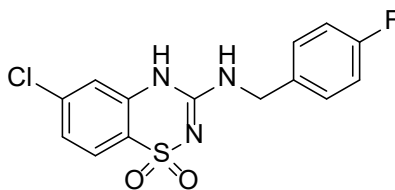
7-Fluoro-3-((4-fluorobenzyl)amino)-4*H*-benzo[*e*][1,2,4]thiadiazine 1,1-dioxide (3.8a).

The white compound was obtained from **3.4a** by following the experimental conditions described for Method **A** (81% yield):

¹H NMR (400 MHz, DMSO-*d*₆): δ = 4.46 (s, 2H), 7.16 (2H, t, *J*=8.8 Hz), 7.27 (q, 1H), 7.38 (m, 2H), 7.45 (1H, t, *J*=8.8 Hz), 7.52 (1H, dd, *J*=7.5, 2.8 Hz), 7.68 (br, 1H), 10.68 ppm (br, 1H).

¹³C NMR (100 MHz, DMSO-*d*₆): δ = 43.66, 109.23, 115.48, 119.60, 120.77, 123.80, 129.77, 132.92, 135.20, 151.80, 156.84, 159.26, 160.58, 163.00 ppm.

HRMS (ESI): *m/z* calcd for C₁₄H₁₁F₂N₃O₂S [*M*+Na]⁺: 346.0437, found: 346.0428.



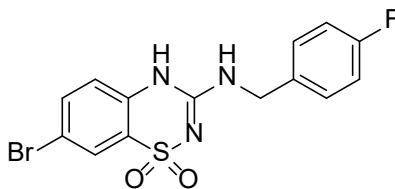
6-Chloro-3-((4-fluorobenzyl)amino)-4H-benzo[e][1,2,4]thiadiazine 1,1-dioxide (3.8b).

The white compound was obtained from **3.4b** by following the experimental conditions described for Method **A** (77% yield):

¹H NMR (400 MHz, DMSO-*d*₆): δ = 4.47 (s, 2H), 7.18 (2H, t, *J*=8.8 Hz), 7.28 (q, 1H), 7.39 (q, 2H), 7.46 (1H, t, *J*=8.8 Hz), 7.53 (1H, dd, *J*=7.5, 2.8 Hz), 7.67 (br, 1H), 10.83 ppm (br, 1H).

¹³C NMR (100 MHz, DMSO-*d*₆): δ = 43.65, 109.50, 115.69, 119.50, 120.79, 123.86, 129.76, 132.84, 135.19, 151.75, 156.85, 159.27, 160.58, 163.00 ppm.

HRMS (ESI): *m/z* calcd for C₁₄H₁₁ClF₂N₃O₂S [*M*+Na]⁺: 362.0142, found: 362.0160.



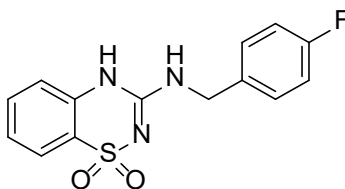
7-Bromo-3-((4-fluorobenzyl)amino)-4H-benzo[e][1,2,4]thiadiazine 1,1-dioxide (3.8c).

The white compound was obtained from **3.4c** by following the experimental conditions described for Method **A** (63% yield):

¹H NMR (400 MHz, DMSO-*d*₆): δ = 4.45 (2H, d, *J*=5.8 Hz), 7.18 (3H, d, *J*=8.8 Hz), 7.38 (q, 2H), 7.72 (2H, dd, *J*=8.7, 2.2 Hz), 7.78 (1H, d, *J*=2.2 Hz), 10.94 ppm (s, 1H).

¹³C NMR (100 MHz, DMSO-*d*₆): δ = 43.66, 115.12, 115.50, 115.71, 119.63, 124.56, 125.40, 129.77, 135.11, 135.46, 135.65, 151.49, 160.59, 163.00 ppm.

HRMS (ESI): *m/z* calcd for C₁₄H₁₁BrFN₃O₂S [*M*+Na]⁺: 405.9637, found: 405.9602.



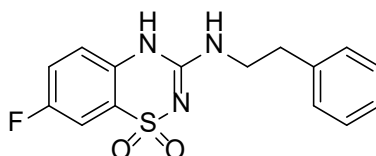
3-((4-Fluorobenzyl)amino)-4H-benzo[e][1,2,4]thiadiazine 1,1-dioxide (3.8d).

The white compound was obtained from **3.4d** by following the experimental conditions described for Method **A** (66% yield):

¹H NMR (400 MHz, DMSO-*d*₆): δ = 4.45 (2H, d, *J*=5.8 Hz), 7.18 (3H, t, *J*=8.8 Hz), 7.26 (2H, d, *J*=7.4 Hz), 7.39 (q, 2H), 7.55 (2H, t, *J*=7.2 Hz), 7.69 (1H, d, *J*=7.8 Hz), 10.77 ppm (s, 1H).

^{13}C NMR (100 MHz, DMSO- d_6): δ = 43.56, 115.49, 115.70, 117.02, 123.07, 123.70, 124.24, 129.77, 132.87, 135.30, 136.13, 151.59, 160.58, 162.99 ppm.

HRMS (ESI): m/z calcd for $\text{C}_{14}\text{H}_{12}\text{FN}_3\text{O}_2\text{S}$ $[M+\text{Na}]^+$: 328.0531, found: 328.0530.



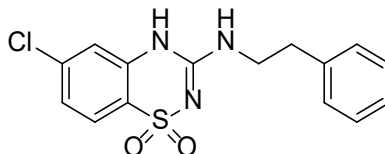
7-Fluoro-3-(phenethylamino)-4H-benzo[e][1,2,4]thiadiazine 1,1-dioxide (3.9a).

The white compound was obtained from **3.4a** by following the experimental conditions described for Method **A** (76% yield):

^1H NMR (400 MHz, DMSO- d_6): δ = 2.86 (2H, t, J =7.2 Hz), 3.48 (q, 2H), 7.20- 7.34 (m, 7H), 7.45 (1H, t, J =7.3 Hz), 7.52 (1H, dd, J =7.5, 2.8 Hz), 10.55 ppm (s, 1H).

^{13}C NMR (100 MHz, DMSO- d_6): δ = 35.08, 43.42, 109.23, 119.47, 120.49, 120.72, 123.79, 126.74, 128.90, 129.15, 132.85, 139.32, 151.69, 156.76, 159.21 ppm.

HRMS (ESI): m/z calcd for $\text{C}_{15}\text{H}_{14}\text{FN}_3\text{O}_2\text{S}$ $[M+\text{Na}]^+$: 342.0688, found: 342.0687.



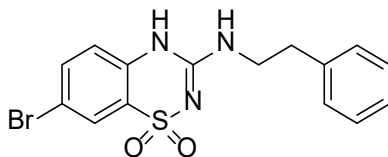
6-Chloro-3-(phenethylamino)-4H-benzo[e][1,2,4]thiadiazine 1,1-dioxide (3.9b).

The white compound was obtained from **3.4b** by following the experimental conditions described for Method **A** (73% yield):

¹H NMR (400 MHz, DMSO-*d*₆): δ = 2.86 (2H, t, *J* = 7.2 Hz), 3.47 (q, 2H), 7.20- 7.34 (m, 8H), 7.68 (1H, dd, *J* = 8.4 Hz), 10.71 ppm (br, 1H).

¹³C NMR (100 MHz, DMSO-*d*₆): δ = 35.00, 42.43, 116.52, 121.86, 124.22, 125.43, 126.74, 128.89, 129.15, 132.85, 136.94, 137.52, 139.29, 151.39 ppm.

HRMS (ESI): *m/z* calcd for C₁₅H₁₄ClN₃O₂S [*M*+Na]⁺: 358.0392, found: 358.0388.



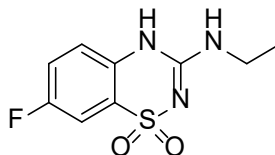
7-Bromo-3-(phenethylamino)-4*H*-benzo[*e*][1,2,4]thiadiazine 1,1-dioxide (3.9c).

The white compound was obtained from **3.4c** by following the experimental conditions described for Method **A** (65% yield):

¹H NMR (400 MHz, DMSO-*d*₆): δ = 2.86 (2H, t, *J* = 7.3 Hz), 3.48 (q, 2H), 7.15- 7.34 (m, 7H), 7.70 (1H, dd, *J* = 8.7, 2.2 Hz), 7.77 (1H, d, *J* = 2.2 Hz), 10.79 ppm (br, 1H).

¹³C NMR (100 MHz, DMSO-*d*₆): δ = 35.03, 42.42, 115.01, 119.51, 124.52, 125.39, 126.75, 128.90, 129.14, 135.44, 135.58, 139.27, 151.43 ppm.

HRMS (ESI): *m/z* calcd for C₁₅H₁₄BrN₃O₂S [*M*+Na]⁺: 401.9887, found: 401.9857.



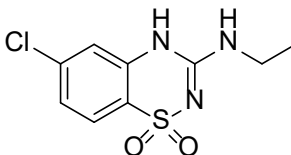
3-(Ethylamino)-7-fluoro-4*H*-benzo[*e*][1,2,4]thiadiazine 1,1-dioxide (3.10a).

The white compound was obtained from **3.4a** by following the experimental conditions described for Method **A** (71% yield):

¹H NMR (400 MHz, DMSO-*d*₆): δ = 1.12 (3H, t, *J*=7.1 Hz), 3.26 (m, 2H), 7.18 (br, 1H), 7.26 (m, 1H), 7.42 (m, 1H), 7.49 (1H, dd, *J*=7.5, 2.8 Hz), 10.66 ppm (s, 1H).

¹³C NMR (100 MHz, DMSO-*d*₆): δ = 14.99, 36.03, 109.42, 119.44, 123.82, 132.89, 151.59, 156.78, 159.71 ppm.

HRMS (ESI): *m/z* calcd for C₉H₁₀FN₃O₂S [*M*+Na]⁺: 266.0375, found: 266.0385.



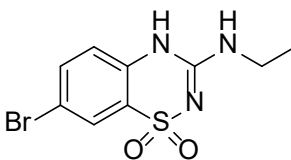
6-Chloro-3-(ethylamino)-4*H*-benzo[*e*][1,2,4]thiadiazine 1,1-dioxide (3.10b).

The white compound was obtained from **3.4b** by following the experimental conditions described for Method **A** (79% yield):

¹H NMR (400 MHz, DMSO-*d*₆): δ = 1.12 (3H, t, *J*=7.1 Hz), 3.25 (m, 2H), 7.19 (br, 1H), 7.27 (m, 1H), 7.42- 7.50 (m, 2H), 10.66 ppm (s, 1H).

¹³C NMR (100 MHz, DMSO-*d*₆): δ = 15.00, 36.03, 109.43, 119.44, 120.45, 132.88, 151.58, 156.75, 159.17 ppm.

HRMS (ESI): *m/z* calcd for C₉H₁₀ClN₃O₂S [*M*+Na]⁺: 282.0079, found: 282.0110.



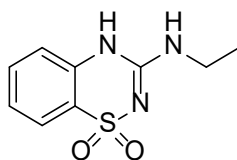
7-Bromo-3-(ethylamino)-4*H*-benzo[e][1,2,4]thiadiazine 1,1-dioxide (3.10c).

The white compound was obtained from **3.4c** by following the experimental conditions described for Method **A** with the slight modification that the crude material was dissolved in a 1:1 hydromethanolic solution of sodium bicarbonate instead of an aqueous solution of sodium bicarbonate (69% yield):

¹H NMR (400 MHz, DMSO-*d*₆): δ= 1.12 (3H, t, *J*=7.1 Hz), 3.25 (m, 2H), 7.19 (1H, d, *J*=8.5 Hz), 7.23 (br, 1H), 7.71 (1H, dd, *J*=8.7, 2.2 Hz), 7.75 (1H, d, *J*=2.2 Hz), 10.72 ppm (s, 1H).

¹³C NMR (100 MHz, DMSO-*d*₆): δ= 14.96, 36.05, 114.92, 119.54, 124.60, 125.35, 135.54, 151.33 ppm.

HRMS (ESI): *m/z* calcd for C₉H₁₀BrN₃O₂S [*M*+Na]⁺: 325.9574, found: 325.9550.

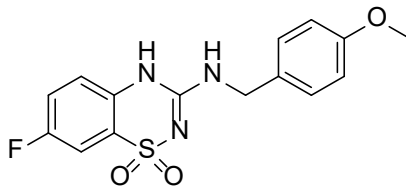
**3-(Ethylamino)-4*H*-benzo[e][1,2,4]thiadiazine 1,1-dioxide (3.10d).**

The white compound was obtained from **3.4d** by following the experimental conditions described for Method **A** (74% yield):

¹H NMR (400 MHz, DMSO-*d*₆): δ= 1.12 (3H, t, *J*=7.1 Hz), 3.25 (m, 2H), 7.07 (br, 1H), 7.19 (1H, d, *J*=8 Hz), 7.24 (1H, t, *J*=8 Hz), 7.53 (1H, t, *J*=8.7 Hz), 7.64 (1H, dd, *J*=7.8, 2 Hz), 10.56 ppm (s, 1H).

¹³C NMR (100 MHz, DMSO-*d*₆): δ= 15.03, 35.93, 116.90, 123.09, 123.25, 124.06, 132.76, 136.21, 151.45 ppm.

HRMS (ESI): *m/z* calcd for C₉H₁₁N₃O₂S [*M*+Na]⁺: 248.0469, found: 248.0466.



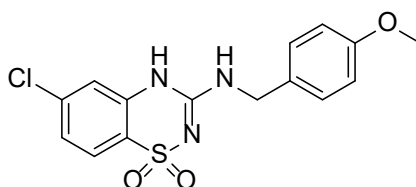
7-Fluoro-3-((4-methoxybenzyl)amino)-4H-benzo[e][1,2,4]thiadiazine 1,1-dioxide (3.11a).

The white compound was obtained from **3.4a** by following the experimental conditions described for Method **A** (82% yield):

¹H NMR (400 MHz, DMSO-*d*₆): δ= 3.73 (s, 3H), 4.40 (s, 2H), 6.92 (2H, d, *J*=8.5 Hz), 7.27 (m, 3H), 7.45 (2H, t, *J*=8.7 Hz), 7.51 (1H, dd, *J*=7.5, 2.8 Hz), 7.60 ppm (br, 1H).

¹³C NMR (100 MHz, DMSO-*d*₆): δ= 43.85, 55.51, 109.21, 114.25, 119.54, 120.48, 120.72, 123.81, 129.14, 130.83, 133.06, 151.80, 156.77, 158.90, 159.19 ppm.

HRMS (ESI): *m/z* calcd for C₁₅H₁₄FN₃O₃S [*M*+Na]⁺: 358.0637, found: 358.0616.



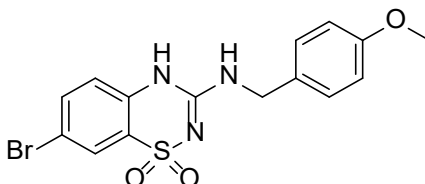
6-Chloro-3-((4-methoxybenzyl)amino)-4H-benzo[e][1,2,4]thiadiazine 1,1-dioxide (3.11b).

The white compound was obtained from **3.4b** by following the experimental conditions described for Method **A** (77% yield):

¹H NMR (400 MHz, DMSO-*d*₆): δ= 3.73 (s, 3H), 4.40 (s, 2H), 6.92 (2H, d, *J*=8.5 Hz), 7.28 (m, 4H), 7.69 (1H, d, *J*=8.7 Hz), 7.74 ppm (br, 1H).

^{13}C NMR (100 MHz, DMSO- d_6): δ = 43.87, 55.51, 114.25, 116.63, 121.87, 124.23, 125.41, 129.19, 130.65, 130.90, 137.01, 137.60, 151.40, 158.93 ppm.

HRMS (ESI): m/z calcd for $\text{C}_{15}\text{H}_{14}\text{ClN}_3\text{O}_3\text{S}$ $[M+\text{Na}]^+$: 374.0342, found: 374.0332.



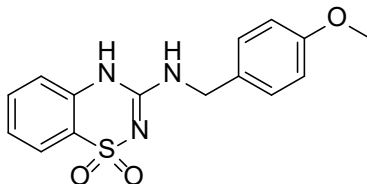
7-Bromo-3-((4-methoxybenzyl)amino)-4H-benzo[e][1,2,4]thiadiazine 1,1-dioxide (3.11c).

The white compound was obtained from **3.4c** by following the experimental conditions described for Method **A** (75% yield):

^1H NMR (400 MHz, DMSO- d_6): δ = 3.73 (s, 3H), 4.39 (2H, d, J =5.8 Hz), 6.92 (m, 2H), 7.19 (1H, d, J =8.7 Hz), 7.26 (2H, d, J =8.7 Hz), 7.65 (br, 1H), 7.71 (1H, dd, J =8.7, 2.2 Hz), 7.78 (1H, d, J =2.2 Hz), 10.85 ppm (s, 1H).

^{13}C NMR (100 MHz, DMSO- d_6): δ = 43.86, 55.54, 114.28, 115.05, 119.59, 124.59, 125.39, 129.17, 130.66, 135.47, 135.61, 151.53, 158.94 ppm.

HRMS (ESI): m/z calcd for $\text{C}_{15}\text{H}_{14}\text{BrN}_3\text{O}_3\text{S}$ $[M+\text{Na}]^+$: 417.9836, found: 417.9811.



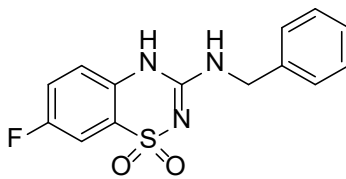
3-((4-Methoxybenzyl)amino)-4H-benzo[e][1,2,4]thiadiazine 1,1-dioxide (3.11d).

The white compound was obtained from **3.4d** by following the experimental conditions described for Method **A** (69% yield):

¹H NMR (400 MHz, DMSO-*d*₆): δ = 3.73 (s, 3H), 4.39 (2H, d, *J*=5.8 Hz), 6.93 (1H, d, *J*=8.7 Hz), 7.18 (1H, d, *J*=8.2 Hz), 7.37 (m, 3H), 7.49 (br, 1H), 7.55 (2H, t, *J*=8.3 Hz), 7.66 (1H, dd, *J*=7.8, 2 Hz), 10.68 ppm (s, 1H).

¹³C NMR (100 MHz, DMSO-*d*₆): δ = 43.75, 55.53, 114.27, 116.98, 123.10, 123.30, 124.18, 129.16, 130.85, 132.84, 136.15, 151.53, 158.91 ppm.

HRMS (ESI): *m/z* calcd for C₁₅H₁₅N₃O₃S [*M*+Na]⁺: 340.0731, found: 340.0722 .



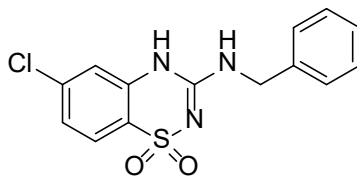
3-(Benzylamino)-7-fluoro-4H-benzo[e][1,2,4]thiadiazine 1,1-dioxide (3.12a).

The white compound was obtained from **3.4a** by following the experimental conditions described for Method **A** (61% yield):

¹H NMR (400 MHz, DMSO-*d*₆): δ = 4.48 (2H, d, *J*=5.8 Hz), 7.26 (m, 2H), 7.34 (m, 4H), 7.51 (m, 2H), 7.65 (br, 1H), 10.70 ppm (br, 1H).

¹³C NMR (100 MHz, DMSO-*d*₆): δ = 44.35, 109.25, 109.49, 119.45, 120.54, 123.87, 127.84, 129.07, 132.94, 138.97, 151.86, 156.83, 159.25 ppm.

HRMS (ESI): *m/z* calcd for C₁₄H₁₂FN₃O₂S [*M*+Na]⁺: 328.0531, found: 328.0523.



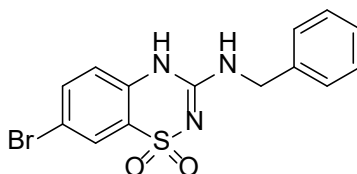
3-(Benzylamino)-6-chloro-4H-benzo[e][1,2,4]thiadiazine 1,1-dioxide (3.12b).

The white compound was obtained from **3.4b** by following the experimental conditions described for Method **A** (56% yield):

¹H NMR (400 MHz, DMSO-*d*₆): δ= 4.48 (s, 2H), 7.29 (m, 3H), 7.34 (m, 4H) 7.69 (1H, d, *J*=8.8 Hz), 7.82 (br, 1H), 10.46 ppm (br, 1H).

¹³C NMR (100 MHz, DMSO-*d*₆): δ= 44.34, 116.69, 121.88, 124.23, 125.42, 127.58, 127.68, 128.87, 136.99, 137.69, 138.86, 151.57 ppm.

HRMS (ESI): *m/z* calcd for C₁₄H₁₂ClN₃O₂S [*M*+Na]⁺: 344.0236, found: 344.0235.



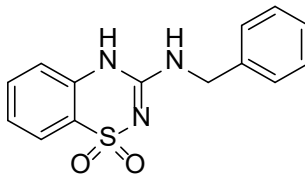
3-(Benzylamino)-7-bromo-4H-benzo[e][1,2,4]thiadiazine 1,1-dioxide (3.12c).

The white compound was obtained from **3.4c** by following the experimental conditions described for Method **A** (70%, yield):

¹H NMR (400 MHz, DMSO-*d*₆): δ= 4.48 (2H, d, *J*=5.8 Hz), 7.21 (1H, d, *J*=8.7 Hz), 7.27 (m, 1H), 7.34 (m, 4H), 7.72 (2H, dd, *J*=8.7, 2.2 Hz), 7.78 (1H, d, *J*=2.2 Hz), 10.87 ppm (s, 1H).

¹³C NMR (100 MHz, DMSO-*d*₆): δ= 44.33, 115.08, 119.63, 124.57, 125.39, 127.59, 127.67, 128.87, 135.50, 135.64, 138.84, 151.57 ppm.

HRMS (ESI): m/z calcd for $C_{14}H_{12}BrN_3O_2S$ $[M+Na]^+$: 387.9731, found: 387.9710.



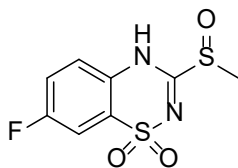
3-(Benzylamino)-4H-benzo[e][1,2,4]thiadiazine 1,1-dioxide (3.12d).

The white compound was obtained from **3.4d** by following the experimental conditions described for Method **A** (67% yield):

1H NMR (400 MHz, DMSO- d_6): δ = 4.49 (2H, d, J =5.8 Hz), 7.22 (1H, d, J =8.2 Hz), 7.26 (m, 2H), 7.34 (4H, d, J =4.5 Hz), 7.55 (2H, t, J =8.3 Hz), 7.70 (1H, d, J =7.8 Hz), 10.74 ppm (s, 1H).

^{13}C NMR (100 MHz, DMSO- d_6): δ = 44.26, 117.03, 123.10, 123.31, 124.22, 127.56, 127.67, 128.87, 136.16, 139.03, 151.65 ppm.

HRMS (ESI): m/z calcd for $C_{14}H_{13}N_3O_2S$ $[M+Na]^+$: 310.0626, found: 310.0621.



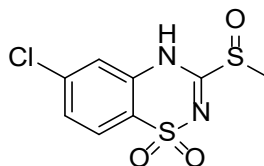
7-Fluoro-3-(methylsulfinyl)-4H-benzo[e][1,2,4]thiadiazine 1,1-dioxide (3.4aa).

The 7-fluoro-3-methylsulfonyl-4H-1,2,4-benzothiadiazine 1,1-dioxide (**3.4a**, 0.5 g, 2.03 mmol) was suspended in an aqueous solution of sodium carbonate (2.2 g/25 ml) and the aqueous solution 2N NaOH was added until the mixture was completely dissolved. At room temperature, bromine (0.2 mL, 2.03 mmol) was added under vigorous stirring for 30

mins, the resulting suspension was adjusted to pH 2-3 by adding 6N HCl. The insoluble compound was collected by filtration, washed twice with water, and suspended under stirring in methanol (10 mL). The resultant white precipitate was collected by filtration, washed with water and methanol, and air dried (0.443 g, 83% yield):

¹H NMR (400 MHz, DMSO-*d*₆): δ = 3.45 (s, 3H), 7.66 (m, 1H), 7.76-7.81 ppm (m, 2H).

HRMS (ESI): *m/z* calcd for C₈H₇FN₂O₃S₂ [*M*+Na]⁺: 284.9780, found: 284.9831.

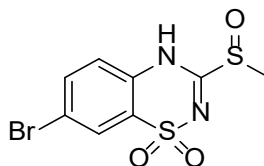


6-Chloro-3-(methylsulfinyl)-4*H*-benzo[*e*][1,2,4]thiadiazine 1,1-dioxide (3.4ba).

The white compound was obtained from **3.4b** (1 g, 3.81 mmol) by following the experimental conditions described for **3.4aa** (0.965 g, 91% yield):

¹H NMR (400 MHz, DMSO-*d*₆): δ = 3.44 (s, 3H), 7.66 (m, 1H), 7.74-7.80 ppm (m, 2H).

HRMS (ESI): *m/z* calcd for C₈H₇ClN₂O₃S₂ [*M*+Na]⁺: 300.9484, found: 300.9526.

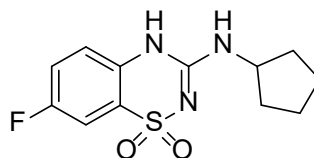


7-Bromo-3-(methylsulfinyl)-4*H*-benzo[*e*][1,2,4]thiadiazine 1,1-dioxide (3.4ca).

The white compound was obtained from **3.4c** (1 g, 3.26 mmol) by following the experimental conditions described for **3.4aa** (0.725 g, 75% yield):

¹H NMR (400 MHz, DMSO-*d*₆): δ= 3.45 (s, 3H), 7.66 (m, 1H), 7.76-7.81 ppm (m, 1H).

HRMS (ESI): *m/z* calcd for C₈H₇BrN₂O₂S₂ [*M*+Na]⁺: 328.9030, found: 328.9018.



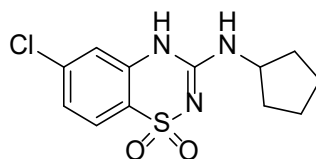
7-Fluoro-3-(cyclopentylamino)-4*H*-benzo[*e*][1,2,4]thiadiazine 1,1-dioxide (3.13a).

A mixture of 7-fluoro-3-methylsulfinyl-4*H*-1,2,4-benzothiadiazine 1,1-dioxide (**3.4aa**) (0.25 g, 0.953 mmol) and cyclopentylamine (0.3 mL, 2.89 mmol) was dissolved in 1,4-dioxane (5 mL) and heated in a sealed vessel overnight at 160 °C. The solvent and excess amine was removed in vacuo, and the residue was dissolved in a hydromethanolic (1:1) 2% w/v solution of NaOH (10mL). The alkaline solution was treated with charcoal and was filtered, and the filtrate was adjusted to pH 4-5 with 6N HCl. The precipitate was collected by filtration, washed with water, and air dried. The dried compound was suspended in an aqueous solution of sodium bicarbonate NaHCO₃ (1 g/40 mL). The alkaline solution was treated with charcoal and filtered, and the filtrate was adjusted to pH 4-5 with 6 N HCl. The white precipitate was collected by filtration, washed with water, and air dried. The white compound was recrystallized from methanol/water (0.185 g, 68% yield):

¹H NMR (400 MHz, DMSO-*d*₆): δ= 1.46 -1.66 (m, 6H), 1.90 (m, 2H), 4.07 (m, 1H), 7.27 (s, 2H), 7.45 (m, 2H), 10.35 ppm (s, 1H).

¹³C NMR (100 MHz, DMSO-*d*₆): δ= 23.72, 32.71, 52.82, 109.42, 119.46, 120.66, 132.74, 151.31, 156.78, 159.20 ppm.

HRMS (ESI): *m/z* calcd for C₁₂H₁₄FN₃O₂S [*M*+Na]⁺: 306.0688, found: 306.0675.



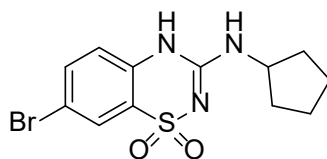
6-Chloro-3-(cyclopentylamino)-4H-benzo[e][1,2,4]thiadiazine 1,1-dioxide (3.13b).

The white compound was obtained from **3.4ba** (0.25 g, 0.897 mmol) by following the experimental conditions described for **3.4a** (0.166 g, 61% yield):

¹H NMR (400 MHz, DMSO-*d*₆): δ = 1.48- 1.67 (m, 6H), 1.91 (m, 2H), 4.06 (m, 1H), 7.29 (2H, dd, *J*=8.5, 2 Hz), 7.39 (br, 1H), 7.69 (1H, d, *J*=8.7 Hz), 10.32 ppm (s, 1H).

¹³C NMR (100 MHz, DMSO-*d*₆): δ = 22.65, 32.66, 52.85, 116.63, 121.98, 124.23, 125.38, 136.91, 137.44, 150.99 ppm.

HRMS (ESI): *m/z* calcd for C₁₂H₁₄ClN₃O₂S [*M*+Na]⁺: 322.0392, found: 322.0407.



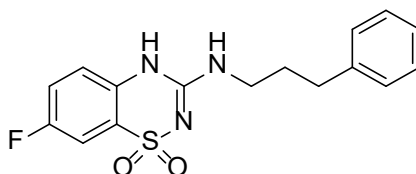
7-Bromo-3-(cyclopentylamino)-4H-benzo[e][1,2,4]thiadiazine 1,1-dioxide (3.13c).

The white compound was obtained from **3.4ca** (0.25 g, 0.77 mmol) by following the experimental conditions described for **3.4a** with the slight modification that the crude material was dissolved in a 1:1 hydromethanolic solution of sodium bicarbonate instead of an aqueous solution of sodium bicarbonate (0.132 g, 49% yield):

¹H NMR (400 MHz, DMSO-*d*₆): δ = 1.48 -1.67 (m, 6H), 1.91 (m, 2H), 4.06 (m, 1H), 7.19 (br, 2H), 7.28 (br, 1H), 7.76 (m, 1H), 10.40 ppm (s, 1H).

^{13}C NMR (100 MHz, DMSO- d_6): δ = 23.64, 32.69, 52.84, 114.99, 119.63, 124.65, 125.34, 135.40, 135.54, 151.05 ppm.

HRMS (ESI): m/z calcd for $\text{C}_{12}\text{H}_{14}\text{BrN}_3\text{O}_2\text{S}$ $[M+\text{Na}]^+$: 365.9887, found: 365.9879.



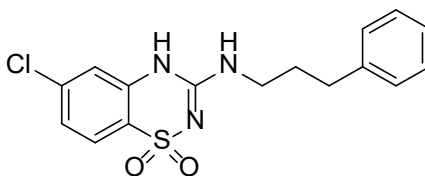
7-Fluoro-3-((3-phenylpropyl)amino)-4H-benzo[e][1,2,4]thiadiazine 1,1-dioxide (3.14a).

The white compound was obtained from **3.4a** by following the experimental conditions described for Method **A** (76% yield):

^1H NMR (400 MHz, DMSO- d_6): δ = 1.83 (m, 2H), 2.63 (2H, t, J =7.8 Hz), 3.24 (q, 2H) 7.16-7.30 (m, 7H), 7.42- 7.51 (m, 2H), 10.68 ppm (br, 1H).

^{13}C NMR (100 MHz, DMSO- d_6): δ = 31.01, 32.78, 109.20, 109.45, 119.40, 120.47, 120.70, 123.90, 126.28, 128.79, 132.87, 141.86, 151.75, 156.78, 159.19 ppm.

HRMS (ESI): m/z calcd for $\text{C}_{16}\text{H}_{16}\text{FN}_3\text{O}_2\text{S}$ $[M+\text{Na}]^+$: 356.0844, found: 356.0811.



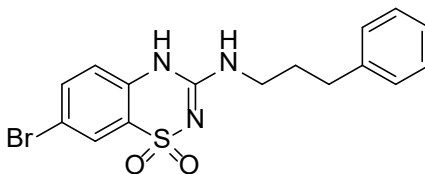
6-Chloro-3-((3-phenylpropyl)amino)-4H-benzo[e][1,2,4]thiadiazine 1,1-dioxide (3.14b).

The white compound was obtained from **3.4b** by following the experimental conditions described for Method **A** (65% yield):

¹H NMR (400 MHz, DMSO-*d*₆): δ= 1.83 (m, 2H), 2.63 (2H, t, *J*=7.8 Hz), 3.23 (q, 2H), 7.17-7.37 (m, 8H), 7.67 (1H, d, *J*=8.5 Hz), 10.66 ppm (s, 1H).

¹³C NMR (100 MHz, DMSO-*d*₆): δ= 30.93, 31.16, 32.79, 116.59, 121.92, 124.18, 125.40, 126.29, 128.75, 128.80, 136.90, 137.60, 141.86, 151.44 ppm.

HRMS (ESI): *m/z* calcd for C₁₆H₁₆ClN₃O₂S [*M*+Na]⁺: 372.0549, found: 372.0544.



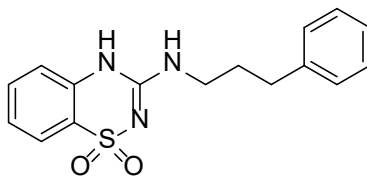
7-Bromo-3-((3-phenylpropyl)amino)-4*H*-benzo[*e*][1,2,4]thiadiazine 1,1-dioxide (3.14c).

The white compound was obtained from **3.4c** by following the experimental conditions described for Method **A** with the slight modification that the crude material was dissolved in a 1:1 hydromethanolic solution of sodium bicarbonate instead of an aqueous solution of sodium bicarbonate (74% yield):

¹H NMR (400 MHz, DMSO-*d*₆): δ= 1.83 (m, 2H), 2.63 (2H, t, *J*=7.8 Hz), 3.26 (q, 2H), 7.16-7.31 (m, 7H), 7.71 (1H, dd, *J*=8.7, 2.2 Hz), 7.76 (1H, d, *J*=2.2 Hz), 10.73 ppm (br, 1H).

¹³C NMR (100 MHz, DMSO-*d*₆): δ= 30.95, 32.78, 114.97, 119.56, 124.61, 125.36, 126.28, 128.74, 128.79, 135.50, 135.55, 141.85, 151.49 ppm.

HRMS (ESI): *m/z* calcd for C₁₆H₁₆BrN₃O₂S [*M*+Na]⁺: 416.0044, found: 416.0036.



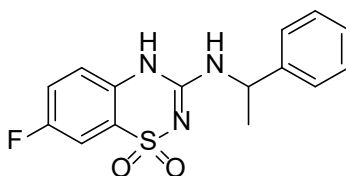
3-((3-phenylpropyl)amino)-4H-benzo[e][1,2,4]thiadiazine 1,1-dioxide (3.14d).

The white compound was obtained from **3.4d** by following the experimental conditions described for Method **A** (61% yield):

¹H NMR (400 MHz, DMSO-*d*₆): δ = 1.83 (m, 2H), 2.64 (2H, t, *J* = 7.5 Hz), 3.24 (q, 2H), 7.17-7.31 (m, 8H), 7.54 (1H, t, *J* = 8.3 Hz), 7.65 (1H, d, *J* = 7.8 Hz), 10.59 ppm (s, 1H).

¹³C NMR (100 MHz, DMSO-*d*₆): δ = 31.04, 32.80, 116.94, 123.10, 123.27, 124.09, 126.28, 128.75, 128.80, 132.78, 136.19, 141.89, 151.61 ppm.

HRMS (ESI): *m/z* calcd for C₁₆H₁₇N₃O₂S [*M*+Na]⁺: 338.0939, found: 338.0938.



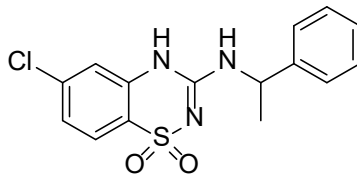
7-Fluoro-3-((1-phenylethyl)amino)-4H-benzo[e][1,2,4]thiadiazine 1,1-dioxide (3.15a).

The white compound was obtained from **3.4a** by following the experimental conditions described for Method **B** (76% yield):

¹H NMR (400 MHz, DMSO-*d*₆): δ = 1.48 (3H, d, *J* = 7.0 Hz), 5.02 (m, 1H), 7.27 (m, 2H), 7.39 (m, 4H), 7.48 (m, 2H), 7.70 (br, 1H), 10.52 ppm (s, 1H).

¹³C NMR (100 MHz, DMSO-*d*₆): δ = 32.91, 50.47, 109.48, 119.67, 120.54, 122.89, 126.41, 127.55, 128.91, 132.66, 143.84, 150.95, 156.85, 159.27 ppm.

HRMS (ESI): m/z calcd for $C_{15}H_{14}FN_3O_2S$ $[M+Na]^+$: 342.0688, found: 342.0676.



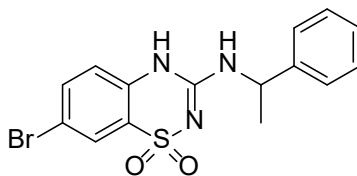
6-Chloro-3-((1-phenylethyl)amino)-4H-benzo[e][1,2,4]thiadiazine 1,1-dioxide (3.15b).

The white compound was obtained from **3.4b** by following the experimental conditions described for Method **B** (59% yield):

1H NMR (400 MHz, DMSO- d_6): δ = 1.48 (3H, d, J =7 Hz), 5.02 (m, 1H), 7.28 (m, 3H), 7.38 (m, 4H), 7.66 (1H, d, J =8.3 Hz), 7.84 (s, 1H), 10.58 ppm (s, 1H).

^{13}C NMR (100 MHz, DMSO- d_6): δ = 22.87, 50.48, 116.64, 120.80, 121.88, 124.34, 125.47, 126.43, 127.57, 128.92, 137.00, 137.63, 143.74, 150.68 ppm.

HRMS (ESI): m/z calcd for $C_{15}H_{14}ClN_3O_2S$ $[M+Na]^+$: 358.0392, found: 358.0385.



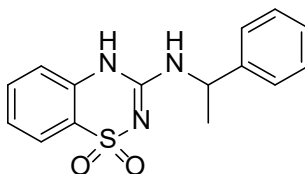
7-Bromo-3-((1-phenylethyl)amino)-4H-benzo[e][1,2,4]thiadiazine 1,1-dioxide (3.15c).

The white compound was obtained from **3.4c** by following the experimental conditions described for Method **B** with the slight modification that the crude material was dissolved in a 1:1 hydromethanolic solution of sodium bicarbonate instead of an aqueous solution of sodium bicarbonate (46% yield):

¹H NMR (400 MHz, DMSO-*d*₆): δ = 1.49 (3H, d, *J*=7 Hz), 5.02 (m, 1H), 7.19 (1H, d, *J*=8.7 Hz), 7.26 (m, 1H), 7.38 (m, 4H), 7.71 (2H, dd, *J*=8.7, 2.2 Hz), 7.76 (1H, d, *J*=2.2 Hz), 10.57 ppm (s, 1H).

¹³C NMR (100 MHz, DMSO-*d*₆): δ = 22.84, 50.50, 115.12, 119.69, 124.58, 125.38, 126.43, 127.14, 127.57, 128.91, 129.23, 135.31, 135.61, 143.73, 150.71 ppm.

HRMS (ESI): *m/z* calcd for C₁₅H₁₄BrN₃O₂S [*M*+Na]⁺: 401.9887, found: 401.9885.



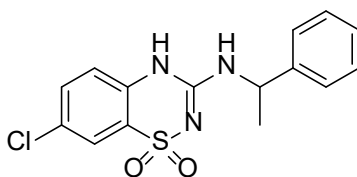
3-((1-Phenylethyl)amino)-4H-benzo[e][1,2,4]thiadiazine 1,1-dioxide (3.15d).

The white compound was obtained from **3.4d** by following the experimental conditions described for Method **B** (52% yield):

¹H NMR (400 MHz, DMSO-*d*₆): δ = 1.47 (3H, d, *J*=6.9 Hz), 5.03 (m, 1H), 7.19 (1H, d, *J*=8.2 Hz), 7.25 (m, 2H), 7.39 (m, 4H), 7.54 (2H, t, *J*=8.3 Hz), 7.58 (br, 1H), 7.67 (1H, d, *J*=7.6 Hz), 10.42 ppm (s, 1H).

¹³C NMR (100 MHz, DMSO-*d*₆): δ = 22.96, 50.36, 117.06, 123.08, 123.28, 124.26, 126.41, 127.54, 128.92, 132.86, 135.98, 143.91, 150.82 ppm.

HRMS (ESI): *m/z* calcd for C₁₅H₁₅N₃O₂S [*M*+Na]⁺: 324.0782, found: 324.0782.



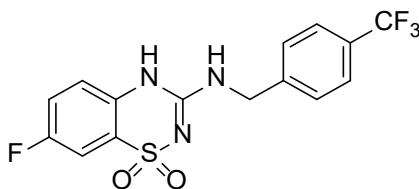
7-Chloro-3-((1-phenylethyl)amino)-4*H*-benzo[e][1,2,4]thiadiazine 1,1-dioxide (3.15e).

The white compound was obtained from **3.4e** by following the experimental conditions described for Method **B** (59% yield):

¹H NMR (400 MHz, DMSO-*d*₆): δ= 1.49 (3H, d, *J*=7.0 Hz), 5.02 (m, 1H), 7.25 (m, 2H), 7.38 (m, 4H), 7.60 (1H, dd, *J*=8.7, 2.4 Hz), 7.65 (1H, d, *J*=2.4 Hz), 7.76 (br, 1H), 10.62 ppm (s, 1H).

¹³C NMR (100 MHz, DMSO-*d*₆): δ= 22.88, 50.49, 119.42, 122.59, 124.23, 126.42, 127.58, 127.69, 128.92, 132.89, 134.95, 143.75, 150.79 ppm.

HRMS (ESI): *m/z* calcd for C₁₅H₁₄ClN₃O₂S [*M*+Na]⁺: 358.0392, found: 358.0361.



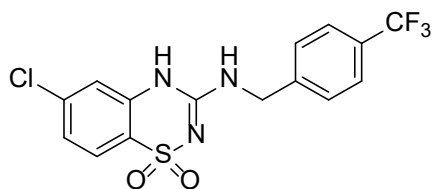
7-Fluoro-3-((4-(trifluoromethyl)benzyl)amino)-4*H*-benzo[e][1,2,4]thiadiazine 1,1-dioxide (3.16a).

The white compound was obtained from **3.4a** by following the experimental conditions described for Method **A** (53% yield):

¹H NMR (400 MHz, DMSO-*d*₆): δ= 4.58 (2H, d, *J*=5.9 Hz), 7.30 (m, 1H), 7.45- 7.56 (m, 4H), 7.71 (2H, d, *J*=8.2 Hz), 7.76 (br, 1H), 11.00 ppm (br, 1H).

¹³C NMR (100 MHz, DMSO-*d*₆): δ= 43.94, 109.27, 119.52, 120.62, 123.41, 123.82, 125.69, 126.11, 128.18, 132.81, 144.05, 151.82, 156.88, 159.30 ppm.

HRMS (ESI): *m/z* calcd for C₁₅H₁₁F₄N₃O₂S [*M*+Na]⁺: 396.0405, found: 396.0388.



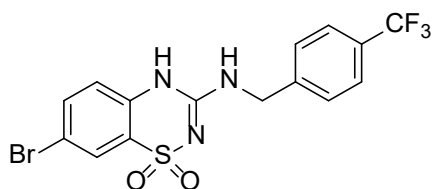
6-Chloro-3-((4-(trifluoromethyl)benzyl)amino)-4H-benzo[e][1,2,4]thiadiazine 1,1-dioxide (3.16b).

The white compound was obtained from **3.4b** by following the experimental conditions described for Method **A** (48% yield):

¹H NMR (400 MHz, DMSO-*d*₆): δ = 4.50 (2H, d, *J* = 5.8 Hz), 7.30 (s, 1H), 7.32 (1H, d, *J* = 2 Hz), 7.37 (2H, d, *J* = 8.5 Hz), 7.45 (2H, d, *J* = 8.7 Hz), 7.70 (1H, d, *J* = 8.7 Hz), 7.86 (s, 1H), 10.90 ppm (s, 1H).

¹³C NMR (100 MHz, DMSO-*d*₆): δ = 43.66, 116.65, 119.26, 121.50, 121.81, 121.87, 124.35, 125.45, 129.55, 137.01, 137.53, 138.48, 147.83, 151.48 ppm.

HRMS (ESI): *m/z* calcd for C₁₅H₁₁ClF₃N₃O₂S [*M*+Na]⁺: 412.0110, found: 412.1504.



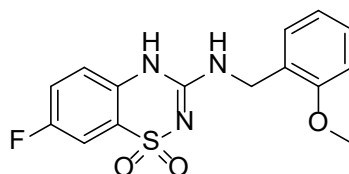
7-Bromo-3-((4-(trifluoromethyl)benzyl)amino)-4H-benzo[e][1,2,4]thiadiazine 1,1-dioxide (3.16c).

The white compound was obtained from **3.4c** by following the experimental conditions described for Method **A** (39% yield):

¹H NMR (400 MHz, DMSO-*d*₆): δ = 4.58 (2H, d, *J* = 5.2 Hz), 7.22 (1H, d, *J* = 8.7 Hz), 7.55 (2H, d, *J* = 8.1 Hz), 7.73 (m, 3H), 7.78 (1H, d, *J* = 2.2 Hz), 7.83 (br, 1H), 11.04 ppm (s, 1H).

¹³C NMR (100 MHz, DMSO-*d*₆): δ= 43.94, 115.16, 119.28, 123.41, 124.50, 125.41, 125.71, 126.11, 127.99, 128.21, 128.30, 135.51, 135.69, 143.97, 151.61 ppm.

HRMS (ESI): *m/z* calcd for C₁₅H₁₁BrF₃N₃O₂S [*M*+Na]⁺: 455.9605, found: 455.9591.



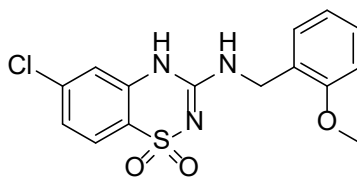
7-Fluoro-3-((2-methoxybenzyl)amino)-4*H*-benzo[*e*][1,2,4]thiadiazine 1,1-dioxide (3.17a).

The white compound was obtained from **3.4a** by following the experimental conditions described for Method **A** (71% yield):

¹H NMR (400 MHz, DMSO-*d*₆): δ= 3.48 (s, 3H), 4.43 (2H, d, *J*=5.7 Hz), 6.93 (1H, t, *J*=7.3 Hz), 7.02 (1H, d, *J*=8.1 Hz), 7.28 (m, 3H), 7.46 (2H, t, *J*=8.7 Hz), 7.52 (1H, dd, *J*=7.5, 2.8 Hz), 10.78 ppm (s, 1H).

¹³C NMR (100 MHz, DMSO-*d*₆): δ= 55.83, 109.51, 111.03, 119.47, 120.68, 123.79, 126.14, 128.38, 129.05, 132.78, 151.84, 156.83, 157.21, 159.25 ppm.

HRMS (ESI): *m/z* calcd for C₁₅H₁₄FN₃O₃S [*M*+Na]⁺: 358.0637, found: 358.0608.



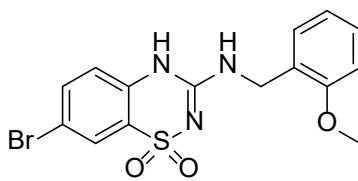
6-Chloro-3-((2-methoxybenzyl)amino)-4*H*-benzo[*e*][1,2,4]thiadiazine 1,1-dioxide (3.17b).

The white compound was obtained from **3.4b** by following the experimental conditions described for Method **A** (67% yield):

¹H NMR (400 MHz, DMSO-*d*₆): δ = 3.48 (s, 3H), 4.43 (2H, d, *J*=5.7 Hz), 6.93 (1H, t, *J*=7.3 Hz), 7.03 (1H, d, *J*=8.2 Hz), 7.28 (m, 4H), 7.66 (br, 1H), 7.68 (1H, d, *J*=8.3 Hz), 10.47 ppm (br, 1H).

¹³C NMR (100 MHz, DMSO-*d*₆): δ = 55.86, 111.08, 116.57, 120.68, 121.84, 124.25, 125.43, 126.04, 128.44, 129.08, 136.99, 137.53, 151.55, 157.23 ppm.

HRMS (ESI): *m/z* calcd for C₁₅H₁₄ClN₃O₃S [*M*+Na]⁺: 374.0342, found: 374.0336.



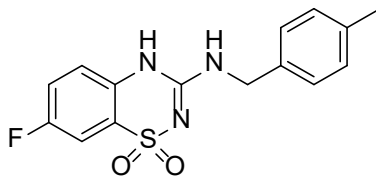
7-Bromo-3-((2-methoxybenzyl)amino)-4*H*-benzo[*e*][1,2,4]thiadiazine 1,1-dioxide (3.17c).

The white compound was obtained from **3.4c** by following the experimental conditions described for Method **A** (56% yield):

¹H NMR (400 MHz, DMSO-*d*₆): δ = 3.84 (s, 3H), 4.42 (2H, d, *J*=5.3 Hz), 6.93 (1H, t, *J*=7.3 Hz), 7.03 (1H, d, *J*=8.2 Hz), 7.18 (1H, d, *J*=8.5 Hz), 7.22 (1H, d, *J*=7.2 Hz), 7.28 (1H, t, *J*=7.7 Hz), 7.46 (br, 1H), 7.72 (1H, dd, *J*=8.7, 2 Hz), 7.77 (1H, d, *J*=2 Hz), 10.69 ppm (br, 1H).

¹³C NMR (100 MHz, DMSO-*d*₆): δ = 55.86, 111.08, 115.00, 119.60, 120.69, 124.51, 125.40, 126.06, 128.42, 129.08, 135.61, 151.61, 157.22 ppm.

HRMS (ESI): *m/z* calcd for C₁₅H₁₄BrN₃O₃S [*M*+Na]⁺: 417.9836, found: 417.9816.



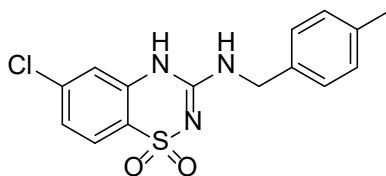
7-Fluoro-3-((4-methylbenzyl)amino)-4H-benzo[e][1,2,4]thiadiazine 1,1-dioxide (3.18a).

The white compound was obtained from **3.4a** by following the experimental conditions described for Method **A** (74% yield):

¹H NMR (400 MHz, DMSO-*d*₆): δ= 2.28 (s, 3H), 4.44 (2H, d, *J*=5.7 Hz), 7.16 (2H, d, *J*=7.8 Hz), 7.22 (2H, d, *J*=7.8 Hz), 7.28 (m, 1H), 7.46 (m, 1H), 7.52 (1H, dd, *J*=7.5, 2.8 Hz), 7.64 (br, 1H), 10.81 ppm (s, 1H).

¹³C NMR (100 MHz, DMSO-*d*₆): δ= 21.13, 44.10, 109.49, 119.54, 120.53, 120.77, 123.89, 127.66, 129.40, 132.84, 135.86, 136.68, 151.75, 156.83, 157.21, 159.25 ppm.

HRMS (ESI): *m/z* calcd for C₁₅H₁₄FN₃O₂S [*M*+Na]⁺: 342.0688, found: 342.0672.



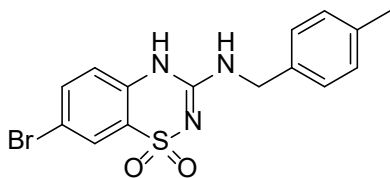
6-Chloro-3-((4-methylbenzyl)amino)-4H-benzo[e][1,2,4]thiadiazine 1,1-dioxide (3.18b).

The white compound was obtained from **3.4b** by following the experimental conditions described for Method **A** (78% yield):

¹H NMR (400 MHz, DMSO-*d*₆): δ= 2.28 (s, 3H), 4.41 (2H, d, *J*=4.2 Hz), 7.17 (2H, d, *J*=7.9 Hz), 7.22 (2H, d, *J*=7.9 Hz), 7.28 (s, 1H), 7.30 (s, 1H), 7.68 (1H, d, *J*=8.3 Hz), 7.76 (br, 1H), 10.64 ppm (br, 1H).

¹³C NMR (100 MHz, DMSO-*d*₆): δ= 21.14, 44.10, 116.66, 121.89, 124.23, 125.42, 127.70, 129.40, 135.76, 136.70, 136.96, 137.65, 151.49 ppm.

HRMS (ESI): *m/z* calcd for C₁₅H₁₄ClN₃O₂S [M+Na]⁺: 358.0392, found: 358.0388.



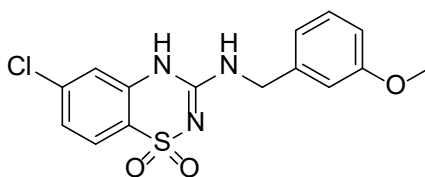
7-Bromo-3-((4-methylbenzyl)amino)-4*H*-benzo[*e*][1,2,4]thiadiazine 1,1-dioxide (3.18c).

The white compound was obtained from **3.4c** by following the experimental conditions described for Method **A** (61% yield):

¹H NMR (400 MHz, DMSO-*d*₆): δ= 2.28 (s, 3H), 4.43 (2H, d, *J*=4.6 Hz), 7.15- 7.23 (m, 5H), 7.67 (br, 1H), 7.72 (1H, dd, *J*=8.7, 2.2 Hz), 7.77 (1H, d, *J*=2.2 Hz), 10.83 ppm (s, 1H).

¹³C NMR (100 MHz, DMSO-*d*₆): δ= 21.48, 44.10, 116.67, 121.90, 124.23, 125.42, 127.70, 129.40, 135.77, 136.70, 136.95, 137.65, 151.48 ppm.

HRMS (ESI): *m/z* calcd for C₁₅H₁₄BrN₃O₂S [M+Na]⁺: 401.9887, found: 401.9885.



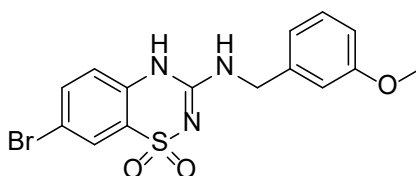
6-Chloro-3-((3-methoxybenzyl)amino)-4*H*-benzo[*e*][1,2,4]thiadiazine 1,1-dioxide (3.19b).

The white compound was obtained from **3.4b** by following the experimental conditions described for Method **A** (81% yield):

¹H NMR (400 MHz, DMSO-*d*₆): δ= 3.74 (s, 3H), 4.46 (2H, d, *J*=5.3 Hz), 6.85 (1H, dd, *J*=8, 2 Hz), 6.94 (m, 2H), 7.27 (1H, d, *J*=7.8 Hz), 7.29 (2H, d, *J*=7 Hz), 7.70 (1H, d, *J*=8.8 Hz), 7.79 (br, 1H), 10.79 ppm (s, 1H).

¹³C NMR (100 MHz, DMSO-*d*₆): δ= 44.29, 55.45, 112.99, 113.38, 116.66, 119.81, 121.78, 124.30, 125.43, 129.95, 137.03, 137.54, 140.42, 151.47, 159.81 ppm.

HRMS (ESI): *m/z* calcd for C₁₅H₁₄ClN₃O₃S [*M*+Na]⁺: 374.0342, found: 374.0335.



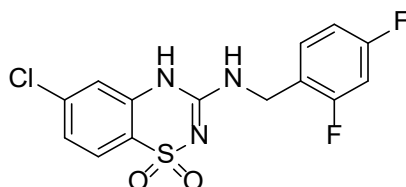
7-Bromo-3-((3-methoxybenzyl)amino)-4*H*-benzo[*e*][1,2,4]thiadiazine 1,1-dioxide (3.19c).

The white compound was obtained from **3.4c** by following the experimental conditions described for Method **A** with the slight modification that the crude material was dissolved in a 1:1 hydromethanolic solution of sodium bicarbonate instead of an aqueous solution of sodium bicarbonate (74% yield):

¹H NMR (400 MHz, DMSO-*d*₆): δ= 3.74 (s, 3H), 4.44 (s, 2H), 6.85 (1H, d, *J*=7.9 Hz), 6.92 (2H, d, *J*=10.5 Hz), 7.20 (1H, d, *J*=8.6 Hz), 7.26 (1H, t, *J*=7.8 Hz), 7.72 (2H, dd, *J*=8.7, 2 Hz), 7.77 (1H, d, *J*=2 Hz), 10.79 ppm (br, 1H).

¹³C NMR (100 MHz, DMSO-d₆): δ= 44.28, 55.47, 113.01, 113.36, 115.05, 119.68, 119.79, 124.57, 125.39, 129.95, 135.62, 140.45, 151.59, 159.81 ppm.

HRMS (ESI): *m/z* calcd for C₁₅H₁₄BrN₃O₃S [*M*+Na]⁺: 417.9836, found: 417.9819.



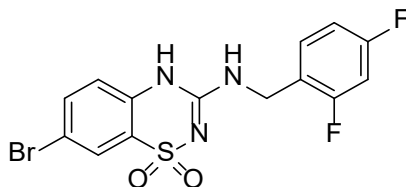
6-Chloro-3-((2,4-difluorobenzyl)amino)-4H-benzo[e][1,2,4]thiadiazine 1,1-dioxide (3.20b).

The white compound was obtained from **3.4b** by following the experimental conditions described for Method **A** (69% yield):

¹H NMR (400 MHz, DMSO-d₆): δ= 4.47 (2H, d, *J*=5.6 Hz), 7.10 (1H, t, *J*=8.5 Hz), 7.24-7.32 (m, 3H), 7.45 (q, 1H), 7.69 (1H, d, *J*=8.5 Hz), 7.79 (br, 1H), 10.84 ppm (s, 1H).

¹³C NMR (100 MHz, DMSO-d₆): δ= 38.08, 104.26, 111.77, 116.67, 121.78, 124.40, 125.47, 131.23, 137.04, 137.44, 151.38, 159.34, 160.77, 161.68, 163.33 ppm.

HRMS (ESI): *m/z* calcd for C₁₅H₁₀ClF₂N₃O₂S [*M*+Na]⁺: 380.0048, found: 380.0051.



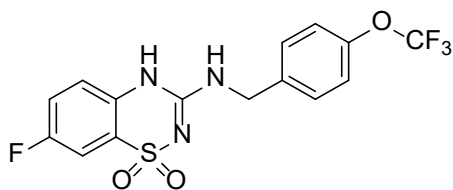
7-Bromo-3-((2,4-difluorobenzyl)amino)-4H-benzo[e][1,2,4]thiadiazine 1,1-dioxide (3.20c).

The white compound was obtained from **3.4c** by following the experimental conditions described for Method **A** (73% yield):

¹H NMR (400 MHz, DMSO-*d*₆): δ = 4.48 (2H, d, *J*=5.5 Hz), 7.10 (1H, t, *J*=8.5 Hz), 7.20 (1H, d, *J*=8.7 Hz), 7.27 (m, 1H), 7.45 (q, 1H), 7.70 (br, 1H), 7.73 (1H, dd, *J*=8.7, 2.2 Hz), 7.78 (1H, d, *J*=2.2 Hz), 10.93 ppm (s, 1H).

¹³C NMR (100 MHz, DMSO-*d*₆): δ = 38.09, 104.27, 111.99, 115.20, 119.66, 122.06, 124.45, 125.42, 131.20, 135.39, 135.69, 151.43, 159.20, 160.76, 161.79, 163.32 ppm.

HRMS (ESI): *m/z* calcd for C₁₅H₁₀BrF₂N₃O₂S [*M*+Na]⁺: 423.9542, found: 423.9538.



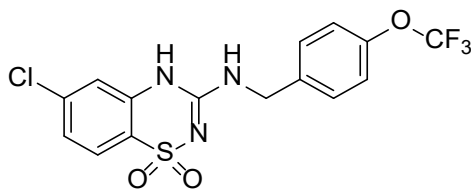
7-Fluoro-3-((4-(trifluoromethoxy)benzyl)amino)-4*H*-benzo[*e*][1,2,4]thiadiazine 1,1-dioxide (3.21a).

The white compound was obtained from **3.4a** by following the experimental conditions described for Method **C** (59% yield):

¹H NMR (400 MHz, DMSO-*d*₆): δ = 4.51 (2H, d, *J*=5.7 Hz), 7.29 (q, 1H), 7.37 (2H, d, *J*=8.2 Hz), 7.44- 7.52 (m, 4H), 7.73 (br, 1H), 10.91 ppm (s, 1H).

¹³C NMR (100 MHz, DMSO-*d*₆): δ = 43.64, 109.51, 119.26, 119.59, 120.60, 121.51, 123.85, 129.50, 132.80, 138.63, 147.80, 151.77, 156.87, 159.29 ppm.

HRMS (ESI): *m/z* calcd for C₁₅H₁₁F₄N₃O₃S [*M*+Na]⁺: 412.0354, found: 412.0304.



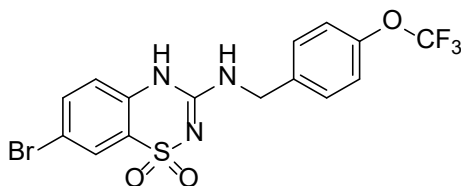
6-Chloro-3-((4-(trifluoromethoxy)benzyl)amino)-4H-benzo[e][1,2,4]thiadiazine 1,1-dioxide (3.21b).

The white compound was obtained from **3.4b** by following the experimental conditions described for Method **C** (64% yield):

¹H NMR (400 MHz, DMSO-*d*₆): δ = 4.51 (2H, d, *J* = 5.7 Hz), 7.30 (2H, d, *J* = 7.8 Hz), 7.37 (2H, d, *J* = 8.6 Hz), 7.45 (2H, d, *J* = 8.6 Hz), 7.69 (1H, d, *J* = 8.6 Hz), 7.85 (br, 1H), 10.90 ppm (s, 1H).

¹³C NMR (100 MHz, DMSO-*d*₆): δ = 43.65, 116.66, 119.26, 121.51, 121.81, 121.85, 124.35, 125.45, 129.54, 137.03, 137.52, 138.49, 147.84, 151.47 ppm.

HRMS (ESI): *m/z* calcd for C₁₅H₁₁ClF₃N₃O₃S [*M*+Na]⁺: 428.0059, found: 428.0062.



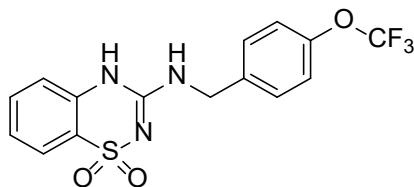
7-Bromo-3-((4-(trifluoromethoxy)benzyl)amino)-4H-benzo[e][1,2,4]thiadiazine 1,1-dioxide (3.21c).

The white compound was obtained from **3.4c** by following the experimental conditions described for Method **C** (68% yield):

¹H NMR (400 MHz, DMSO-*d*₆): δ= 4.50 (2H, d, *J*=5 Hz), 7.21 (1H, d, *J*=8.7 Hz), 7.36 (2H, d, *J*=8.2 Hz), 7.45 (2H, d, *J*=8.5 Hz), 7.74 (1H, d, *J*=8.6, 2 Hz), 7.78 (2H, d, *J*=2 Hz), 10.84 ppm (s, 1H).

¹³C NMR (100 MHz, DMSO-*d*₆): δ= 43.65, 115.10, 116.72, 119.26, 119.68, 121.49, 121.81, 124.54, 125.40, 129.53, 135.55, 135.64, 138.52, 147.82, 151.58 ppm.

HRMS (ESI): *m/z* calcd for C₁₅H₁₁BrF₃N₃O₃S [*M*+Na]⁺: 471.9554, found: 471.9540.



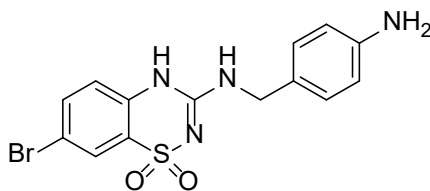
3-((4-(Trifluoromethoxy)benzyl)amino)-4H-benzo[e][1,2,4]thiadiazine 1,1-dioxide (3.21d).

The white compound was obtained from **3.4d** by following the experimental conditions described for Method **C** (72% yield):

¹H NMR (400 MHz, DMSO-*d*₆): δ= 4.52 (2H, d, *J*=5.8 Hz), 7.22 (1H, d, *J*=8.2 Hz), 7.26 (1H, t, *J*=7.6 Hz), 7.37 (2H, d, *J*=8.2 Hz), 7.46 (2H, d, *J*=8.6 Hz), 7.56 (1H, t, *J*=8.2 Hz), 7.61 (br, 1H), 7.67 (1H, d, *J*=7.2 Hz), 10.83 ppm (s, 1H).

¹³C NMR (100 MHz, DMSO-*d*₆): δ= 43.55, 117.04, 119.27, 121.50, 121.81, 123.05, 123.30, 124.27, 129.50, 132.89, 136.12, 138.71, 147.79, 151.62 ppm.

HRMS (ESI): *m/z* calcd for C₁₅H₁₂F₃N₃O₃S [*M*+Na]⁺: 394.0449, found: 394.0439.



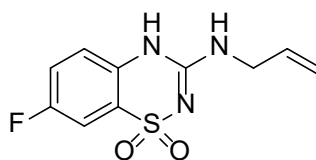
3-((4-Aminobenzyl)amino)-7-bromo-4H-benzo[e][1,2,4]thiadiazine 1,1-dioxide (3.22c).

The white compound was obtained from **3.4c** by following the experimental conditions described for Method **B** (48% yield):

¹H NMR (400 MHz, DMSO-*d*₆): δ= 4.26 (s, 2H), 5.03 (s, 2H) 6.52 (s, 2H), 7.00 (s, 2H), 7.16 (s, 1H), 7.46 (s, 1H), 7.76 (d, 2H), 10.15 ppm (s, 1H).

¹³C NMR (100 MHz, DMSO-*d*₆): δ= 44.28, 114.02, 114.17, 114.73, 119.76, 124.63, 125.35, 128.93, 130.36, 135.49, 135.89, 148.39, 151.56 ppm.

HRMS (ESI): *m/z* calcd for C₁₄H₁₃BrN₄O₂S [*M*+Na]⁺: 402.9840, found: 402.9819.



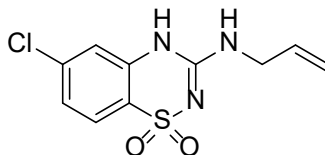
3-(Allylamino)-7-fluoro-4H-benzo[e][1,2,4]thiadiazine 1,1-dioxide (3.23a).

The white compound was obtained from **3.4a** by following the experimental conditions described for Method **C** (81% yield):

¹H NMR (400 MHz, DMSO-*d*₆): δ= 3.88 (m, 3H), 5.12- 5.23 (m, 2H), 5.88 (m, 1H), 7.28 (q, 1H), 7.36 (br, 1H), 7.43- 7.57 (m, 2H), 10.75 ppm (s, 1H).

¹³C NMR (100 MHz, DMSO-*d*₆): δ= 43.15, 109.47, 116.23, 119.52, 120.75, 123.86, 132.80, 134.92, 151.65, 156.82, 159.24 ppm.

HRMS (ESI): m/z calcd for $C_{10}H_{10}FN_3O_2S$ $[M+Na]^+$: 278.0375, found: 278.0351.



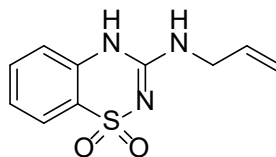
3-(allylamino)-6-chloro-4H-benzo[e][1,2,4]thiadiazine 1,1-dioxide (3.23b).

The white compound was obtained from **3.4b** by following the experimental conditions described for Method **C** (76% yield):

1H NMR (400 MHz, DMSO- d_6): δ = 3.88 (m, 3H), 5.15 (m, 1H), 5.29 (m, 1H), 5.88 (m, 1H), 7.29 (s, 1H), 7.31 (1H, d, J =8.7 Hz), 7.50 (br, 1H), 7.68 (d, 1H), 10.74 ppm (br, 1H).

^{13}C NMR (100 MHz, DMSO- d_6): δ = 43.16, 116.32, 116.61, 121.85, 124.28, 125.42, 134.81, 136.69, 137.53, 151.33 ppm.

HRMS (ESI): m/z calcd for $C_{10}H_{10}ClN_3O_2S$ $[M+Na]^+$: 294.0079, found: 294.0068.



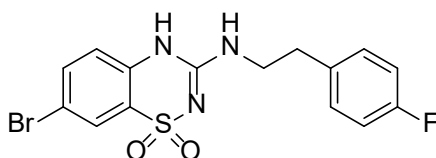
3-(allylamino)-4H-benzo[e][1,2,4]thiadiazine 1,1-dioxide (3.23d).

The white compound was obtained from **3.4d** by following the experimental conditions described for Method **C** (88% yield):

1H NMR (400 MHz, DMSO- d_6): δ = 3.88 (m, 3H), 5.12- 5.23 (m, 2H), 5.88 (q, 1H), 7.21 (1H, d, J =8.2 Hz), 7.25 (2H, t, J =8.3 Hz), 7.55 (1H, t, J =8.3 Hz), 7.65 (1H, dd, J =7.8, 2 Hz), 10.64 ppm (s, 1H).

^{13}C NMR (100 MHz, DMSO- d_6): δ = 43.05, 116.19, 116.98, 123.05, 123.28, 124.19, 132.82, 135.01, 136.13, 151.49 ppm.

HRMS (ESI): m/z calcd for $\text{C}_{10}\text{H}_{11}\text{N}_3\text{O}_2\text{S}$ [$M+\text{Na}$] $^+$: 260.0469, found: 260.0338.



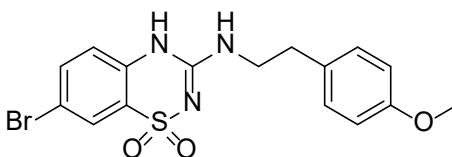
7-Bromo-3-((4-fluorophenethyl)amino)-4H-benzo[e][1,2,4]thiadiazine 1,1-dioxide (3.24c).

The white compound was obtained from **3.4c** by following the experimental conditions described for Method **A** (73% yield):

^1H NMR (400 MHz, DMSO- d_6): δ = 2.84 (2H, t, J =7.2 Hz), 3.47 (q, 2H), 7.14 (m, 4H), 7.29 (m, 2H), 7.73 (1H, dd, J =8.7, 2.2 Hz), 7.77 (1H, d, J =2.2 Hz), 10.78 ppm (br, 1H).

^{13}C NMR (100 MHz, DMSO- d_6): δ = 34.15, 42.41, 115.01, 115.46, 115.66, 119.51, 124.53, 125.39, 130.91, 130.99, 135.44, 135.58, 151.46, 160.19, 162.59 ppm.

HRMS (ESI): m/z calcd for $\text{C}_{15}\text{H}_{13}\text{BrFN}_3\text{O}_2\text{S}$ [$M+\text{Na}$] $^+$: 419.9793, found: 419.9792.



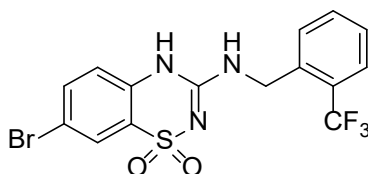
7-Bromo-3-((4-methoxyphenethyl)amino)-4H-benzo[e][1,2,4]thiadiazine 1,1-dioxide (3.25c).

The white compound was obtained from **3.4c** by following the experimental conditions described for Method **A** (67% yield):

¹H NMR (400 MHz, DMSO-*d*₆): δ = 2.78 (2H, t, *J* = 7.2 Hz), 3.43 (q, 2H), 3.72 (s, 3H), 6.89 (2H, d, *J* = 8.6 Hz), 7.14 (br, 1H), 7.16 (3H, d, *J* = 8.6 Hz), 7.71 (1H, dd, *J* = 8.7, 2.2 Hz), 7.77 (1H, d, *J* = 2.2 Hz), 10.75 ppm (br, 1H).

¹³C NMR (100 MHz, DMSO-*d*₆): δ = 34.13, 42.66, 55.45, 114.42, 115.00, 119.52, 124.53, 125.38, 130.12, 130.06, 135.44, 135.58, 151.42, 158.27 ppm.

HRMS (ESI): *m/z* calcd for C₁₆H₁₆BrN₃O₃S [*M*+Na]⁺: 431.9993, found: 431.9996.



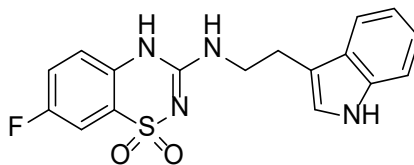
7-Bromo-3-((2-(trifluoromethyl)benzyl)amino)-4H-benzo[e][1,2,4]thiadiazine 1,1-dioxide (3.26c).

The white compound was obtained from **3.4c** by following the experimental conditions described for Method **A** (42% yield):

¹H NMR (400 MHz, DMSO-*d*₆): δ = 4.67 (2H, d, *J* = 5.4 Hz), 7.22 (1H, d, *J* = 8.7 Hz), 7.54 (m, 1H), 7.67- 7.79 (m, 5H), 11.09 ppm (br, 1H).

¹³C NMR (100 MHz, DMSO-*d*₆): δ = 41.12, 114.22, 119.71, 123.53, 124.44, 125.45, 126.37, 128.15, 128.85, 133.72, 135.45, 135.73, 137.07, 151.61 ppm.

HRMS (ESI): *m/z* calcd for C₁₅H₁₂BrF₃N₃O₂S [*M*+Na]⁺: 455.9605, found: 455.9588.



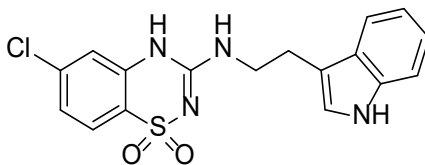
3-((2-(1*H*-indol-3-yl)ethyl)amino)-7-fluoro-4*H*-benzo[*e*][1,2,4]thiadiazine 1,1-dioxide (3.27a).

A mixture of 7-fluoro-3-methylsulfanyl-4*H*-1,2,4-benzothiadiazine 1,1-dioxide (**3.4a**, 0.25 g, 1.02 mmol) and tryptamine (0.19 g, 1.21 mmol) was dissolved in 1,4-dioxane (10 mL) and refluxed for 72 h. The reaction was allowed to cool, and the solvent and excess amine removed in vacuo and the resulting residue dissolved in an aqueous 2% w/v solution of sodium hydroxide (7 mL). This solution was treated with charcoal and was filtered. The filtrate was adjusted to pH 3-4 using 6N HCl. The precipitated compound was collected by filtration, washed with water twice and air dried. The dried compound was suspended in an aqueous solution of sodium bicarbonate (NaHCO₃) (1 g/40 mL). The alkaline solution was treated with charcoal and filtered, and the filtrate was adjusted to pH 4-5 with 6N HCl. The white precipitate was collected by filtration, washed twice with water, and air dried (0.197 g, 53% yield):

¹H NMR (400 MHz, DMSO-*d*₆): δ= 2.97 (2H, t, *J*=7.2 Hz), 3.56 (q, 2H), 6.99 (1H, t, *J*=7.7 Hz), 7.09 (2H, t, *J*=7.8 Hz), 7.22 (m, 2H), 7.35 (1H, d, *J*=8.1 Hz), 7.45 (1H, t, *J*=8.7 Hz), 7.53 (1H, dd, *J*=7.5, 2.8 Hz), 7.59 (1H, d, *J*=7.8 Hz), 10.72 (br, 1H), 10.90 ppm (br, 1H).

¹³C NMR (100 MHz, DMSO-*d*₆): δ= 25.21, 41.70, 109.50, 111.53, 111.87, 118.78, 119.37, 120.73, 121.49, 123.37, 123.84, 127.59, 132.85, 136.74, 151.73, 156.77, 159.18 ppm.

HRMS (ESI): *m/z* calcd for C₁₇H₁₅FN₄O₂S [*M*+Na]⁺: 381.0797, found: 381.0749.



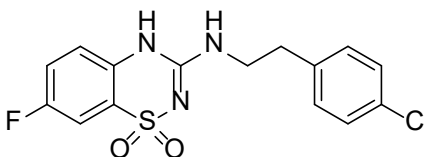
3-((2-(1H-indol-3-yl)ethyl)amino)-6-chloro-4H-benzo[e][1,2,4]thiadiazine 1,1-dioxide (3.27b).

The white compound was obtained from **3.4b** by following the experimental conditions described for **36a** (62% yield):

¹H NMR (400 MHz, DMSO-*d*₆): δ = 2.97 (2H, t, *J* = 7.2 Hz), 3.55 (q, 2H), 6.99 (1H, t, *J* = 7.9 Hz), 7.08 (1H, t, *J* = 7.9 Hz), 7.22 (1H, d, *J* = 2.5 Hz), 7.23 (br, 1H), 7.30 (2H, dd, *J* = 8.4, 2.0 Hz), 7.34 (1H, d, *J* = 8.1 Hz), 7.61 (1H, d, *J* = 7.8 Hz), 7.68 (1H, d, *J* = 8.4 Hz), 10.71 (br, 1H), 10.90 ppm (br, 1H).

¹³C NMR (100 MHz, DMSO-*d*₆): δ = 25.15, 41.71, 111.51, 111.87, 116.47, 118.78, 121.49, 123.38, 124.18, 125.44, 126.53, 127.59, 136.74, 136.93, 137.55, 151.43, 161.92 ppm.

HRMS (ESI): *m/z* calcd for C₁₇H₁₅ClN₄O₂S [*M*+Na]⁺: 397.0501, found: 397.0498.



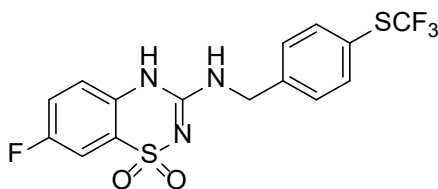
3-((4-Chlorophenethyl)amino)-7-fluoro-4H-benzo[e][1,2,4]thiadiazine 1,1-dioxide (3.28a).

The white compound was obtained from **3.4a** by following the experimental conditions described for Method **A** (81% yield):

¹H NMR (400 MHz, DMSO-*d*₆): δ= 2.85 (2H, t, *J*=7.1 Hz), 3.47 (q, 2H), 7.14 (br, 1H), 7.24 (m, 1H), 7.30 (1H, d, *J*=8.3 Hz), 7.36 (2H, d, *J*=8.3 Hz), 7.45 (1H, t, *J*=8.7 Hz), 7.51 (1H, dd, *J*=7.5, 2.8 Hz), 10.70 ppm (s, 1H).

¹³C NMR (100 MHz, DMSO-*d*₆): δ= 34.32, 42.18, 109.48, 119.45, 120.74, 128.79, 131.08, 131.39, 131.60, 132.78, 138.36, 151.67, 159.22, 166.91 ppm.

HRMS (ESI): *m/z* calcd for C₁₅H₁₃ClFN₃O₂S [*M*+Na]⁺: 376.0298, found: 376.0270.



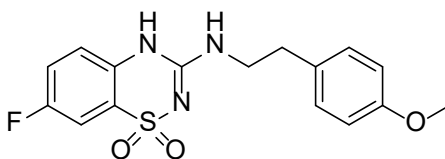
7-Fluoro-3-((4-((trifluoromethyl)thio)benzyl)amino)-4*H*-benzo[*e*][1,2,4]thiadiazine 1,1-dioxide (3.29a).

The white compound was obtained from **3.4a** by following the experimental conditions described for Method **A** (72% yield):

¹H NMR (400 MHz, DMSO-*d*₆): δ= 4.57 (2H, d, *J*=5.9 Hz), 7.30 (m, 1H), 7.44- 7.53 (m, 4H), 7.7 (2H, d, *J*=8.1 Hz), 7.77 (br, 1H), 11.05 ppm (s, 1H).

¹³C NMR (100 MHz, DMSO-*d*₆): δ= 43.87, 109.51, 119.50, 120.84, 121.77, 123.83, 128.54, 129.00, 131.60, 132.82, 136.79, 143.08, 151.86, 156.88, 159.30 ppm.

HRMS (ESI): *m/z* calcd for C₁₅H₁₁F₄N₃O₂S₂ [*M*+Na]⁺: 428.0126, found: 428.0131.



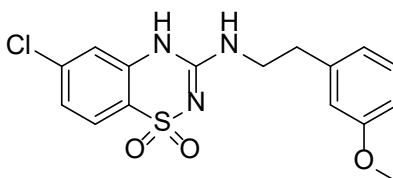
7-Fluoro-3-((4-methoxyphenethyl)amino)-4*H*-benzo[*e*][1,2,4]thiadiazine 1,1-dioxide (3.30a).

The white compound was obtained from **3.4a** by following the experimental conditions described for Method **A** (63% yield):

¹H NMR (400 MHz, DMSO-*d*₆): δ= 2.79 (2H, t, *J*=7.2 Hz), 3.44 (q, 2H), 3.72 (s, 3H), 6.88 (2H, d, *J*=8.6 Hz), 7.10 (br, 1H), 7.16 (2H, d, *J*=8.5 Hz), 7.24 (br, 1H), 7.44 (1H, t, *J*=8.7 Hz), 7.52 (1H, dd, *J*=7.5, 2.8 Hz) 10.73 ppm (br, 1H).

¹³C NMR (100 MHz, DMSO-*d*₆): δ= 34.20, 42.66, 55.42, 109.47, 114.30, 119.40, 120.47, 120.71, 123.75, 130.12, 131.09, 132.82, 151.70, 156.78, 158.26, 159.20 ppm.

HRMS (ESI): *m/z* calcd for C₁₆H₁₆FN₃O₃S [*M*+Na]⁺: 372.0794, found: 372.0720.



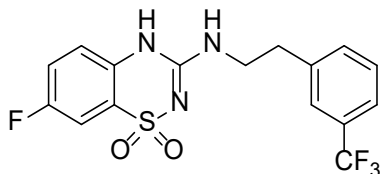
6-Chloro-3-((3-methoxyphenethyl)amino)-4*H*-benzo[*e*][1,2,4]thiadiazine 1,1-dioxide (3.31b).

The white compound was obtained from **3.4b** by following the experimental conditions described for Method **A** (77% yield):

¹H NMR (400 MHz, DMSO-*d*₆): δ= 2.83 (2H, t, *J*=7.1 Hz), 3.48 (q, 2H), 3.74 (s, 3H), 6.80 (1H, d, *J*=8.2 Hz), 6.87 (m, 2H), 7.23 (m, 3H), 7.29 (1H, dd, *J*=8.4, 2 Hz), 7.68 (1H, d, *J*=8.4 Hz), 10.67 ppm (br, 1H).

¹³C NMR (100 MHz, DMSO-*d*₆): δ= 34.98, 42.29, 55.36, 112.19, 114.78, 116.53, 121.37, 121.86, 124.23, 125.42, 129.91, 136.94, 137.51, 140.86, 151.38, 159.79 ppm.

HRMS (ESI): m/z calcd for $C_{16}H_{16}ClN_3O_3S$ $[M+Na]^+$: 388.0498, found: 388.0542.



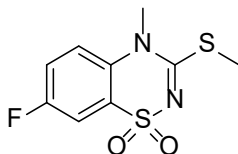
7-Fluoro-3-((3-(trifluoromethyl)phenethyl)amino)-4H-benzo[e][1,2,4]thiadiazine 1,1-dioxide (3.32a).

The white compound was obtained from **3.4a** by following the experimental conditions described for Method **A** (75% yield):

1H NMR (400 MHz, DMSO- d_6): δ = 2.97 (2H, t, J =7 Hz), 3.52 (q, 2H), 7.25 (br, 2H), 7.45 (1H, t, J =8.7 Hz), 7.50 (1H, dd, J =7.5, 2.8 Hz), 7.57 (q, 3H), 7.63 (s, 1H), 10.71 ppm (br, 1H).

^{13}C NMR (100 MHz, DMSO- d_6): δ = 34.69, 42.06, 109.45, 119.45, 120.48, 120.72, 123.51, 123.83, 125.72, 129.84, 132.78, 133.40, 140.81, 151.74, 156.87, 159.24 ppm.

HRMS (ESI): m/z calcd for $C_{16}H_{13}F_4N_3O_2S$ $[M+Na]^+$: 410.0562, found: 410.0497.



7-Fluoro-4-methyl-3-(methylthio)-4H-benzo[e][1,2,4]thiadiazine 1,1-dioxide (3.33a).

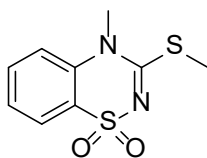
To a solution of 7-fluoro-3-methylsulfanyl-4H-1,2,4-benzothiadiazine 1,1-dioxide (**3.4a**, 1 g, 3.8 mmol) in acetonitrile/DMF, 4:1 (15 mL) at room temperature was added K_2CO_3 (0.48 g, 3.45 mmol) and methyl iodide (1 mL, 6.9 mmol). The mixture was stirred for 10 h and

the solvent was removed in vacuo. The solid residue was taken up in water (20 mL). The resulting aqueous suspension was adjusted to pH 2 by means of formic acid, and the precipitate was collected by filtration and washed with water. The crude compound was recrystallized in methanol/water to provide the title compound as a white powder (0.93 g, 89% yield):

¹H NMR (400 MHz, DMSO-*d*₆): δ = 2.55 (s, 3H), 3.71 (s, 3H), 7.68 (m, 2H), 7.73 (m, 1H).

¹³C NMR (100 MHz, DMSO-*d*₆): δ = 16.09, 36.41, 110.29, 120.66, 121.48, 125.01, 135.26, 158.17, 160.63, 166.35 ppm.

HRMS (ESI): *m/z* calcd for C₉H₉FN₂O₂S₂ [*M*+Na]⁺: 282.9987, found: 282.9954.



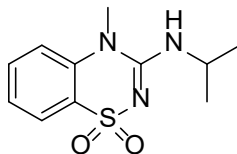
4-Methyl-3-(methylthio)-4*H*-benzo[*e*][1,2,4]thiadiazine 1,1-dioxide (3.33d).

The white compound was obtained from **3.4d** by following the experimental conditions described for **42a** (76% yield):

¹H NMR (400 MHz, DMSO-*d*₆): δ = 2.54 (s, 3H), 3.70 (s, 3H), 7.60 (m, 2H), 7.79 (1H, t, *J*=8.6 Hz), 7.86 ppm (1H, dd, *J*=7.8, 2.0 Hz).

¹³C NMR (100 MHz, DMSO-*d*₆): δ = 15.98, 36.13, 117.45, 123.96, 126.74, 133.82, 138.43, 166.09 ppm.

HRMS (ESI): *m/z* calcd for C₉H₁₀N₂O₂S₂ [*M*+Na]⁺: 265.0081, found: 264.992.



3-(Isopropylamino)-4-methyl-4H-benzo[e][1,2,4]thiadiazine 1,1-dioxide (3.34d).

To a solution of 4-methyl-3-methylsulfanyl-4H-1,2,4-benzothiadiazine 1,1-dioxide (**3.33d**, 0.2 g, 0.79 mmol) in 1,4-dioxane (3 mL) in a sealed vessel was added isopropylamine (0.2 mL, 3.16 mmol) and the mixture heated for 24 h at 130 °C. The excess solvent and amine were removed by distillation under reduced pressure, and the residue was suspended in water (15 mL). The mixture was stirred for 1 h at room temperature, the resultant precipitate was collected by filtration, washed twice with water, and recrystallized from methanol/water to yield the title compound as a white powder (0.11 g, 55% yield):

¹H NMR (400 MHz, DMSO-*d*₆): δ = 1.21 (6H, d, *J* = 6.5 Hz), 3.46 (s, 3H), 4.05 (q, 1H), 7.36 (1H, t, *J* = 7.5 Hz), 7.45 (2H, d, *J* = 8.3 Hz), 7.65 (1H, t, *J* = 8.5 Hz), 7.70 ppm (1H, dd, *J* = 7.8, 2.0 Hz).

¹³C NMR (100 MHz, DMSO-*d*₆): δ = 22.53, 35.09, 44.80, 66.80, 117.22, 122.76, 124.42, 126.45, 132.77, 139.26, 153.37 ppm.

HRMS (ESI): *m/z* calcd for C₁₁H₁₅N₃O₂S [*M*+Na]⁺: 276.0552, found: 276.0782.

Chapter 4. Discovery of Halogenated Benzothiadiazine Derivatives as Novel VEGF Inhibitors

4.1. Introduction

Angiogenesis is a physiological process which is tightly regulated by the balance between angiogenic and antiangiogenic factors in normal tissues.²¹⁰ Vascular permeability factor (VPF) or vascular endothelial growth factor (VEGF), is one of the best characterized angiogenic factors. It plays a critical role in the vascular system in both pathological angiogenesis, such as cancer and normal physiological functions including bone formation, hematopoiesis, wound healing, and development.^{104, 211, 212} The main function of VEGF is to modulate vessel permeability, remodeling, endothelial cell survival, proliferation and migration.^{213, 214} In tumor cells, VEGF is highly overexpressed which induces other proangiogenic factors and leads to the formation of new blood vessels.²¹⁵ Vascular endothelial growth factor and its receptors are dysregulated by activation, overexpression, or mutation that leads to tumorigenesis and metastasis by initiating downstream signaling transduction pathways resulting in angiogenesis, vascular permeability enhancement, and tumor development.¹⁰¹

The narrow therapeutic index is one of the major drawbacks of using the traditional chemotherapeutic agents to treat cancer in addition to the lack of specificity, severe side effects, and development of drug resistance. Therefore, anti-angiogenesis as a new therapy strategy was developed to target tumors and assist in overcoming the side effects of the chemotherapeutic agents. Currently, the antiangiogenic drugs against VEGF have been shown to normalize tumor vasculature and, as a result, offer an improvement in chemotherapeutic delivery. Therefore, anti-VEGF drugs are most effective in clinical practice when combined with other chemotherapeutic anticancer agents.²¹⁶ Anti-VEGF treatments are designed to target both the pro-angiogenic activity and the antiapoptotic

functions of VEGF.²¹⁵ Thus, vascular endothelial growth factor is a focus of interest concerning vascular research and oncology.

The target of action of the diazoxide derivatives were envisioned as VEGF inhibitors because diazoxide has been shown to inhibit VEGF mediated angiogenesis in *in vivo* Matrigel plug assay in mice.²⁰⁹ Moreover, the structural similarity between our compounds with many known VEGF inhibitors, such as pazopanib, indicated a possible role as VEGF inhibitors. These compounds share the guanidine template, which is the active unit in many VEGF inhibitors.²¹⁷ The guanidine unit is set deeply into the hydrophilic site of the hydrophobic pocket and forms a strong hydrogen bond with amino acid Asp331.²¹⁸ A similar structural unit is also common in VEGF inhibitor drugs such as sorafenib, sunitinib, regorafenib, in which they usually have urea moiety in their chemical structures.²¹⁹ The urea unit is a bioisostere of the guanidine group, which contributes to the biological activity of these drugs.²²⁰ According to a recent study, the sulfonylurea unit was important for VEGF inhibitors in place of urea scaffolds, and the resulting derivatives showed great activity for VEGF inhibition.²¹⁹ Moreover, the functional sulfonamide unit has been extensively studied for VEGF inhibition. The aromatic sulfonamide derivatives are known to have many biological activities, including antimicrobial,²²¹ antiinflammatory,²²² and anticancer activity.²²³ I speculated that novel anti-angiogenesis agents might be found among cyclic sulfonamide derivatives. Hence, the current chapter involves synthesis of new derivatives based on cyclic sulfonamide template that could be explored for VEGF inhibition. The electron withdrawing groups such as halogen atoms as a substitution in the compounds seem to be beneficial for stability and activity of the VEGF inhibitors.²²⁴ These attributes guide us to envision the synthesis of novel derivatives of cyclic sulfonamides and evaluate these compounds as antiangiogenic agents for cancer therapy.

The discovery of tumor blood vessel formation and the subsequent concept of suppressing angiogenesis was a significant breakthrough in antineoplastic treatment and improved our knowledge of the biology of cancer. In order to identify new angiogenesis inhibitors; herein, I report the synthesis of a library of novel benzothiadiazine derivatives to understand structural effect on VEGF inhibition activity and their biological activities against triple negative breast cancer MDA-MB-468, and HEK293 human embryonic kidney cell lines. Selective DZX derivatives were screened for the activity on the VEGF induced proliferation on human umbilical vein endothelial cells (HUVECs). A promising result was achieved in this research wherein several of these novel derivatives **3.9b**, **3.11-3.14b**, **3.20-3.21b**, **4.5-4.7b**, and **4.7-4.17e** could suppress the major signaling pathways in tumor angiogenesis VEGF, which showed moderate cytotoxicity against cancer cell lines and no effect on the low tumorigenic cells up to 50 μ M. Understanding signaling mechanisms in tumor angiogenesis will improve the development of novel therapies and lead to the discovery of more efficient angiogenesis treatments in cancers.

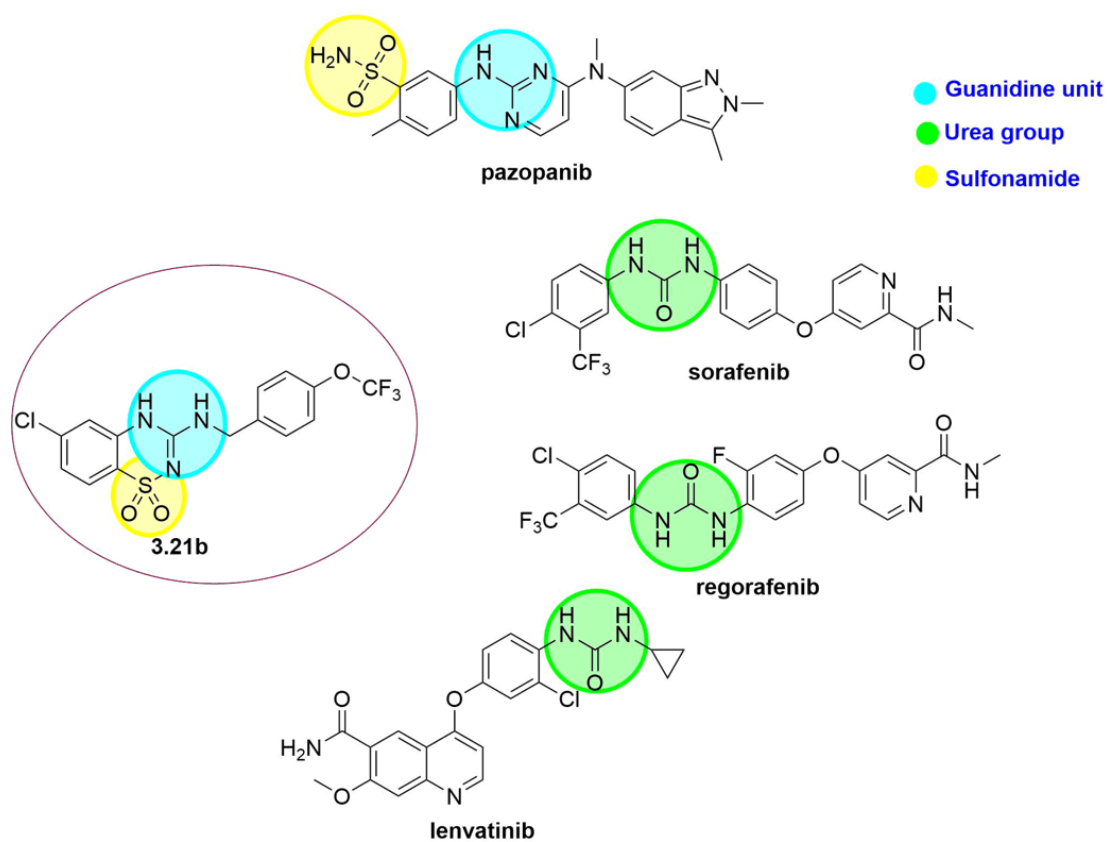


Figure 4.1. Structure similarity between diazoxide derivative **3.21b** and FDA-approved VEGF inhibitors.

4.2. Results and Discussion

4.2.1. Chemistry

The parent compound diazoxide can be accessed by a number of reported syntheses, our adopted route blends elements of several.^{194, 197-200} Additionally, a number of derivatives of DZX with various side chains have been synthesized as K_{ATP} channel activators that are selective to pancreatic β -cells, although no determination of antineoplastic effects of these compounds have been reported.¹⁹⁷ I sought to modify the side chain through a different amine to form a guanidine template which is important in many known VEGF inhibitors. Furthermore, I also envisioned adding different halogen substituents in the phenyl ring of the diazoxide structure in different positions of those derivatives which were described in the chapter 3. The synthesis of the new diazoxide derivatives was carried out according to **Schemes 3.1-3.3** in chapter 3 (**Table 4.1-4.3**).²⁰¹

I also attempted the synthesis of benzothiadiazine derivatives with cyanide groups as substitution on the aromatic ring of the DZX derivative. Based on the literature, introduction of cyano group tend to improve the inhibition of VEGF.^{225, 226} Unfortunately, the synthesis of these derivatives did not result in the formation of the product leading to the formation of an undesired product (product is not characterized). On the other hand, a few CN-benzothiadiazine derivatives are known, synthesized by the reflux of the halogen benzothiadiazine with copper cyanide. Due to the time constraints, this method was not employed to synthesize the CN-benzothiadiazine derivatives. Future synthetic studies will involve the synthesis of CN-benzothiadiazine derivatives based on the above-described procedure.²²⁷

4.2.2. VEGF Inhibition Assay

As described in the previous chapter, the CII derivative DZX is also linked to VEGF, wherein halogen substitution on the benzothiadiazine ring provided slightly increased CII

inhibition activity over saturated counterparts. To further evaluate if DZX derivatives which have been synthesized in chapter 3 show anti-angiogenesis properties, they have been evaluated for VEGF inhibition activity. The VEGF inhibition activity was assessed by our collaborators at the Texas Tech University Health Sciences Center following a literature reported method using HUVEC cells treated with VEGF as previously described.²²⁸ The VEGF treated cells were employed as a positive control with dimethyl sulfoxide (DMSO) as a negative control. To assess the antiangiogenic activity of the synthesized DZX derivatives *in vitro*, our collaborators at the Texas Tech University Health Sciences Center examined the effect of DZX derivatives on VEGF-induced proliferation in HUVECs using MTT assay. Several compounds were found to inhibit VEGF-induced HUVEC proliferation with high statistical significance compared to VEGF treated cells and the DMSO control. Toxicity to low tumorigenic cells was confirmed in the human embryonic kidney cell lines (HEK293), wherein most of the potent diazoxide derivatives did not affect cell viability.

Several of the synthesized diazoxide derivatives were initially screened at 20 μ M concentration. The 7-fluorobenzothiadiazine substituted derivatives provided lower activity of VEGF inhibition (**Figure 4.2**). When the 7-fluoro substituent on the benzothiadiazine ring was interchanged with 7-bromo substitution, the inhibitory activity of the derivatives notably increased, as shown with **3.9c**, **3.14c** and **3.20c**. The 6-chlorobenzothiadiazine derivatives showed the most potent activity to reduce HUVEC-VEGF treated cell proliferation over 7-fluorobenzothiadiazine and 7-bromobenzothiadiazine. The homologation series of benzylamine derivatives without substitution (**3.12b**), phenethyl (**3.9b**), and phenyl propyl (**3.14b**) were found to be highly active for inhibition of proliferation in the VEGF treated cells with 118%-200%. The derivatives **3.12b** with benzylamine as a substitution has 4-fold cells inhibition to VEGF treated cells. The 6-chlorobenzothiadiazine substituted in benzothiadiazine ring is very important for the

activity of phenyl propyl (**3.14b**) which suppression of VEGF-mediated cells growth by 178% in contrast to the inactive 7-fluorobenzothiadiazine **3.14a** (0% cells inhibition) and 7-bromobenzothiadiazine derivatives **3.14c** (24% cells inhibition). We therefore chose to focus our efforts to design VEGF inhibitors on chlorine substituted derivatives. Electron-donating substitution with a methoxy group increases the VEGF inhibitory activity dependent on position; 4-OMe (**3.11b**) > 3-OMe (**3.19b**) > 2-OMe (**3.17b**). Adding electron-donating methyl substitution to the benzylamine ring increases the VEGF inhibitory activity as shown with **4.5b**, **4.6b**, and **3.18b**. The electron-withdrawing groups on the benzylamine ring have high activity as shown in 4-OCF₃ (**3.21b**) and 2-OCF₃ (**4.7b**). Moreover, the cyclopentylamine (**3.13b**) have 3-fold activity to inhibit the cell proliferation of HUVEC-VEGF treated cells by 174% at 20 μ M concentration.

Most of the 7-chlorobenzothiadiazine series showed potency to reduce percentage proliferation of the VEGF treated cells. The benzyl amine derivative (**4.8e**) showed highly active to suppresses VEGF-mediated cells growth (124% cells inhibition) than phenethylamine (**4.6e**) (82%), phenylpropylamine (**4.11e**) (92%), and phenylbutylamine (**4.16e**) (116%) slightly similar the activity as 6-chlorobenzothiadiazine **3.12b**, **3.9b**, and **3.14b**. These results suggest that increased lipophilicity in DZX derivatives had similar VEGF activity. The electron-withdrawing groups on the benzylamine ring such as 2,4-difluorobenzylamine increase the activity to inhibit VEGF by 3.5-fold (133%) as shown in 7-chloro derivative **4.14e** and 2.5-fold (167%) with 6-chloro derivative **3.20b**. The 7-chlorobenzothiadiazine substituted cyclopentylamine (**4.10e**) side chain derivative possessed high activity similar to the activity of 6-chloro substituted **3.13b** DZX derivatives. Adding electron-donating methyl substitution on the benzylamine ring increases the VEGF inhibitory activity by 3 to 4-fold as shown with 2-Me **4.9e** > 4-Me **4.12e** > 3-Me **4.15e** derivatives compared to 6-chlorobenzothiadiazine derivatives 3-Me (**4.5b**)

>2-Me (**4.6b**) >4-Me (**3.18b**). Increase in the polarity of the compound side chain by adding picolylamine (**4.17e**) diminished the activity to inhibit VEGF-mediated cells growth by 67% (**Figure 4.2**).

Some of the lead compounds were analyzed for phosphorylated VEGFR2 using Western blot in HUVEC cells. Cells were treated with test compounds (20 μ M) along with VEGF (10 ng/mL) for 5 min. The DMSO was used as a negative control, whereas DMSO + VEGF was used as a positive control. Cells were lysed using RIPA buffer (10 mmol/L Tris-HCl, 1 mmol/L EDTA, 0.5 mmol/L EGTA, 1% Triton X-100, 0.1% sodium deoxycholate, 0.1% SDS and 140 mmol/L NaCl), supplemented with protease and phosphatase inhibitors (Halt Protease and Phosphatase Inhibitor). Cell lysates were centrifuged, and the supernatants were mixed with appropriate amount of 5X SDS loading buffer proteins were resolved on polyacrylamide gel and transferred onto nitrocellulose/PVDF membrane and treated with pVEGFR2 antibody. The membrane was developed using chemiluminescence, and the bands were analyzed using densitometry. From **figure 4.3**, phosphorylation of VEGFR2 was highly upregulated in the presence of VEGF, whereas the treatment with DZX derivatives resulted in attenuation of the expression of pVEGFR2. Diazoxide derivative **3.13b** did not affect the expression of pVEGFR2, while other DZX derivatives **3.12b**, **3.20b**, **4.7b**, **4.9e** showed 46-59% attenuation in phosphorylated pVEGFR2 expression compared to VEGF treated control. Compounds **3.21b**, **4.10e**, **4.13e**, and **DZX** were found to be most potent towards attenuation of pVEGFR2 expression (75-97% downregulation). These results signify that DZX derivatives have the potential to further explore them as VEGF inhibitors.

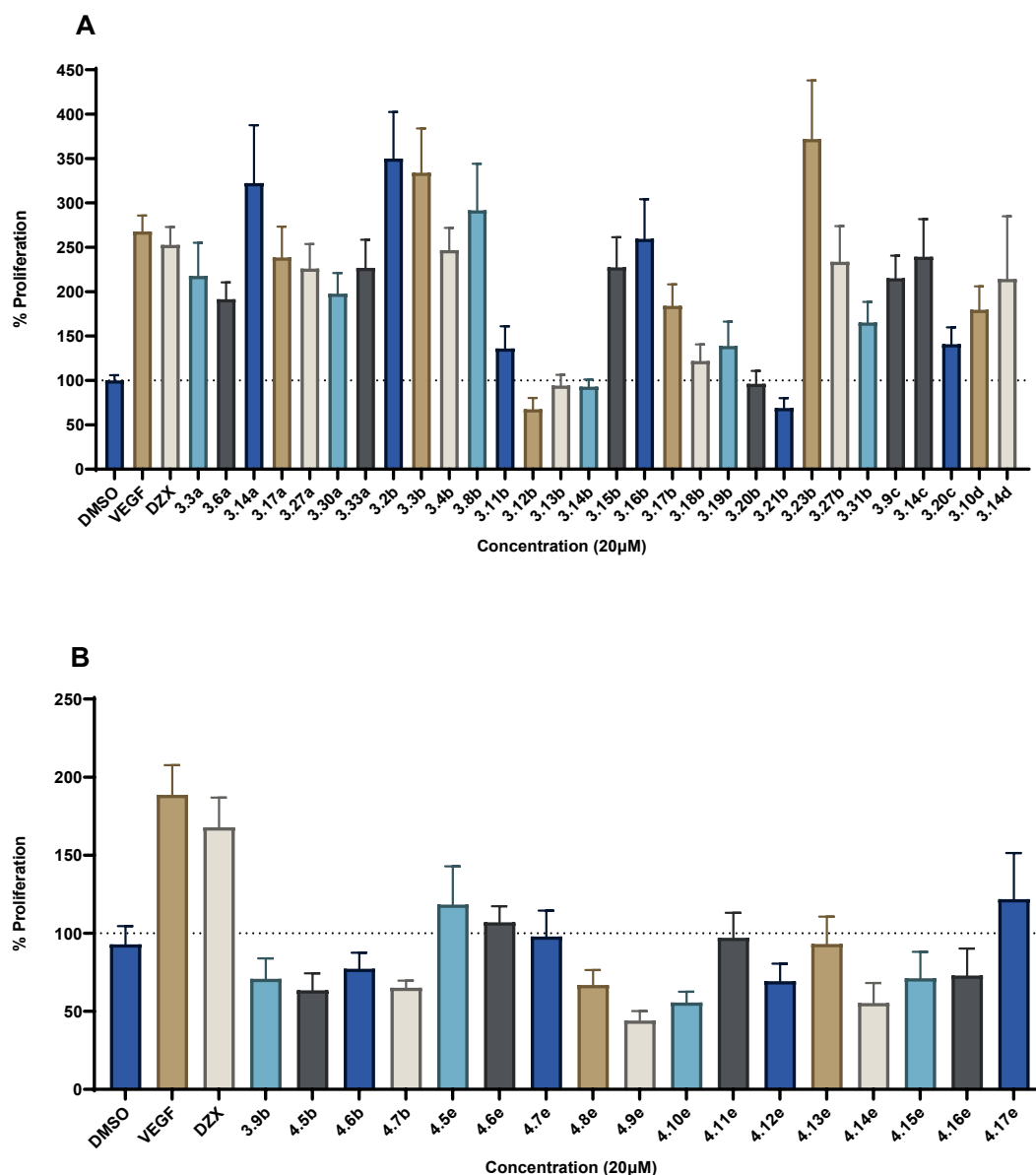


Figure 4.2. Cytotoxic effect of diazoxide derivatives at 20 μ M concentration in HUVEC cells in the presence of VEGF (10 ng/mL). A) Cell proliferation inhibition of VEGF (10 ng/mL) treated HUVEC cells by diazoxide derivatives previously synthesized in chapter 3. B) Cell proliferation inhibition of VEGF (10 ng/mL) treated HUVEC cells by diazoxide derivatives newly synthesized in this chapter. Values represent the mean \pm SEM of n = 3 experiments.

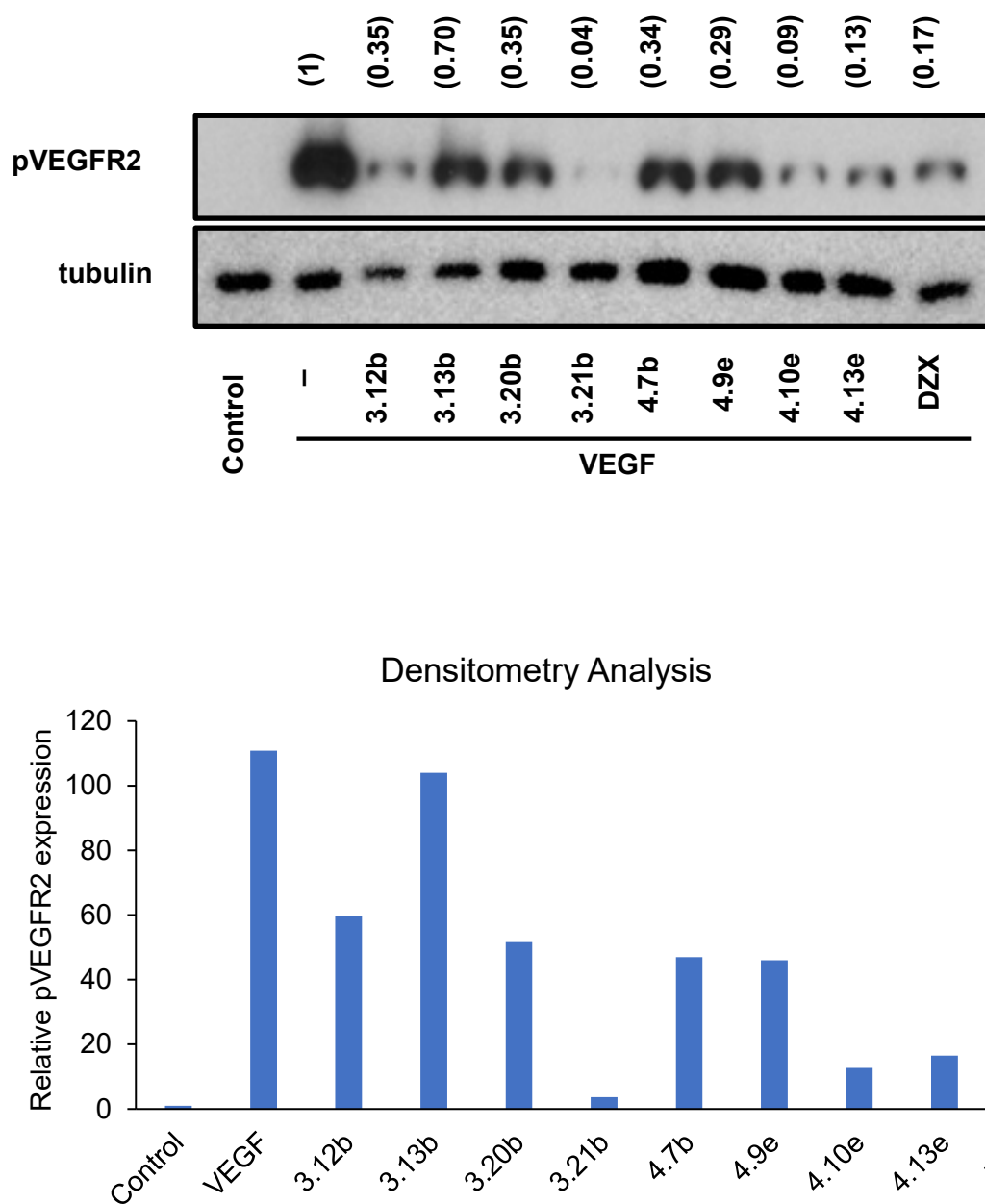
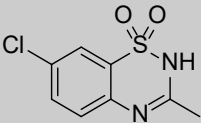
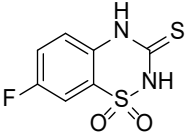
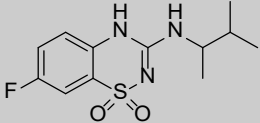
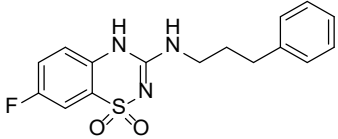
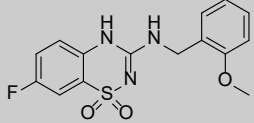
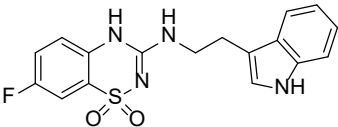
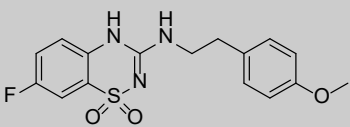
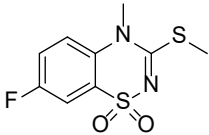
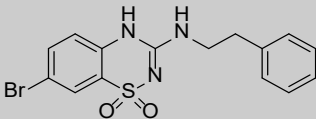
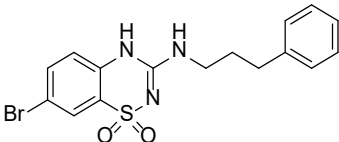
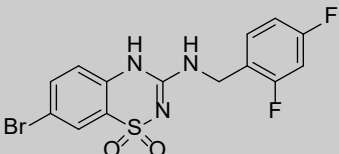
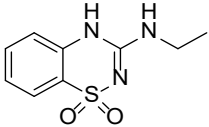
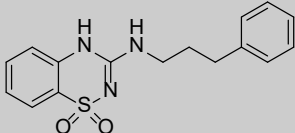


Figure 4.3. Western blotting demonstrating the effect of selective DZX derivatives on the expression of phosphorylation of vascular endothelial growth factor receptor-2 (VEGFR-2) in HUVEC cells with the addition of VEGF (10 ng/mL) and DZX derivatives concentration (20 μ M).

Compound	Structure	Mw	cLogP ^a	PSA ^b	% Cells Inhibition ^c
DZX		230.67	1.0	58.53	15 ±20
3.3a		232.25	0.76	58.20	50 ±35
3.6a		285.34	1.66	70.56	76 ±18
3.14a		333.38	2.37	70.56	0
3.17a		335.35	1.58	79.79	29 ±33
3.27a		358.39	1.98	82.59	41 ±26
3.30a		349.38	1.91	79.79	70 ±22

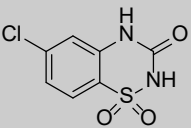
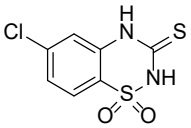
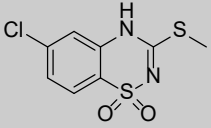
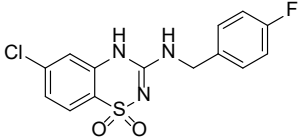
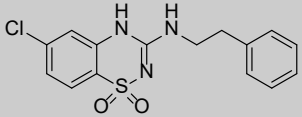
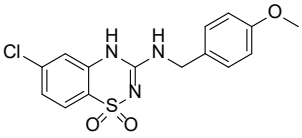
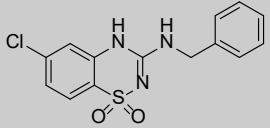
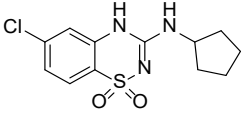
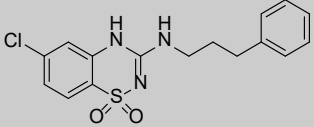
3.33a		290.30	1.84	49.74	41 ±30
3.9c		380.26	2.71	70.56	47 ±24
3.14c		394.29	3.09	70.56	24 ±41
3.20c		402.21	2.67	70.56	127 ±18
3.10d		225.27	0.28	70.56	81 ±25
3.14d		315.39	2.22	70.56	39 ±68

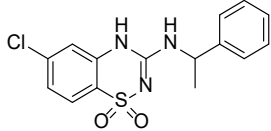
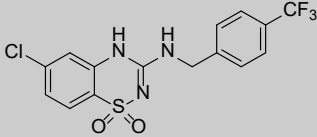
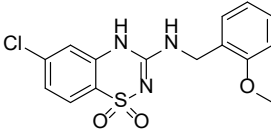
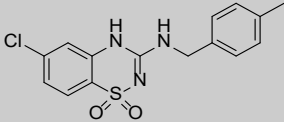
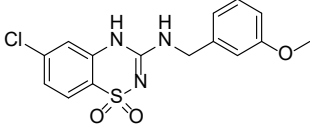
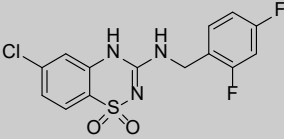
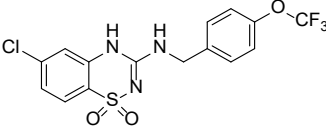
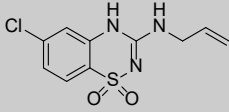
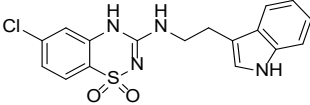
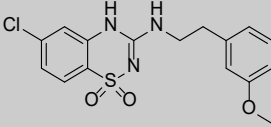
^a Calculated by ChemDraw Professional 16.0.

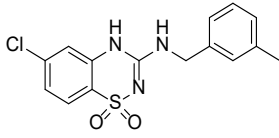
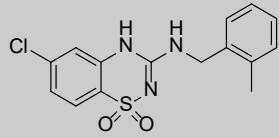
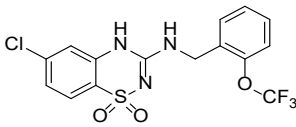
^b Polar surface area (pH 7.4), calculated by ChemDraw Professional 16.0.

^c Percentage of suppression VEGF-mediated cells growth. Values represent the mean ±SEM of n = 3 experiments.

Table 4.1. Structure, molecular weight, calculated logP, polar surface area, and % of proliferation inhibition relative to VEGF treated cells of diazoxide derivatives with 7-fluoro, 7-bromo substitution and a non-halogenated ring.

Compound	Structure	Mw	cLogP ^a	PSA ^b	% Cells Inhibition ^c
3.2b		232.64	1.52	75.27	0
3.3b		248.7	1.33	58.2	0
3.4b		262.73	1.54	58.53	21 ±23
3.8b		339.77	2.37	70.56	0
3.9b		335.81	2.56	70.56	118 ±12
3.11b		351.81	2.15	79.79	132 ±24
3.12b		321.78	2.23	70.56	200 ±12
3.13b		299.77	1.93	70.56	174 ± 12
3.14b		349.83	2.94	70.56	178 ±8

3.15b		335.81	2.54	70.56	38 ±33
3.16b		389.28	3.11	70.56	1 ±43
3.17b		351.81	2.15	79.79	79 ±23
3.18b		335.81	2.73	70.56	146 ±18
3.19b		351.81	2.15	79.79	126 ±26
3.20b		357.76	2.52	70.56	167 ±14
3.21b		405.78	3.26	79.79	196 ±11
3.23b		271.72	1.24	70.56	0
3.27b		374.84	2.55	82.59	24 ±38
3.31b		365.83	2.48	79.79	99 ±22

4.5b		335.81	2.73	70.56	125 ±10
4.6b		335.81	2.68	70.56	111 ±9
4.7b		405.78	3.26	79.79	124 ±4

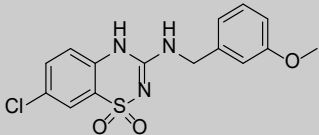
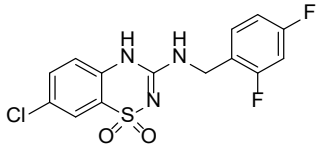
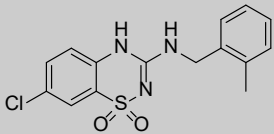
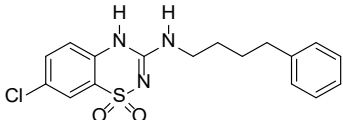
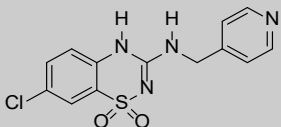
^a Calculated by ChemDraw Professional 16.0.

^b Polar surface area (pH 7.4), calculated by ChemDraw Professional 16.0.

^c Percentage of suppression VEGF-mediated cells growth. Values represent the mean ±SEM of n = 3 experiments.

Table 4.2. Structure, molecular weight, calculated logP, polar surface area, and % of proliferation inhibition relative to VEGF treated cells of diazoxide derivatives with 6-chloro substitution.

Compound	Structure	Mw	cLogP ^a	PSA ^b	% Cells Inhibition ^c
4.5e		339.77	2.37	70.56	70 ±23
4.6e		335.81	2.56	70.56	82 ±10
4.7e		351.81	2.15	79.79	91 ±15
4.8e		321.78	2.23	70.56	122 ±9
4.9e		335.81	2.73	70.56	145 ±6
4.10e		299.77	1.93	70.56	133 ±6
4.11e		349.83	2.94	70.56	92 ±15
4.12e		335.81	2.73	70.56	119 ±10

4.13e		351.81	2.15	79.79	96 ±16
4.14e		357.76	2.52	70.56	133 ±12
4.15e		335.81	2.68	70.56	117 ±15
4.16e		363.86	3.47	70.56	116 ±16
4.17e		322.77	0.73	82.92	67 ±27

^a Calculated by ChemDraw Professional 16.0.

^b Polar surface area (pH 7.4), calculated by ChemDraw Professional 16.0.

^c Percentage of suppression VEGF-mediated cells growth. Values represent the mean ±SEM of n = 3 experiments.

Table 4.3. Structure, molecular weight, calculated logP, and polar surface area of diazoxide derivatives with 7-chloro substitution.

4.2.3 Cytotoxicity Assay

Taking AA5 derivative **16c** as a reference compound, clinical chemotherapeutic sorafenib as positive control and DMSO as negative control, the most active diazoxide derivatives were evaluated to determine their cell growth inhibition ability against different cell lines including human embryonic kidney cells (HEK293), and triple-negative breast cancer cells (MDA-MB-468) by MTS cell proliferation assay which was performed according to the manufacturer's recommended protocol.²⁰⁵

Initially, the cytotoxicity of the DZX derivatives which have an excellent activity to inhibit HUVEC-VEGF treated cells have been evaluated by using the low tumorigenic HEK293 cells at 50 μ M concentration. These results showed that most of these compounds (18 compounds) were unable to inhibit the proliferation of the HEK293 cells by more than 50% at 50 μ M concentration. Three diazoxide derivatives inhibited the proliferation of HEK293 cells more than 50% with the range of inhibition between 65-72% (**Figure 4.4 A**). However, the inhibition of these three compounds is lower than the clinical VEGF inhibitor sorafenib, which inhibits proliferation of HEK293 cells by 99% at 50 μ M. 6-Chloro-3-((2-(trifluoro-methoxy)benzyl)amino)-4*H*-benzo[e][1,2,4]thiadiazine 1,1-dioxide (**4.7b**) is the most toxic derivative for 6-chloro substitution with an IC_{50} value of 30.48 μ M. The diazoxide derivatives with 7-chloro substitution, **4.11e** and **4.16e**, also exhibited toxicity with IC_{50} values of 30.85 μ M and 23.41 μ M, respectively (**Table 4.4**). Six diazoxide derivatives did not show inhibition of the HEK293 cell proliferation more than 10%. In general, the percentage inhibition of the other potent VEGF inhibitors compounds on HEK293 cells are in the range between 0-49% (**Figure 4.4 A**).

The potent VEGF inhibitor compounds showed modest activity at 50 μ M against the most aggressive triple negative breast cancer cells (MDA-MB-468), The IC_{50} values for the most potent compound **4.7b** was 14.93 μ M. Moreover, compound **4.7b** showed

good activity and moderate selectivity against MDA-MB-468 cancer cell lines over low tumorigenic HEK293 cells ($IC_{50} = 30.48 \mu M$). The 7-chlorobenzothiadiazine derivative **4.12e** showed the second most potent activity to reduce MDA-MB-468 cell viability with an IC_{50} value of $43.10 \mu M$. The 7-chlorobenzothiadiazine derivative (2,4-difluorophenyl) methanamine (**4.14e**) afforded $IC_{50} = 45.49 \mu M$ which had lower IC_{50} value than the 6-chlorobenzothiadiazine derivative (**3.20b**) with $IC_{50} = 84.63 \mu M$. 6-Chloro-3-((4-(trifluoromethoxy)benzyl)amino)-4*H*-benzo[e][1,2,4] thiadiazine 1,1-dioxide (**3.21b**) possessed an IC_{50} value of $48.01 \mu M$ in MDA-MB-468 and $IC_{50} = 77.16 \mu M$ in low tumorigenic HEK293 cells (**Table 4.4**). The other diazoxide derivatives were found to be inactive in inhibiting MDA-MB-468 cell proliferation ($>50 \mu M$) (**Figure 4.4 B**).

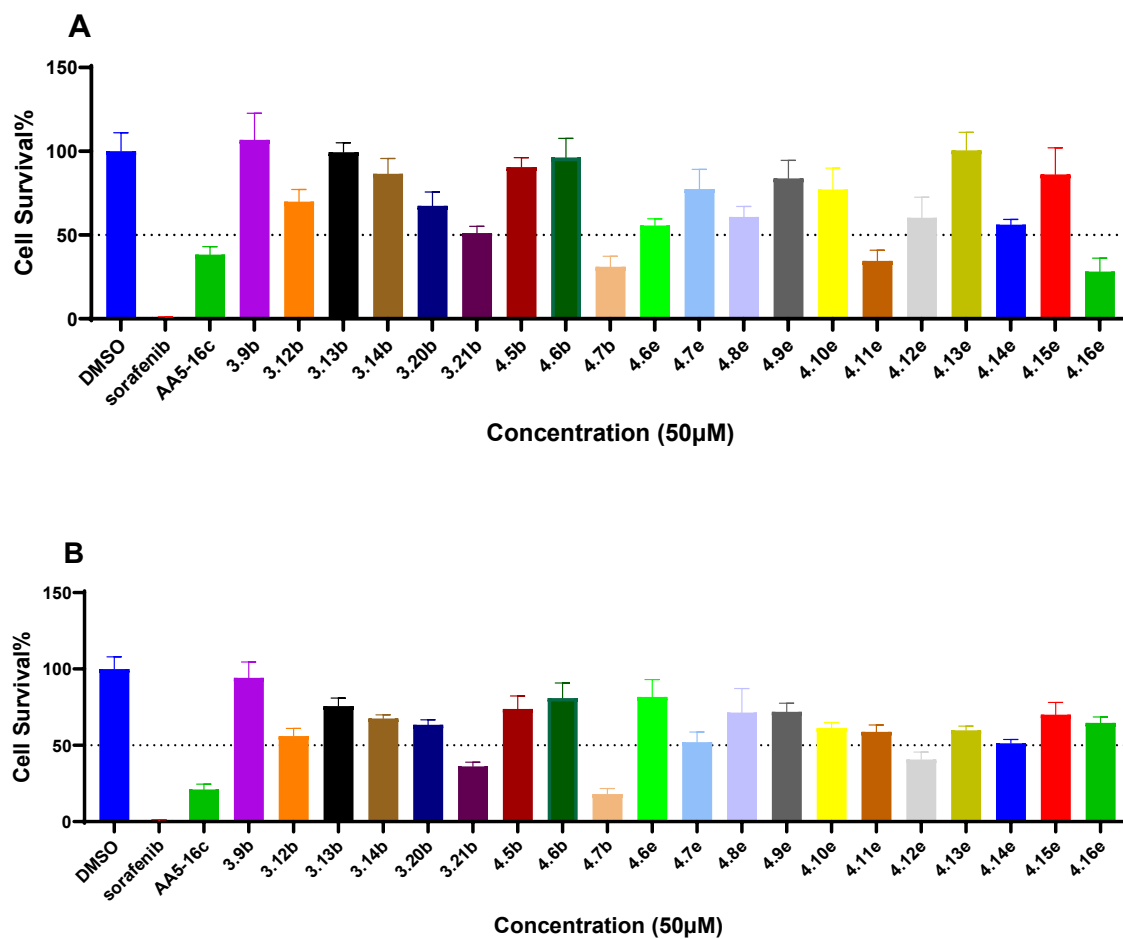
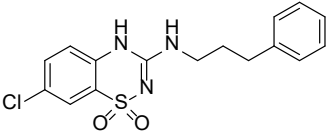
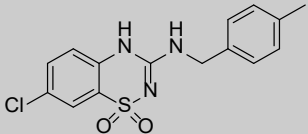
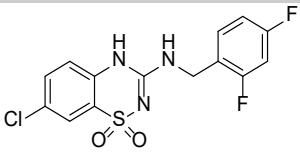
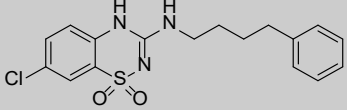


Figure 4.4. Cytotoxic effect of potent diazoxide derivatives (50 μM, 72-hour treatment): **A)** Cytotoxic effect of diazoxide derivatives on human embryonic kidney (HEK293) cells. **B)** Cytotoxic effect of diazoxide derivatives on triple negative breast cancer (MDA-MB-468) cells. Values represent the mean \pm SD of n= 3 experiments.

Compound	Structure	MDA-MB-468	HEK293
		IC ₅₀ (μM) ^a	IC ₅₀ (μM) ^a
Sorafenib		7.31 ± 1.9	2.95 ± 0.1
AA5-16c		6.71 ± 0.8	25.93 ± 2.4
3.12b		64.16 ± 14.2	101.90 ± 16.1
3.13b		147.80 ± 26.3	N.D. ^b
3.14b		91.91 ± 16.8	110.81 ± 7.4
3.20b		84.63 ± 9.6	129.40 ± 12.2
3.21b		48.01 ± 14.3	77.16 ± 5.2
4.7b		14.93 ± 2.5	30.48 ± 4.1
4.7e		62.90 ± 4.2	N.D.

4.11e		N.D.	30.85 ±3.9
4.12e		43.10 ±7.5	N.D.
4.14e		45.49 ±9.1	58.94 ±13.7
4.16e		N.D.	23.41 ±3.2

^aValues are the mean ±SD of n = 3 experiments at 72 hours.

^bNot Determined

Table 4.4. Cytotoxicity of the potent VEGF inhibitors of diazoxide derivatives and the clinical chemotherapeutic sorafenib in triple negative breast cancer MDA-MB-468 cells and low tumorigenic human endothelial kidney (HEK293) cells.

4.3. Conclusions

In summary, the development and use of antiangiogenic agents, especially those targeting the common growth factor VEGF, has become an integral component of antineoplastic regimens for many cancer types. A novel benzothiadiazine derivatives **3.9b**, **3.11b-3.14b**, **3.20b**, **3.21b**, **4.5b-4.7b**, and **4.7e-4.17e** were identified possess enhanced activity to inhibit the HUVEC-VEGF treated cells. Also, DZX derivatives **3.21b**, **4.10e**, **4.13e**, and the parent compound **DZX** were found to be most potent towards attenuation of pVEGFR2 expression. These potent derivatives reduced the cell viability of triple negative breast cancer MDA-MB-468 cells and low toxicity for the low tumorigenic HEK293 cells. The current SAR of the DZX derivative as VEGF inhibitors can be summarized as shown in **Figure 4.5**. These novel structural analogues of angiogenesis inhibitors that were discovered might be useful to improve the suppression of the tumor especially in combination treatment with the chemotherapeutic agent. Future studies involve IC₅₀ determination of potent VEGF inhibitors and improve the SAR based on the activity.

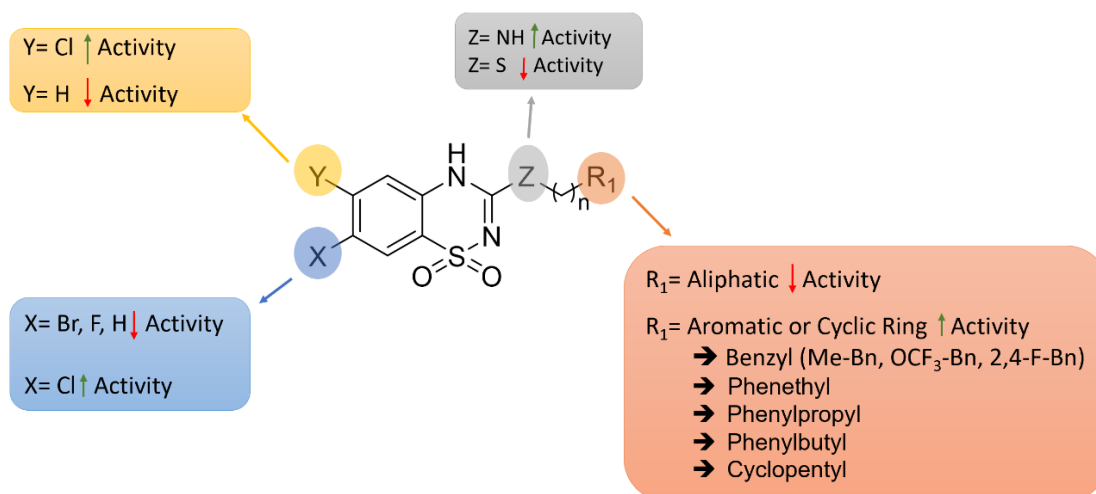


Figure 4.5. Structure activity relationship of the DZX derivative as VEGF inhibitors.

4.4. Experimental Section

4.4.1. Biology

4.4.1.1. Cell Culture and Reagents

Cells were maintained at 37 °C with 5% CO₂ in a humidified environment. Cell lines Primary Human Umbilical Vein Endothelial Cells (HUVEC), human embryonic kidney cells (HEK293), and triple-negative breast cancer cells (MDA-MB-468) were purchased from the American Type culture Collection (ATCC). The HUVEC cells were routinely cultured in M199 medium (Corning, Cat# MT10060CV), supplemented with 15% Fetal Bovine Serum (FBS, GIBCO™, Cat# 10438026), 150 µg/mL Endothelial Cell Growth Supplement (ECGS), 5 U/mL heparin sodium and 1X Antibiotic-Antimycotic solution (GIBCO™, Cat# 15240-062). MDA-MB-468 cells were cultured in Dulbecco's Modified Eagle Medium (DMEM, Fisher Scientific, Cat# 50-188-267FP) and HEK293 cells in Eagle's Minimum Essential Medium (ATCC®, Cat# 30-2003™), supplemented with FBS (ATCC®, Cat# 30-2020) to a final concentration of 10% and Penicillin-Streptomycin Solution (Corning™, Cat# MT30001CI) according to the supplier's recommended protocol. Vascular endothelial growth factor (VEGF, Cat# SRP3182) were purchased from Sigma. Diazoxide (Alfa Aesar™, Cat# AAJ66010ME) and Sorafenib™ (Tocris Bioscience™, Cat# 68-141-0) were purchased from Fisher Scientific. Stock solutions of all compounds were prepared in DMSO and were serially diluted for cell culture treatment maintaining the final DMSO concentration at less than 1%. Cell Titer 96 AQueous one solution cell proliferation assay (3-(4,5-dimethylthiazol-2-yl)-5-(3-carboxymethoxyphenyl)-2-(4-sulfophenyl)-2H-tetrazolium) (MTS) assay was purchased from Promega (Cat# G3580).

4.4.1.2 Cytotoxicity Assays

To determine the cell growth inhibition ability of the synthesized compounds, MTS assay used according to the manufacturer's recommended protocol. Stock solutions of the synthesized compounds were prepared in DMSO. Cells were seeded at a density of 1×10^5 cells in 96-well plates. After 24 hours, cells were treated at the indicated concentrations of test compounds, limiting the final DMSO concentration to less than 1%. After incubation at 37 °C in an environment of 5% CO₂ for 48-72 hours, 10 µL of MTS reagent (CellTiter 96® AQueous One Solution Reagent) was added to each well and incubated at the above-mentioned conditions for 2-4 h. Absorbance was recorded at 570 nm on a BioTek Synergy Mx multimode plate reader and the viability of cells were plotted as percentage of controls.

4.4.1.3 VEGF Assay

Cell proliferation of HUVECs was evaluated through the MTT (3-[4, 5-dimethylthiazol-2-yl]-2, 5-dimethyltetrazolium bromide) colorimetric assay, as previously described.²²⁹ The HUVECs were seeded at a density of 10,000 cells/well in 24 well plates in serum-containing medium and cultured overnight. Cells were starved with 300 µL of assay media (0.1% BSA+0.1% FBS in basal medium) for 24 h. Then, cells were treated with 500 µL of assay medium (control group), VEGF (10ng/mL, positive control group) or VEGF along with compounds (20 µM). After 48 h of culture, 50 µL of MTT stock (5 mg/mL in PBS) was added to each well and incubated for 2 h at 37 °C to allow the formation of dark blue formazan crystals in the metabolically active cells. The medium was removed, the cells were washed with PBS (pH 7.4), and 100 µL of acidified isopropanol (0.33 mL HCl in 100 mL isopropanol) was added to each well and incubated for 5 min with thorough agitation to solubilize the formazan crystals. An equal volume of the solution was

transferred to a 96-well plate and the absorbance was immediately measured using a microplate reader at a wavelength of 570 nm. Results were confirmed by direct measurement of the cells using a standard hemocytometer.

4.4.1.4 Statistical Analysis

Experiments were repeated at least thrice, and the statistical significance was calculated using the unpaired *t* test. A *p* value of <0.05 was considered statistically significant. IC₅₀ values were calculated by GraphPad prism software.

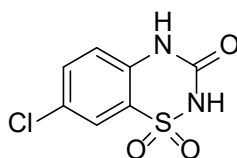
4.4.2 Chemistry

General

All reactions were carried out in oven- or flame-dried glassware under positive nitrogen pressure unless otherwise noted. Reaction progress was monitored by thin-layer chromatography (TLC) carried out on silica gel plates (2.5 cm x 7.5 cm, 200 μm thick, 60 F254) and visualized by using UV (254 nm) or by potassium permanganate or phosphomolybdic acid stain as indicator. Commercial grade solvents and reagents were purchased from Fisher Scientific (Houston, TX) or Millipore-Sigma (Milwaukee, WI) and were used without further purification except as indicated. Anhydrous solvents were purchased from Across Organics and stored under an atmosphere of dry nitrogen over molecular sieves.

¹H and ¹³C NMR spectra were recorded in the indicated solvent on a Bruker 400 MHz Advance III HD spectrometer at 400 and 100 MHz for ¹H and ¹³C respectively with solvent peak as an internal standard. Multiplicities are indicated by s (single), d (doublet), dd (doublet of doublets), t (triplet), q (quartet), m (multiplet), and br (broad). Chemical shifts

(δ) are reported in parts per million (ppm), and coupling constants (J), in Hertz. High-resolution mass spectroscopy (HRMS) was performed on a TripleTOF 5600 (SCIEX) using an ESI source conducted at the Texas Tech University Health Sciences Center School of Pharmacy in Dallas, TX for all the synthesized compounds in chapter 3. Also, the high-resolution mass spectroscopy (HRMS) was performed on 6230 LC/TOF (Agilent). The spectral data was extracted from total ion chromatogram (TIC).



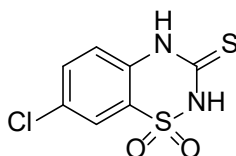
7-Chloro-3-oxo-3,4-dihydro-2H-1,2,4-benzothiadiazine 1,1-dioxide (4.2e).

A solution of chlorosulfonyl isocyanate (3.3 mL, 37.6 mmol) in nitromethane (50 mL) was mixed in a closed dried vessel under nitrogen pressure and cooled to $- (5-10) ^\circ\text{C}$ (ice and salt bath). The 4-chloroaniline (**4.1e**, 4 g, 31.4 mmol) was added dropwise. The contents were vigorously stirred for 15 mins followed by the addition of anhydrous aluminium chloride (5.44 g, 40.8 mmol) and the mixture was refluxed for 1h. The hot solution was poured onto ice (200 g) and stirred for an additional 30 mins until all ice is melted and the resulting precipitate was collected by filtration and washed with water. The crude solid was treated with an aqueous solution of sodium bicarbonate (5 g/100 mL) followed by heating until the solid precipitate was dissolved. The solution was treated with charcoal and was filtered, the filtrate solution was adjusted to pH 1 using 12N HCl. The resulting pure white precipitate was filtered, washed with water, and air dried (5.8 g, 80% yield):

^1H NMR (400 MHz, DMSO- d_6): δ = 7.29 (1H, d, J =7.3 Hz), 7.7 (1H, d, J =7.7), 7.83 (s, 1H), 11.45 ppm (s, 1H).

^{13}C NMR (100 MHz, DMSO- d_6): δ = 119.62, 122.09, 124.05, 127.69, 134.27, 134.53, 151.57 ppm.

HRMS (ESI): m/z calcd for $\text{C}_7\text{H}_5\text{ClN}_2\text{O}_3\text{S}$ [$M+\text{Na}$] $^+$: 254.9607, found: 254.9648.



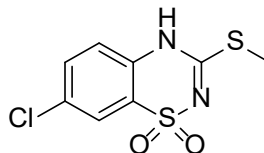
7-Chloro-3-thioxo-3,4-dihydro-2H-1,2,4-benzothiadiazine 1,1-dioxide (4.3e).

A suspension of 7-chloro-3-oxo-3,4-dihydro-2H-1,2,4-benzothiadiazine 1,1-dioxide (**4.2e**, 4.5 g, 19.34 mmol) and phosphorus pentasulfide (8.4 g, 19.34 mmol) was dissolved in anhydrous pyridine (50 mL) and refluxed under nitrogen pressure overnight. The reaction was allowed to cool, and the solvent removed in vacuo, the crude product was dissolved in an aqueous solution of sodium hydroxide (NaOH) (5 g/100 mL). This solution was treated with charcoal and was filtered. The filtrate was acidified to pH 1 using 12N HCl. The precipitated compound was collected by filtration, washed with water, and was allowed to air dry. The dried compound was suspended in an aqueous solution of sodium bicarbonate (NaHCO_3) (10 g/200 mL) and heated until the solid was dissolved. This solution was treated with charcoal and filtered. The filtrate was adjusted to pH 1 using 12N HCl, and the white precipitate was collected by filtration, washed with water, and air dried. (4.08 g, 81% yield):

^1H NMR (400 MHz, DMSO- d_6): δ = 7.25 (1H, d, J =7.2), 7.49 (1H, dd, J =7.5, 2.8 Hz), 7.55 (s, 1H), 11.35 ppm (br, 1H).

^{13}C NMR (100 MHz, DMSO- d_6): δ = 109.88, 121.31, 122.43, 124.51, 132.66, 158.16, 160.83 ppm.

HRMS (ESI): m/z calcd for $C_7H_5ClN_2O_2S_2$ $[M+Na]^+$: 270.9379, found: 270.9318.



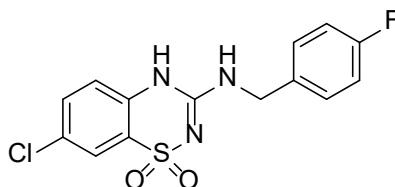
7-Chloro-3-methylsulfany-4H-1,2,4-benzothiadiazine 1,1-dioxide (4.4e).

7-Chloro-3-thioxo-3,4-dihydro-2H-1,2,4-benzothiadiazine 1,1-dioxide (**4.3e**, 4.0 g, 15.22 mmol) was suspended in a 1:1 hydromethanolic solution of sodium bicarbonate (5 g/ 200 mL). Methyl iodide was added (2 mL, 30.44 mmol) and the solution was stirred for 1h. The resulting suspension was adjusted to pH 5 using 6N HCl. The suspension was concentrated under reduced pressure, and the white precipitate was collected by filtration, washed with water, and air dried (93% yield):

1H NMR (400 MHz, DMSO- d_6): δ = 2.53 (s, 2H), 7.31 (1H, dd, J =8.8, 2.2 Hz), 7.72 (1H, dd, J =8.8, 2.3 Hz), 7.84 (1H, d, J =2.3 Hz), 12.66 ppm (s, 1H).

^{13}C NMR (100 MHz, DMSO- d_6): δ = 13.87, 119.72, 123.16, 123.20, 129.68, 133.88, 133.94, 161.79 ppm.

HRMS (ESI): m/z calcd for $C_8H_7ClN_2O_2S_2$ $[M+Na]^+$: 284.9535, found: 284.9486.



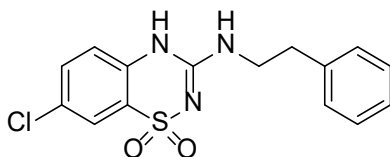
7-Chloro-3-((4-fluorobenzyl)amino)-4H-benzo[e][1,2,4]thiadiazine 1,1-dioxide (4.5e).

7-Chloro-3-methylsulfanyl-4H-1,2,4-benzothiadiazine 1,1-dioxide (**4.4e**, 0.25 g, 1 mmol) and 4-fluorobenzylamine (0.23 mL, 1.9 mmol) were dissolved in 1,4-dioxane (8 mL) in a sealed vessel and heated for 24h at 140 °C. The solvent and the excess amine were removed in vacuo, and the residue was dissolved in an aqueous 2% w/v solution of NaOH (6 mL). This solution was treated with charcoal and was filtered. The filtrate was adjusted to pH 1 using 6N HCl. The precipitated compound was collected by filtration, washed with water and air dried. The dried compound was suspended in an aqueous solution of sodium bicarbonate NaHCO₃ (1 g/40 mL). The alkaline solution was treated with charcoal and filtered; the filtrate was adjusted to pH 4-5 with 6N HCl. The white precipitate was collected by filtration, washed twice with water, and air dried (79% yield):

¹H NMR (400 MHz, DMSO-d₆): δ= 4.46 (s, 2H), 7.18 (2H, t, *J*=8.8 Hz), 7.26 (1H, d, *J*=8.8 Hz), 7.39 (q, 2H), 7.59 (1H, dd, *J*=8.7, 2.2 Hz), 7.67 (1H, d, *J*=2.2 Hz), 7.76 (br, 1H), 10.94 ppm (br, 1H).

¹³C NMR (100 MHz, DMSO-d₆): δ= 43.64, 115.49, 115.70, 119.42, 122.60, 124.21, 127.54, 129.71, 129.79, 132.87, 135.17, 151.73, 160.59, 163.01 ppm.

HRMS (ESI): *m/z* calcd for C₁₄H₁₁ClFN₃O₂S [*M*+Na]⁺: 362.0142, found: 362.0160.



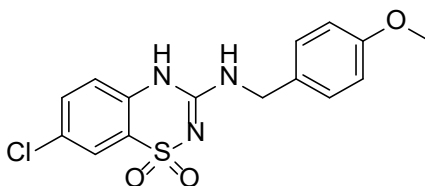
7-Chloro-3-(phenethylamino)-4H-benzo[e][1,2,4]thiadiazine 1,1-dioxide (4.6e).

The white compound was obtained from **4.4e** by following the experimental conditions described for **4.5e** (77% yield):

¹H NMR (400 MHz, DMSO-*d*₆): δ= 2.85 (2H, t, *J*=7.2 Hz), 3.48 (s, 2H), 7.20- 7.34 (m, 7H), 7.56 (1H, dd, *J*=8.7Hz), 7.67 (s 1H), 10.91 ppm (br, 1H).

¹³C NMR (100 MHz, DMSO-*d*₆): δ= 35.05, 42.43, 119.30, 121.61, 124.19, 125.83, 126.82, 127.56, 128.90, 129.12, 129.15, 132.84, 135.15, 139.28, 151.52 ppm.

HRMS (ESI): *m/z* calcd for C₁₅H₁₄ClN₃O₂S [*M*+Na]⁺: 358.0392, found: 358.0379.



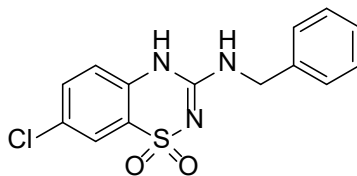
7-Chloro-3-((4-methoxybenzyl)amino)-4*H*-benzo[*e*][1,2,4]thiadiazine 1,1-dioxide (4.7e).

The white compound was obtained from **4.4e** by following the experimental conditions described for **4.5e** (77% yield):

¹H NMR (400 MHz, DMSO-*d*₆): δ= 3.73 (s, 3H), 4.40 (2H, d, *J*=5.6 Hz), 6.92 (2H, d, *J*=8.6 Hz), 7.26 (m, 3H), 7.62 (2H, dd, *J*=8.7, 2.4 Hz), 7.62 (1H, d, *J*=2.4 Hz), 10.75 ppm (br, 1H).

¹³C NMR (100 MHz, DMSO-*d*₆): δ= 43.87, 55.55, 114.29, 119.40, 122.61, 124.26, 127.59, 129.17, 130.70, 130.90, 132.87, 135.19, 151.51, 158.94 ppm.

HRMS (ESI): *m/z* calcd for C₁₅H₁₄ClN₃O₃S [*M*+Na]⁺: 374.03421, found: 374.0338.



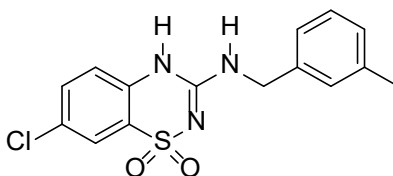
3-(Benzylamino)-7-chloro-4H-benzo[e][1,2,4]thiadiazine 1,1-dioxide (4.8e).

The white compound was obtained from **4.4e** by following the experimental conditions described for **4.5e** (76% yield):

¹H NMR (400 MHz, DMSO-*d*₆): δ = 4.47 (s, 2H), 7.25 (m, 2H), 7.34 (m, 4H), 7.69 (1H, d, *J*=8.7 Hz), 7.66 (s, 2H), 10.69 ppm (br, 1H).

¹³C NMR (100 MHz, DMSO-*d*₆): δ = 44.34, 119.51, 122.59, 124.25, 127.51, 127.57, 127.67, 127.77, 128.86, 132.84, 135.39, 135.42, 138.92, 151.47, 151.75 ppm.

HRMS (ESI): *m/z* calcd for C₁₄H₁₂ClN₃O₂S [*M*+Na]⁺: 344.0236, found: 344.0308.



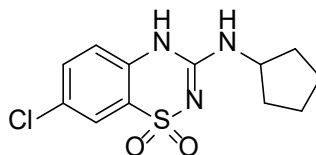
7-Chloro-3-((3-methylbenzyl)amino)-4H-benzo[e][1,2,4]thiadiazine 1,1-dioxide (4.9e).

The white compound was obtained from **4.4e** by following the experimental conditions described for **4.5e** (65% yield):

¹H NMR (400 MHz, DMSO-*d*₆): δ = 2.30 (s, 3H), 4.45 (2H, d, *J*=5.6 Hz), 7.35 (m, 3H), 7.24 (2H, t, *J*=7.8 Hz), 7.61 (1H, dd, *J*=8.7, 2.3 Hz), 7.68 (1H, d, *J*=2.4 Hz), 10.78 ppm (br, 1H).

¹³C NMR (100 MHz, DMSO-*d*₆): δ = 21.49, 44.32, 119.41, 122.61, 124.25, 124.76, 127.63, 128.23, 128.26, 128.80, 132.89, 135.15, 137.98, 138.673, 151.58 ppm.

HRMS (ESI): m/z calcd for $C_{15}H_{14}ClN_3O_2S$ $[M+Na]^+$: 358.0392, found: 358.0387.



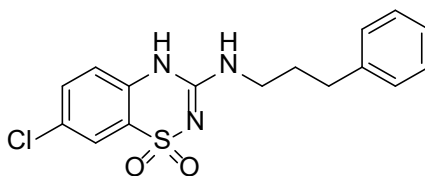
7-Chloro-3-(cyclopentylamino)-4H-benzo[e][1,2,4]thiadiazine 1,1-dioxide (4.10e).

The white compound was obtained from **4.4e** by following the experimental conditions described for **4.5e** (51% yield):

1H NMR (400 MHz, DMSO- d_6): δ = 1.44 -1.66 (m, 6H), 1.90 (m, 2H), 4.06 (m, 1H), 7.24 (2H, d, J =7.8 Hz), 7.58 (2H, dd, J =8.7, 2.3 Hz), 7.65 (2H, d, J =2.3 Hz), 10.39 ppm (s, 1H).

^{13}C NMR (100 MHz, DMSO- d_6): δ = 23.64, 32.69, 52.85, 119.38, 122.55, 124.33, 127.55, 132.79, 135.04, 151.11 ppm.

HRMS (ESI): m/z calcd for $C_{12}H_{14}ClN_3O_2S$ $[M+Na]^+$: 322.0392, found: 322.0351.



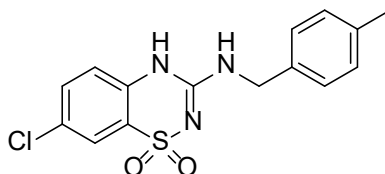
7-Chloro-3-((3-phenylpropyl)amino)-4H-benzo[e][1,2,4]thiadiazine 1,1-dioxide (4.11e).

The white compound was obtained from **4.4e** by following the experimental conditions described for **4.5e** (53% yield):

1H NMR (400 MHz, DMSO- d_6): δ = 1.83 (m, 2H), 2.64 (2H, t, J =8 Hz), 3.26 (q, 2H), 7.17-7.31 (m, 7H), 7.55 (1H, dd, J =8.7, 2.4 Hz), 7.66 (1H, d, J =2.4), 10.71 ppm (s, 1H).

^{13}C NMR (100 MHz, DMSO- d_6): δ = 30.96, 32.79, 119.33, 122.58, 124.27, 124.30, 126.29, 127.53, 128.74, 128.80, 128.91, 132.82, 135.16, 141.86, 151.55 ppm.

HRMS (ESI): m/z calcd for $\text{C}_{16}\text{H}_{16}\text{ClN}_3\text{O}_2\text{S}$ $[M+\text{Na}]^+$: 372.0549, found: 372.0546.



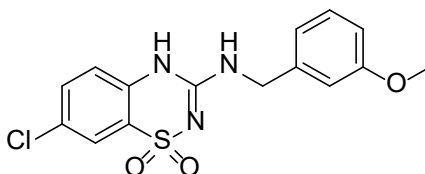
7-Chloro-3-((4-methylbenzyl)amino)-4H-benzo[e][1,2,4]thiadiazine 1,1-dioxide (4.12e).

The white compound was obtained from **4.4e** by following the experimental conditions described for **4.5e** (78% yield):

^1H NMR (400 MHz, DMSO- d_6): δ = 2.29 (s, 3H), 4.43 (2H, d, J =5.7 Hz), 7.17 (2H, d, J =8.2 Hz), 7.22 (2H, d, J =8.2 Hz), 7.26 (s, 1H), 7.30 (s, 1H), 7.66 (1H, dd, J =8.7, 2.4 Hz), 7.68 (2H, d, J =2.4), 10.82 ppm (br, 1H).

^{13}C NMR (100 MHz, DMSO- d_6): δ = 21.14, 44.12, 119.38, 122.61, 124.25, 127.63, 127.69, 129.41, 132.89, 135.13, 135.76, 136.71, 151.55 ppm.

HRMS (ESI): m/z calcd for $\text{C}_{15}\text{H}_{14}\text{ClN}_3\text{O}_2\text{S}$ $[M+\text{Na}]^+$: 358.0392, found: 358.0389.



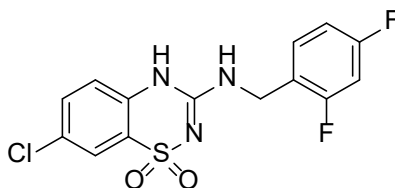
7-Chloro-3-((3-methoxybenzyl)amino)-4H-benzo[e][1,2,4]thiadiazine 1,1-dioxide (4.13e).

The white compound was obtained from **4.4e** by following the experimental conditions described for **4.5e** (76% yield):

¹H NMR (400 MHz, DMSO-*d*₆): δ = 3.74 (s, 3H), 4.45 (2H, d, *J*=5.7 Hz), 6.86 (1H, d, *J*=7.2 Hz), 6.92 (2H, d, *J*=8.7 Hz), 7.27 (1H, t, *J*=8.4 Hz), 7.61 (1H, d, *J*=8.7 Hz), 7.67 (s, 2H), 10.84 ppm (br, 1H).

¹³C NMR (100 MHz, DMSO-*d*₆): δ = 44.29, 55.48, 113.02, 113.37, 119.41, 119.80, 122.62, 124.24, 127.67, 129.97, 132.91, 135.31, 140.45, 151.58, 159.82 ppm.

HRMS (ESI): *m/z* calcd for C₁₅H₁₄ClN₃O₃S [*M*+Na]⁺: 374.0342, found: 374.0338.



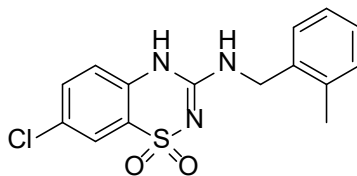
7-Chloro-3-((2,4-difluorobenzyl)amino)-4H-benzo[e][1,2,4]thiadiazine 1,1-dioxide (4.14e).

The white compound was obtained from **4.4e** by following the experimental conditions described for **4.5e** (69% yield):

¹H NMR (400 MHz, DMSO-*d*₆): δ = 4.48 (2H, d, *J*=5.7 Hz), 7.09 (1H, t, *J*=8.7 Hz), 7.24(m, 2H), 7.44 (q, 1H), 7.67 (m, 3H), 10.84 ppm (br, 1H).

¹³C NMR (100 MHz, DMSO-*d*₆): δ = 38.10, 104.26, 104.57, 111.74, 111.95, 119.43, 122.07, 122.65, 124.14, 127.76, 131.18, 132.94, 135.06, 151.52 ppm.

HRMS (ESI): *m/z* calcd for C₁₅H₁₀ClF₂N₃O₂S [*M*+Na]⁺: 380.0048, found: 380.0041.



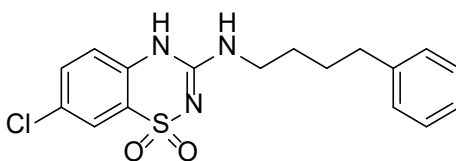
7-Chloro-3-((4-methylbenzyl)amino)-4H-benzo[e][1,2,4]thiadiazine 1,1-dioxide (4.15e).

The white compound was obtained from **4.4e** by following the experimental conditions described for **4.5e** (78% yield):

¹H NMR (400 MHz, DMSO-*d*₆): δ = 2.26 (s, 3H), 4.48 (2H, d, *J* = 4.8 Hz), 7.20 (m, 3H), 7.26 (m, 2H), 7.40 (2H, dd, *J* = 8.8, 2.4 Hz), 7.67 (s, 1H), 10.71 ppm (br, 1H).

¹³C NMR (100 MHz, DMSO-*d*₆): δ = 19.09, 42.45, 119.44, 122.62, 124.22, 126.35, 127.60, 127.65, 130.76, 132.88, 135.18, 136.03, 136.48, 151.60 ppm.

HRMS (ESI): *m/z* calcd for C₁₅H₁₄ClN₃O₂S [*M*+Na]⁺: 358.0392, found: 358.0399.

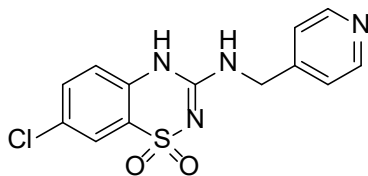


7-Chloro-3-((4-phenylbutyl)amino)-4H-benzo[e][1,2,4]thiadiazine 1,1-dioxide (4.16e).

The white compound was obtained from **4.4e** by following the experimental conditions described for **4.5e** (78% yield):

¹H NMR (400 MHz, DMSO-*d*₆): δ = 1.53 (m, 4H), 2.61 (2H, t, *J* = 7.7 Hz), 3.26 (2H, t, *J* = 6.8 Hz), 7.22 (m, 6H), 7.61 (1H, d, *J* = 8.8 Hz), 7.66 (s, 1H), 10.67 ppm (br, 1H).

HRMS (ESI): *m/z* calcd for C₁₇H₁₈ClN₃O₂S [*M*+Na]⁺: 386.8486, found: 386.8473.



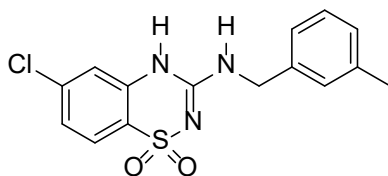
7-Chloro-3-((pyridin-4-ylmethyl)amino)-4H-benzo[e][1,2,4]thiadiazine 1,1-dioxide (4.17e).

The white compound was obtained from **4.4e** by following the experimental conditions described for **4.5e** (56% yield):

¹H NMR (400 MHz, DMSO-*d*₆): δ = 4.50 (2H, d, *J*=5.7 Hz), 7.29 (1H, d, *J*=8.8 Hz), 7.32 (1H, d, *J*=8.8 Hz), 7.62 (1H, dd, *J*=8.7, 2.0 Hz), 7.68 (1H, d, *J*=2.0 Hz), 7.77 (br, 1H), 8.53 (2H, d, *J*=4.6 Hz), 11.09 ppm (br, 1H).

¹³C NMR (100 MHz, DMSO-*d*₆): δ = 40.40, 119.44, 122.40, 122.64, 124.15, 127.78, 132.97, 135.10, 148.12, 150.04, 151.71 ppm.

HRMS (ESI): *m/z* calcd for C₁₃H₁₁ClN₄O₂S [*M*+Na]⁺: 345.7571, found: 345.7448.



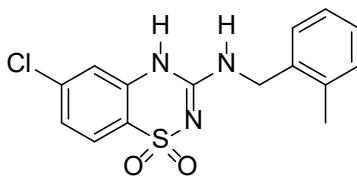
6-Chloro-3-((3-methylbenzyl)amino)-4H-benzo[e][1,2,4]thiadiazine 1,1-dioxide (4.5b).

The white compound was obtained from **3.4b** by following the experimental conditions described for **4.5e** (78% yield):

¹H NMR (400 MHz, DMSO-*d*₆): δ= 2.29 (s, 3H), 4.44 (2H, d, *J*=5 Hz), 7.05- 7.15 (m, 3H), 7.24 (1H, t, *J*=7.5 Hz), 7.29 (2H, *J*= 9.0 Hz), 7.70 (1H, d, *J*=7.5 Hz), 7.70 (1H, d, *J*=8.2 Hz), 7.75 (br, 1H), 10.60 ppm (br, 1H).

¹³C NMR (100 MHz, DMSO-*d*₆): δ= 21.48, 44.32, 116.68, 121.91, 124.26, 123.78, 125.43, 128.23, 128.28, 128.80, 136.97, 137.62, 137.97, 138.72, 151.49 ppm.

HRMS (ESI): *m/z* calcd for C₁₅H₁₄ClN₃O₂S [*M*+Na]⁺: 358.0392, found: 358.0339.



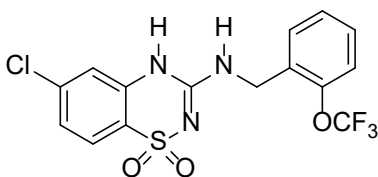
6-Chloro-3-((2-methylbenzyl)amino)-4*H*-benzo[*e*][1,2,4]thiadiazine 1,1-dioxide (4.6b).

The white compound was obtained from **3.4b** by following the experimental conditions described for **4.5e** (93% yield):

¹H NMR (400 MHz, DMSO-*d*₆): δ= 2.32 (s, 3H), 4.41 (s, 2H), 7.19 (s, 3H), 7.28 (3H, t, *J*= 9 Hz), 7.64 (br, 1H), 7.67 (1H, d, *J*=8.2 Hz), 10.33 ppm (br, 1H).

¹³C NMR (100 MHz, DMSO-*d*₆): δ= 19.09, 42.53, 116.73, 121.90, 124.24, 125.43, 126.34, 127.65, 127.72, 130.52, 136.04, 136.48, 136.97, 151.56 ppm.

HRMS (ESI): *m/z* calcd for C₁₅H₁₄ClN₃O₂S [*M*+Na]⁺: 358.0392, found: 358.0287.



6-Chloro-3-((2-(trifluoromethoxy)benzyl)amino)-4*H*-benzo[e][1,2,4]thiadiazine 1,1-dioxide (4.7b).

The white compound was obtained from **3.4b** by following the experimental conditions described for **4.5e** (64% yield):

¹H NMR (400 MHz, DMSO-*d*₆): δ= 4.55 (2H, d, *J*=5.8 Hz), 7.30 (2H, d, *J*=7.8 Hz), 7.32 (2H, d, *J*=8.6 Hz), 7.47 (2H, d, *J*=8.6 Hz), 7.75 (br, 1H), 7.84 (1H, d, *J*=8.6 Hz), 10.93 ppm (s, 1H).

¹³C NMR (100 MHz, DMSO-*d*₆): δ= 113.89, 116.66, 120.82, 121.07, 124.43, 125.50, 126.16, 126.52, 128.01, 129.63, 131.20, 137.25, 157.85, 151.52, 161.90 ppm.

HRMS (ESI): *m/z* calcd for C₁₅H₁₁ClF₃N₃O₃S [*M*+Na]⁺: 428.0059, found: 428.0021.

Chapter 5. Design, Synthesis, and Evaluation of Novel Carbonic Anhydrase Inhibitors as Anticancer Agents

5.1. Introduction

The carbonic anhydrases (CA) are a family of ubiquitous zinc enzymes which play a catalytic role in the reversible hydration of carbon dioxide (CO_2) and water (H_2O) to bicarbonate (HCO_3^-) and proton.¹²⁰ In humans, the carbonic anhydrases enzymes have 16 isoforms that vary by localization and catalytic activity include: the cytosolic CA's are CA I, CA II, CA III, CA VII, CA XIII; also, the membrane-bound CAs are CA IV, CA IX, CA XII, CA XIV, CA XV; but the CA Va and CA Vb are mitochondrial, and CA VI is secreted in saliva and colostrum. Besides, there are three catalytically inactive forms of CA (CA VIII, CA X, and CA XI) referred to as CA related proteins.¹²³ Carbonic anhydrase IX and CA XII are highly overexpression genes in response to hypoxia in a variety of human solid tumors and play a critical role in regulating tumor acidification, proliferation, and progression.¹³⁸

The overexpression of CA IX and CA XII leads to induced cancer cell growth, activation of the metastatic cascade, and reduced response to chemotherapy.¹²⁵ Targeting both CA IX and CA XII in cancers that overexpress these biomarkers and suppress their activity will be therapeutically beneficial in the treatment of tumors. There are several CA inhibitors that have shown potent anticancer activity. The classic CA inhibitors are sulfonamide derivatives which have been determined as potent CA IX and XII inhibitors with high activity to attenuate cancer cell growth both *in vitro* and *in vivo* (**Table 5.1**).¹²⁰ Recently, non-classic CA inhibitor coumarin-based small molecules were reported with high efficacy and selectively for inhibiting the enzymatic activity of the physiologically dominant tumor-associated isoenzyme human CA IX and CA XII.²³⁰ Carbonic anhydrase inhibitors with sulfonamides containing a coumarin moiety have been reported to possess high efficacy for inhibiting the enzymatic activity of the physiologically dominant tumor-

associated isoenzyme human CA IX. Moreover, sulfonamides containing coumarin moieties have potent anticancer activity.¹⁶⁶

Here, the synthesis of a series of CA inhibitors have been reported based around the coumarin scaffold with substituted sulfonamide moieties to have the benefit of both sulfonamides and coumarin to inhibit the CA enzymes. I envisioned that these derivatives would potentially possess high selectivity and potency for inhibiting the tumor-associated CA IX and CA XII. Several of the synthesized compounds have anticancer activity against the aggressive cancer cells triple negative breast cancer MDA-MB-468 cells with IC₅₀ values in the range between 25.74- 39.32 μ M. By collaborating with Dr. Claudiu T Supuran's lab in Università degli Studi di Firenze, Florence, Italy, our lab will continue further studies to identify the potent compounds and completing the structure-activity relationship study. Due to the COVID-19 pandemic efforts to evaluate the CA inhibition activity and SAR of these compounds has been impacted.

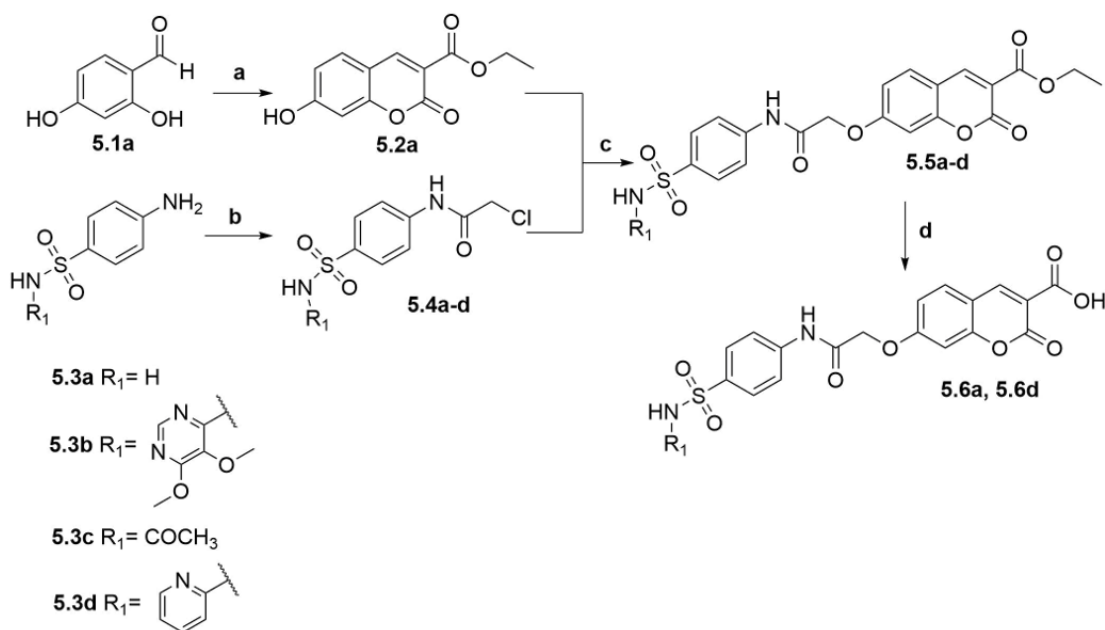
Compound	Structure	K _i (μM)		
		CA II	CA IX	CA XII
Acetazolamide		0.012	0.026	0.006
U-104		9.6	0.045	0.004
Dichlorphenamide		0.038	0.05	0.05
Dorzolamide		0.009	0.052	0.004
GC-204		>100	0.009	0.043
GC-205		>100	0.2	0.18
1.4		>100	0.2	0.2
1.2		94.3	0.61	7.7

Table 5.1. Structures, and inhibition value of CA II, IX, and XII for several carbonic anhydrase inhibitors.^{120, 161, 163, 165, 231}

5.2. Results and Discussion

5.2.1. Chemistry

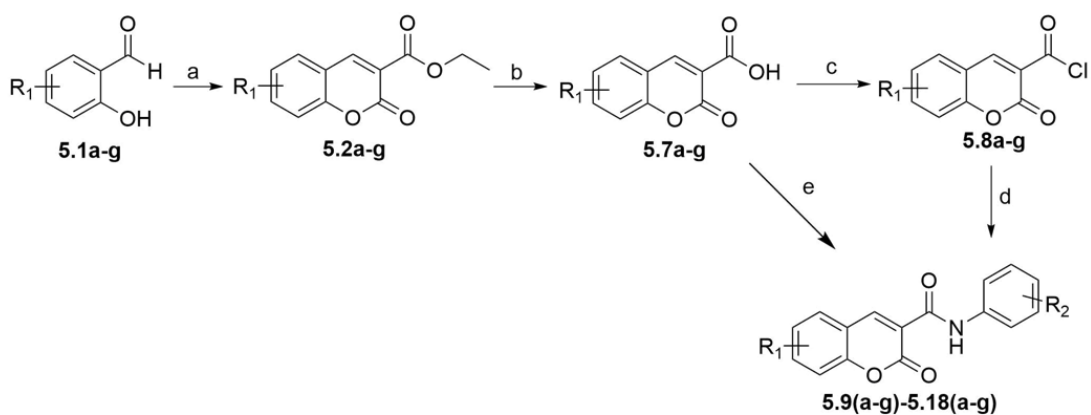
Although several substituted coumarins have been described in the literature, little information is known about the importance of these coumarin structures as a CA inhibitor. The coumarin derivatives (*2H*-chromen-2-one derivatives) can be accessed by a number of reported syntheses.²³²⁻²³⁴ Herein, coumarin ethyl ester was synthesized according to the protocol outlined in **Scheme 5.1**. Initially, the ethyl 7-hydroxy-2-oxo-2*H*-chromene-3-carboxylate (**5.2a**) was prepared starting from a reaction of the commercially available 2,4-dihydroxybenzaldehyde (**5.1a**) with diethyl malonate in the presence of piperidine. The synthesis of sulfonamide derivatives with the chloroacetamide linker were synthesized as summarized as **Scheme 5.1**.^{235, 236} Starting with various of appropriate commercially available sulfonamide derivatives (**5.3a-d**) were reacted in tetrahydrofuran with 2-chloroacetyl chloride at 0 °C in the presence of anhydrous potassium carbonate and a catalytic amount of potassium iodide to give corresponding chloroacetamide derivatives (**5.4a-d**) in good yields.²³⁷ After that, the mixture of ethyl 7-hydroxy-2-oxo-2*H*-chromene-3-carboxylate (**5.2a**) and sulfonamide derivatives (**5.4a-d**) in DMF were reacted in the presence of potassium carbonate along with potassium iodide led to the formation of coumarin sulfonamides (**5.5a-d**) in moderate yields (**Table 5.2**).²³⁴ Finally, hydrolysis of the ethyl ester group by using NaOH in hydroethanolic solution yielded 2-oxo-7-(2-oxo-2-((4-sulfamoylphenyl)amino)ethoxy)-2*H*-chromene-3-carboxylic acid (**5.6a**) and 2-oxo-7-(2-oxo-2-((4-(*N*-(pyridin-2-yl) sulfamoyl)phenyl) amino)ethoxy)-2*H*-chromene-3-carboxylic acid (**5.6d**) in good yield (**Table 5.2**).



Scheme 5.1. Synthesis carbonic anhydrase inhibitors 5.5a-d and 5.6a, 5.6d.

Reagents and Conditions: **a)** Diethyl malonate, piperidine, 60 °C, 3 h, 87%; **b)** Chloroacetyl chloride, K_2CO_3 , KI, THF, 2 h, 0 °C, 76-93%; **c)** Na_2CO_3 , DMF, 155 °C, 12 h, 49-61%; **d)** NaOH, ethanol, 1 h, RT, 87%

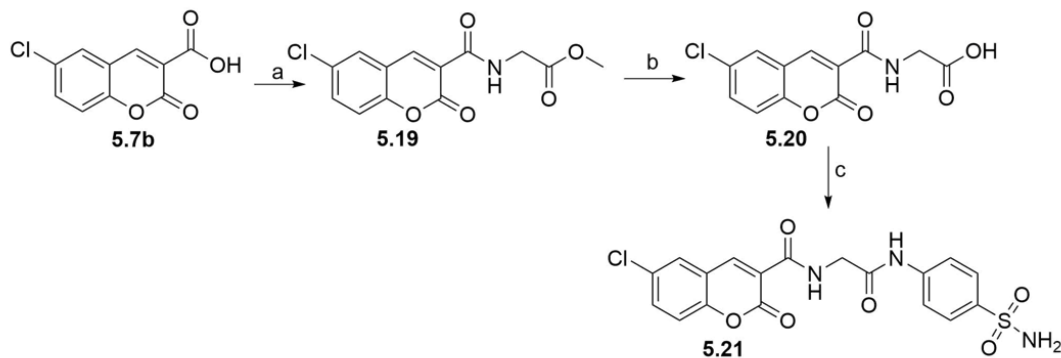
Several coumarin derivatives (**5.2a-g**) were achieved by following the synthesis of **5.2a** in **scheme 5.1**. The ethyl ester group was hydrolyzed to obtain the compound **5.7a-g** in high yield. Thionyl chloride was refluxed with compounds **5.7a-g** to obtain coumarin acid chloride. Finally, amide coupling reaction was used by adding appropriate sulfonamide derivatives to coumarin acid chloride in the presence of pyridine or triethylamine resulted in compound **5.9a-g**.²³² On the other hand, alternate amide coupling was used for some compounds to achieve an excellent yield by using 1-ethyl-3-(3-dimethylaminopropyl) carbodiimide hydrochloride (EDC) and 1-hydroxybenzotriazole hydrate (HOBt•H₂O) with triethylamine (TEA) (**Scheme 5.2**) (**Table 5.3**).²³⁸⁻²⁴⁰



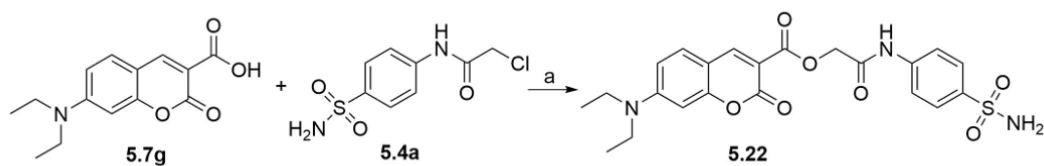
Scheme 5.2. Synthesis carbonic anhydrase inhibitors 5.9a-g. *Reagents and Conditions:* **a)** Diethyl malonate, piperidine, 3 h, 60 °C, 70-92%; **b)** NaOH, methanol, RT, 84-99%; **c)** SOCl₂, 75 °C, 5 h, 71-96% ;**d)** Appropriate sulfonamide amines, pyridine, DMF, 12 h, 80 °C, 49-96%; **e)** Appropriate sulfonamide amines, EDC , HOBt·H₂O, Et₃N, DMF, RT, 5 h, 73%.

Another derivative was designed with different linkers between the coumarin acids and the sulfonamide derivatives, as described in **schemes 5.3** and **5.4**. 6-Chloro-2-oxo-2*H*-chromene-3-carboxylic acid (**5.7b**) was reacted with glycine methyl ester hydrochloride in the presence of triethylamine and thionyl to yield compound **5.19**. The methyl ester was hydrolyzed by using NaOH in hydroethanolic solution to allow access to (6-chloro-2-oxo-2*H*-chromene-3-carbonyl)glycine (**5.20**). Finally, amide coupling was used by adding appropriate sulfonamide derivatives to **5.20** by using EDC and HOBt•H₂O with triethylamine to obtain 6-chloro-2-oxo-*N*-(2-oxo-2-((4-sulfamoylphenyl) amino) ethyl)-2*H*-chromene-3-carboxamide (**5.21**) (**Scheme 5.3**).^{238, 241}

The ester linker was synthesized to combine the coumarin acids and the sulfonamide derivatives. This derivative was synthesized based on higher rate of hydrolysis and potentially releasing subunits of sulfonamide and coumarin with the interaction of CA which in turn could individually inhibit the activity of CA separately. 2-Oxo-2-((4-sulfamoylphenyl)amino)ethyl 7-(diethylamino)-2-oxo-2*H*-chromene-3-carboxylate (**5.22**) was obtained by reaction of 7-(diethylamino)-2-oxo-2*H*-chromene-3-carboxylic acid (**5.7g**) with 2-chloro-*N*-(4-sulfamoylphenyl) acetamide (**5.4a**) in the presence of anhydrous potassium carbonate and a catalytic amount of potassium iodide to afford a moderate yield of **5.22** (**Scheme 5.4**).²³⁴



Scheme 5.3. Synthesis of carbonic anhydrase inhibitors 5.21. *Reagents and Conditions:* **a)** Glycine methyl ester hydrochloride, SOCl_2 , Et_3N , DCM, RT, 20 mins, 91%; **b)** NaOH, methanol, 1 h, RT, 89%; **c)** Appropriate sulfonamide amines, EDC, $\text{HOBT}\cdot\text{H}_2\text{O}$, Et_3N , DMF, 5 h, RT, 67%.



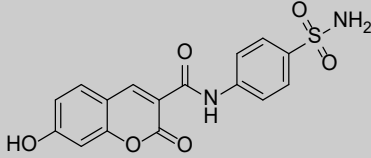
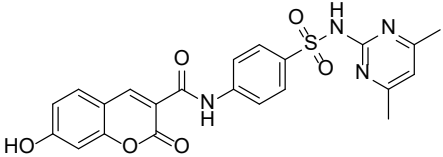
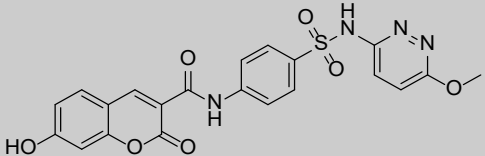
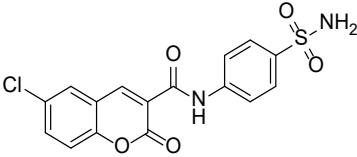
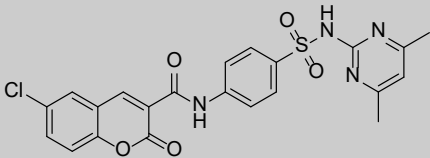
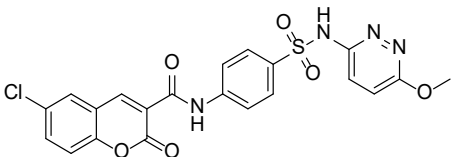
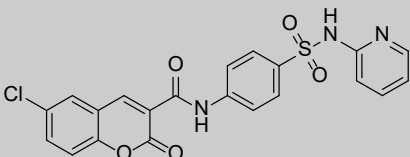
Scheme 5.4. Synthesis of carbonic anhydrase inhibitors 5.22. *Reagents and Conditions:* **a)** K_2CO_3 , KI, DMF, 155 °C, 12 h, 54%

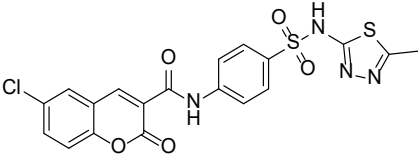
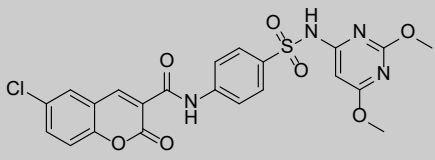
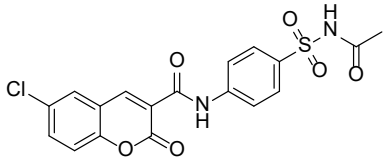
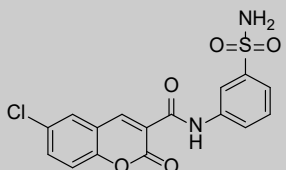
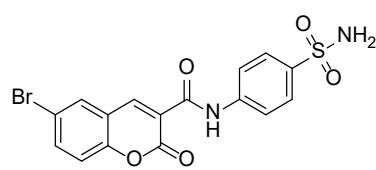
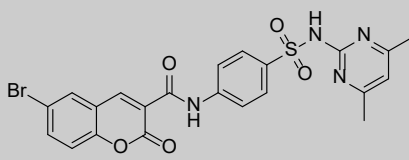
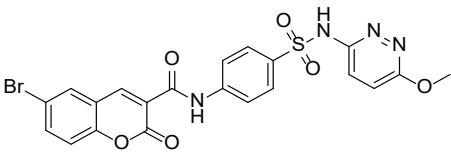
Compound	Structure	Mw	cLogP ^a	PSA ^b
5.5a		446.43	1.37	151.09
5.5b		584.56	3.17	180.28
5.5c		488.47	0.97	154.17
5.5d		523.10	2.78	149.46
5.6a		418.38	0.64	162.09
5.6d		495.46	2.05	160.46

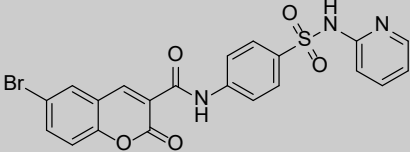
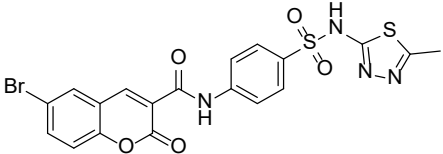
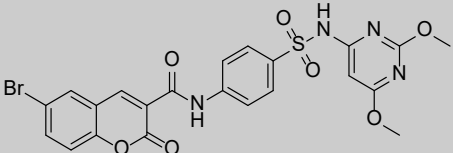
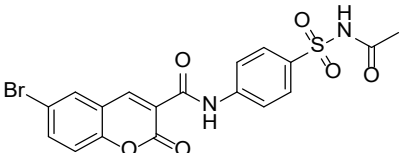
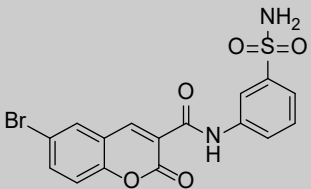
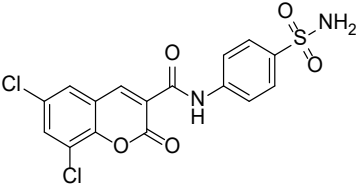
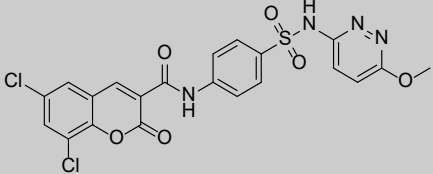
^aCalculated by ChemDraw Professional 16.0.

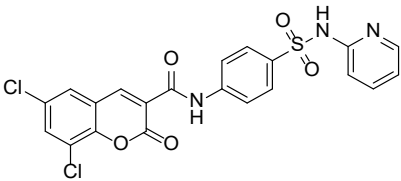
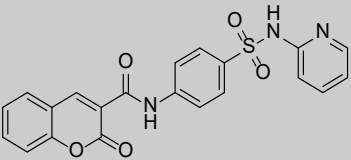
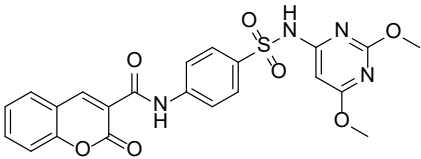
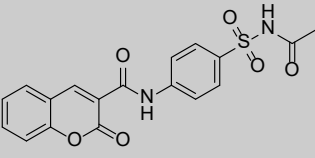
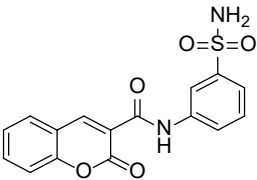
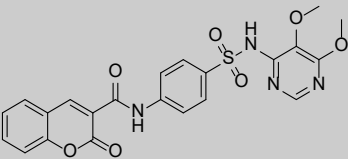
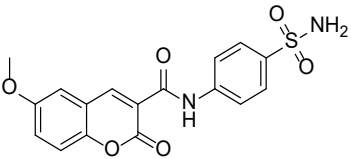
^bPolar surface area (pH 7.4), calculated by ChemDraw Professional 16.0.

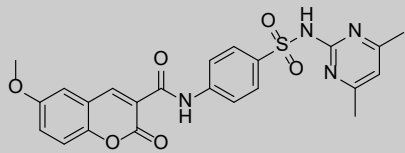
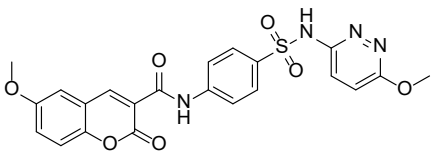
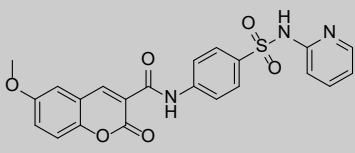
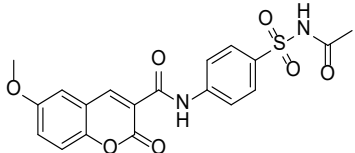
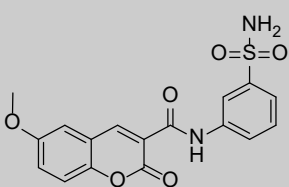
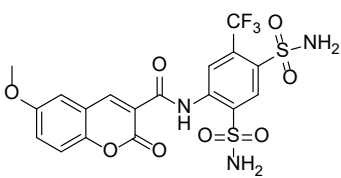
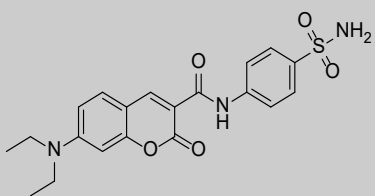
Table 5.2. Structure, molecular weight, calculated cLogP and polar surface area of synthesized carbonic anhydrase inhibitors in scheme 5.1.

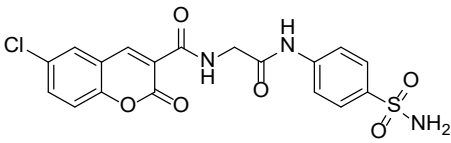
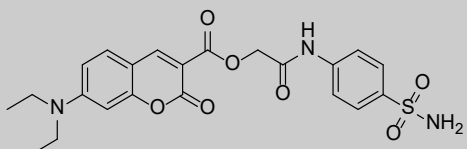
Compound	Structure	Mw	cLogP ^a	PSA ^b
5.9a		360.34	0.44	135.79
5.10a		466.47	2.11	146.52
5.11a		468.44	1.57	155.75
5.9b		378.78	1.64	115.56
5.10b		484.91	3.31	126.29
5.11b		486.88	2.77	135.52
5.12b		455.87	3.05	113.93

5.13b		476.91	2.63	126.29
5.14b		516.91	4.19	144.75
5.15b		420.82	1.32	118.64
5.16b		378.78	1.64	115.56
5.9c		423.24	1.79	115.56
5.10c		529.37	3.46	126.29
5.11c		531.34	2.92	135.52

5.12c		500.32	3.20	113.93
5.13c		521.36	2.78	126.29
5.14c		561.36	4.34	144.75
5.15c		465.27	1.47	118.64
5.16c		423.24	1.79	115.56
5.9d		413.23	2.35	115.56
5.11d		521.33	3.48	135.52

5.12d		490.31	3.76	113.93
5.12e		421.43	2.32	113.93
5.14e		482.47	3.47	144.75
5.15e		386.38	0.60	118.64
5.16e		344.34	0.92	115.56
5.17e		482.47	2.72	144.75
5.9f		374.37	0.89	179.24

5.10f		480.50	2.56	135.52
5.11f		482.47	2.02	144.75
5.12f		451.45	2.30	123.16
5.15f		416.40	0.58	127.87
5.16f		374.37	0.89	124.79
5.18f		521.44	-0.30	184.95
5.9g		415.46	2.20	118.80

5.21		435.48	1.14	144.66
5.22		473.50	2.22	145.10

^aCalculated by ChemDraw Professional 16.0.

^bPolar surface area (pH 7.4), calculated by ChemDraw Professional 16.0.

Table 5.3. Structure, molecular weight, calculated logP and polar surface area of synthesized carbonic anhydrase inhibitors in schemes 5.2-5.4.

5.2.2. Prediction of the activity of synthesized carbonic anhydrase inhibitor

Many reports showed sulfonamide or coumarin-based molecules are able to inhibit the carbonic anhydrase enzymes IX and XII and effect tumor pH, leading to inhibition of growth in both primary tumors and metastases.^{123, 138, 242} Several sulfonamide or coumarin compounds that inhibit CA IX are in clinical development or in use (**Figures 1.6** and **1.7**).¹²⁰ A recent report discovered that the carbonic anhydrase inhibitors with sulfonamide containing coumarin moiety have nanomolar potency to inhibit the enzymatic activity of the physiologically dominant tumor-associated isoenzyme human CA IX (**Table 5.4**).¹⁶⁶ Therefore, I envisioned to synthesize a series of sulfonamide containing coumarin conjugates that could inhibit tumor associated human carbonic anhydrases IX and XII. The compounds which have coumarin's containing sulfonamide moieties could have the potential to be novel and potent antitumor agents.

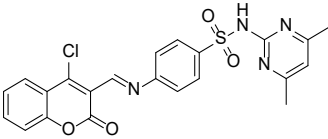
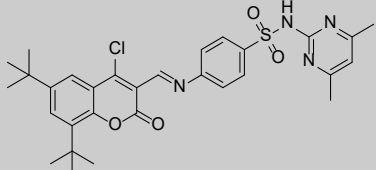
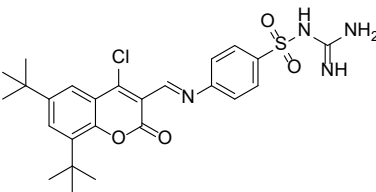
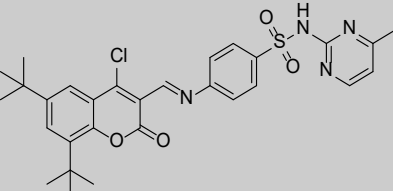
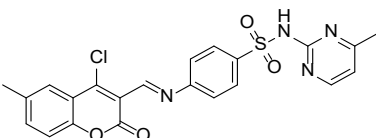
Compound	Structure	IC ₅₀ (μM)		
		CA II	CA IX	MCF-7
5.23		0.023	0.124	0.020
5.24		0.173	0.090	0.008
5.25		0.103	0.074	0.018
5.26		0.063	0.024	0.032
5.27		0.061	0.048	0.061

Table 5.4. Carbonic anhydrase inhibitors sulfonamides containing coumarin moieties, Anticancer activities (IC₅₀) on human breast cancer cell line (MCF-7).¹⁶⁶

5.2.3. Cytotoxicity Assay

Recently, carbonic anhydrase IX has been shown to be overexpressed in aggressive breast cancers. Carbonic anhydrase IX plays a major role that drives the growth, migration, and metastasis of the cancer cells. Therefore, it has received more attention as a potential target for triple negative breast cancer.^{243, 244} The cytotoxicity of some coumarins and sulfonamide derivatives have been shown to inhibit the proliferation of many aggressive cancer cells including triple-negative breast cancer cell lines with moderate inhibition.^{243, 245} Based on the inhibitory capabilities of sulfonamides and coumarins in TNBC, I explored the cytotoxic effect of the synthesized compounds in the TNBC MDA-MB-468 cell line. All the synthesized compounds were initially screened for cytotoxic effect at 50 μ M over 72 hours (**Figure 5.2**). Cytotoxicity studies were performed using MTS assay. The derivatives that reduced cell viability by 50% or more at 50 μ M concentration were further evaluated for IC₅₀ (**Table 3.3**). The clinical agent 5-fluorouracil is employed as a positive control with dimethyl sulfoxide (DMSO) as a negative control.

When the sulfonamide derivatives were conjugated to the 7-hydroxyl in the coumarin, the inhibition in TNBC cell viability was diminished. Ethyl 2-oxo-7-(2-oxo-2-((4-sulfamoylphenyl)amino)ethoxy)-2*H*-chromene-3-carboxylate (**5.5a**) which afforded a 39% reduction in cell viability was most active of this class. However, converting the coumarin ester to carboxylic acid (**5.6a**) afforded just 14% reduction of MDA-MB-468 cell viability. On the other hand, replacing the sulfanilamide in **5.5a** to sulfadoxine (**5.5b**) or sulfacetamide (**5.5c**) reduces cell survival of TNBC cells by approximately 18% and 26%, respectively (**Figure 5.2A**).

The synthesized compounds with the amide coupling between the coumarin carboxylic acid and sulfonamide derivatives displayed higher inhibition in compounds that depend on the substitution on coumarin. 7-Hydroxyl coumarin compounds with three

different sulfonamide derivatives include sulfanilamide (**5.9a**), sulfamethazine (**5.10a**), and sulfamethoxypyridazine (**5.11a**) have cell viability inhibition between 28-45% at 50 μM concentration. The chlorine in position 6 is very important in the derivatives as shown in 6-chloro-*N*-(4-(*N*-(6-methoxypyridazin-3-yl) sulfamoyl) phenyl) -2-oxo-2*H*-chromene-3-carboxamide (**5.11b**), where this compound reduced cell survival of TNBC cells by 79% and possessed an IC_{50} value of 26.48 μM with 4-fold selectivity towards TNBC cells over low tumorigenic HEK293 cells (IC_{50} = 106.71 μM) (**Table 5.3**). Compound **5.12b**, the sulfapyridine, and **5.13b**, the sulfamethizole reduced cell survival of MDA-MB-468 cells by 46% and 45%, respectively, while the sulfanilamide (**5.9b**) and 3-aminobenzene-sulfonamide (**5.16b**) derivatives resulted in 43% and 4% cell viability, respectively. Replacing the 6-chloro to 6-bromo reduced the activity as shown in 6-bromo-*N*-(4-(*N*-(6-methoxypyridazin-3-yl)sulfamoyl) phenyl)-2-oxo-2*H*-chromene-3-carboxamide (**5.11c**) that possessed an IC_{50} value of 36.64 μM , lower than **5.11b**, but has higher selectivity towards TNBC cells over low tumorigenic HEK293 cells (IC_{50} = >200 μM). Also, the 6-bromo derivatives with sulfapyridine (**5.12c**), and sulfanilamide (**5.9c**), as a substitution, reduced cell survival of MDA-MB-468 by 31% and 6%, respectively.

The sulfanilamide derivative with 6,8-dichloro coumarin (**5.9d**, IC_{50} = 27.10 μM) is more active than derivatives with 6-chloro or 6-bromo coumarins with higher selectivity towards MDA-MB-468 cells over HEK293 cells (IC_{50} = >200 μM). Replacing the sulfanilamide (**5.9d**) with sulfamethoxypyridazine (**5.11d**) reduced the activity with an IC_{50} value of 39.32 μM , while the sulfapyridine derivative with 6,8-dichloro coumarin (**5.12d**) afforded the most active compound (IC_{50} = 25.74 μM) with more than 3-fold selectivity towards TNBC cells over HEK293 cells (IC_{50} = 92.52 μM) (**Table 5.3**). Most synthesized compounds with a saturated ring in coumarin or with 6-methoxy were found to be inactive (IC_{50} >50 μM). The coumarin derivatives with a saturated ring 2-oxo-*N*-(4-(*N*-(pyridin-2-yl)

sulfamoyl) phenyl) -2*H*-chromene-3-carboxamide (**5.12e**) inhibited cell survival of MDA-MB-468 cells by 33%, but the 6-methoxy derivative showed 23% cell viability inhibition. Adding amide or ester linker between the coumarin acid and the sulfonamide derivatives increased the polarity of the compounds, but this change did not improve the cytotoxicity of these derivatives. The 6-chloro-2-oxo-*N*-(2-oxo-2-((4-sulfamoylphenyl)amino)ethyl)-2*H*-chromene-3-carboxamide (**5.21**) afforded 29% cell viability inhibition while 2-oxo-2-((4-sulfamoyl phenyl)amino) ethyl 7-(diethylamino)-2-oxo-2*H*-chromene -3-carboxylate (**5.22**) showed 27% cell viability inhibition.

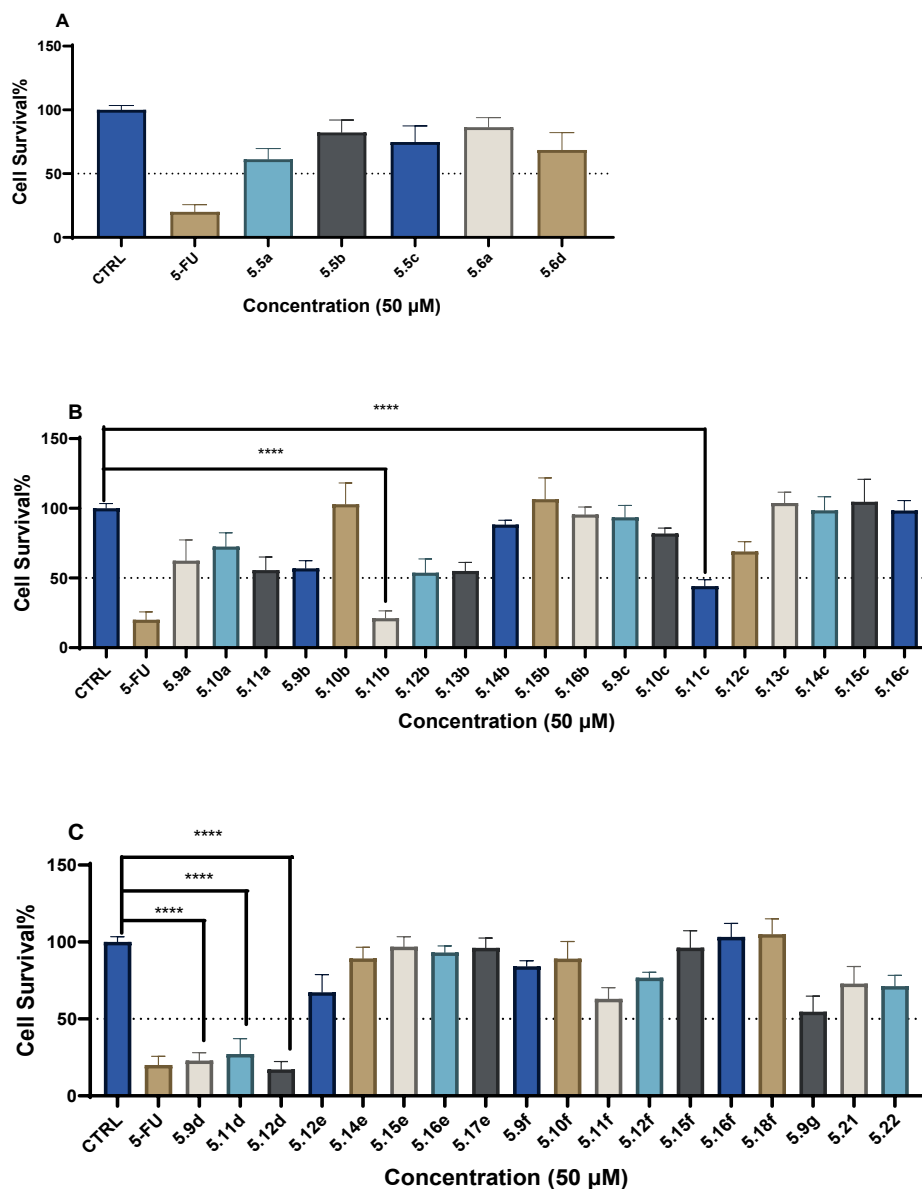
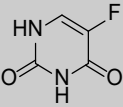
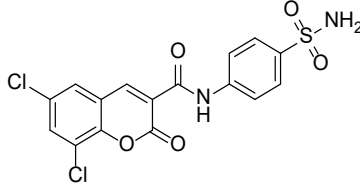
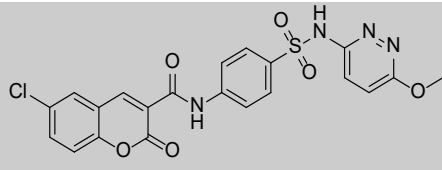
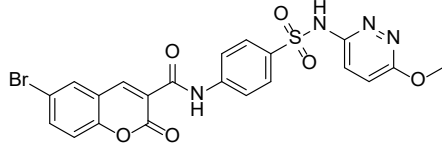
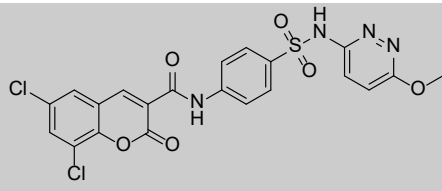
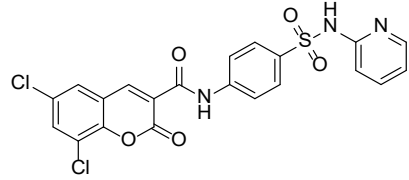


Figure 5.1. Cytotoxic effect of synthesized carbonic anhydrase inhibitors at 50 μ M for 72-hour treatment in triple negative breast cancer MDA-MB-468 cells. A) Cytotoxic effect of carbonic anhydrase inhibitors **5.5a-c**, **5.6a** and **5.6d**. **B) & C)** Cytotoxic effect of synthesized carbonic anhydrase inhibitors **5.9a-5.18f**, **5.21**, and **5.22**. Values represent the mean \pm SD of $n = 4$ experiments. Unpaired t test; **** $p < 0.0001$.

Compound	Structure	MDA-MB-468 IC ₅₀ (μM) ^a	HEK293 IC ₅₀ (μM) ^a
5-Fluorouracil		6.83 ±2.9	7.06 ±0.8
5.9d		27.10 ±3.7	>200
5.11b		26.48 ±2.2	106.71 ±6.1
5.11c		36.64 ±7.0	>200
5.11d		39.32 ±7.4	137.64 ±3.3
5.12d		25.74 ±4.3	92.52 ±9.0

^aValues are the mean ±SD of n = 3 experiments at 72-hour.

Table 5.5. Cytotoxicity of selective synthesized carbonic anhydrase inhibitors and the clinical chemotherapeutic 5-fluorouracil in TNBC MDA-MB-468 cells and low tumorigenic human endothelial kidney (HEK293) cells.

5.3. Conclusions

In summary, a library of novel carbonic anhydrase inhibitors have been synthesized that possess activity to reduce the cell viability of MDA-MB-468 triple-negative breast cancer cells with the IC_{50} between 25.74 μ M to 39.32 μ M. Five of the reported derivatives **5.9d**, **5.11b-d**, and **5.12d** showed higher selectivity to MDA-MB-468 cells over low tumorigenic HEK293 cells with better selectivity than the clinical agent 5-fluorouracil but low potency. Currently, the structure active relationship of the synthesized carbonic anhydrase inhibitors can be summarized according to the cytotoxicity on MDA-MB-468 cancer cell line as shown in **Figure 5.2**. We are working with our collaborator in Università degli Studi di Firenze, Florence, Italy to evaluate and confirm the carbonic anhydrase inhibition of the synthesized compounds. Due to the COVID-19 pandemic efforts to evaluate the CA inhibition activity and SAR of these compounds has been impacted. These compounds may be promising towards future studies as anticancer agent. Therefore, our lab will continue studying these compounds to complete the structure activity relationship as carbonic anhydrase inhibitors.

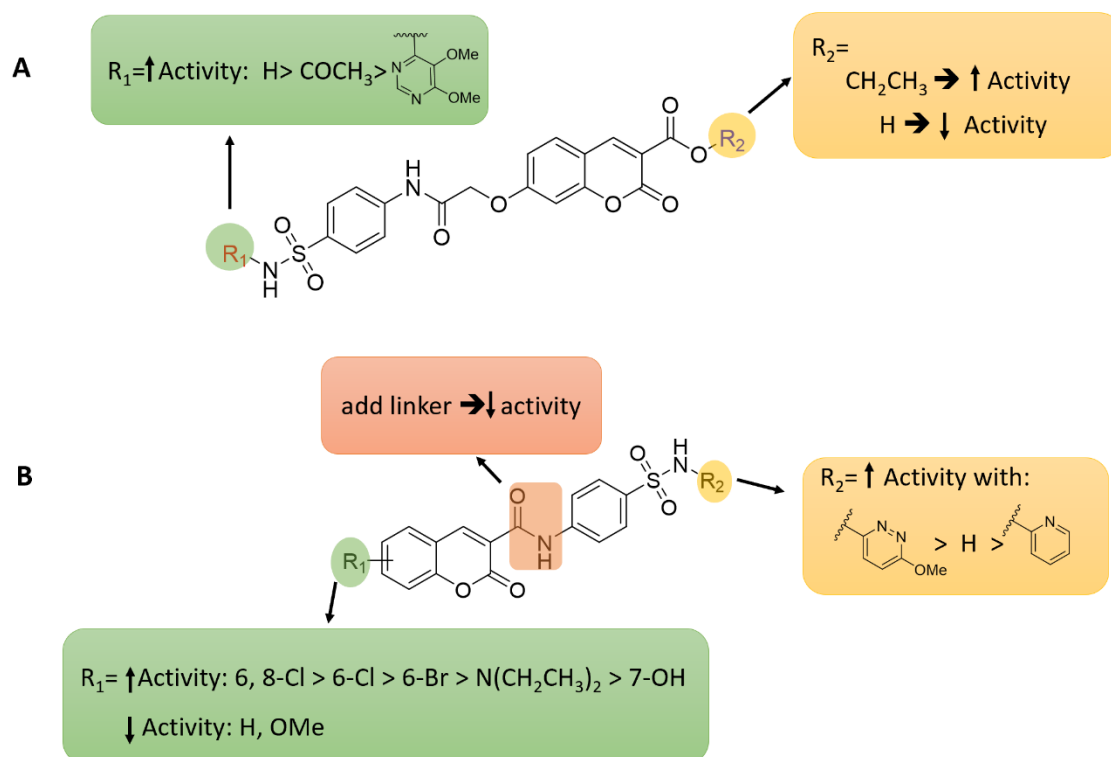


Figure 5.2. Structure activity relationship of the synthesized carbonic anhydrase inhibitors according to the cytotoxicity on MDA-MB-468 cancer cell line. A) SAR of synthesized carbonic anhydrase inhibitors as in scheme 5.1. **B)** SAR of synthesized carbonic anhydrase inhibitors as in schemes 5.2-5.4.

5.4. Experimental Section

5.4.1. Biology

5.4.1.1. Cell Culture and Reagents

Cells were maintained at 37 °C with 5% CO₂ in a humidified environment. Triple-negative breast cancer cells (MDA-MB-468) and human embryonic kidney cells (HEK293) were purchased from American Type Culture Collection (ATCC). The cells were cultured in Dulbecco's Modified Eagle Medium (DMEM) (Fisher Scientific, Catalog No. 50-188-267FP) for MDA-MB-468 cells and in Eagle's Minimum Essential Medium (ATCC®, Catalog No. 30-2003™) for HEK293 cells, supplemented with fetal bovine serum (ATCC®, Catalog No. 30-2020) to a final concentration of 10% and Penicillin-Streptomycin Solution (Corning™, Catalog No. MT30001CI) according to the supplier's recommended protocol. 5-Fluorouracil 99%, ACROS Organics™ (Catalog No. AC228440010) was purchased from Fisher Scientific. Stock solutions of all compounds were prepared in DMSO and were serially diluted for cell culture treatment maintaining the final DMSO concentration at less than 1%. CellTiter 96 aQueous one solution cell proliferation assay (3-(4,5-dimethylthiazol-2-yl)-5-(3-carboxymethoxyphenyl)-2-(4-sulfophenyl)- 2*H*-tetrazolium) (MTS) assay kit (Catalog No. G3580) was purchased from Promega.

5.4.1.2. Cytotoxicity Assays

To determine the cell growth inhibition ability of the synthesized compounds, MTS assay was used according to the manufacturer's recommended protocol. Stock solutions of the synthesized compounds were prepared in DMSO. Cells were seeded at a density of 1 x 10⁵ cells in 96-well plates. After 24 hours, cells were treated at the indicated concentrations of test compounds, limiting the final DMSO concentration to less than 1%.

After incubation at 37 °C in an environment of 5% CO₂ for 48-72 hours, 10 µL of MTS reagent (CellTiter 96® AQueous One Solution Reagent) was added to each well and incubated at the above-mentioned conditions for 2-4 h. Absorbance was recorded at 570 nm on a BioTek Synergy Mx multimode plate reader and the viability of cells was plotted as percentage of controls.

5.4.1.4. Statistical Analysis

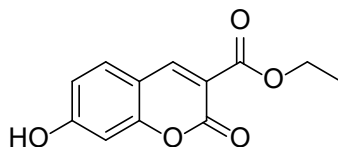
Experiments were repeated at least thrice, and the statistical significance was calculated using one-way ANOVA. A *p* value of <0.0001 was considered statistically significant. IC₅₀ values were calculated by GraphPad prism software.

5.4.2. Chemistry

General

All reactions were carried out in oven- or flame-dried glassware under positive nitrogen pressure unless otherwise noted. Reaction progress was monitored by thin-layer chromatography (TLC) carried out on silica gel plates (2.5 cm x 7.5 cm, 200 µm thick, 60 F254) and visualized by using UV (254 nm) or by potassium permanganate or phosphomolybdic acid stain as indicator. Flash column chromatography was performed with silica gel (40-63 µm, 60 Å) or on a Biotage® (Biotage® Selekt). Commercial grade solvents and reagents were purchased from Fisher Scientific (Houston, TX) or Sigma Aldrich (Milwaukee, WI) and were used without further purification except as indicated. Anhydrous solvents were purchased from Acros Organics and stored under an atmosphere of dry nitrogen over molecular sieves.

^1H and ^{13}C NMR spectra were recorded in the indicated deuterated solvent on a Bruker 400 MHz Advance III HD spectrometer at 400 and 100 MHz for ^1H and ^{13}C respectively with solvent peak as an internal standard. Multiplicities are indicated by s (single), d (doublet), dd (doublet of doublets), t (triplet), q (quartet), m (multiplet), and br (broad). Chemical shifts (δ) are reported in parts per million (ppm) and coupling constants (J) in Hertz. High-resolution mass spectroscopy (HRMS) was performed on a 6230 LC/TOF (Agilent) using an ESI source conducted. The spectral data was extracted from total ion chromatogram (TIC).



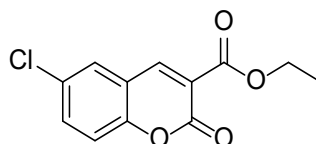
Ethyl 7-hydroxy-2-oxo-2H-chromene-3-carboxylate (5.2a).

To a mixture of 2,4-dihydroxybenzaldehyde (**5.1a**, 2 g, 14.48 mmol) in ethanol (5 mL) at room temperature, the diethyl malonate (5.81 g, 2.43 mL, 15.23 mmol) was added along with piperidine (0.29 mL, 2.9 mmol). The mixture was stirred and heated to 60 °C for 2 h. Then, it was cooled to room temperature and filtered off washed with water and ethanol and air dried to yield a yellow solid (2.954 g, 87% yield):

^1H NMR (400 MHz, DMSO- d_6): δ = 1.30 (3H, t, J =7.1 Hz), 4.27 (q, 2H), 6.73 (s, 1H), 6.86 (1H, d, J =8.5 Hz), 7.77 (1H, d, J =8.5 Hz), 8.67 (s, 1H), 11.06 ppm (s, 1H).

^{13}C NMR (100 MHz, DMSO- d_6): δ = 14.60, 61.27, 102.25, 110.89, 112.57, 114.45, 132.56, 149.87, 156.84, 157.56, 163.40, 164.50 ppm.

HRMS (ESI): m/z calcd for $\text{C}_{12}\text{H}_{10}\text{O}_5$ [$M+\text{Na}$] $^+$: 257.1939, found: 257.1907.



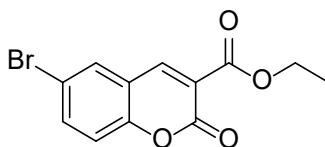
Ethyl 6-chloro-2-oxo-2H-chromene-3-carboxylate (5.2b).

The white compound was obtained from 5-chlorosalicylaldehyde (**5.1b**, 2 g, 12.77 mmol) by following the experimental conditions described for **5.2a** (2.97 g, 92% yield):

¹H NMR (400 MHz, DMSO-*d*₆): δ = 1.31 (3H, t, *J*=7.1 Hz), 4.30 (q, 2H), 7.50 (1H, d, *J*=8.8 Hz), 7.76 (1H, dd, *J*=8.9, 2.5 Hz), 8.06 (1H, d, *J*=3.5 Hz), 8.72 ppm (s, 1H).

¹³C NMR (100 MHz, DMSO-*d*₆): δ = 14.50, 61.86, 118.64, 119.27, 119.62, 128.92, 129.53, 134.29, 147.82, 153.61, 155.99, 164.80 ppm.

HRMS (ESI): *m/z* calcd for C₁₂H₉ClO₄ [*M*+Na]⁺: 275.6391, found: 275.6358.



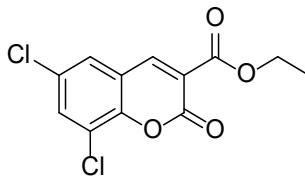
Ethyl 6-bromo-2-oxo-2H-chromene-3-carboxylate (5.2c).

The white compound was obtained from 5-bromosalicylaldehyde (**5.1c**, 2 g, 9.95 mmol) by following the experimental conditions described for **5.2a** (2.38 g, 81% yield):

¹H NMR (400 MHz, DMSO-*d*₆): δ = 1.32 (3H, t, *J*=7.1 Hz), 4.30 (q, 2H), 7.42 (1H, d, *J*=8.8 Hz), 7.86 (1H, dd, *J*=8.8, 2.5 Hz), 8.17 (1H, d, *J*=2.5 Hz), 8.70 ppm (s, 1H).

¹³C NMR (100 MHz, DMSO-*d*₆): δ = 14.52, 60.99, 118.61, 119.81, 120.01, 128.86, 129.43, 134.07, 147.45, 153.56, 156.55, 164.18 ppm.

HRMS (ESI): *m/z* calcd for C₁₂H₉BrO₄ [*M*+Na]⁺: 320.0902, found: 320.0872.



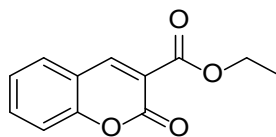
Ethyl 6,8-dichloro-2-oxo-2H-chromene-3-carboxylate (5.2d).

The white compound was obtained from 5,3-dichlorosalicylaldehyde (**5.1d**, 2 g, 10.47 mmol) by following the experimental conditions described for **5.2a** (2.12 g, 70% yield):

¹H NMR (400 MHz, DMSO-*d*₆): δ = 1.32 (3H, t, *J*=8.7 Hz), 4.20 (q, 2H), 8.04 (1H, d, *J*=2.9 Hz), 8.07 (1H, d, *J*=2.9 Hz), 8.66 ppm (s, 1H).

¹³C NMR (100 MHz, DMSO-*d*₆): δ = 116.75, 118.44, 120.02, 129.09, 129.66, 133.93, 148.56, 153.48, 156.88, 164.04 ppm.

HRMS (ESI): *m/z* calcd for C₁₂H₉Cl₂O₄ [*M*+Na]⁺: 311.0923, found: 311.0902.



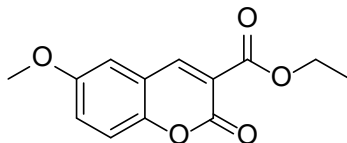
Ethyl 2-oxo-2H-chromene-3-carboxylate (5.2e).

The white compound was obtained from salicylaldehyde (**5.1e**, 2 g, 16.38 mmol) by following the experimental conditions described for **5.2a** (3.07 g, 86% yield):

¹H NMR (400 MHz, DMSO-*d*₆): δ = 1.31 (3H, t, *J*=8.7 Hz), 4.29 (q, 2H), 7.40 (m, 2H), 7.73 (1H, t, *J*=8.3 Hz), 7.90 (1H, d, *J*=7.7 Hz), 8.74 ppm (s, 1H).

¹³C NMR (100 MHz, DMSO-*d*₆): δ = 14.52, 61.69, 116.60, 118.26, 125.29, 130.72, 134.92, 149.09, 154.98, 156.42, 163.04 ppm

HRMS (ESI): *m/z* calcd for C₁₂H₁₀O₄ [*M*+Na]⁺: 241.1946, found: 241.1933.



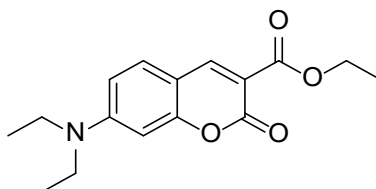
Ethyl 6-methoxy-2-oxo-2H-chromene-3-carboxylate (5.2f).

The yellow compound was obtained from 5-methoxysalicylaldehyde (**5.1f**, 2 g, 13.15 mmol) by following the experimental conditions described for **5.2a** (2.89 g, 89% yield):

¹H NMR (400 MHz, DMSO-*d*₆): δ = 1.31 (3H, t, *J* = 7.1 Hz), 3.81 (s, 3H), 4.3 (q, 2H), 7.32 (1H, dd, *J* = 9, 2.7 Hz), 7.35 (1H, d, *J* = 9 Hz), 7.46 (1H, d, *J* = 2.7 Hz), 8.67 ppm (s, 1H).

¹³C NMR (100 MHz, DMSO-*d*₆): δ = 14.51, 56.23, 61.67, 112.29, 117.70, 118.28, 118.61, 122.72, 148.89, 149.45, 156.14, 156.55, 163.05 ppm.

HRMS (ESI): *m/z* calcd for C₁₃H₁₂O₅ [*M*+Na]⁺: 271.2204, found: 271.2201.



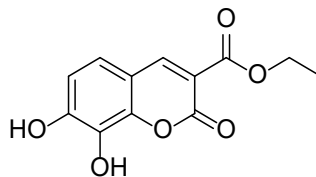
Ethyl 7-(diethylamino)-2-oxo-2H-chromene-3-carboxylate (5.2g).

The brown compound was obtained from 4-(diethylamino)salicylaldehyde (**5.1g**, 2 g, 10.35 mmol) by following the experimental conditions described for **5.2a** (2.13 g, 71% yield):

¹H NMR (400 MHz, DMSO-*d*₆): δ = 1.13 (6H, t, *J* = 7.1 Hz), 1.26 (3H, t, *J* = 7.1 Hz), 3.48 (q, 4H), 4.23 (q, 2H), 6.52 (1H, d, *J* = 2.3 Hz), 6.75 (1H, dd, *J* = 9, 2.3 Hz), 7.60 (1H, d, *J* = 9 Hz), 8.53 ppm (s, 1H).

¹³C NMR (100 MHz, DMSO-*d*₆): δ = 12.78, 14.68, 44.80, 60.76, 96.26, 107.43, 107.86, 110.20, 132.17, 149.62, 153.24, 157.44, 158.48, 163.01 ppm.

HRMS (ESI): m/z calcd for $C_{16}H_{19}NO_4$ $[M+Na]^+$: 312.3155, found: 312.3150.



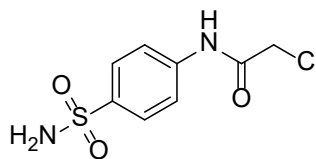
Ethyl 7,8-dihydroxy-2-oxo-2H-chromene-3-carboxylate (5.2h).

The brown compound was obtained from 2,3,4-trihydroxybenzaldehyde (**5.1h**, 2 g, 12.98 mmol) by following the experimental conditions described for **5.2a** (2.88 g, 89% yield):

1H NMR (400 MHz, DMSO- d_6): δ = 1.29 (3H, t, J =7.1 Hz), 4.27 (q, 2H), 6.87 (1H, d, J =8.6 Hz), 7.28 (1H, d, J =8.5 Hz), 8.62 (s, 1H), 9.55 (s, 1H), 10.63 ppm (s, 1H).

^{13}C NMR (100 MHz, DMSO- d_6): δ = 14.61, 61.26, 102.25, 110.89, 112.57, 114.41, 132.79, 149.89, 155.14, 157.53, 163.32, 164.34 ppm.

HRMS (ESI): m/z calcd for $C_{12}H_{10}O_6$ $[M+Na]^+$: 273.1931, found: 273.1930.



2-Chloro-N-(4-sulfamoylphenyl)acetamide (5.4a).

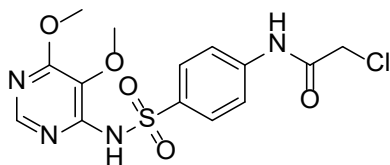
Potassium carbonate (K_2CO_3) (1.2 g, 8.72 mmol) was added to a solution of sulfanilamide (**5.3a**, 1 g, 5.81 mmol) in THF (20 mL). Chloroacetyl chloride (0.56 mL, 6.97 mmol) was added to the above solution dropwise and under N_2 atmosphere at 0 °C with stirring. After that, the reaction mixture was stirred for 2 h and then the water was added to quench the reaction. The reaction mixture was extracted with ethyl acetate, the organic layer washed

with brine and dried over sodium sulfate, the solvent was removed in vacuo and purified by recrystallization in hexane:MeOH to yield a white solid (1.349 g, 93% yield):

¹H NMR (400 MHz, DMSO-*d*₆): δ= 4.30 (s, 2H), 7.27 (s, 2H), 7.78 (q, 4H), 10.61 ppm (s, 1H).

¹³C NMR (100 MHz, DMSO-*d*₆): δ= 44.01, 119.44, 127.26, 139.40, 141.79, 165.63 ppm.

HRMS (ESI): *m/z* calcd for C₈H₉ClN₂O₃S [*M*+Na]⁺: 271.6736, found: 271.6683.



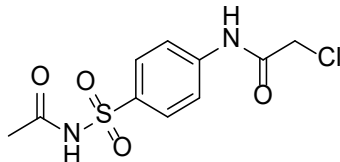
2-Chloro-*N*-(4-(*N*-(5,6-dimethoxypyrimidin-4-yl)sulfamoyl)phenyl)acetamide (5.4b).

The white compound was obtained from sulfadoxine (**5.3b**, 1 g, 3.22 mmol) by following the experimental conditions described for **5.4a** (0.983 g, 79% yield):

¹H NMR (400 MHz, DMSO-*d*₆): δ= 3.70 (s, 3H), 3.90 (s, 3H), 4.29 (s, 2H), 7.78 (2H, d, *J*=8.7 Hz), 7.96 (2H, d, *J*=8.7 Hz), 8.11 (s, 1H), 10.67 (s, 1H), 11.04 ppm (br, 1H).

¹³C NMR (100 MHz, DMSO-*d*₆): δ= 43.99, 54.50, 60.69, 119.22, 127.70, 129.31, 135.55, 142.80, 150.78, 162.06, 165.76 ppm.

HRMS (ESI): *m/z* calcd for C₁₄H₁₅ClN₄O₅S [*M*+Na]⁺: 409.7968, found: 409.7937.



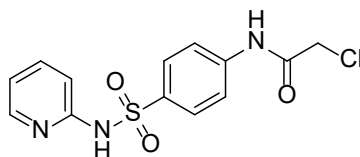
***N*-(4-(*N*-Acetylsulfamoyl)phenyl)-2-chloroacetamide (5.4c).**

The white compound was obtained from sulfacetamide (**5.3c**, 1 g, 4.67 mmol) by following the experimental conditions described for **5.4a** (1.076 g, 80% yield):

¹H NMR (400 MHz, DMSO-*d*₆): δ = 3.32 (s, 3H), 4.31 (s, 2H), 7.78 (2H, d, *J*=8.7 Hz), 7.89 (2H, d, *J*=8.7 Hz), 10.72 (s, 1H), 11.99 ppm (s, 1H).

¹³C NMR (100 MHz, DMSO-*d*₆): δ = 23.65, 44.00, 119.38, 129.43, 134.08, 143.41, 165.84, 169.14 ppm.

HRMS (ESI): *m/z* calcd for C₁₀H₁₁ClN₂O₄S [*M*+Na]⁺: 313.7102, found: 313.7082.



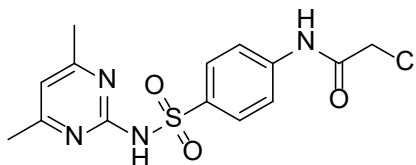
2-Chloro-*N*-(4-(*N*-(pyridin-2-yl)sulfamoyl)phenyl) acetamide (5.4d**).**

The white compound was obtained from sulfapyridine (**5.3d**, 1 g, 4.01 mmol) by following the experimental conditions described for **5.4a** (0.992 g, 76% yield):

¹H NMR (400 MHz, DMSO-*d*₆): δ = 4.27 (s, 2H), 6.86 (1H, t, *J*=7.5 Hz), 7.14 (1H, d, *J*=8.8 Hz), 7.72 (2H, d, *J*=8.7 Hz), 7.83 (2H, d, *J*=8.7 Hz), 8.00 (2H, d, *J*=8.6 Hz), 10.62 (s, 1H), 11.03 ppm (br, 1H).

¹³C NMR (100 MHz, DMSO-*d*₆): δ = 44.39, 119.34, 126.23, 126.77, 130.79, 132.64, 140.22, 144.23, 148.45, 150.56, 165.85 ppm.

HRMS (ESI): *m/z* calcd for C₁₃H₁₂ClN₃O₃S [*M*+Na]⁺: 348.7574, found: 348.7552.



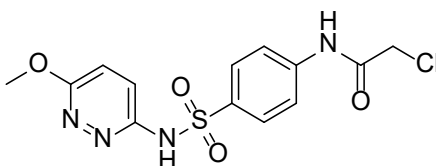
2-Chloro-*N*-(4-(*N*-(4,6-dimethylpyrimidin-2-yl)sulfamoyl)phenyl)acetamide (5.4e).

The white compound was obtained from sulfamethazine (**5.3e**, 1 g, 3.6 mmol) by following the experimental conditions described for **5.4a** (1.11 g, 87% yield):

¹H NMR (400 MHz, DMSO-*d*₆): δ = 2.24 (s, 6H), 4.28 (s, 2H), 6.74 (s, 1H), 7.74 (2H, d, J =8.7 Hz), 7.97 (2H, d, J =8.7 Hz), 10.62 (s, 1H), 11.66 ppm (br, 1H).

¹³C NMR (100 MHz, DMSO-*d*₆): δ = 23.28, 44.00, 113.89, 118.83, 129.82, 135.71, 142.48, 156.62, 165.68, 167.81 ppm.

HRMS (ESI): m/z calcd for C₁₄H₁₅ClN₄O₃S [M +Na]⁺: 377.7982, found: 377.7981.



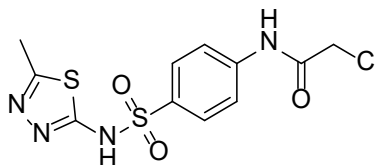
2-Chloro-*N*-(4-(*N*-(6-methoxypyridazin-3-yl)sulfamoyl)phenyl)acetamide (5.4f).

The white compound was obtained from sulfamethoxypyridazine (**5.3f**, 1 g, 3.57 mmol) by following the experimental conditions described for **5.4a** (1.01 g, 79% yield):

¹H NMR (400 MHz, DMSO-*d*₆): δ = 3.84 (s, 3H), 4.28 (s, 2H), 7.37 (s, 1H), 7.73 (2H, d, J =8.6 Hz), 7.82 (2H, d, J =8.6 Hz), 10.60 (s, 1H), 13.68 ppm (br, 1H).

¹³C NMR (100 MHz, DMSO-*d*₆): δ = 43.99, 54.95, 119.29, 119.42, 127.84, 137.85, 142.02, 153.36, 158.70, 165.63 ppm.

HRMS (ESI): m/z calcd for C₁₃H₁₃ClN₄O₄S [M +Na]⁺: 379.7712, found: 379.7709.



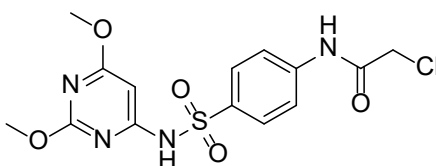
2-Chloro-N-(4-(N-(5-methyl-1,3,4-thiadiazol-2-yl)sulfamoyl)phenyl)acetamide (5.4g).

The white compound was obtained from sulfamethizole (**5.3g**, 1 g, 3.7 mmol) by following the experimental conditions described for **5.4a** (0.988 g, 77% yield):

¹H NMR (400 MHz, DMSO-*d*₆): δ= 2.42 (s, 3H), 4.26 (s, 2H), 7.76 (s, 4H), 10.64 (s, 1H), 13.92 ppm (s, 1H).

¹³C NMR (100 MHz, DMSO-*d*₆): δ= 16.52, 44.00, 119.56, 127.47, 137.00, 142.37, 154.92, 165.66, 168.29ppm.

HRMS (ESI): *m/z* calcd for C₁₁H₁₁ClN₄O₂S₂ [*M*+Na]⁺: 353.7991, found: 353.7914.



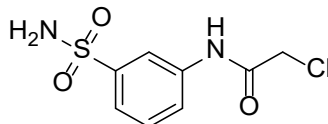
2-Chloro-N-(4-(N-(2,6-dimethoxypyrimidin-4-yl)sulfamoyl)phenyl)acetamide (5.4h).

The white compound was obtained from sulfadimethoxine (**5.3h**, 1 g, 3.22 mmol) by following the experimental conditions described for **5.4a** (0.895 g, 71% yield):

¹H NMR (400 MHz, DMSO-*d*₆): δ= 3.75 (s, 3H), 3.79 (s, 3H), 4.29 (s, 2H), 5.96 (s, 1H), 7.81 (1H, d, *J*=8.8 Hz), 7.92 (2H, d, *J*=8.8 Hz), 10.70 (s, 1H), 11.52 ppm (br, 1H).

¹³C NMR (100 MHz, DMSO-*d*₆): δ= 43.98, 54.21, 54.95, 85.06, 119.51, 129.03, 134.74, 143.11, 160.31, 165.79, 172.12 ppm.

HRMS (ESI): *m/z* calcd for C₁₄H₁₅ClN₄O₅S [*M*+Na]⁺: 409.7968, found: 409.7917.



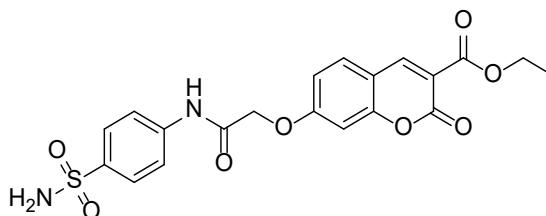
2-Chloro-*N*-(3-sulfamoylphenyl)acetamide (5.4i).

The white compound was obtained from 3-aminobenzenesulfonamide (**5.3i**, 1 g, 5.81 mmol) by following the experimental conditions described for **5.4a** (1.12 g, 78% yield):

¹H NMR (400 MHz, DMSO-*d*₆): δ= 4.29 (s, 2H), 7.38 (s, 2H), 7.56 (m, 2H), 7.73 (m, 1H), 8.61 ppm (s, 1H).

¹³C NMR (100 MHz, DMSO-*d*₆): δ= 43.96, 116.85, 121.39, 122.72, 130.08, 139.29, 145.17, 165.53 ppm.

HRMS (ESI): *m/z* calcd for C₈H₉ClN₂O₃S [*M*+Na]⁺: 271.6736, found: 271.6713.



Ethyl 2-oxo-7-(2-oxo-2-((4-sulfamoylphenyl)amino)ethoxy)-2*H*-chromene-3-carboxylate (5.5a).

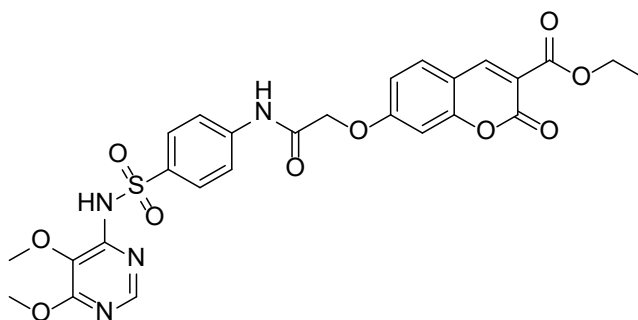
To a solution of ethyl 7-hydroxy-2-oxo-2*H*-chromene-3-carboxylate (**5.2a** 0.2 g, 0.85 mmol) in dry *N,N*-dimethylformamide (15 mL), anhydrous K₂CO₃ (0.18 g, 1.28 mmol) was added. The solution was stirred for 15 mins at 70-80 °C and 2-chloro-*N*-(4-sulfamoylphenyl) acetamide (**5.4a**, 0.23 g, 0.94 mmol) was added, followed by a pinch of potassium iodide (KI) and heated overnight. After that, the water (10 mL) was added to the reaction mixture, followed by 1 mL 6N HCl. The resulting solid was filtered, washed

with water, and air dried and purification by flash column chromatography (hexane/EtOAc 20:1) afforded the title compound as a brown powder (0.21 g, 55% yield):

¹H NMR (400 MHz, DMSO-*d*₆): δ= 1.30 (3H, t, *J*=7.1 Hz), 3.70 (s, 3H), 4.90 (s, 3H), 4.29 (q, 2H), 4.95 (s, 2H), 7.09 (m, 2H), 7.27 (s, 2H), 7.79 (s, 4H), 7.87 (1H, d, *J*=8.5 Hz), 8.73 (s, 1H), 10.52 ppm (s, 1H).

¹³C NMR (100 MHz, DMSO-*d*₆): δ= 14.58, 61.44, 67.73, 101.61, 112.41, 113.99, 114.25, 119.67, 127.18, 132.16, 139.35, 141.65, 149.50, 156.64, 157.13, 163.23, 163.64, 166.65 ppm.

HRMS (ESI): *m/z* calcd for C₂₀H₁₈N₂O₈S [*M*+Na]⁺: 469.4179, found: 469.4098.



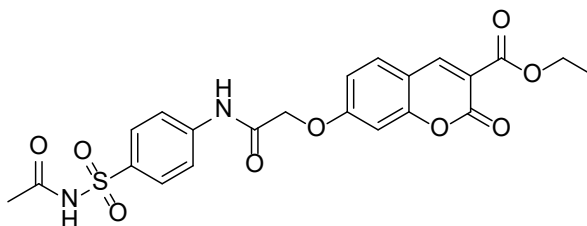
Ethyl 7-(2-((4-(*N*-(5,6-dimethoxypyrimidin-4-yl) sulfamoyl)phenyl) amino)-2-oxoethoxy)-2-oxo-2*H*-chromene-3-carboxylate (5.5b).

The yellow compound was obtained from 2-chloro-*N*-(4-(*N*-(5,6-dimethoxypyrimidin-4-yl)sulfamoyl)phenyl)acetamide (**5.4b**) by following the experimental conditions described for **5.5a** (0.197 g, 61% yield):

¹H NMR (400 MHz, DMSO-*d*₆): δ= 1.31 (3H, t, *J*=7.0 Hz), 4.27 (q, 2H), 4.95 (s, 2H), 7.07 (m, 2H), 7.81 (2H, d, *J*=8.8 Hz), 7.87 (1H, d, *J*=8.5 Hz), 7.95 (2H, d, *J*=8.8 Hz), 8.11 (s, 1H), 8.73 (s, 1H), 10.56 (s, 1H), 11.04 ppm (br, 1H).

^{13}C NMR (100 MHz, DMSO- d_6): δ = 14.58, 54.50, 60.71, 61.44, 67.70, 101.67, 112.42, 113.96, 114.26, 119.43, 127.69, 129.30, 132.16, 135.45, 149.50, 150.80, 151.07, 157.13, 162.07, 163.24, 163.62, 166.79 ppm.

HRMS (ESI): m/z calcd for $\text{C}_{26}\text{H}_{24}\text{N}_4\text{O}_{10}\text{S}$ [$M+\text{Na}$] $^+$: 607.5418, found: 607.5406.



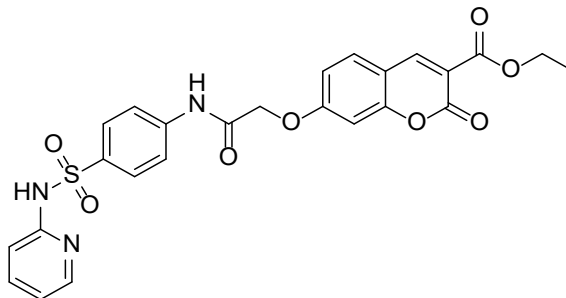
Ethyl 7-(2-((4-(*N*-acetylsulfamoyl)phenyl)amino)-2-oxoethoxy)-2-oxo-2*H*-chromene-3-carboxylate (5.5c).

The yellow compound was obtained from *N*-(4-(*N*-acetylsulfamoyl) phenyl)-2-chloroacetamide (**5.4c**) by following the experimental conditions described for **5.5a** (0.22 g, 58% yield):

^1H NMR (400 MHz, DMSO- d_6): δ = 1.31 (3H, t, J =7.0 Hz), 1.91 (s, 1H), 4.29 (q, 2H), 4.96 (s, 2H), 7.08 (2H, d, J =9.9 Hz), 7.87 (m, 5H), 8.73 (s, 1H), 10.63 (s, 1H), 11.98 ppm (s, 1H).

^{13}C NMR (100 MHz, DMSO- d_6): δ = 14.58, 23.65, 61.44, 67.69, 101.68, 112.43, 113.95, 114.27, 119.58, 119.65, 129.38, 132.16, 133.99, 149.50, 156.63, 157.13, 163.24, 163.62, 166.88, 169.13 ppm.

HRMS (ESI): m/z calcd for $\text{C}_{22}\text{H}_{20}\text{N}_2\text{O}_9\text{S}$ [$M+\text{Na}$] $^+$: 511.4545, found: 511.4518.

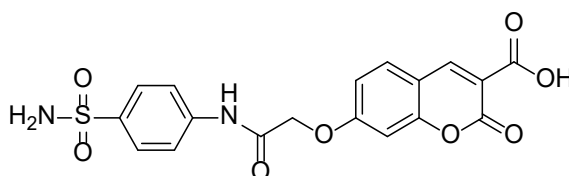


Ethyl 2-oxo-7-(2-oxo-2-((4-(*N*-(pyridin-2-yl) sulfamoyl) phenyl)amino) ethoxy)-2*H* chromene-3-carboxylate (5.5d).

The yellow compound was obtained from 2-chloro-*N*-(4-(*N*-(pyridin-2 yl)sulfamoyl)phenyl) acetamide (**5.4d**) by following the experimental conditions described for **5.5a** (0.87 g, 49% yield):

¹H NMR (400 MHz, DMSO-*d*₆): δ = 1.30 (3H, t, *J*=6.7 Hz), 4.23 (q, 2H), 4.80 (s, 2H), 6.75 (1H, t, *J*= 6.5 Hz), 7.19 (2H, d, *J*= 8.7 Hz), 7.51 (2H, d, *J*=8.7 Hz), 7.70 (m, 5H), 8.02 (2H, d, *J*=6.5 Hz), 8.49 (br, 1H), 10.28 ppm (s, 1H).

HRMS (ESI): *m/z* calcd for C₂₅H₂₁N₃O₈S [*M*+Na]⁺: 546.5023, found: 546.5003.



2-Oxo-7-(2-oxo-2-((4-sulfamoylphenyl) amino) ethoxy) -2*H*-chromene-3-carboxylic acid (5.6a).

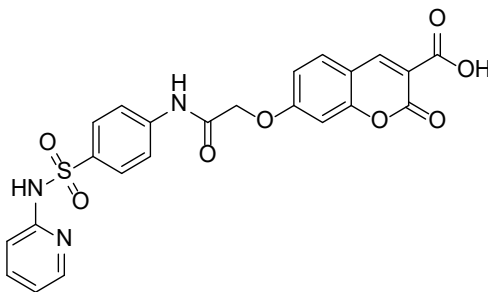
To a solution of ethyl 2-oxo-7-(2-oxo-2-((4-sulfamoylphenyl)amino)ethoxy) -2*H*-chromene-3-carboxylate (**5.5a**, 0.1 g, 0.22 mmol) in methanol (5 mL) and water (2 mL) was added NaOH (0.02 g, 0.44 mmol). The solution was heated to reflux for 16 h, then cooled and concentrated in vacuo. The crude product was diluted with water (10 mL) and acidified

with an aqueous solution of 6N HCl. The resulting solid was filtered, washed with water, and air-dried to provide to the product as a white solid. (0.08 g, 86% yield).

¹H NMR (400 MHz, DMSO-*d*₆): δ= 4.92 (s, 3H), 4.31 (q, 2H), 4.97 (s, 2H), 7.09 (m, 2H), 7.27 (s, 2H), 7.77 (s, 4H), 7.84 (1H, d, *J*=8.5 Hz), 8.71 (s, 1H), 10.52 (s, 1H), 11.64 ppm (br, 1H).

¹³C NMR (100 MHz, DMSO-*d*₆): δ= 67.72, 101.61, 112.43, 114.08, 114.56, 119.67, 127.11, 132.16, 139.43, 141.65, 149.53, 156.61, 157.27, 163.23, 163.64, 166.64 ppm.

HRMS (ESI): *m/z* calcd for C₁₈H₁₄N₂O₈S [*M*+Na]⁺: 441.3651, found: 441.3490.



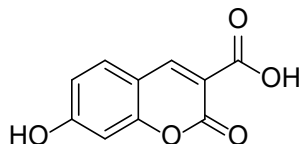
2-Oxo-7-(2-oxo-2-((4-(*N*- (pyridin-2-yl) sulfamoyl) phenyl) amino)ethoxy)-2*H*-chromene-3-carboxylic acid (5.6d).

The white compound was obtained from ethyl 2-oxo-7-(2-oxo-2-((4-(*N*-(pyridin-2-yl) sulfamoyl)phenyl) amino)ethoxy)-2*H* chromene-3-carboxylate (**5.5d**, 0.1 g, 0.19 mmol) by following the experimental conditions described for **5.6a** (0.084 g, 87% yield):

¹H NMR (400 MHz, DMSO-*d*₆): δ= 4.80 (s, 2H), 6.75 (1H, t, *J*= 6.5 Hz), 7.19 (2H, d, *J*=8.7 Hz), 7.51 (2H, d, *J*=8.7 Hz), 7.70 (m, 5H), 8.02 (2H, d, *J*=6.5 Hz), 8.49 (br, 1H), 10.28 ppm (s, 1H).

¹³C NMR (100 MHz, DMSO-*d*₆): δ= 57.24, 110.59, 117.12, 118.33, 118.45, 1126.29 132.79, 139.30, 114.88, 141.85, 142.28, 142.58, 153.90, 159.40, 165.29 ppm.

HRMS (ESI): m/z calcd for $C_{23}H_{17}N_3O_8S$ $[M+Na]^+$: 518.4490, found: 518.4149.



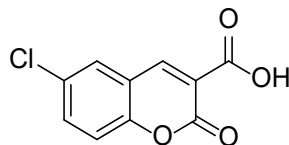
7-Hydroxy-2-oxo-2H-chromene-3-carboxylic acid (5.7a).

To a solution of ethyl 7-hydroxy-2-oxo-2H-chromene-3-carboxylate (**5.2a**, 2 g, 8.54 mmol) in MeOH (15 mL) and water (12 mL) was added 2N NaOH solution (40 mL). The solution was heated to reflux for 12 h, then cooled and concentrated in vacuo. The crude product was diluted with water (10 mL) and acidified with an aqueous solution of 6N HCl. The resulting solid was filtered, washed with water, and air-dried to provide the product as a yellow solid. (1.71 g, 97% yield):

1H NMR (400 MHz, DMSO- d_6): δ = 6.73 (s, 1H), 6.85 (1H, dd, J =8.6,2.1 Hz), 7.72 (1H, d, J =8.6 Hz), 8.66 (s, 1H), 11.10 (br, 1H), 12.93 ppm (br, 1H).

^{13}C NMR (100 MHz, DMSO- d_6): δ = 103.16, 111.03, 113.01, 114.53, 132.48, 149.75, 157.40, 158.32, 164.14, 164.57 ppm.

HRMS (ESI): m/z calcd for $C_{10}H_6O_5$ $[M+Na]^+$: 229.1406, found: 229.1401.



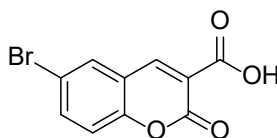
6-Chloro-2-oxo-2H-chromene-3-carboxylic acid (5.7b).

The white compound was obtained from ethyl 6-chloro-2-oxo-2*H*-chromene-3-carboxylate (**5.2b**, 2 g, 7.92 mmol) by following the experimental conditions described for **5.7a** (1.725 g, 97% yield):

¹H NMR (400 MHz, DMSO-*d*₆): δ= 7.49 (1H, d, *J*=8.8 Hz), 7.75 (1H, dd, *J*=8.8, 2.5 Hz), 8.04 (1H, d, *J*=2.5 Hz), 8.69 (s, 1H), 13.38 ppm (br, 1H).

¹³C NMR (100 MHz, DMSO-*d*₆): δ= 118.63, 119.82, 120.03, 128.88, 129.44, 134.07, 147.44, 153.57, 156.56, 164.18 ppm.

HRMS (ESI): *m/z* calcd for C₁₀H₅ClO₄ [*M*+Na]⁺: 247.5861, found: 247.5859.



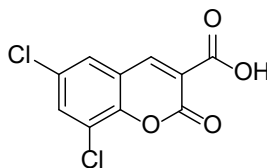
6-Bromo-2-oxo-2*H*-chromene-3-carboxylic acid (5.7c**).**

The white compound was obtained from ethyl 6-bromo-2-oxo-2*H*-chromene-3-carboxylate (**5.2c**, 2 g, 6.73 mmol) by following the experimental conditions described for **5.7a** (1.8 g, 99% yield):

¹H NMR (400 MHz, DMSO-*d*₆): δ= 7.42 (1H, d, *J*=8.8 Hz), 7.86 (1H, dd, *J*=8.8, 2.5 Hz), 8.17 (1H, d, *J*=2.5 Hz), 8.69 (s, 1H), 13.37 ppm (br, 1H).

¹³C NMR (100 MHz, DMSO-*d*₆): δ= 118.69, 119.84, 120.18, 128.92, 129.39, 134.09, 148.01, 153.12, 156.38, 164.66 ppm.

HRMS (ESI): *m/z* calcd for C₁₀H₅BrO₄ [*M*+Na]⁺: 292.037, found: 292.036.



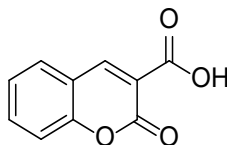
6,8-Dichloro-2-oxo-2H-chromene-3-carboxylic acid (5.7d).

The white compound was obtained from ethyl 6,8-dichloro-2-oxo-2H-chromene-3-carboxylate (**5.2d**, 2 g, 6.97 mmol) by following the experimental conditions described for **5.7a** (1.65 g, 91% yield):

¹H NMR (400 MHz, DMSO-*d*₆): δ= 8.04 (1H, d, *J*=2.5 Hz), 8.06 (1H, d, *J*= 2.5 Hz), 8.71 (s, 1H), 13.51 ppm (br, 1H).

¹³C NMR (100 MHz, DMSO-*d*₆): δ= 116.75, 118.44, 120.02, 129.09, 129.66, 133.93, 148.56, 153.48, 156.88, 164.04 ppm.

HRMS (ESI): *m/z* calcd for C₁₀H₄Cl₂O₄ [*M*+Na]⁺: 282.0308, found: 282.0301.



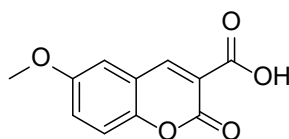
2-Oxo-2H-chromene-3-carboxylic acid (5.7e).

The white compound was obtained from ethyl 2-oxo-2H-chromene-3-carboxylate (**5.2e**, 2 g, 9.17 mmol) by following the experimental conditions described for **5.7a** (1.7 g, 98% yield):

¹H NMR (400 MHz, DMSO-*d*₆): δ= 7.42 (m, 2H), 7.73 (1H, t, *J*=7.6 Hz), 7.91 (1H, d, *J*=7.6 Hz), 8.74 (s, 1H), 13.24 ppm (br, 1H).

^{13}C NMR (100 MHz, DMSO- d_6): δ = 116.54, 118.40, 118.75, 125.32, 130.61, 134.69, 148.79, 154.89, 157.14, 164.39 ppm.

HRMS (ESI): m/z calcd for $\text{C}_{10}\text{H}_6\text{O}_4$ [$M+\text{Na}$] $^+$: 213.1414, found: 213.1410.



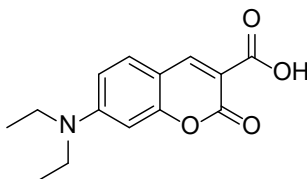
6-Methoxy-2-oxo-2H-chromene-3-carboxylic acid (5.7f):

The yellow compound was obtained from ethyl 6-methoxy-2-oxo-2H-chromene-3-carboxylate (**5.2f**, 2 g, 8.06 mmol) by following the experimental conditions described for **5.7a** (1.71 g, 96% yield):

^1H NMR (400 MHz, DMSO- d_6): δ = 3.80 (s, 3H), 4.74 (br, 1H), 7.31 (1H, dd, J =9, 3 Hz), 7.35 (1H, d, J =9 Hz), 7.44 (1H, d, J =3 Hz), 8.66 ppm (s, 1H).

^{13}C NMR (100 MHz, DMSO- d_6): δ = 56.28, 112.30, 117.71, 118.84, 118.99, 122.51, 148.57, 149.37, 156.18, 157.46, 164.46 ppm.

HRMS (ESI): m/z calcd for $\text{C}_{11}\text{H}_8\text{O}_5$ [$M+\text{Na}$] $^+$: 243.1673, found: 243.1673.



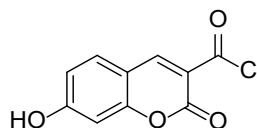
7-(Diethylamino)-2-oxo-2H-chromene-3-carboxylic acid (5.7g).

The brown compound was obtained from ethyl 7-(diethylamino)-2-oxo-2*H*-chromene-3-carboxylate (**5.2g**, 2 g, 6.91 mmol) by following the experimental conditions described for **5.7a** (1.531 g, 84% yield):

¹H NMR (400 MHz, DMSO-*d*₆): δ= 1.14 (6H, t, *J*=7.0 Hz), 3.47 (q, 4H), 6.56 (1H, d, *J*=2.0 Hz), 6.81 (1H, dd, *J*=9.0, 2.0 Hz), 7.63 (1H, d, *J*=9.0 Hz), 8.58 (s, 1H), 12.49 ppm (s, 1H).

¹³C NMR (100 MHz, DMSO-*d*₆): δ= 12.78, 44.85, 96.38, 107.60, 107.83, 110.51, 132.30, 149.90, 153.36, 158.35, 159.98, 164.94 ppm.

HRMS (ESI): *m/z* calcd for C₁₄H₁₅NO₄ [*M*+Na]⁺: 284.2621, found: 284.2619.



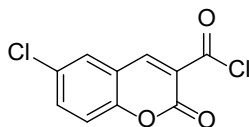
7-Hydroxy-2-oxo-2*H*-chromene-3-carbonyl chloride (**5.8a**).

A mixture of 7-hydroxy-2-oxo-2*H*-chromene-3-carboxylic acid (**5.7a**, 0.2 g 0.97 mmol) and thionyl chloride (5 mL) was heated at 80 °C for 9 h. The excess of thionyl chloride was then removed in vacuo. To the residue, the toluene (10 mL) was added twice and removed in vacuo to provide the product as a yellow solid which was used for the next step without further purification (0.19 g, 87% yield):

¹H NMR (400 MHz, DMSO-*d*₆): δ= 6.75 (s, 1H), 6.86 (1H, dd, *J*=8.6, 2.1 Hz), 7.76 (1H, d, *J*=8.6 Hz), 8.68 (s, 1H), 11.08 ppm (br, 1H).

¹³C NMR (100 MHz, DMSO-*d*₆): δ= 102.26, 111.05, 112.91, 114.49, 132.47, 149.86, 157.44, 158.02, 164.43, 164.66 ppm.

HRMS (ESI): *m/z* calcd for C₁₀H₅ClO₄ [*M*+Na]⁺: 247.5861, found: 247.5860.



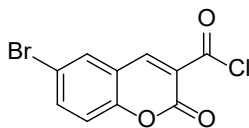
6-Chloro-2-oxo-2H-chromene-3-carbonyl chloride (5.8b).

The brown compound was obtained from 6-chloro-2-oxo-2H-chromene-3-carboxylic acid (**5.7b**, 0.2 g, 0.89 mmol) by following the experimental conditions described for **5.8a** (0.149 g, 84% yield):

¹H NMR (400 MHz, DMSO-*d*₆): δ= 7.49 (1H, d, *J*=8.8 Hz), 7.77 (1H, dd, *J*=8.8, 2.4 Hz), 8.05 (1H, d, *J*=2.4 Hz), 8.70 ppm (s, 1H).

¹³C NMR (100 MHz, DMSO-*d*₆): δ= 118.63, 119.82, 120.03, 128.88, 129.44, 134.08, 147.45, 153.57, 156.56, 164.19 ppm.

HRMS (ESI): *m/z* calcd for C₁₀H₄Cl₂O₃ [*M*+Na]⁺: 266.0314, found: 266.0311.



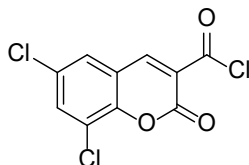
6-Bromo-2-oxo-2H-chromene-3-carbonyl chloride (5.8c).

The brown compound was obtained from 6-bromo-2-oxo-2H-chromene-3-carboxylic acid (**5.7c**, 0.2 g, 0.74 mmol) by following the experimental conditions described for **5.8a** (0.188 g, 87% yield):

¹H NMR (400 MHz, DMSO-*d*₆): δ= 7.42 (1H, d, *J*=8.2 Hz), 7.86 (1H, dd, *J*=8.2, 2.0 Hz), 8.17 (1H, d, *J*=2.0 Hz), 8.69 ppm (s, 1H).

¹³C NMR (100 MHz, DMSO-*d*₆): δ= 118.16, 119.90, 121.76, 128.92, 129.39, 134.09, 148.01, 153.72, 156.11, 164.64 ppm.

HRMS (ESI): m/z calcd for $C_{10}H_4BrClO_3$ $[M+Na]^+$: 310.4825, found: 310.4824.



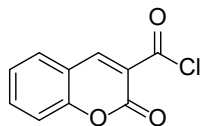
6,8-Dichloro-2-oxo-2H-chromene-3-carbonyl chloride (5.8d).

The white compound was obtained from 6,8-dichloro-2-oxo-2H-chromene-3-carboxylic acid (**5.7d**, 0.2 g, 0.77 mmol) by following the experimental conditions described for **5.8a** (0.153 g, 71% yield):

1H NMR (400 MHz, DMSO- d_6): δ = 8.04 (1H, d, J =2.4 Hz), 8.07 (1H, d, J =2.4 Hz), 8.71 ppm (s, 1H).

^{13}C NMR (100 MHz, DMSO- d_6): δ = 116.73, 118.43, 120.02, 129.11, 129.66, 133.89, 148.57, 153.53, 156.88, 164.04 ppm.

HRMS (ESI): m/z calcd for $C_{10}H_3Cl_3O_3$ $[M+Na]^+$: 300.4768, found: 300.4746.



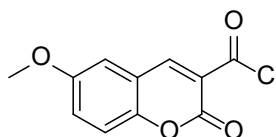
2-Oxo-2H-chromene-3-carbonyl chloride (5.8e).

The white compound was obtained from 6,8-dichloro-2-oxo-2H-chromene-3-carboxylic acid (**5.7e**, 0.2 g, 1.05 mmol) by following the experimental conditions described for **5.8a** (0.2 g, 91% yield):

^1H NMR (400 MHz, DMSO- d_6): δ = 7.43 (m, 2H), 7.75 (1H, t, J =7.6 Hz), 7.91 (1H, d, J =7.6 Hz), 8.72 ppm (s, 1H).

^{13}C NMR (100 MHz, DMSO- d_6): δ = 116.62, 118.43, 118.75, 125.35, 130.61, 134.69, 148.76, 154.89, 157.14, 164.41 ppm.

HRMS (ESI): m/z calcd for $\text{C}_{10}\text{H}_5\text{ClO}_3$ $[M+\text{Na}]^+$: 231.5869, found: 231.5838.



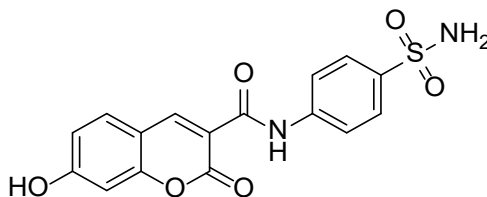
6-Methoxy-2-oxo-2H-chromene-3-carbonyl chloride (5.8f).

The white compound was obtained from 6-methoxy-2-oxo-2H-chromene-3-carboxylic acid (**5.7f**, 0.2 g, 0.90 mmol) by following the experimental conditions described for **5.8a** (0.208 g, 96% yield):

^1H NMR (400 MHz, DMSO- d_6): δ = 3.82 (s, 3H), 7.34 (1H, dd, J =8.7, 2.5 Hz), 7.38 (1H, d, J =8.7 Hz), 7.47 (1H, d, J =3 Hz), 8.69 ppm (s, 1H).

^{13}C NMR (100 MHz, DMSO- d_6): δ = 56.31, 112.36, 117.74, 118.87, 119.06, 122.52, 148.57, 149.40, 156.20, 157.44, 164.47 ppm.

HRMS (ESI): m/z calcd for $\text{C}_{11}\text{H}_7\text{ClO}_4$ $[M+\text{Na}]^+$: 261.6126, found: 261.6109.



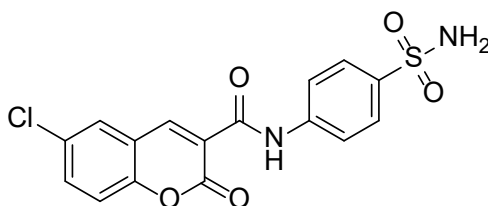
7-Hydroxy-2-oxo-N-(4-sulfamoylphenyl)-2H-chromene-3-carboxamide (5.9a).

A solution of 7-hydroxy-2-oxo-2*H*-chromene-3-carbonyl chloride (**5.8a**, 0.2 g, 0.89 mmol) and sulfanilamide (**5.3a**, 0.17 g, 0.98 mmol) in the presence pyridine or triethylamine (1 mL) in DMF (5 mL) was stirred under reflux 12 h. The solution was cooled, and 5 mL of 6N HCl was added and the resulting solid was filtered off and washed with water (10 mL) and air dried to yield a white powder (0.211 g, 66% yield).

¹H NMR (400 MHz, DMSO-*d*₆): δ= 6.84 (1H, d, *J*=2.4 Hz), 6.92 (1H, dd, *J*=8.6, 2.4 Hz), 7.30 (s, 2H), 7.89 (m, 5H), 8.87 (1H, d, *J*=8.6 Hz), 10.89 ppm (s, 1H).

¹³C NMR (100 MHz, DMSO-*d*₆): δ= 102.42, 106.48, 111.51, 113.90, 115.28, 120.02, 127.33, 132.73, 139.58, 141.36, 149.14, 157.03, 161.20, 161.77, 165.09 ppm.

HRMS (ESI): *m/z* calcd for C₁₆H₁₂N₂O₆S [*M*+Na]⁺: 383.3285, found: 383.3193.



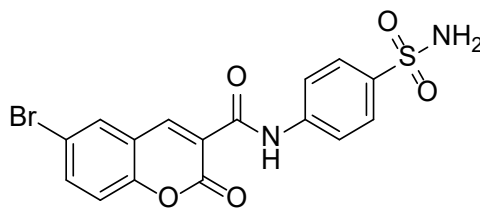
6-Chloro-2-oxo-*N*-(4-sulfamoylphenyl)-2*H*-chromene-3-carboxamide (5.9b**).**

The white compound was obtained from 6-chloro-2-oxo-2*H*-chromene-3-carbonyl chloride (**5.8b**, 0.2 g, 0.82 mmol) by following the experimental conditions described for **5.9a** (0.287 g, 92% yield):

¹H NMR (400 MHz, DMSO-*d*₆): δ= 7.32 (s, 2H), 7.61 (1H, d, *J*=8.9 Hz), 7.83 (m, 3H), 7.89 (2H, d, *J*=8.9 Hz), 8.16 (1H, d, *J*=2.6 Hz), 8.78 (s, 1H), 10.86 ppm (s, 1H).

¹³C NMR (100 MHz, DMSO-*d*₆): δ= 118.81, 120.18, 120.23, 121.66, 127.35, 129.47, 129.61, 134.27, 139.92, 141.14, 146.73, 153.00, 160.20, 160.66 ppm.

HRMS (ESI): *m/z* calcd for C₁₆H₁₁ClN₂O₅S [*M*+Na]⁺: 401.7737, found: 401.7717.



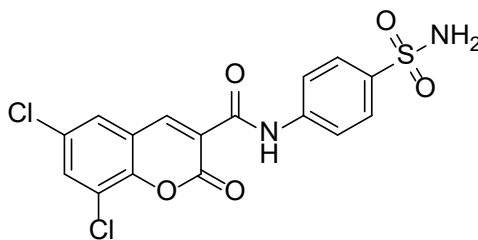
6-Bromo-2-oxo-*N*-(4-sulfamoylphenyl)-2*H*-chromene-3-carboxamide (5.9c).

The white compound was obtained from 6-bromo-2-oxo-2*H*-chromene-3-carbonyl chloride (**5.8c**, 0.2 g, 0.70 mmol) by following the experimental conditions described for **5.9a** (0.243 g, 83% yield):

¹H NMR (400 MHz, DMSO-*d*₆): δ = 7.32 (s, 2H), 7.55 (1H, d, *J*=8.8 Hz), 7.85 (1H, d, *J*=8.8 Hz), 7.89 (m, 3H), 8.29 (1H, d, *J*=2.5 Hz), 8.86 (s, 1H), 10.85 ppm (s, 1H).

¹³C NMR (100 MHz, DMSO-*d*₆): δ = 117.29, 119.05, 120.18, 120.72, 121.62, 127.34, 132.63, 137.02, 139.93, 141.14, 146.65, 153.42, 160.15, 160.66 ppm.

HRMS (ESI): *m/z* calcd for C₁₆H₁₁BrN₂O₅S [*M*+Na]⁺: 446.2247, found: 446.2236.



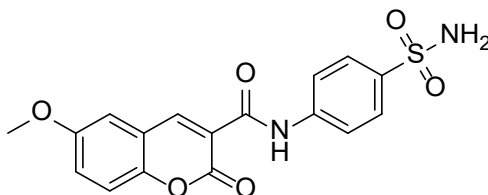
6,8-Dichloro-2-oxo-*N*-(4-sulfamoylphenyl)-2*H*-chromene-3-carboxamide (5.9d).

The white compound was obtained from 6,8-dichloro-2-oxo-2*H*-chromene-3-carbonyl chloride (**5.8d**, 0.2 g, 0.72 mmol) by following the experimental conditions described for **5.9a** (0.214 g, 72% yield):

¹H NMR (400 MHz, DMSO-*d*₆): δ= 7.33 (s, 2H), 7.86 (2H, d, *J*=8.8 Hz), 7.89 (2H, d, *J*=8.8 Hz), 8.14 (s, 2H), 8.84 (s, 1H), 10.78 ppm (s, 1H).

¹³C NMR (100 MHz, DMSO-*d*₆): δ= 120.21, 121.25, 121.42, 122.71, 127.35, 128.71, 129.35, 133.51, 140.03, 141.06, 148.77, 159.16, 160.42, 162.75 ppm.

HRMS (ESI): *m/z* calcd for C₁₆H₁₀Cl₂N₂O₅S [*M*+Na]⁺: 436.2178, found: 436.2176.



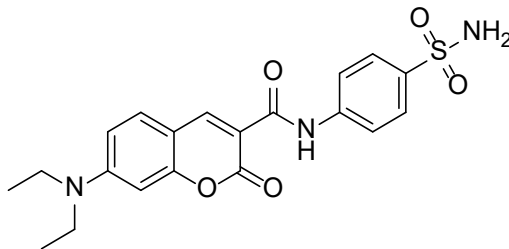
6-Methoxy-2-oxo-*N*-(4-sulfamoylphenyl)-2*H*-chromene-3-carboxamide (5.9f).

The white compound was obtained from 2-oxo-2*H*-chromene-3-carbonyl chloride (**5.8f**, 0.2 g, 0.84 mmol) by following the experimental conditions described for **5.9a** (0.298 g, 95% yield):

¹H NMR (400 MHz, DMSO-*d*₆): δ= 3.84 (s, 1H), 7.32 (s, 2H), 7.39 (1H, d, *J*=8.2 Hz), 7.49 (1H, d, *J*=8.9 Hz), 7.59 (1H, d, *J*=2.2 Hz), 7.85 (2H, d, *J*=8.6 Hz), 7.90 (2H, d, *J*=8.6 Hz), 8.89 (s, 1H), 10.95 ppm (s, 1H).

¹³C NMR (100 MHz, DMSO-*d*₆): δ= 56.34, 112.36, 117.90, 119.36, 120.12, 120.20, 122.68, 127.35, 139.85, 141.19, 148.14, 148.93, 156.54, 160.83, 160.96 ppm.

HRMS (ESI): *m/z* calcd for C₁₇H₁₄N₂O₆S [*M*+Na]⁺: 397.3553, found: 397.3518.



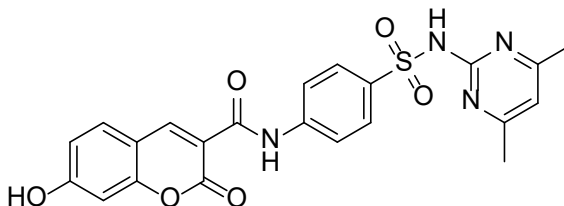
7-(Diethylamino)-2-oxo-N-(4-sulfamoylphenyl)-2H-chromene-3-carboxamide (5.9g).

To a solution of 7-(diethylamino)-2-oxo-2H-chromene-3-carboxylic acid (**5.7g**, 0.2 g, 0.77 mmol), 1-ethyl-3-(3-dimethylaminopropyl)carbodiimide hydrochloride (EDC) (0.14 g, 0.92 mmol), 1-hydroxybenzotriazole hydrate (HOBt·H₂O) (0.124 g, 0.92 mmol) and triethylamine (TEA) (0.5 mL) in DMF (7 mL) was added sulfanilamide (**5.3a**, 0.132 g, 0.77 mmol). The solution was stirred at room temperature for 12 h. The water (5 mL) was added to the solution with few drops of 6N HCl and the resulting solid was filtered off and washed with water and air-dried to yield a yellow powder (0.233 g, 73% yield).

¹H NMR (400 MHz, DMSO-d₆): δ= 1.15 (6H, t, *J*=7.1 Hz), 3.52 (q, 4H), 6.68 (1H, d, *J*=2.1 Hz), 6.86 (1H, dd, *J*=8.9, 2.1 Hz), 7.29 (s, 2H), 7.73 (1H, d, *J*=9 Hz), 7.82 (2H, d, *J*=8.6 Hz), 7.88 (2H, d, *J*=8.6 Hz), 8.77 (s, 1H), 10.98 ppm (s, 1H).

¹³C NMR (100 MHz, DMSO-d₆): δ= 12.80, 44.92, 96.44, 108.41, 109.10, 111.00, 119.82, 127.31, 132.46, 139.30, 141.57, 148.95, 153.44, 157.96, 161.65, 162.64 ppm.

HRMS (ESI): *m/z* calcd for C₂₀H₂₁N₃O₅S [*M*+Na]⁺: 438.4500, found: 438.4418.



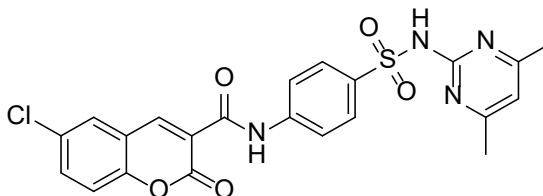
***N*-(4-(*N*-(4,6-dimethylpyrimidin-2-yl) sulfamoyl)phenyl) -7-hydroxy -2-oxo-2*H*-chromene-3-carboxamide (5.10a).**

The white compound was obtained from 7-hydroxy-2-oxo-2*H*-chromene-3-carbonyl chloride (**5.8a**, 0.2 g, 0.84 mmol) and sulfamethazine (**5.3e**, 0.233 g, 0.84 mmol) by following the experimental conditions described for **5.9a** (0.21 g, 54% yield):

¹H NMR (400 MHz, DMSO-*d*₆): δ= 2.26 (s, 6H), 6.76 (s, 1H), 6.85 (1H, d, *J*=2.1 Hz), 6.92 (1H, dd, *J*=8.6, 2.1 Hz), 7.89 (m, 3H), 7.98 (2H, d, *J*=8.7 Hz), 8.86 (s, 1H), 10.89 (s, 1H), 11.18 (s, 1H), 11.66 ppm (s, 1H).

¹³C NMR (100 MHz, DMSO-*d*₆): δ= 23.32, 102.40, 111.63, 114.30, 115.08, 119.41, 129.86, 132.75, 135.97, 141.99, 149.15, 156.67, 156.94, 161.19, 161.60, 164.63 ppm.

HRMS (ESI): *m/z* calcd for C₂₂H₁₈N₄O₆S [*M*+Na]⁺: 489.4538, found: 489.4497.



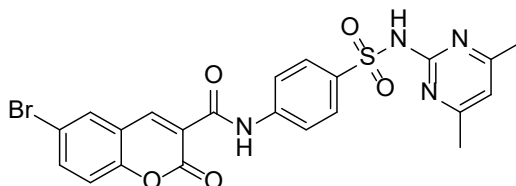
6-Chloro-*N*-(4-(*N*-(4,6-dimethylpyrimidin-2-yl) sulfamoyl)phenyl) -2-oxo-2*H*-chromene-3-carboxamide (5.10b).

The white compound was obtained from 6-chloro-2-oxo-2*H*-chromene-3-carbonyl chloride (**5.8b**, 0.2 g, 0.82 mmol) and sulfamethazine (**5.3e**, 0.228 g, 0.82 mmol) by following the experimental conditions described for **5.9a** (0.254 g, 63% yield):

¹H NMR (400 MHz, DMSO-*d*₆): δ= 2.26 (s, 6H), 6.75 (s, 1H), 7.60 (1H, d, *J*=8.8 Hz), 7.79 (1H, dd, *J*=8.6, 2.5 Hz), 7.89 (2H, d, *J*=8.8 Hz), 8.00 (2H, d, *J*=8.8 Hz), 8.14 (1H, d, *J*=2.5 Hz), 8.84 (s, 1H), 10.85 (s, 1H), 11.81 ppm (s, 1H).

¹³C NMR (100 MHz, DMSO-*d*₆): δ= 23.31, 112.52, 118.79, 119.45, 119.84, 120.19, 121.64, 129.46, 129.61, 129.87, 130.39, 134.25, 136.31, 141.77, 146.70, 150.28, 152.98, 156.61, 160.14, 160.66 ppm.

HRMS (ESI): *m/z* calcd for C₂₂H₁₇ClN₄O₅S [*M*+Na]⁺: 507.8985, found: 507.8975.



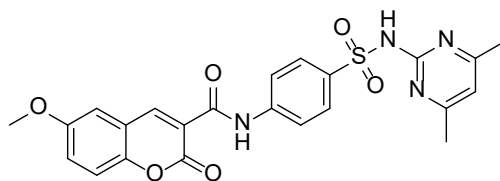
6-Bromo-N-(4-(N-(4,6-dimethylpyrimidin-2-yl)sulfamoyl)phenyl)-2-oxo-2H-chromene-3-carboxamide (5.10c).

The white compound was obtained from 6-bromo-2-oxo-2H-chromene-3-carbonyl chloride (**5.8c**, 0.2 g, 0.70 mmol) and sulfamethazine (**5.3e**, 0.194 g, 0.70 mmol) by following the experimental conditions described for **5.9a** (0.269 g, 72% yield):

¹H NMR (400 MHz, DMSO-*d*₆): δ= 2.26 (s, 6H), 6.76 (s, 1H), 7.54 (1H, d, *J*=8.8 Hz), 7.89 (2H, d, *J*=8.8 Hz), 7.94 (1H, dd, *J*=8.8, 2.3 Hz), 8.00 (2H, d, *J*=8.8 Hz), 8.27 (1H, d, *J*=2.3 Hz), 8.84 (s, 1H), 10.85 (s, 1H), 11.68 ppm (s, 1H).

¹³C NMR (100 MHz, DMSO-*d*₆): δ= 23.32, 112.52, 117.28, 119.04, 119.54, 120.69, 121.65, 129.88, 129.90, 132.62, 137.01, 141.78, 146.60, 153.40, 156.62, 160.09, 160.68 ppm.

HRMS (ESI): *m/z* calcd for C₂₂H₁₇BrN₄O₅S [*M*+Na]⁺: 552.3499, found: 552.3443.



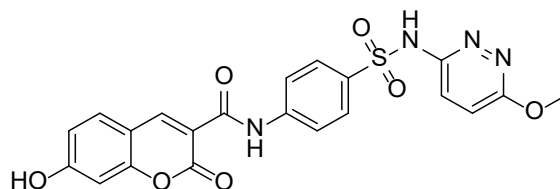
***N*-(4-(*N*- (4,6-dimethylpyrimidin-2-yl) sulfamoyl)phenyl) -6-methoxy-2-oxo-2*H*-chromene-3-carboxamide (5.10f).**

The white compound was obtained from 6-methoxy-2-oxo-2*H*-chromene-3-carbonyl chloride (**5.8f**, 0.2 g, 0.84 mmol) and sulfamethazine (**5.3e**, 0.234 g, 0.84 mmol) by following the experimental conditions described for **5.9a** (0.367 g, 91% yield):

¹H NMR (400 MHz, DMSO-*d*₆): δ= 2.27 (s, 6H), 3.83 (s, 1H), 6.76 (s, 1H), 7.39 (1H, dd, *J*=9.0, 2.9 Hz), 7.49 (1H, d, *J*=9.0 Hz), 7.57 (1H, d, *J*=2.9 Hz), 7.90 (2H, d, *J*=8.8 Hz), 8.00 (2H, d, *J*=8.8 Hz), 8.87 (s, 1H), 10.95 (s, 1H), 11.72 ppm (s, 1H).

¹³C NMR (100 MHz, DMSO-*d*₆): δ= 23.31, 56.30, 112.32, 113.84, 117.87, 119.31, 119.49, 120.16, 122.86, 123.42, 136.20, 141.83, 148.08, 148.90, 156.52, 160.80, 160.92 ppm.

HRMS (ESI): *m/z* calcd for C₂₃H₂₀N₄O₆S [*M*+Na]⁺: 503.4807, found: 503.4782.



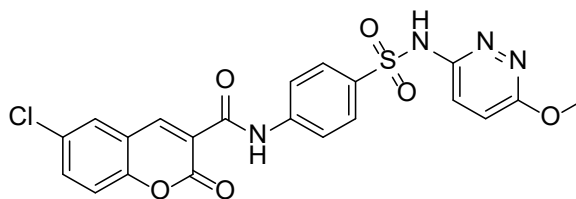
7-Hydroxy-*N*- (4-(*N*-(6-methoxypyridazin-3-yl) sulfamoyl)phenyl) -2-oxo-2*H*-chromene-3-carboxamide (5.11a).

The white compound was obtained from 7-hydroxy-2-oxo-2*H*-chromene-3-carbonyl chloride (**5.8a**, 0.2 g, 0.84 mmol) and sulfamethoxypyridazine (**5.3f**, 0.235 g, 0.84 mmol) by following the experimental conditions described for **5.9a** (0.237 g, 60% yield):

¹H NMR (400 MHz, DMSO-*d*₆): δ= 3.84 (s, 3H), 6.85 (1H, d, *J*=2.0 Hz), 6.91 (1H, dd, *J*=8.6, 2.0 Hz), 7.38 (1H, d, *J*=8.5 Hz), 7.76 (br, 1H), 7.85 (m, 6H), 8.87 (s, 1H), 10.87 (s, 1H), 11.22 ppm (br, 1H).

¹³C NMR (100 MHz, DMSO-*d*₆): δ= 54.96, 102.39, 111.16, 111.62, 114.25, 115.09, 120.23, 127.90, 132.74, 141.56, 149.17, 153.63, 156.94, 161.14, 161.61, 164.71 ppm.

HRMS (ESI): *m/z* calcd for C₂₁H₁₆N₄O₇S [*M*+Na]⁺: 491.4265, found: 491.4241.



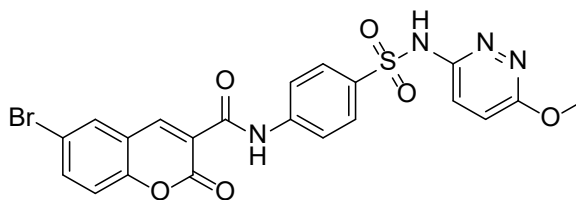
6-Chloro-*N*-(4-(*N*-(6-methoxypyridazin-3-yl)sulfamoyl)phenyl)-2-oxo-2*H*-chromene-3-carboxamide (5.11b).

The white compound was obtained from 6-chloro-2-oxo-2*H*-chromene-3-carbonyl chloride (**5.8b**, 0.2 g, 0.82 mmol) and sulfamethoxypyridazine (**5.3f**, 0.228 g, 0.82 mmol) by following the experimental conditions described for **5.9a** (0.326 g, 82% yield):

¹H NMR (400 MHz, DMSO-*d*₆): δ= 3.84 (s, 3H), 7.39 (br, 1H), 7.62 (1H, d, *J*=8.7 Hz), 7.86 (m, 5H), 8.15 (1H, d, *J*=2.2 Hz), 8.85 (s, 1H), 10.84 (s, 1H), 13.84 ppm (br, 1H).

¹³C NMR (100 MHz, DMSO-*d*₆): δ= 54.98, 118.80, 120.21, 120.72, 121.69, 127.87, 129.45, 129.75, 134.25, 141.42, 146.17, 146.72, 153.00, 160.12, 160.66 ppm.

HRMS (ESI): *m/z* calcd for C₂₁H₁₅ClN₄O₆S [*M*+Na]⁺: 509.8711, found: 509.8709.



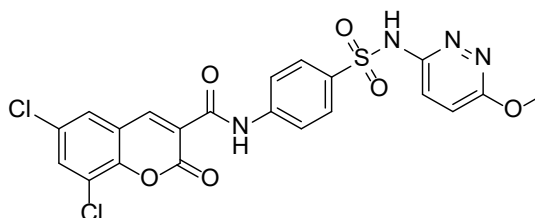
6-Bromo-*N*-(4-(*N*-(6-methoxypyridazin-3-yl)sulfamoyl)phenyl)-2-oxo-2*H*-chromene-3-carboxamide (5.11c).

The white compound was obtained from 6-bromo-2-oxo-2*H*-chromene-3-carbonyl chloride (**5.8c**, 0.2 g, 0.70 mmol) and sulfamethoxypyridazine (**5.3f**, 0.196 g, 0.70 mmol) by following the experimental conditions described for **5.9a** (0.309 g, 83% yield):

¹H NMR (400 MHz, DMSO-*d*₆): δ = 3.84 (s, 3H), 7.40 (br, 1H), 7.55 (1H, d, *J*=8.8 Hz), 7.86 (m, 4H), 7.92 (2H, dd, *J*=8.8, 2.4 Hz), 8.28 (1H, d, *J*=2.4 Hz), 8.84(s, 1H), 10.84 (s, 1H), 13.81 ppm (br,1H).

¹³C NMR (100 MHz, DMSO-*d*₆): δ = 54.98, 117.28, 119.04, 120.22, 120.70, 121.65, 127.88, 132.61, 137.01, 141.37, 146.61, 153.41, 160.08, 160.66 ppm.

HRMS (ESI): *m/z* calcd for C₂₁H₁₅BrN₄O₆S [*M*+Na]⁺: 554.3226, found: 554.3213.



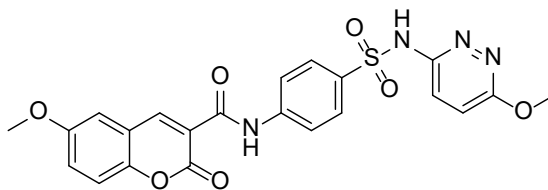
6,8-Dichloro-*N*-(4-(*N*-(6-methoxypyridazin-3-yl)sulfamoyl)phenyl)-2-oxo-2*H*-chromene-3-carboxamide (5.11d).

The white compound was obtained from 6,8-dichloro-2-oxo-2*H*-chromene-3-carbonyl chloride (**5.8d**, 0.2 g, 0.72 mmol) and sulfamethoxypyridazine (**5.3f**, 0.202 g, 0.72 mmol) by following the experimental conditions described for **5.9a** (0.263 g, 70% yield):

¹H NMR (400 MHz, DMSO-*d*₆): δ= 3.85 (s, 3H), 7.40 (br, 1H), 7.87 (m, 5H), 8.13 (s, 2H), 7.82 (s, 1H), 10.77 (s, 1H), 13.83 ppm (br, 1H).

¹³C NMR (100 MHz, DMSO-*d*₆): δ 54.98, 120.25, 121.24, 121.42, 122.77, 127.94, 128.26, 128.68, 129.34, 133.49, 141.33, 146.13, 148.76, 151.44, 153.93, 159.09, 160.44 ppm.

HRMS (ESI): *m/z* calcd for C₂₁H₁₄Cl₂N₄O₆S [*M*+Na]⁺: 544.3155, found: 544.3148.



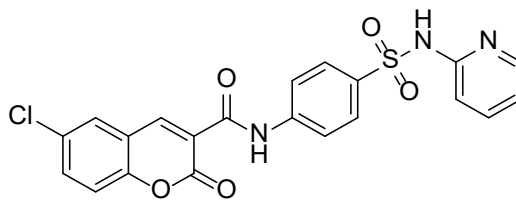
6-Methoxy-N-(4-(N-(6-methoxypyridazin-3-yl)sulfamoyl)phenyl)-2-oxo-2H-chromene-3-carboxamide (5.11f).

The white compound was obtained from 6-methoxy-2-oxo-2*H*-chromene-3-carbonyl chloride (**5.8f**, 0.2 g, 0.84 mmol) and sulfamethoxypyridazine (**5.3f**, 0.235 g, 0.84 mmol) by following the experimental conditions described for **5.9a** (0.328 g, 81% yield):

¹H NMR (400 MHz, DMSO-*d*₆): δ= 3.83 (6H, d, *J*=4.0 Hz), 7.37 (m, 2H), 7.47 (1H, d, *J*=8.8 Hz), 7.56 (1H, d, *J*=4.0 Hz), 7.76 (m, 2H), 7.89 (s, 4H), 8.86 (s, 1H), 10.93 ppm (s, 1H).

¹³C NMR (100 MHz, DMSO-*d*₆): δ= 54.97, 56.31, 107.28, 112.34, 117.87, 119.33, 120.18, 122.84, 127.91, 129.83, 130.19, 135.64, 141.41, 148.09, 148.91, 156.52, 160.89 ppm.

HRMS (ESI): *m/z* calcd for C₂₂H₁₈N₄O₇S [*M*+Na]⁺: 505.4531, found: 505.4522.



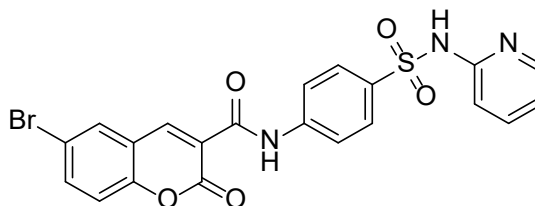
6-Chloro-2-oxo-N-(4-(N-(pyridin-2-yl)sulfamoyl)phenyl)-2H-chromene-3-carboxamide (5.12b).

The white compound was obtained from 6-chloro-2-oxo-2H-chromene-3-carbonyl chloride (**5.8b**, 0.2 g, 0.82 mmol) and sulfapyridine (**5.3d**, 0.204 g, 0.82 mmol) by following the experimental conditions described for **5.9a** (0.298 g, 80% yield):

¹H NMR (400 MHz, DMSO-*d*₆): δ = 6.88 (1H, t, *J*=7.5 Hz), 7.17 (1H, d, *J*=8.6 Hz), 7.61 (1H, d, *J*=8.6 Hz), 7.72 (1H, t, *J*=8.5 Hz), 7.87 (m, 6H), 8.02 (br, 1H), 8.15 (s, 1H), 8.84 (s, 1H), 10.84 ppm (s, 1H).

¹³C NMR (100 MHz, DMSO-*d*₆): δ = 101.98, 113.19, 119.02, 119.79, 120.41, 120.88, 121.64, 128.29, 132.60, 137.71, 141.29, 149.67, 153.42, 160.18, 160.95 ppm.

HRMS (ESI): *m/z* calcd for C₂₁H₁₄ClN₃O₅S [*M*+Na]⁺: 478.8573, found: 478.8459.



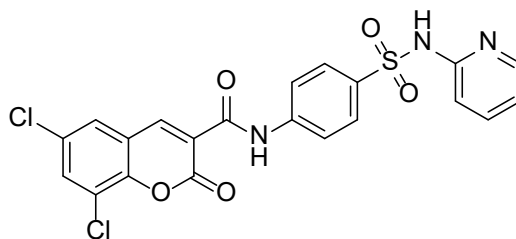
6-Bromo-2-oxo-N-(4-(N-(pyridin-2-yl)sulfamoyl)phenyl)-2H-chromene-3-carboxamide (5.12c).

The white compound was obtained from 6-bromo-2-oxo-2*H*-chromene-3-carbonyl chloride (**5.8c**, 0.2 g, 0.70 mmol) and sulfapyridine (**5.3d**, 0.18 g, 0.70 mmol) by following the experimental conditions described for **5.9a** (0.288 g, 82% yield):

¹H NMR (400 MHz, DMSO-*d*₆): δ= 6.88 (1H, t, *J*=7.5 Hz), 7.17 (1H, d, *J*=8.6 Hz), 7.54 (1H, d, *J*=8.6 Hz), 7.72 (1H, t, *J*=7.5 Hz), 7.88 (m, 6H), 8.02 (br, 1H), 8.28 (1H, d, *J*=2.4 Hz), 8.84 (s, 1H), 10.3 ppm (s, 1H).

¹³C NMR (100 MHz, DMSO-*d*₆): δ= 101.65, 112.88, 117.27, 119.04, 120.11, 120.70, 121.69, 128.39, 132.61, 137.00, 141.52, 146.57, 153.41, 160.05, 160.69 ppm.

HRMS (ESI): *m/z* calcd for C₂₁H₁₄BrN₃O₅S [*M*+Na]⁺: 523.3089, found: 523.3059.



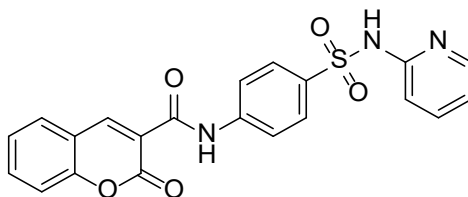
6,8-Dichloro-2-oxo-*N*-(4-(*N*-(pyridin-2-yl)sulfamoyl)phenyl)-2*H*-chromene-3-carboxamide (5.12d**).**

The white compound was obtained from 6,8-dichloro-2-oxo-2*H*-chromene-3-carbonyl chloride (**5.8d**, 0.2 g, 0.72 mmol) and sulfapyridine (**5.3d**, 0.18 g, 0.72 mmol) by following the experimental conditions described for **5.9a** (0.210 g, 59% yield):

¹H NMR (400 MHz, DMSO-*d*₆): δ= 6.88 (1H, t, *J*=6.6 Hz), 7.17 (1H, d, *J*=8.4 Hz), 7.73 (1H, t, *J*=7.1 Hz), 7.89 (m, 5H), 8.02 (br, 1H), 8.13 (s, 2H), 8.81 (s, 1H), 10.76 ppm (s, 1H).

^{13}C NMR (100 MHz, DMSO- d_6): δ = 114.17, 120.15, 121.24, 121.41, 122.78, 128.39, 128.68, 129.33, 133.49, 137.60, 140.99, 141.44, 146.11, 148.76, 153.57, 159.07, 160.46 ppm.

HRMS (ESI): m/z calcd for $\text{C}_{21}\text{H}_{13}\text{Cl}_2\text{N}_3\text{O}_5\text{S}$ [$M+\text{Na}$] $^+$: 513.3020, found: 513.3007.



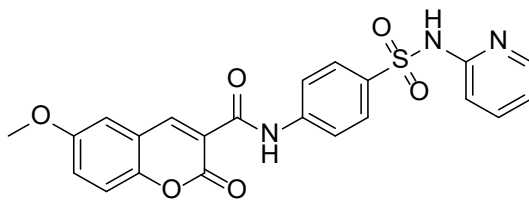
2-Oxo-N-(4-(N-(pyridin-2-yl)sulfamoyl)phenyl)-2H-chromene-3-carboxamide (5.12e).

The white compound was obtained from 2-oxo-2H-chromene-3-carbonyl chloride (**5.8e**, 0.2 g, 0.96 mmol) and sulfapyridine (**5.3d**, 0.24 g, 0.96 mmol) by following the experimental conditions described for **5.9a** (0.389 g, 96% yield):

^1H NMR (400 MHz, DMSO- d_6): δ = 6.87 (1H, t, J =6.2 Hz), 7.17 (1H, d, J =8.6 Hz), 7.47 (1H, t, J =7.4 Hz), 7.56 (1H, d, J =8.4 Hz), 7.78 (m, 2H), 7.88 (q, 4H), 8.02 (2H, d, J =7.0 Hz), 8.90 (s, 1H), 10.88 (s, 1H), 11.94 ppm (br, 1H).

^{13}C NMR (100 MHz, DMSO- d_6): δ = 114.17, 116.07, 116.74, 118.85, 120.07, 120.36, 120.40, 125.79, 128.39, 130.82, 134.90, 137.39, 140.75, 141.61, 148.08, 154.40, 160.63, 160.93 ppm.

HRMS (ESI): m/z calcd for $\text{C}_{21}\text{H}_{15}\text{N}_3\text{O}_5\text{S}$ [$M+\text{Na}$] $^+$: 444.4133, found: 444.4093.



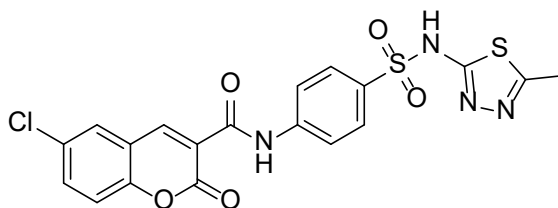
2-Oxo-N-(4-(N-(pyridin-2-yl)sulfamoyl)phenyl)-2H-chromene-3-carboxamide (5.12f).

The white compound was obtained from 6-methoxy-2-oxo-2H-chromene-3-carbonyl chloride (**5.8f**, 0.2 g, 0.84 mmol) and sulfapyridine (**5.3d**, 0.21 g, 0.84 mmol) by following the experimental conditions described for **5.9a** (0.249 g, 66% yield):

¹H NMR (400 MHz, DMSO-*d*₆): δ = 3.84 (s, 3H), 6.88 (1H, t, *J* = 6.1 Hz), 7.18 (1H, d, *J* = 8.6 Hz), 7.38 (1H, d, *J* = 7.4 Hz), 7.50 (s, 1H), 7.59 (s, 1H), 7.73 (m, 2H), 7.89 (q, 4H), 8.02 (2H, d, *J* = 7.0 Hz), 8.87 (s, 1H), 10.93 ppm (s, 1H).

¹³C NMR (100 MHz, DMSO-*d*₆): δ = 56.33, 112.37, 114.16, 117.89, 119.34, 120.16, 120.27, 122.84, 128.47, 140.81, 141.56, 148.06, 148.92, 156.52, 160.89 ppm.

HRMS (ESI): *m/z* calcd for C₂₂H₁₇N₃O₆S [*M*+Na]⁺: 474.4393, found: 474.4329.



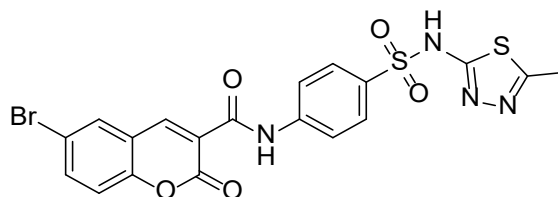
6-Chloro-N-(4-(N-(5-methyl-1,3,4-thiadiazol-2-yl)sulfamoyl)phenyl)-2-oxo-2H-chromene-3-carboxamide (5.13b).

The white compound was obtained from 6-chloro-2-oxo-2H-chromene-3-carbonyl chloride (**5.8b**, 0.2 g, 0.82 mmol) and sulfamethizole (**5.3g**, 0.222 g, 0.82 mmol) by following the experimental conditions described for **5.9a** (0.288 g, 74% yield):

¹H NMR (400 MHz, DMSO-*d*₆): δ= 2.47 (s, 3H), 7.62 (1H, d, *J*=8.8 Hz), 7.80 (m, 3H), 7.88 (2H, d, *J*=8.8 Hz), 8.15 (s, 1H), 8.85 (s, 1H), 10.87 (s, 1H), 13.94 ppm (br, 1H).

¹³C NMR (100 MHz, DMSO-*d*₆): δ= 16.53, 118.80, 120.02, 120.30, 121.66, 127.54, 129.46, 129.61, 134.26, 137.53, 141.69, 146.71, 153.00, 155.10, 160.13, 160.69, 168.35 ppm.

HRMS (ESI): *m/z* calcd for C₁₉H₁₃ClN₄O₅S₂ [*M*+Na]⁺: 499.8982, found: 499.8806.



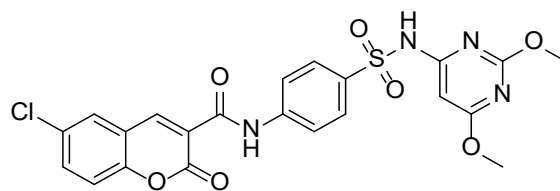
6-Bromo-N- (4-(N-(5-methyl-1,3,4-thiadiazol-2-yl) sulfamoyl)phenyl) -2-oxo-2H-chromene-3-carboxamide (5.13c).

The white compound was obtained from 6-bromo-2-oxo-2H-chromene-3-carbonyl chloride (**5.8c**, 0.2 g, 0.70 mmol) and sulfamethizole (**5.3g**, 0.189 g, 0.70 mmol) by following the experimental conditions described for **5.9a** (0.277 g, 76% yield):

¹H NMR (400 MHz, DMSO-*d*₆): δ= 2.47 (s, 3H), 7.55 (1H, d, *J*=8.8 Hz), 7.82 (2H, d, *J*=8.8 Hz), 7.90 (m, 3H), 8.28 (2H, d, *J*=2.4 Hz), 8.84 (s, 1H), 10.86 (s, 1H), 13.93 ppm (br, 1H).

¹³C NMR (100 MHz, DMSO-*d*₆): δ= 16.53, 117.29, 119.04, 120.30, 120.70, 121.64, 127.55, 132.62, 137.02, 137.53, 141.70, 146.63, 153.41, 155.00, 160.08, 160.69, 168.34 ppm.

HRMS (ESI): *m/z* calcd for C₁₉H₁₃BrN₄O₅S₂ [*M*+Na]⁺: 544.3507, found: 544.3498.



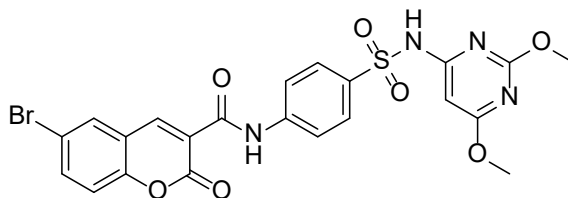
6-Chloro-*N*-(4-(*N*-(2,6-dimethoxypyrimidin-4-yl) sulfamoyl)phenyl) -2-oxo-2*H*-chromene-3-carboxamide (5.14b).

The white compound was obtained from 6-chloro-2-oxo-2*H*-chromene-3-carbonyl chloride (**5.8b**, 0.2 g, 0.82 mmol) and sulfadimethoxine (**5.3h**, 0.254 g, 0.82 mmol) by following the experimental conditions described for **5.9a** (0.312 g, 73% yield):

¹H NMR (400 MHz, DMSO-*d*₆): δ= 3.77 (s, 3H), 3.80 (s, 3H), 5.96 (s, 1H), 7.61 (1H, d, *J*=8.8 Hz), 7.81 (1H, dd, *J*=8.8, 2.4 Hz), 7.95 (m, 4H), 8.14 (1H, d, *J*= 2.4 Hz), 8.85 (s, 1H), 10.90 (s, 1H), 11.59 ppm (br, 1H).

¹³C NMR (100 MHz, DMSO-*d*₆): δ= 54.29, 55.02, 85.07, 118.81, 120.18, 120.27, 121.66, 129.10, 129.26, 129.62, 134.29, 135.27, 142.44, 146.75, 153.01, 160.06, 160.31, 160.84, 164.66, 172.14 ppm.

HRMS (ESI): *m/z* calcd for C₂₂H₁₇ClN₄O₇S [*M*+Na]⁺: 539.8971, found: 539.8857.



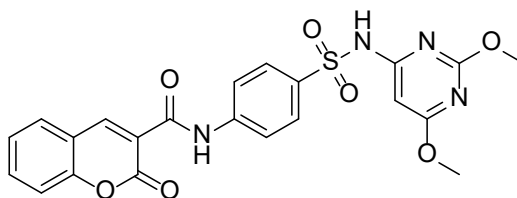
6-Bromo-*N*-(4-(*N*-(2,6-dimethoxypyrimidin-4-yl) sulfamoyl)phenyl) -2-oxo-2*H*-chromene -3-carboxamide (5.14c).

The white compound was obtained from 6-bromo-2-oxo-2*H*-chromene-3-carbonyl chloride (**5.8c**, 0.2 g, 0.70 mmol) and sulfadimethoxine (**5.3h**, 0.217 g, 0.70 mmol) by following the experimental conditions described for **5.9a** (0.322 g, 82% yield):

¹H NMR (400 MHz, DMSO-*d*₆): δ= 3.77 (s, 3H), 3.80 (s, 3H), 5.96 (s, 1H), 7.54 (1H, d, *J*=8.8 Hz), 7.95 (m, 5H), 8.15 (1H, d, *J*=2.4 Hz), 8.84 (s, 1H), 10.90 (s, 1H), 11.56 ppm (br, 1H).

¹³C NMR (100 MHz, DMSO-*d*₆): δ= 54.29, 55.03, 85.07, 117.29, 119.04, 120.27, 120.67, 121.60, 129.10, 132.63, 137.04, 142.44, 146.69, 153.42, 160.01, 160.31, 160.82, 162.75, 172.15 ppm.

HRMS (ESI): *m/z* calcd for C₂₂H₁₇BrN₄O₇S [*M*+Na]⁺: 584.3486, found: 584.3497.



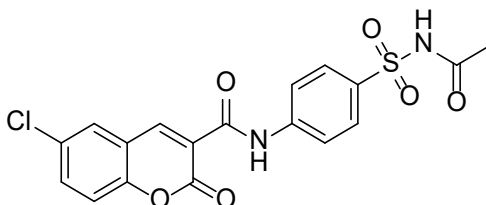
***N*-(4-(*N*-(2,6-dimethoxypyrimidin-4-yl)sulfamoyl)phenyl)-2-oxo-2*H*-chromene-3-carboxamide (**5.14e**).**

The white compound was obtained from 2-oxo-2*H*-chromene-3-carbonyl chloride (**5.8e**, 0.2 g, 0.96 mmol) and sulfadimethoxine (**5.3h**, 0.298 g, 0.96 mmol) by following the experimental conditions described for **5.9a** (0.377 g, 81% yield):

¹H NMR (400 MHz, DMSO-*d*₆): δ= 3.77 (s, 3H), 3.80 (s, 3H), 5.96 (s, 1H), 7.47 (1H, t, *J*=7.6 Hz), 7.56 (1H, d, *J*=8.4 Hz), 7.56 (1H, t, *J*=8.6 Hz), 7.95 (m, 5H), 8.90 (s, 1H), 10.94 (s, 1H), 11.57 ppm (br, 1H).

^{13}C NMR (100 MHz, DMSO- d_6): δ = 54.28, 55.02, 85.06, 116.74, 118.82, 120.21, 120.28, 125.79, 129.08, 130.83, 134.94, 135.16, 142.52, 148.18, 154.40, 160.31, 160.59, 151.06, 164.69, 172.13 ppm.

HRMS (ESI): m/z calcd for $\text{C}_{22}\text{H}_{18}\text{N}_4\text{O}_7\text{S}$ $[M+\text{Na}]^+$: 505.4531, found: 505.4489.



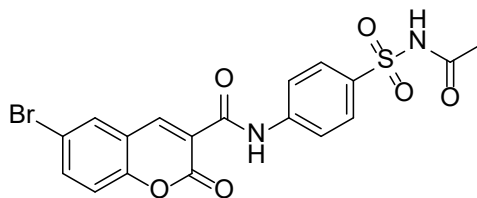
***N*-(4-(*N*-acetylsulfamoyl)phenyl)-6-chloro-2-oxo-2*H*-chromene-3-carboxamide (5.15b).**

The white compound was obtained from 6-chloro-2-oxo-2*H*-chromene-3-carbonyl chloride (**5.8b**, 0.2 g, 0.82 mmol) and sulfacetamide (**5.3c**, 0.176 g, 0.82 mmol) by following the experimental conditions described for **5.9a** (0.302 g, 88% yield):

^1H NMR (400 MHz, DMSO- d_6): δ = 1.93 (s, 3H), 7.61 (1H, d, J =8.8 Hz), 7.81 (1H, dd, J =8.8, 2.5 Hz), 7.93 (m, 4H), 8.14 (1H, d, J =2.5 Hz), 8.86 (s, 1H), 10.93 (s, 1H), 12.04 ppm (br, 1H).

^{13}C NMR (100 MHz, DMSO- d_6): δ = 23.68, 116.61, 118.83, 120.14, 120.68, 121.74, 129.50, 134.30, 134.62, 139.04, 142.76, 146.75, 153.03, 160.05, 160.62, 169.20 ppm.

HRMS (ESI): m/z calcd for $\text{C}_{18}\text{H}_{13}\text{ClN}_2\text{O}_6\text{S}$ $[M+\text{Na}]^+$: 443.8101, found: 443.8025.



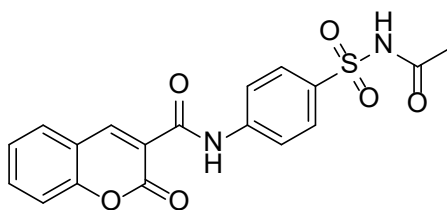
***N*-(4-(*N*-acetylsulfamoyl)phenyl)-6-bromo-2-oxo-2*H*-chromene-3-carboxamide (5.15c).**

The white compound was obtained from 6-bromo-2-oxo-2*H*-chromene-3-carbonyl chloride (**5.8c**, 0.2 g, 0.70 mmol) and sulfacetamide (**5.3c**, 0.15 g, 0.70 mmol) by following the experimental conditions described for **5.9a** (0.285 g, 87% yield):

¹H NMR (400 MHz, DMSO-*d*₆): δ = 1.93 (s, 3H), 7.54 (1H, d, *J*=8.8 Hz), 7.93 (m, 5H), 8.28 (1H, d, *J*=2.4 Hz), 8.85 (s, 1H), 10.93 (s, 1H), 12.05 ppm (s, 1H).

¹³C NMR (100 MHz, DMSO-*d*₆): δ = 23.68, 117.29, 119.05, 120.13, 120.68, 121.63, 129.49, 132.64, 134.61, 137.06, 142.74, 146.73, 153.43, 160.03, 160.87, 169.18 ppm.

HRMS (ESI): *m/z* calcd for C₁₈H₁₃BrN₂O₆S [*M*+Na]⁺: 488.2614, found: 488.2591.



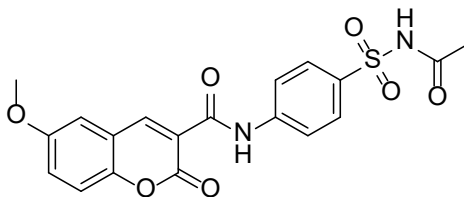
***N*-(4-(*N*-acetylsulfamoyl)phenyl)-2-oxo-2*H*-chromene-3-carboxamide (5.15e).**

The white compound was obtained from 2-oxo-2*H*-chromene-3-carbonyl chloride (**5.8e**, 0.2 g, 0.96 mmol) and sulfacetamide (**5.3c**, 0.21 g, 0.96 mmol) by following the experimental conditions described for **5.9a** (0.329 g, 89% yield):

¹H NMR (400 MHz, DMSO-*d*₆): δ= 1.93 (s, 3H), 7.49 (1H, t, *J*=7.9 Hz), 7.58 (1H, d, *J*=8.8 Hz), 7.80 (1H, t, *J*=8.8 Hz), 7.94 (m, 4H), 8.02 (1H, d, *J*=8.9 Hz), 8.93 (s, 1H), 10.97 (s, 1H), 12.05 ppm (br, 1H).

¹³C NMR (100 MHz, DMSO-*d*₆): δ= 23.71, 116.74, 118.85, 120.08, 120.39, 125.81, 129.48, 130.85, 134.60, 134.96, 142.82, 148.20, 154.43, 160.59, 161.15, 169.25 ppm.

HRMS (ESI): *m/z* calcd for C₁₈H₁₄N₂O₆S [*M*+Na]⁺: 409.366, found: 409.3641.



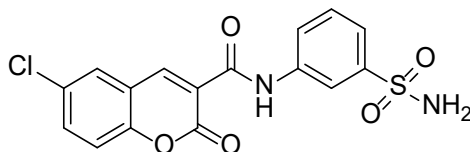
***N*-(4-(*N*-acetylsulfamoyl)phenyl)-6-methoxy-2-oxo-2*H*-chromene-3-carboxamide (5.15f).**

The white compound was obtained from 6-methoxy-2-oxo-2*H*-chromene-3-carbonyl chloride (**5.8f**, 0.2 g, 0.84 mmol) and sulfacetamide (**5.3c**, 0.18 g, 0.84 mmol) by following the experimental conditions described for **5.9a** (0.297 g, 85% yield):

¹H NMR (400 MHz, DMSO-*d*₆): δ= 1.93 (s, 3H), 3.85 (s, 3H), 7.40 (1H, dd, *J*=9.0, 2.8 Hz), 7.50 (1H, d, *J*=9.0 Hz), 7.59 (1H, dd, *J*=2.8 Hz), 7.94 (m, 4H), 8.89 (s, 1H), 11.01 (s, 1H), 12.05 ppm (br, 1H).

¹³C NMR (100 MHz, DMSO-*d*₆): δ= 23.70, 56.34, 112.40, 117.92, 119.33, 120.09, 120.32, 122.89, 129.49, 134.56, 142.80, 148.16, 148.96, 156.54, 160.81, 161.11, 169.21 ppm.

HRMS (ESI): *m/z* calcd for C₁₉H₁₆N₂O₇S [*M*+Na]⁺: 439.3920, found: 439.3902.



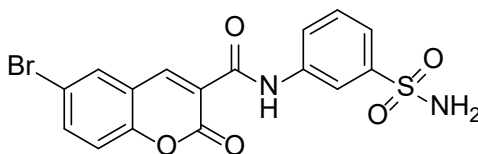
6-Chloro-2-oxo-*N*-(3-sulfamoylphenyl)-2*H*-chromene-3-carboxamide (5.16b).

The white compound was obtained from 6-chloro-2-oxo-2*H*-chromene-3-carbonyl chloride (**5.8b**, 0.2 g, 0.82 mmol) and 3-aminobenzenesulfonamide (**5.3i**, 0.141 g, 0.84 mmol) by following the experimental conditions described for **5.9a** (0.273 g, 85% yield):

¹H NMR (400 MHz, DMSO-*d*₆): δ= 7.43 (s, 2H), 7.61(m, 3H), 7.82 (1H, dd, *J*=8.8, 2.5 Hz), 7.87 (m, 1H), 8.16 (1H, d, *J*=2.5 Hz), 8.28 (s, 1H), 8.85 (s, 1H), 10.83 ppm (s,1H).

¹³C NMR (100 MHz, DMSO-*d*₆): δ= 117.42, 118.81, 120.24, 121.86, 123.37, 129.44, 129.59, 130.24, 134.20, 138.70, 145.35, 146.48, 153.00, 160.12, 160.61, 162.76 ppm.

HRMS (ESI): *m/z* calcd for C₁₆H₁₁ClN₂O₅S [*M*+Na]⁺: 401.7737, found: 401.7703.



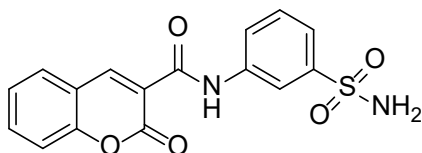
6-Bromo-2-oxo-*N*-(3-sulfamoylphenyl)-2*H*-chromene-3-carboxamide (5.16c).

The white compound was obtained from 6-bromo-2-oxo-2*H*-chromene-3-carbonyl chloride (**5.8c**, 0.2 g, 0.70 mmol) and 3-aminobenzenesulfonamide (**5.3i**, 0.121 g, 0.70 mmol) by following the experimental conditions described for **5.9a** (0.267 g, 90% yield):

¹H NMR (400 MHz, DMSO-*d*₆): δ= 7.43 (s, 2H), 7.60 (m, 3H), 7.92 (m, 2H), 8.29 (s, 2H), 8.84 (s, 1H), 10.82 ppm (s,1H).

^{13}C NMR (100 MHz, DMSO- d_6): δ = 117.27, 117.42, 119.04, 120.72, 121.85, 123.36, 130.23, 132.60, 136.60, 138.69, 145.35, 146.43, 153.00, 160.08, 160.59, 162.75 ppm.

HRMS (ESI): m/z calcd for $\text{C}_{16}\text{H}_{11}\text{BrN}_2\text{O}_5\text{S}$ $[M+\text{Na}]^+$: 446.2247, found: 446.2251.



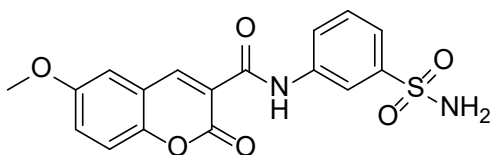
2-Oxo-*N*-(3-sulfamoylphenyl)-2*H*-chromene-3-carboxamide (5.16e).

The white compound was obtained from 2-oxo-2*H*-chromene-3-carbonyl chloride (**5.8e**, 0.2 g, 0.96 mmol) and 3-aminobenzenesulfonamide (**5.3i**, 0.17 g, 0.96 mmol) by following the experimental conditions described for **5.9a** (0.248 g, 75% yield):

^1H NMR (400 MHz, DMSO- d_6): δ = 7.43 (m, 3H), 7.60 (m, 3H), 7.80 (1H, t, J = 8.3 Hz), 7.90 (1H, d, J =6.7 Hz), 8.03 (1H, d, J =7.7 Hz), 8.29 (s, 1H), 8.91 (s, 1H), 10.87 ppm (s, 1H).

^{13}C NMR (100 MHz, DMSO- d_6): δ = 116.76, 117.38, 118.88, 120.51, 121.76, 123.33, 125.79, 130.22, 130.79, 134.85, 138.78, 145.34, 147.91, 154.39, 160.65, 160.85 ppm.

HRMS (ESI): m/z calcd for $\text{C}_{16}\text{H}_{12}\text{N}_2\text{O}_5\text{S}$ $[M+\text{Na}]^+$: 367.3292, found: 367.3224.



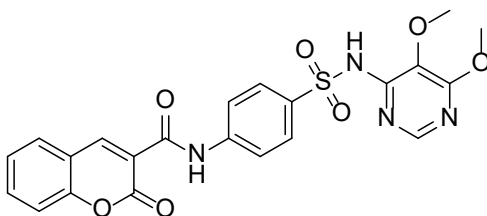
6-Methoxy-2-oxo-*N*-(3-sulfamoylphenyl)-2*H*-chromene-3-carboxamide (5.16f).

The white compound was obtained from 2-oxo-2*H*-chromene-3-carbonyl chloride (**5.8f**, 0.2 g, 0.84 mmol) and 3-aminobenzenesulfonamide (**5.3i**, 0.145 g, 0.96 mmol) by following the experimental conditions described for **5.9a** (0.211 g, 69% yield):

¹H NMR (400 MHz, DMSO-*d*₆): δ= 3.85 (s, 3H), 7.43 (m, 3H), 7.50 (1H, t, *J*=8.9 Hz), 7.60 (m, 3H), 7.89 (1H, t, *J*=8.7 Hz), 8.30 (s, 1H), 8.88 (s, 1H), 10.91 ppm (s, 1H).

¹³C NMR (100 MHz, DMSO-*d*₆): δ= 56.35, 112.35, 117.36, 117.91, 119.36, 120.49, 121.76, 122.80, 123.34, 130.22, 138.76, 145.34, 147.87, 148.92, 156.54, 160.87 ppm.

HRMS (ESI): *m/z* calcd for C₁₇H₁₄N₂O₆S [*M*+Na]⁺: 397.3553, found: 397.3492.



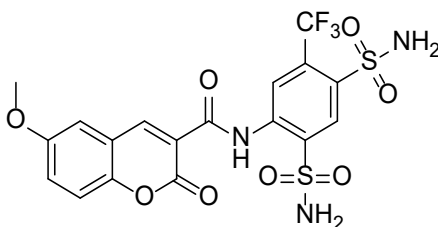
***N*-(4-(*N*-(5,6-dimethoxypyrimidin-4-yl)sulfamoyl)phenyl)-2-oxo-2*H*-chromene-3-carboxamide (**5.17e**).**

The white compound was obtained from 2-oxo-2*H*-chromene-3-carbonyl chloride (**5.8e**, 0.2 g, 0.96 mmol) and sulfadoxin (**5.3b**, 0.298 g, 0.96 mmol) by following the experimental conditions described for **5.9a** (0.299 g, 64% yield):

¹H NMR (400 MHz, DMSO-*d*₆): δ= 3.71 (s, 3H), 3.91 (s, 3H), 7.49 (1H, t, *J*=7.4 Hz), 7.57 (1H, d, *J*=8.4 Hz), 7.79 (1H, t, *J*=7.7 Hz), 7.93 (2H, d, *J*=8.7 Hz), 8.01 (3H, d, *J*=8.7 Hz), 8.13 (s, 1H), 8.91 (s, 1H), 10.93 (s, 1H), 11.11 ppm (s, 1H).

¹³C NMR (100 MHz, DMSO-*d*₆): δ= 54.52, 60.70, 116.75, 118.85, 119.91, 120.37, 125.80, 127.75, 129.37, 130.83, 134.93, 136.02, 142.24, 148.13, 150.78, 151.07, 154.41, 160.60, 161.05, 162.09 ppm.

HRMS (ESI): m/z calcd for $C_{22}H_{18}N_4O_7S$ $[M+Na]^+$: 505.4531, found: 505.4510.



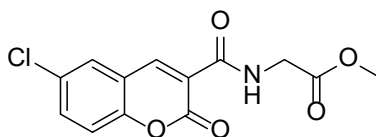
***N*-(2,4-disulfamoyl-5-(trifluoromethyl)phenyl)-6-methoxy-2-oxo-2*H*-chromene-3-carboxamide (5.18f).**

The yellow compound was obtained from 2-oxo-2*H*-chromene-3-carbonyl chloride (**5.8f**, 0.2 g, 0.84 mmol) and 4-amino-6-(trifluoromethyl)benzene-1,3-disulfonamide (**5.3j**, 0.268 g, 0.96 mmol) by following the experimental conditions described for **5.9a** (0.217 g, 49% yield):

^1H NMR (400 MHz, DMSO- d_6): δ = 3.85 (s, 3H), 7.43 (1H, dd, J =8.9, 2.6 Hz), 7.55 (1H, d, J =9.0 Hz), 7.64 (1H, d, J =2.6 Hz), 7.89 (m, 4H), 8.66 (s, 1H), 8.86 (s, 1H), 9.06 (s, 1H) 11.54 ppm (s, 1H).

^{13}C NMR (100 MHz, DMSO- d_6): δ = 56.34, 117.11, 118.71, 119.28, 120.47, 121.63, 123.12, 125.96, 130.75, 131.19, 135.07, 139.89, 143.42, 147.16, 156.39, 160.25, 160.89 ppm.

HRMS (ESI): m/z calcd for $C_{18}H_{14}F_3N_3O_8S_2$ $[M+Na]^+$: 544.4306, found: 544.4283.



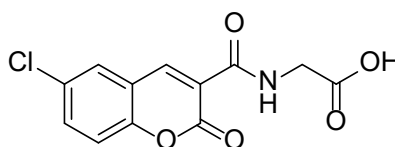
Methyl (6-chloro-2-oxo-2*H*-chromene-3-carbonyl)glycinate (5.19).

6-Chloro-2-oxo-2*H*-chromene-3-carboxylic acid (**5.7b**, 0.2 g, 0.89 mmol) was added to a solution of glycine methyl ester hydrochloride (0.123 g, 0.95 mmol) and TEA in dichloromethane. The reaction was stirred for 10 min and SOCl₂ (0.07 mL, 0.89 mmol) was added at room temperature and the mixture was stirred for 20 minutes. The reaction solution was extracted with dichloromethane, the organic layer washed with brine and dried over sodium sulfate, the solvent was removed in vacuo to the title compound as a yellow powder (0.239 g, 91% yield):

¹H NMR (400 MHz, DMSO-*d*₆): δ= 3.67 (s, 3H), 4.15 (1H, d, *J*=5.6 Hz), 7.57 (1H, d, *J*=8.8 Hz), 7.81 (1H, dd, *J*=8.8, 2.2 Hz), 8.16 (1H, d, *J*=2.2 Hz), 8.88 (s, 1H), 9.07 ppm (1H, t, *J*=7.1 Hz).

¹³C NMR (100 MHz, DMSO-*d*₆): δ= 41.88, 52.34, 118.68, 119.79, 120.26, 129.28, 129.71, 134.17, 147.45, 143.11, 160.32, 161.62, 170.33 ppm.

HRMS (ESI): *m/z* calcd for C₁₃H₁₀ClNO₅ [*M*+Na]⁺: 318.6637, found: 318.6619.



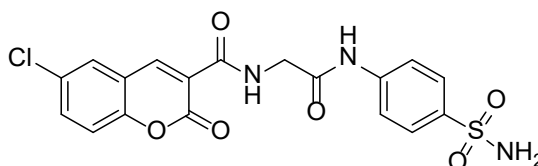
(6-chloro-2-oxo-2*H*-chromene-3-carbonyl) glycine (5.20**).**

The white compound was obtained from methyl (6-chloro-2-oxo-2*H*-chromene-3-carbonyl) glycinate (**5.19**) by following the experimental conditions described for **5.7a** (0.217 g, 89% yield):

¹H NMR (400 MHz, DMSO-*d*₆): δ= 4.15 (1H, d, *J*=5.6 Hz), 7.56 (1H, dd, *J*=8.8, 2 Hz), 7.77 (1H, dd, *J*=8.8, 2 Hz), 8.14 (1H, d, *J*=2.5 Hz), 8.88 (s, 1H), 9.01 (s, 1H), 12.82 ppm (br, 1H).

^{13}C NMR (100 MHz, DMSO- d_6): δ = 41.88, 52.34, 118.68, 119.79, 120.26, 129.28, 129.71, 134.17, 147.45, 143.11, 160.32, 161.62, 170.33 ppm.

HRMS (ESI): m/z calcd for $\text{C}_{12}\text{H}_8\text{ClNO}_5$ [$M+\text{Na}$] $^+$: 304.6369, found: 304.6388.



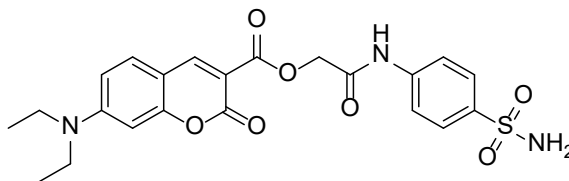
6-Chloro-2-oxo-*N*-(2-oxo-2-((4-sulfamoylphenyl)amino)ethyl)-2*H*-chromene-3-carboxamide (5.21).

To a solution of (6-chloro-2-oxo-2*H*-chromene-3-carbonyl) glycine (**5.20**, 0.2 g, 0.71 mmol), EDC (0.132 g, 0.85 mmol), HOBt·H₂O (0.115 g, 0.85 mmol) and triethylamine (0.5 mL) in DMF (7 mL) was added sulfanilamide (**5.3a**, 0.122 g, 0.71 mmol). The solution was stirred at room temperature for 12 h. Water (5 mL) was added to the solution with few drops of 6N HCl and the resulting solid was filtered off and washed with water and air dried to yield a white powder (0.208 g, 67% yield).

^1H NMR (400 MHz, DMSO- d_6): δ = 3.85 (s, 2H), 7.48 (s, 2H), 7.61 (1H, d, J =8.8 Hz), 7.78 (m, 4H), 7.89 (2H, d, J =8.8 Hz), 8.14 (1H, d, J =2.5 Hz), 8.82 (s, 1H), 10.86 ppm (s, 1H).

^{13}C NMR (100 MHz, DMSO- d_6): δ = 44.20, 117.55, 119.69, 120.45, 121.79, 126.53, 128.46, 130.21, 135.77, 139.81, 141.15, 146.63, 153.89, 160.11, 165.12 ppm.

HRMS (ESI): m/z calcd for $\text{C}_{18}\text{H}_{14}\text{ClN}_3\text{O}_6\text{S}$ [$M+\text{Na}$] $^+$: 458.8246, found: 458.8233.



2-Oxo-2-((4-sulfamoylphenyl)amino)ethyl-7-(diethylamino)-2-oxo-2H-chromene-3-carboxylate (5.22).

To a solution of ethyl 7-(diethylamino)-2-oxo-2H-chromene-3-carboxylate (**5.2g**, 0.2 g, 0.77 mmol) in dry DMF (15 mL), anhydrous K₂CO₃ (0.18 g, 1.28 mmol) was added. The mixture was stirred for 15 mins at 70-80 °C and 2-chloro-*N*-(4-sulfamoylphenyl) acetamide (**5.4a**, 0.21 g, 0.85 mmol) was added, followed by a pinch of KI, and heated overnight. Water (10 mL) was added to the reaction mixture, followed by 1 mL 6N HCl. The resulting solid was filtered, washed with water and air dried, and purification by flash column chromatography (hexane/EtOAc 20:1) afforded the title compound as a yellow powder (0.198 g, 54% yield):

¹H NMR (400 MHz, DMSO-*d*₆): δ= 1.15 (3H, t, *J*=6.8 Hz), 3.50 (q, 4H), 4.88 (s, 2H), 6.58 (s, 1H), 6.82 (1H, d, *J*=8.3 Hz), 7.27 (s, 1H), 7.70 (1H, d, *J*=9.0 Hz), 7.79 (s, 4H), 8.19 (br, 1H), 8.68 (s, 1H), 10.53 ppm (s, 1H).

¹³C NMR (100 MHz, DMSO-*d*₆): δ= 12.81, 44.89, 63.26, 96.34, 106.62, 107.58, 110.54, 119.25, 127.28, 132.50, 139.21, 141.83, 146.88, 153.65, 157.85, 162.86, 163.46, 165.61 ppm.

HRMS (ESI): *m/z* calcd for C₂₂H₂₃N₃O₇S [*M*+Na]⁺: 496.4863, found: 496.4745.

Chapter 6. References.

1. Garcia, M. C.; Rossen, L. M.; Bastian, B.; Faul, M.; Dowling, N. F.; Thomas, C. C.; Schieb, L.; Hong, Y.; Yoon, P. W.; Iademarco, M. F., Potentially Excess Deaths from the Five Leading Causes of Death in Metropolitan and Nonmetropolitan Counties - United States, 2010-2017. *MMWR Surveill Summ* **2019**, *68* (10), 1-11.
2. Siegel, R. L.; Miller, K. D.; Jemal, A., Cancer statistics, 2020. *CA Cancer J Clin* **2020**, *70* (1), 7-30.
3. Anand, P.; Kunnumakkara, A. B.; Sundaram, C.; Harikumar, K. B.; Tharakan, S. T.; Lai, O. S.; Sung, B.; Aggarwal, B. B., Cancer is a preventable disease that requires major lifestyle changes. *Pharm Res* **2008**, *25* (9), 2097-116.
4. Hanahan, D.; Weinberg, R. A., The hallmarks of cancer. *Cell* **2000**, *100* (1), 57-70.
5. Zeigler-Johnson, C. M.; Rennert, H.; Mittal, R. D.; Jalloh, M.; Sachdeva, R.; Malkowicz, S. B.; Mandhani, A.; Mittal, B.; Gueye, S. M.; Rebbeck, T. R., Evaluation of prostate cancer characteristics in four populations worldwide. *Can J Urol* **2008**, *15* (3), 4056-64.
6. Haas, G. P.; Delongchamps, N.; Brawley, O. W.; Wang, C. Y.; de la Roza, G., The worldwide epidemiology of prostate cancer: perspectives from autopsy studies. *Can J Urol* **2008**, *15* (1), 3866-71.
7. Arruebo, M.; Vilaboa, N.; Saez-Gutierrez, B.; Lambea, J.; Tres, A.; Valladares, M.; Gonzalez-Fernandez, A., Assessment of the evolution of cancer treatment therapies. *Cancers (Basel)* **2011**, *3* (3), 3279-330.
8. Waldman, A. D.; Fritz, J. M.; Lenardo, M. J., A guide to cancer immunotherapy: from T cell basic science to clinical practice. *Nat Rev Immunol* **2020**.

9. Kalyanaraman, B., Teaching the basics of cancer metabolism: Developing antitumor strategies by exploiting the differences between normal and cancer cell metabolism. *Redox Biol* **2017**, *12*, 833-842.
10. Luengo, A.; Gui, D. Y.; Vander Heiden, M. G., Targeting Metabolism for Cancer Therapy. *Cell Chem Biol* **2017**, *24* (9), 1161-1180.
11. Jang, M.; Kim, S. S.; Lee, J., Cancer cell metabolism: implications for therapeutic targets. *Exp Mol Med* **2013**, *45*, e45.
12. Vander Heiden, M. G., Targeting cancer metabolism: a therapeutic window opens. *Nat Rev Drug Discov* **2011**, *10* (9), 671-84.
13. Elion, G. B., The purine path to chemotherapy. *Science* **1989**, *244* (4900), 41-7.
14. Sborov, D. W.; Haverkos, B. M.; Harris, P. J., Investigational cancer drugs targeting cell metabolism in clinical development. *Expert Opin Investig Drugs* **2015**, *24* (1), 79-94.
15. Tennant, D. A.; Duran, R. V.; Gottlieb, E., Targeting metabolic transformation for cancer therapy. *Nat Rev Cancer* **2010**, *10* (4), 267-77.
16. Foretz, M.; Hebrard, S.; Leclerc, J.; Zarrinpashneh, E.; Soty, M.; Mithieux, G.; Sakamoto, K.; Andreelli, F.; Viollet, B., Metformin inhibits hepatic gluconeogenesis in mice independently of the LKB1/AMPK pathway via a decrease in hepatic energy state. *J Clin Invest* **2010**, *120* (7), 2355-69.
17. Cluntun, A. A.; Lukey, M. J.; Cerione, R. A.; Locasale, J. W., Glutamine Metabolism in Cancer: Understanding the Heterogeneity. *Trends Cancer* **2017**, *3* (3), 169-180.
18. Jones, N. P.; Schulze, A., Targeting cancer metabolism--aiming at a tumour's sweet-spot. *Drug Discov Today* **2012**, *17* (5-6), 232-41.

19. Zhang, D.; Li, J.; Wang, F.; Hu, J.; Wang, S.; Sun, Y., 2-Deoxy-D-glucose targeting of glucose metabolism in cancer cells as a potential therapy. *Cancer Lett* **2014**, *355* (2), 176-83.
20. Aft, R. L.; Zhang, F. W.; Gius, D., Evaluation of 2-deoxy-D-glucose as a chemotherapeutic agent: mechanism of cell death. *Br J Cancer* **2002**, *87* (7), 805-12.
21. Murphy, M. P.; Hartley, R. C., Mitochondria as a therapeutic target for common pathologies. *Nat Rev Drug Discov* **2018**, *17* (12), 865-886.
22. Jiang, X.; Li, L.; Ying, Z.; Pan, C.; Huang, S.; Li, L.; Dai, M.; Yan, B.; Li, M.; Jiang, H.; Chen, S.; Zhang, Z.; Wang, X., A Small Molecule That Protects the Integrity of the Electron Transfer Chain Blocks the Mitochondrial Apoptotic Pathway. *Mol Cell* **2016**, *63* (2), 229-239.
23. Wang, H.; Huwaimel, B.; Verma, K.; Miller, J.; Germain, T. M.; Kinarivala, N.; Pappas, D.; Brookes, P. S.; Trippier, P. C., Synthesis and Antineoplastic Evaluation of Mitochondrial Complex II (Succinate Dehydrogenase) Inhibitors Derived from Atpenin A5. *ChemMedChem* **2017**, *12* (13), 1033-1044.
24. Modica-Napolitano, J. S.; Weissig, V., Treatment Strategies that Enhance the Efficacy and Selectivity of Mitochondria-Targeted Anticancer Agents. *Int J Mol Sci* **2015**, *16* (8), 17394-421.
25. Simon, H. U.; Haj-Yehia, A.; Levi-Schaffer, F., Role of reactive oxygen species (ROS) in apoptosis induction. *Apoptosis* **2000**, *5* (5), 415-8.
26. Ray, P. D.; Huang, B. W.; Tsuji, Y., Reactive oxygen species (ROS) homeostasis and redox regulation in cellular signaling. *Cell Signal* **2012**, *24* (5), 981-90.
27. Turrens, J. F., Mitochondrial formation of reactive oxygen species. *J Physiol* **2003**, *552* (Pt 2), 335-44.
28. Yang, Y.; Karakhanova, S.; Werner, J.; Bazhin, A. V., Reactive oxygen species in cancer biology and anticancer therapy. *Curr Med Chem* **2013**, *20* (30), 3677-92.

29. Ramsay, E. E.; Hogg, P. J.; Dilda, P. J., Mitochondrial metabolism inhibitors for cancer therapy. *Pharm Res* **2011**, *28* (11), 2731-44.
30. Sun, F.; Huo, X.; Zhai, Y.; Wang, A.; Xu, J.; Su, D.; Bartlam, M.; Rao, Z., Crystal structure of mitochondrial respiratory membrane protein complex II. *Cell* **2005**, *121* (7), 1043-57.
31. Kluckova, K.; Bezawork-Geleta, A.; Rohlena, J.; Dong, L.; Neuzil, J., Mitochondrial complex II, a novel target for anti-cancer agents. *Biochim Biophys Acta* **2013**, *1827* (5), 552-64.
32. Ernster, L.; Dallner, G., Biochemical, physiological and medical aspects of ubiquinone function. *Biochim Biophys Acta* **1995**, *1271* (1), 195-204.
33. Rohlena, J.; Dong, L. F.; Ralph, S. J.; Neuzil, J., Anticancer drugs targeting the mitochondrial electron transport chain. *Antioxid Redox Signal* **2011**, *15* (12), 2951-74.
34. Selak, M. A.; Armour, S. M.; MacKenzie, E. D.; Boulahbel, H.; Watson, D. G.; Mansfield, K. D.; Pan, Y.; Simon, M. C.; Thompson, C. B.; Gottlieb, E., Succinate links TCA cycle dysfunction to oncogenesis by inhibiting HIF- α prolyl hydroxylase. *Cancer Cell* **2005**, *7* (1), 77-85.
35. Correia, S. C.; Carvalho, C.; Cardoso, S.; Santos, R. X.; Santos, M. S.; Oliveira, C. R.; Perry, G.; Zhu, X.; Smith, M. A.; Moreira, P. I., Mitochondrial preconditioning: a potential neuroprotective strategy. *Front Aging Neurosci* **2010**, *2*.
36. Peczkowska, M.; Cascon, A.; Prejbisz, A.; Kubaszek, A.; Cwikla, B. J.; Furmanek, M.; Erlic, Z.; Eng, C.; Januszewicz, A.; Neumann, H. P., Extra-adrenal and adrenal pheochromocytomas associated with a germline SDHC mutation. *Nat Clin Pract Endocrinol Metab* **2008**, *4* (2), 111-5.
37. Baysal, B. E.; Ferrell, R. E.; Willett-Brozick, J. E.; Lawrence, E. C.; Myssiorek, D.; Bosch, A.; van der Mey, A.; Taschner, P. E.; Rubinstein, W. S.; Myers, E. N.; Richard, C. W., 3rd; Cornelisse, C. J.; Devilee, P.; Devlin, B., Mutations in SDHD, a

mitochondrial complex II gene, in hereditary paraganglioma. *Science* **2000**, *287* (5454), 848-51.

38. Janeway, K. A.; Kim, S. Y.; Lodish, M.; Nose, V.; Rustin, P.; Gaal, J.; Dahia, P. L.; Liegl, B.; Ball, E. R.; Raygada, M.; Lai, A. H.; Kelly, L.; Hornick, J. L.; Pediatric, N. I. H.; Wild-Type, G. C.; O'Sullivan, M.; de Krijger, R. R.; Dinjens, W. N.; Demetri, G. D.; Antonescu, C. R.; Fletcher, J. A.; Helman, L.; Stratakis, C. A., Defects in succinate dehydrogenase in gastrointestinal stromal tumors lacking KIT and PDGFRA mutations. *Proc Natl Acad Sci U S A* **2011**, *108* (1), 314-8.

39. Kluckova, K.; Sticha, M.; Cerny, J.; Mracek, T.; Dong, L.; Drahota, Z.; Gottlieb, E.; Neuzil, J.; Rohlena, J., Ubiquinone-binding site mutagenesis reveals the role of mitochondrial complex II in cell death initiation. *Cell Death Dis* **2015**, *6*, e1749.

40. Tomitsuka, E.; Kita, K.; Esumi, H., An anticancer agent, pyrvinium pamoate inhibits the NADH-fumarate reductase system--a unique mitochondrial energy metabolism in tumour microenvironments. *J Biochem* **2012**, *152* (2), 171-83.

41. Chen, Y.; McMillan-Ward, E.; Kong, J.; Israels, S. J.; Gibson, S. B., Mitochondrial electron-transport-chain inhibitors of complexes I and II induce autophagic cell death mediated by reactive oxygen species. *J Cell Sci* **2007**, *120* (Pt 23), 4155-66.

42. Fulda, S., Tumor resistance to apoptosis. *Int J Cancer* **2009**, *124* (3), 511-5.

43. Neuzil, J.; Dyason, J. C.; Freeman, R.; Dong, L. F.; Prochazka, L.; Wang, X. F.; Scheffler, I.; Ralph, S. J., Mitocans as anti-cancer agents targeting mitochondria: lessons from studies with vitamin E analogues, inhibitors of complex II. *J Bioenerg Biomembr* **2007**, *39* (1), 65-72.

44. Ralph, S. J.; Low, P.; Dong, L.; Lawen, A.; Neuzil, J., Mitocans: mitochondrial targeted anti-cancer drugs as improved therapies and related patent documents. *Recent Pat Anticancer Drug Discov* **2006**, *1* (3), 327-46.

45. Zhuang, J.; Dinsdale, D.; Cohen, G. M., Apoptosis, in human monocytic THP.1 cells, results in the release of cytochrome c from mitochondria prior to their ultracondensation, formation of outer membrane discontinuities and reduction in inner membrane potential. *Cell Death Differ* **1998**, 5 (11), 953-62.
46. Brookes, P. S.; Digerness, S. B.; Parks, D. A.; Darley-Usmar, V., Mitochondrial function in response to cardiac ischemia-reperfusion after oral treatment with quercetin. *Free Radic Biol Medi* **2002**, 32 (11), 1220-8.
47. Halestrap, A. P.; Clarke, S. J.; Javadov, S. A., Mitochondrial permeability transition pore opening during myocardial reperfusion--a target for cardioprotection. *Cardiovasc Res* **2004**, 61 (3), 372-85.
48. Chouchani, E. T.; Pell, V. R.; Gaude, E.; Aksentijevic, D.; Sundier, S. Y.; Robb, E. L.; Logan, A.; Nadtochiy, S. M.; Ord, E. N.; Smith, A. C.; Eyassu, F.; Shirley, R.; Hu, C. H.; Dare, A. J.; James, A. M.; Rogatti, S.; Hartley, R. C.; Eaton, S.; Costa, A. S.; Brookes, P. S.; Davidson, S. M.; Duchon, M. R.; Saeb-Parsy, K.; Shattock, M. J.; Robinson, A. J.; Work, L. M.; Frezza, C.; Krieg, T.; Murphy, M. P., Ischaemic accumulation of succinate controls reperfusion injury through mitochondrial ROS. *Nature* **2014**, 515 (7527), 431-5.
49. Valls-Lacalle, L.; Barba, I.; Miro-Casas, E.; Alburquerque-Bejar, J. J.; Ruiz-Meana, M.; Fuertes-Agudo, M.; Rodriguez-Sinovas, A.; Garcia-Dorado, D., Succinate dehydrogenase inhibition with malonate during reperfusion reduces infarct size by preventing mitochondrial permeability transition. *Cardiovasc Res* **2016**, 109 (3), 374-84.
50. Galina, A., Mitochondria: 3-bromopyruvate vs. mitochondria? A small molecule that attacks tumors by targeting their bioenergetic diversity. *Int J Biochem Cell Biol* **2014**, 54, 266-271.

51. Rodrigues-Ferreira, C.; da Silva, A. P.; Galina, A., Effect of the antitumoral alkylating agent 3-bromopyruvate on mitochondrial respiration: role of mitochondrially bound hexokinase. *J Bioenerg Biomembr* **2012**, *44* (1), 39-49.
52. Ko, Y. H.; Smith, B. L.; Wang, Y.; Pomper, M. G.; Rini, D. A.; Torbenson, M. S.; Hullihen, J.; Pedersen, P. L., Advanced cancers: eradication in all cases using 3-bromopyruvate therapy to deplete ATP. *Biochem Biophys Res Commun* **2004**, *324* (1), 269-75.
53. Ko, Y. H.; Niedzwiecka, K.; Casal, M.; Pedersen, P. L.; Ulaszewski, S., 3-Bromopyruvate as a potent anticancer therapy in honor and memory of the late Professor Andre Goffeau. *Yeast* **2019**, *36* (4), 211-221.
54. Wojtovich, A. P.; Brookes, P. S., The endogenous mitochondrial complex II inhibitor malonate regulates mitochondrial ATP-sensitive potassium channels: implications for ischemic preconditioning. *Biochim Biophys Acta* **2008**, *1777* (7-8), 882-9.
55. Kim, Y. S., Malonate metabolism: biochemistry, molecular biology, physiology, and industrial application. *J Biochem Mol Biol* **2002**, *35* (5), 443-51.
56. Anastacio, M. M.; Kanter, E. M.; Keith, A. D.; Schuessler, R. B.; Nichols, C. G.; Lawton, J. S., Inhibition of Succinate Dehydrogenase by Diazoxide Is Independent of the ATP-Sensitive Potassium Channel Subunit Sulfonylurea Type 1 Receptor. *J Am Coll Surg* **2013**, *216* (6), 1144-9.
57. Valls-Lacalle, L.; Barba, I.; Miro-Casas, E.; Ruiz-Meana, M.; Rodriguez-Sinovas, A.; Garcia-Dorado, D., Selective Inhibition of Succinate Dehydrogenase in Reperfused Myocardium with Intracoronary Malonate Reduces Infarct Size. *Sci Rep* **2018**, *8* (1), 2442.
58. Gruber, J.; Staniek, K.; Krewenka, C.; Moldzio, R.; Patel, A.; Bohmdorfer, S.; Rosenau, T.; Gille, L., Tocopheramine succinate and tocopheryl succinate: mechanism of mitochondrial inhibition and superoxide radical production. *Bioorg Med Chem* **2014**, *22* (2), 684-91.

59. Neuzil, J.; Dyason, J. C.; Freeman, R.; Dong, L. F.; Prochazka, L.; Wang, X. F.; Scheffler, I.; Ralph, S. J., Mitocans as anti-cancer agents targeting mitochondria: lessons from studies with vitamin E analogues, inhibitors of complex II. *J Bioenerg Biomembr* **2007**, 39 (1), 65-72.
60. Gu, X.; Schwartz, J. L.; Pang, X.; Zhou, Y.; Sirois, D. A.; Sridhar, R., Cytotoxicity of liposomal alpha-tocopheryl succinate towards hamster cheek pouch carcinoma (HCPC-1) cells in culture. *Cancer letters* **2006**, 239 (2), 281-91.
61. Malafa, M. P.; Neitzel, L. T., Vitamin E succinate promotes breast cancer tumor dormancy. *J Surg Res* **2000**, 93 (1), 163-70.
62. Malafa, M. P.; Fokum, F. D.; Mowlavi, A.; Abusief, M.; King, M., Vitamin E inhibits melanoma growth in mice. *Surgery* **2002**, 131 (1), 85-91.
63. Quin, J.; Engle, D.; Litwiller, A.; Peralta, E.; Grasc, A.; Boley, T.; Hazelrigg, S., Vitamin E succinate decreases lung cancer tumor growth in mice. *J Surg Res* **2005**, 127 (2), 139-43.
64. Zhang, M.; Altuwaijri, S.; Yeh, S., RRR-alpha-tocopheryl succinate inhibits human prostate cancer cell invasiveness. *Oncogene* **2004**, 23 (17), 3080-8.
65. Neuzil, J.; Dong, L. F.; Rohlena, J.; Truksa, J.; Ralph, S. J., Classification of mitocans, anti-cancer drugs acting on mitochondria. *Mitochondrion* **2013**, 13 (3), 199-208.
66. Dong, L. F.; Jameson, V. J.; Tilly, D.; Cerny, J.; Mahdavian, E.; Marin-Hernandez, A.; Hernandez-Esquivel, L.; Rodriguez-Enriquez, S.; Stursa, J.; Witting, P. K.; Stantic, B.; Rohlena, J.; Truksa, J.; Kluckova, K.; Dyason, J. C.; Ledvina, M.; Salvatore, B. A.; Moreno-Sanchez, R.; Coster, M. J.; Ralph, S. J.; Smith, R. A.; Neuzil, J., Mitochondrial targeting of vitamin E succinate enhances its pro-apoptotic and anti-cancer activity via mitochondrial complex II. *J. Biol. Chem* **2011**, 286 (5), 3717-28.
67. Murphy, M. P.; Smith, R. A., Targeting antioxidants to mitochondria by conjugation to lipophilic cations. *Annu. Rev Pharmacol Toxicol* **2007**, 47, 629-56.

68. Nadanaciva, S.; Bernal, A.; Aggeler, R.; Capaldi, R.; Will, Y., Target identification of drug induced mitochondrial toxicity using immunocapture based OXPHOS activity assays. *Toxicol In Vitro* **2007**, *21* (5), 902-11.
69. Zhang, J. G.; Tirmenstein, M. A.; Nicholls-Grzemeski, F. A.; Fariss, M. W., Mitochondrial electron transport inhibitors cause lipid peroxidation-dependent and -independent cell death: protective role of antioxidants. *Arch Biochem Biophys* **2001**, *393* (1), 87-96.
70. Zhang, J. G.; Fariss, M. W., Thenoyltrifluoroacetone, a potent inhibitor of carboxylesterase activity. *Biochem Pharmacol* **2002**, *63* (4), 751-4.
71. Nath, K.; Guo, L.; Nancolas, B.; Nelson, D. S.; Shestov, A. A.; Lee, S. C.; Roman, J.; Zhou, R.; Leeper, D. B.; Halestrap, A. P.; Blair, I. A.; Glickson, J. D., Mechanism of antineoplastic activity of lonidamine. *Biochim Biophys Acta* **2016**, *1866* (2), 151-162.
72. Liu, Y.; Zhang, X.; Zhou, M.; Nan, X.; Chen, X.; Zhang, X., Mitochondrial-Targeting Lonidamine-Doxorubicin Nanoparticles for Synergistic Chemotherapy to Conquer Drug Resistance. *ACS Appl Mater Interfaces* **2017**, *9* (50), 43498-43507.
73. De Lena, M.; Lorusso, V.; Latorre, A.; Fanizza, G.; Gargano, G.; Caporusso, L.; Guida, M.; Catino, A.; Crucitta, E.; Sambiasi, D.; Mazzei, A., Paclitaxel, cisplatin and lonidamine in advanced ovarian cancer. A phase II study. *Eur J Cancer* **2001**, *37* (3), 364-8.
74. Price, G. S.; Page, R. L.; Riviere, J. E.; Cline, J. M.; Thrall, D. E., Pharmacokinetics and toxicity of oral and intravenous lonidamine in dogs. *Cancer Chemother Pharmacol* **1996**, *38* (2), 129-35.
75. Guo, L.; Shestov, A. A.; Worth, A. J.; Nath, K.; Nelson, D. S.; Leeper, D. B.; Glickson, J. D.; Blair, I. A., Inhibition of Mitochondrial Complex II by the Anticancer Agent Lonidamine. *J Biol Chem* **2016**, *291* (1), 42-57.

76. Dzeja, P. P.; Bast, P.; Ozcan, C.; Valverde, A.; Holmuhamedov, E. L.; Van Wylen, D. G.; Terzic, A., Targeting nucleotide-requiring enzymes: implications for diazoxide-induced cardioprotection. *Am J Physiol Heart Circ Physiol* **2003**, *284* (4), H1048-56.
77. Ralph, S. J.; Moreno-Sanchez, R.; Neuzil, J.; Rodriguez-Enriquez, S., Inhibitors of succinate: quinone reductase/Complex II regulate production of mitochondrial reactive oxygen species and protect normal cells from ischemic damage but induce specific cancer cell death. *Pharm Res* **2011**, *28* (11), 2695-730.
78. Kakei, M.; Nakazaki, M.; Kamisaki, T.; Nagayama, I.; Fukamachi, Y.; Tanaka, H., Inhibition of the ATP-sensitive potassium channel by class I antiarrhythmic agent, cibenzoline, in rat pancreatic beta-cells. *Br J Pharmacol* **1993**, *109* (4), 1226-31.
79. Gill, G. V.; Rauf, O.; MacFarlane, I. A., Diazoxide treatment for insulinoma: a national UK survey. *Postgrad Med J* **1997**, *73* (864), 640-1.
80. Nielsen, F. E.; Bodvarsdottir, T. B.; Worsaae, A.; MacKay, P.; Stidsen, C. E.; Boonen, H. C.; Pridal, L.; Arkhammar, P. O.; Wahl, P.; Ynddal, L.; Junager, F.; Dragsted, N.; Tagmose, T. M.; Mogensen, J. P.; Koch, A.; Treppendahl, S. P.; Hansen, J. B., 6-Chloro-3-alkylamino-4H-thieno[3,2-e]-1,2,4-thiadiazine 1,1-dioxide derivatives potently and selectively activate ATP sensitive potassium channels of pancreatic beta-cells. *J Med Chem* **2002**, *45* (19), 4171-87.
81. Pasdois, P.; Beauvoit, B.; Tariosse, L.; Vinassa, B.; Bonoron-Adele, S.; Dos Santos, P., Effect of diazoxide on flavoprotein oxidation and reactive oxygen species generation during ischemia-reperfusion: a study on Langendorff-perfused rat hearts using optic fibers. *Am J Physiol Heart Circ Physiol* **2008**, *294* (5), H2088-97.
82. Kis, B.; Rajapakse, N. C.; Snipes, J. A.; Nagy, K.; Horiguchi, T.; Busija, D. W., Diazoxide induces delayed pre-conditioning in cultured rat cortical neurons. *J Neurochem* **2003**, *87* (4), 969-80.

83. Busija, D. W.; Gaspar, T.; Domoki, F.; Katakam, P. V.; Bari, F., Mitochondrial-mediated suppression of ROS production upon exposure of neurons to lethal stress: mitochondrial targeted preconditioning. *Adv Drug Deliv Rev* **2008**, *60* (13-14), 1471-7.
84. Liu, D.; Pitta, M.; Lee, J. H.; Ray, B.; Lahiri, D. K.; Furukawa, K.; Mughal, M.; Jiang, H.; Villarreal, J.; Cutler, R. G.; Greig, N. H.; Mattson, M. P., The KATP channel activator diazoxide ameliorates amyloid-beta and tau pathologies and improves memory in the 3xTgAD mouse model of Alzheimer's disease. *J Alzheimers Dis* **2010**, *22* (2), 443-57.
85. Wang, A.; Lim, H.; Cheng, S. Y.; Xie, L., ANTENNA, a Multi-Rank, Multi-Layered Recommender System for Inferring Reliable Drug-Gene-Disease Associations: Repurposing Diazoxide as a Targeted Anti-Cancer Therapy. *IEEE/ACM Trans Comput Biol Bioinform* **2018**, *15* (6), 1960-1967.
86. Kong, M.; Ba, M.; Liang, H.; Shao, P.; Yu, T.; Wang, Y., Regulation of adenosine triphosphate-sensitive potassium channels suppresses the toxic effects of amyloid-beta peptide (25-35). *Neural Regen Res* **2013**, *8* (1), 56-63.
87. Holmuhamedov, E.; Lewis, L.; Bienengraeber, M.; Holmuhamedova, M.; Jahangir, A.; Terzic, A., Suppression of human tumor cell proliferation through mitochondrial targeting. *FASEB J* **2002**, *16* (9), 1010-6.
88. Ding, J.; Ge, D.; Guo, W.; Lu, C., Diazoxide-mediated growth inhibition in human lung cancer cells via downregulation of beta-catenin-mediated cyclin D1 transcription. *Lung* **2009**, *187* (1), 61-7.
89. Miyadera, H.; Shiomi, K.; Ui, H.; Yamaguchi, Y.; Masuma, R.; Tomoda, H.; Miyoshi, H.; Osanai, A.; Kita, K.; Omura, S., Atpenins, potent and specific inhibitors of mitochondrial complex II (succinate-ubiquinone oxidoreductase). *Proc Natl Acad Sci U S A* **2003**, *100* (2), 473-7.

90. Siebels, I.; Drose, S., Q-site inhibitor induced ROS production of mitochondrial complex II is attenuated by TCA cycle dicarboxylates. *Biochimica et biophysica acta* **2013**, *1827* (10), 1156-64.
91. Kawada, M.; Momose, I.; Someno, T.; Tsujiuchi, G.; Ikeda, D., New atpenins, NBRI23477 A and B, inhibit the growth of human prostate cancer cells. *J Antibiot* **2009**, *62* (5), 243-6.
92. Kawada, M.; Inoue, H.; Ohba, S.; Masuda, T.; Momose, I.; Ikeda, D., Leucinstatin A inhibits prostate cancer growth through reduction of insulin-like growth factor-I expression in prostate stromal cells. *Int J Cancer* **2010**, *126* (4), 810-8.
93. Wojtovich, A. P.; Brookes, P. S., The complex II inhibitor atpenin A5 protects against cardiac ischemia-reperfusion injury via activation of mitochondrial KATP channels. *Basic Res Cardiol* **2009**, *104* (2), 121-9.
94. Folkman, J., Angiogenesis. *Annu Rev Med* **2006**, *57*, 1-18.
95. Carmeliet, P.; Jain, R. K., Angiogenesis in cancer and other diseases. *Nature* **2000**, *407* (6801), 249-57.
96. De Palma, M.; Biziato, D.; Petrova, T. V., Microenvironmental regulation of tumour angiogenesis. *Nat Rev Cancer* **2017**, *17* (8), 457-474.
97. Nussenbaum, F.; Herman, I. M., Tumor angiogenesis: insights and innovations. *J Oncol* **2010**, *2010*, 132641.
98. Morikawa, S.; Baluk, P.; Kaidoh, T.; Haskell, A.; Jain, R. K.; McDonald, D. M., Abnormalities in pericytes on blood vessels and endothelial sprouts in tumors. *Am J Pathol* **2002**, *160* (3), 985-1000.
99. Hanahan, D.; Weinberg, R. A., Hallmarks of cancer: the next generation. *Cell* **2011**, *144* (5), 646-74.
100. Bergers, G.; Benjamin, L. E., Tumorigenesis and the angiogenic switch. *Nat Rev Cancer* **2003**, *3* (6), 401-10.

101. Jayson, G. C.; Kerbel, R.; Ellis, L. M.; Harris, A. L., Antiangiogenic therapy in oncology: current status and future directions. *Lancet* **2016**, *388* (10043), 518-29.
102. Ferrara, N.; Kerbel, R. S., Angiogenesis as a therapeutic target. *Nature* **2005**, *438* (7070), 967-74.
103. Houck, K. A.; Leung, D. W.; Rowland, A. M.; Winer, J.; Ferrara, N., Dual regulation of vascular endothelial growth factor bioavailability by genetic and proteolytic mechanisms. *J Biol Chem* **1992**, *267* (36), 26031-7.
104. Chintalgattu, V.; Nair, D. M.; Katwa, L. C., Cardiac myofibroblasts: a novel source of vascular endothelial growth factor (VEGF) and its receptors Flt-1 and KDR. *J Mol Cell Cardiol* **2003**, *35* (3), 277-86.
105. Takahashi, S., Vascular endothelial growth factor (VEGF), VEGF receptors and their inhibitors for antiangiogenic tumor therapy. *Biol Pharm Bull* **2011**, *34* (12), 1785-8.
106. Olsson, A. K.; Dimberg, A.; Kreuger, J.; Claesson-Welsh, L., VEGF receptor signalling - in control of vascular function. *Nat Rev Mol Cell Biol* **2006**, *7* (5), 359-71.
107. Holmes, K.; Roberts, O. L.; Thomas, A. M.; Cross, M. J., Vascular endothelial growth factor receptor-2: structure, function, intracellular signalling and therapeutic inhibition. *Cell Signal* **2007**, *19* (10), 2003-12.
108. Lugano, R.; Ramachandran, M.; Dimberg, A., Tumor angiogenesis: causes, consequences, challenges and opportunities. *Cell Mol Life Sci* **2020**, *77* (9), 1745-1770.
109. Keating, G. M., Sorafenib: A Review in Hepatocellular Carcinoma. *Target Oncol* **2017**, *12* (2), 243-253.
110. Le Tourneau, C.; Raymond, E.; Faivre, S., Sunitinib: a novel tyrosine kinase inhibitor. A brief review of its therapeutic potential in the treatment of renal carcinoma and gastrointestinal stromal tumors (GIST). *Ther Clin Risk Manag* **2007**, *3* (2), 341-8.
111. Ramage, J. K.; Davies, A. H.; Ardill, J.; Bax, N.; Caplin, M.; Grossman, A.; Hawkins, R.; McNicol, A. M.; Reed, N.; Sutton, R.; Thakker, R.; Aylwin, S.; Breen, D.;

- Britton, K.; Buchanan, K.; Corrie, P.; Gillams, A.; Lewington, V.; McCance, D.; Meeran, K.; Watkinson, A.; Tumours, U. K. f. N., Guidelines for the management of gastroenteropancreatic neuroendocrine (including carcinoid) tumours. *Gut* **2005**, *54 Suppl* 4, iv1-16.
112. Al-Husein, B.; Abdalla, M.; Trepte, M.; Deremer, D. L.; Somanath, P. R., Antiangiogenic therapy for cancer: an update. *Pharmacotherapy* **2012**, *32* (12), 1095-111.
113. Kazazi-Hyseni, F.; Beijnen, J. H.; Schellens, J. H., Bevacizumab. *Oncologist* **2010**, *15* (8), 819-25.
114. Meadows, K. L.; Hurwitz, H. I., Anti-VEGF therapies in the clinic. *Cold Spring Harb Perspect Med* **2012**, *2* (10).
115. Singh, A. D.; Parmar, S., Ramucirumab (Cyramza): A Breakthrough Treatment for Gastric Cancer. *P T* **2015**, *40* (7), 430-68.
116. Gorski, D. H.; Beckett, M. A.; Jaskowiak, N. T.; Calvin, D. P.; Mauceri, H. J.; Salloum, R. M.; Seetharam, S.; Koons, A.; Hari, D. M.; Kufe, D. W.; Weichselbaum, R. R., Blockage of the vascular endothelial growth factor stress response increases the antitumor effects of ionizing radiation. *Cancer Res* **1999**, *59* (14), 3374-8.
117. Gridley, D. S.; Lored, L. N.; Slater, J. D.; Archambeau, J. O.; Bedros, A. A.; Andres, M. L.; Slater, J. M., Pilot evaluation of cytokine levels in patients undergoing radiotherapy for brain tumor. *Cancer Detect Prev* **1998**, *22* (1), 20-9.
118. Bayat Mokhtari, R.; Homayouni, T. S.; Baluch, N.; Morgatskaya, E.; Kumar, S.; Das, B.; Yeger, H., Combination therapy in combating cancer. *Oncotarget* **2017**, *8* (23), 38022-38043.
119. Correia, A.; Silva, D.; Correia, A.; Vilanova, M.; Gartner, F.; Vale, N., Study of New Therapeutic Strategies to Combat Breast Cancer Using Drug Combinations. *Biomolecules* **2018**, *8* (4).

120. Supuran, C. T., Carbonic anhydrases: novel therapeutic applications for inhibitors and activators. *Nat Rev Drug Discov* **2008**, 7 (2), 168-81.
121. Singh, S.; Lomelino, C. L.; Mboge, M. Y.; Frost, S. C.; McKenna, R., Cancer Drug Development of Carbonic Anhydrase Inhibitors beyond the Active Site. *Molecules* **2018**, 23 (5).
122. Kannan, K. K.; Notstrand, B.; Fridborg, K.; Lovgren, S.; Ohlsson, A.; Petef, M., Crystal structure of human erythrocyte carbonic anhydrase B. Three-dimensional structure at a nominal 2.2-A resolution. *Proc Natl Acad Sci U S A* **1975**, 72 (1), 51-5.
123. Lomelino, C. L.; Supuran, C. T.; McKenna, R., Non-Classical Inhibition of Carbonic Anhydrase. *Int J Mol Sci* **2016**, 17 (7).
124. Jakubowski, M.; Szahidewicz-Krupska, E.; Doroszko, A., The Human Carbonic Anhydrase II in Platelets: An Underestimated Field of Its Activity. *Biomed Res Int* **2018**, 2018, 4548353.
125. Supuran, C. T., Carbonic anhydrase inhibitors. *Bioorg Med Chem Lett* **2010**, 20 (12), 3467-74.
126. Supuran, C. T.; Scozzafava, A.; Casini, A., Carbonic anhydrase inhibitors. *Med Res Rev* **2003**, 23 (2), 146-89.
127. Kummola, L.; Hamalainen, J. M.; Kivela, J.; Kivela, A. J.; Saarnio, J.; Karttunen, T.; Parkkila, S., Expression of a novel carbonic anhydrase, CA XIII, in normal and neoplastic colorectal mucosa. *BMC Cancer* **2005**, 5, 41.
128. Mboge, M. Y.; Mahon, B. P.; McKenna, R.; Frost, S. C., Carbonic Anhydrases: Role in pH Control and Cancer. *Metabolites* **2018**, 8 (1).
129. Yang, J. S.; Lin, C. W.; Chuang, C. Y.; Su, S. C.; Lin, S. H.; Yang, S. F., Carbonic anhydrase IX overexpression regulates the migration and progression in oral squamous cell carcinoma. *Tumour Biol* **2015**, 36 (12), 9517-24.

130. Lounnas, N.; Rosilio, C.; Nebout, M.; Mary, D.; Griessinger, E.; Neffati, Z.; Chiche, J.; Spits, H.; Hagenbeek, T. J.; Asnafi, V.; Poulsen, S. A.; Supuran, C. T.; Peyron, J. F.; Imbert, V., Pharmacological inhibition of carbonic anhydrase XII interferes with cell proliferation and induces cell apoptosis in T-cell lymphomas. *Cancer Lett* **2013**, 333 (1), 76-88.
131. Parkin, G., Synthetic analogues relevant to the structure and function of zinc enzymes. *Chem Rev* **2004**, 104 (2), 699-767.
132. Carta, F.; Supuran, C. T., Diuretics with carbonic anhydrase inhibitory action: a patent and literature review (2005 - 2013). *Expert Opin Ther Pat* **2013**, 23 (6), 681-91.
133. Supuran, C. T., Structure-based drug discovery of carbonic anhydrase inhibitors. *J Enzyme Inhib Med Chem* **2012**, 27 (6), 759-72.
134. Masini, E.; Carta, F.; Scozzafava, A.; Supuran, C. T., Antiglaucoma carbonic anhydrase inhibitors: a patent review. *Expert Opin Ther Pat* **2013**, 23 (6), 705-16.
135. Supuran, C. T.; Capasso, C., New light on bacterial carbonic anhydrases phylogeny based on the analysis of signal peptide sequences. *J Enzyme Inhib Med Chem* **2016**, 31 (6), 1254-60.
136. Carta, F.; Supuran, C. T.; Scozzafava, A., Sulfonamides and their isosters as carbonic anhydrase inhibitors. *Future Med Chem* **2014**, 6 (10), 1149-65.
137. Supuran, C. T., Carbonic Anhydrase Inhibition and the Management of Hypoxic Tumors. *Metabolites* **2017**, 7 (3).
138. Neri, D.; Supuran, C. T., Interfering with pH regulation in tumours as a therapeutic strategy. *Nat Rev Drug Discov* **2011**, 10 (10), 767-77.
139. Pichake, J.; Kharkar, P. S.; Ceruso, M.; Supuran, C. T.; Toraskar, M. P., Carbonic anhydrase inhibitors: design, synthesis, and biological evaluation of novel sulfonyl semicarbazide derivatives. *ACS Med Chem Lett* **2014**, 5 (7), 793-6.

140. Reiss, W. G.; Oles, K. S., Acetazolamide in the treatment of seizures. *Ann Pharmacother* **1996**, *30* (5), 514-9.
141. Williamson, J.; Oakeshott, P.; Dallimore, J., Altitude sickness and acetazolamide. *BMJ* **2018**, *361*, k2153.
142. Matthews, E.; Portaro, S.; Ke, Q.; Sud, R.; Haworth, A.; Davis, M. B.; Griggs, R. C.; Hanna, M. G., Acetazolamide efficacy in hypokalemic periodic paralysis and the predictive role of genotype. *Neurology* **2011**, *77* (22), 1960-4.
143. Bayat Mokhtari, R.; Baluch, N.; Ka Hon Tsui, M.; Kumar, S.; T, S. H.; Aitken, K.; Das, B.; Baruchel, S.; Yeger, H., Acetazolamide potentiates the anti-tumor potential of HDACi, MS-275, in neuroblastoma. *BMC Cancer* **2017**, *17* (1), 156.
144. Cianchi, F.; Vinci, M. C.; Supuran, C. T.; Peruzzi, B.; De Giuli, P.; Fasolis, G.; Perigli, G.; Pastorekova, S.; Papucci, L.; Pini, A.; Masini, E.; Puccetti, L., Selective inhibition of carbonic anhydrase IX decreases cell proliferation and induces ceramide-mediated apoptosis in human cancer cells. *J Pharmacol Exp Ther* **2010**, *334* (3), 710-9.
145. Mokhtari, R. B.; Kumar, S.; Islam, S. S.; Yazdanpanah, M.; Adeli, K.; Cutz, E.; Yeger, H., Combination of carbonic anhydrase inhibitor, acetazolamide, and sulforaphane, reduces the viability and growth of bronchial carcinoid cell lines. *BMC Cancer* **2013**, *13*, 378.
146. Greig, S. L., Dichlorphenamide: A Review in Primary Periodic Paralysis. *Drugs* **2016**, *76* (4), 501-7.
147. Winum, J. Y.; Casini, A.; Mincione, F.; Starnotti, M.; Montero, J. L.; Scozzafava, A.; Supuran, C. T., Carbonic anhydrase inhibitors: N-(p-sulfamoylphenyl)-alpha-D-glycopyranosylamines as topically acting antiglaucoma agents in hypertensive rabbits. *Bioorg Med Chem Lett* **2004**, *14* (1), 225-9.

148. Dahlen, K.; Epstein, D. L.; Grant, W. M.; Hutchinson, B. T.; Prien, E. L., Jr.; Krall, J. M., A repeated dose-response study of methazolamide in glaucoma. *Arch Ophthalmol* **1978**, *96* (12), 2214-8.
149. Balfour, J. A.; Wilde, M. I., Dorzolamide. A review of its pharmacology and therapeutic potential in the management of glaucoma and ocular hypertension. *Drugs Aging* **1997**, *10* (5), 384-403.
150. Ali, B. M.; Zaitone, S. A.; Shouman, S. A.; Moustafa, Y. M., Dorzolamide synergizes the antitumor activity of mitomycin C against Ehrlich's carcinoma grown in mice: role of thioredoxin-interacting protein. *Naunyn Schmiedebergs Arch Pharmacol* **2015**, *388* (12), 1271-82.
151. Lewis, R. A.; Schoenwald, R. D.; Eller, M. G.; Barfknecht, C. F.; Phelps, C. D., Ethoxzolamide analogue gel. A topical carbonic anhydrase inhibitor. *Arch Ophthalmol* **1984**, *102* (12), 1821-4.
152. Lou, Y.; McDonald, P. C.; Oloumi, A.; Chia, S.; Ostlund, C.; Ahmadi, A.; Kyle, A.; Auf dem Keller, U.; Leung, S.; Huntsman, D.; Clarke, B.; Sutherland, B. W.; Waterhouse, D.; Bally, M.; Roskelley, C.; Overall, C. M.; Minchinton, A.; Pacchiano, F.; Carta, F.; Scozzafava, A.; Touisni, N.; Winum, J. Y.; Supuran, C. T.; Dedhar, S., Targeting tumor hypoxia: suppression of breast tumor growth and metastasis by novel carbonic anhydrase IX inhibitors. *Cancer Res* **2011**, *71* (9), 3364-76.
153. Lock, F. E.; McDonald, P. C.; Lou, Y.; Serrano, I.; Chafe, S. C.; Ostlund, C.; Aparicio, S.; Winum, J. Y.; Supuran, C. T.; Dedhar, S., Targeting carbonic anhydrase IX depletes breast cancer stem cells within the hypoxic niche. *Oncogene* **2013**, *32* (44), 5210-9.
154. Innocenti, A.; Villar, R.; Martinez-Merino, V.; Gil, M. J.; Scozzafava, A.; Vullo, D.; Supuran, C. T., Carbonic anhydrase inhibitors: inhibition of cytosolic/tumor-associated

carbonic anhydrase isozymes I, II, and IX with benzo[b]thiophene 1,1-dioxide sulfonamides. *Bioorg Med Chem Lett* **2005**, *15* (21), 4872-6.

155. Kumar, V.; Mathur, D.; Srivastava, S.; Malhotra, S.; Rana, N.; Singh, S. K.; Singh, B. K.; Prasad, A. K.; Varma, A. J.; Len, C.; Kuhad, R. C.; Saxena, R. K.; Parmar, V. S., Biocatalytic Synthesis of Novel Partial Esters of a Bioactive Dihydroxy 4-Methylcoumarin by *Rhizopus oryzae* Lipase (ROL). *Molecules* **2016**, *21* (11).

156. Comert Onder, F.; Durdagi, S.; Sahin, K.; Ozpolat, B.; Ay, M., Design, Synthesis, and Molecular Modeling Studies of Novel Coumarin Carboxamide Derivatives as eEF-2K Inhibitors. *J Chem Inf Model* **2020**, *60* (3), 1766-1778.

157. Watzka, M.; Geisen, C.; Bevans, C. G.; Sittinger, K.; Spohn, G.; Rost, S.; Seifried, E.; Muller, C. R.; Oldenburg, J., Thirteen novel VKORC1 mutations associated with oral anticoagulant resistance: insights into improved patient diagnosis and treatment. *J Thromb Haemost* **2011**, *9* (1), 109-18.

158. Thakur, A.; Singla, R.; Jaitak, V., Coumarins as anticancer agents: a review on synthetic strategies, mechanism of action and SAR studies. *Eur J Med Chem* **2015**, *101*, 476-95.

159. Carta, F.; Maresca, A.; Scozzafava, A.; Supuran, C. T., Novel coumarins and 2-thioxo-coumarins as inhibitors of the tumor-associated carbonic anhydrases IX and XII. *Bioorg Med Chem* **2012**, *20* (7), 2266-73.

160. Maresca, A.; Temperini, C.; Vu, H.; Pham, N. B.; Poulsen, S. A.; Scozzafava, A.; Quinn, R. J.; Supuran, C. T., Non-zinc mediated inhibition of carbonic anhydrases: coumarins are a new class of suicide inhibitors. *J Am Chem Soc* **2009**, *131* (8), 3057-62.

161. Touisni, N.; Maresca, A.; McDonald, P. C.; Lou, Y.; Scozzafava, A.; Dedhar, S.; Winum, J. Y.; Supuran, C. T., Glycosyl coumarin carbonic anhydrase IX and XII inhibitors strongly attenuate the growth of primary breast tumors. *J Med Chem* **2011**, *54* (24), 8271-7.

162. Mboge, M. Y.; McKenna, R.; Frost, S. C., Advances in Anti-Cancer Drug Development Targeting Carbonic Anhydrase IX and XII. *Top Anticancer Res* **2015**, 5, 3-42.
163. Supuran, C. T., Coumarin carbonic anhydrase inhibitors from natural sources. *J Enzyme Inhib Med Chem* **2020**, 35 (1), 1462-1470.
164. Davis, R. A.; Vullo, D.; Maresca, A.; Supuran, C. T.; Poulsen, S. A., Natural product coumarins that inhibit human carbonic anhydrases. *Bioorg Med Chem* **2013**, 21 (6), 1539-43.
165. Thacker, P. S.; Alvala, M.; Arifuddin, M.; Angeli, A.; Supuran, C. T., Design, synthesis and biological evaluation of coumarin-3-carboxamides as selective carbonic anhydrase IX and XII inhibitors. *Bioorg Chem* **2019**, 86, 386-392.
166. Wang, Z. C.; Qin, Y. J.; Wang, P. F.; Yang, Y. A.; Wen, Q.; Zhang, X.; Qiu, H. Y.; Duan, Y. T.; Wang, Y. T.; Sang, Y. L.; Zhu, H. L., Sulfonamides containing coumarin moieties selectively and potently inhibit carbonic anhydrases II and IX: design, synthesis, inhibitory activity and 3D-QSAR analysis. *Eur J Med Chem* **2013**, 66, 1-11.
167. Krautwald, S.; Nilewski, C.; Mori, M.; Shiomi, K.; Omura, S.; Carreira, E. M., Bioisosteric Exchange of Csp³ -Chloro and Methyl Substituents: Synthesis and Initial Biological Studies of Atpenin A5 Analogues. *Angew Chem Int Ed Engl* **2016**, 55 (12), 4049-53.
168. Selby, T. P.; Hughes, K. A.; Rauh, J. J.; Hanna, W. S., Synthetic atpenin analogs: Potent mitochondrial inhibitors of mammalian and fungal succinate-ubiquinone oxidoreductase. *Bioorg Med Chem Lett* **2010**, 20 (5), 1665-8.
169. Horsefield, R.; Yankovskaya, V.; Sexton, G.; Whittingham, W.; Shiomi, K.; Omura, S.; Byrne, B.; Cecchini, G.; Iwata, S., Structural and computational analysis of the quinone-binding site of complex II (succinate-ubiquinone oxidoreductase): a

mechanism of electron transfer and proton conduction during ubiquinone reduction. *J Biol Chem* **2006**, *281* (11), 7309-16.

170. Ohtawa, M.; Ogihara, S.; Sugiyama, K.; Shiomi, K.; Harigaya, Y.; Nagamitsu, T.; Omura, S., Enantioselective total synthesis of atpenin A5. *J Antibiot* **2009**, *62* (6), 289-294.

171. Trecourt, F.; Mallet, M.; Mongin, O.; Queguiner, G., Total Synthesis of (+/-)-Atpenin-B - an Original Clockwise Functionalization of Alpha-Chloropyridine. *J Org Chem* **1994**, *59* (21), 6173-6178.

172. Schnurch, M.; Spina, M.; Khan, A. F.; Mihovilovic, M. D.; Stanetty, P., Halogen dance reactions - A review. *Chem Soc Rev* **2007**, *36* (7), 1046-1057.

173. Stoyanovsky, D. A.; Jiang, J.; Murphy, M. P.; Epperly, M.; Zhang, X.; Li, S.; Greenberger, J.; Kagan, V.; Bayir, H., Design and Synthesis of a Mitochondria-Targeted Mimic of Glutathione Peroxidase, MitoEbselen-2, as a Radiation Mitigator. *ACS Med Chem Lett* **2014**, *5* (12), 1304-1307.

174. Teixeira, J.; Cagide, F.; Benfeito, S.; Soares, P.; Garrido, J.; Baldeiras, I.; Ribeiro, J. A.; Pereira, C. M.; Silva, A. F.; Andrade, P. B.; Oliveira, P. J.; Borges, F., Development of a Mitochondriotropic Antioxidant Based on Caffeic Acid: Proof of Concept on Cellular and Mitochondrial Oxidative Stress Models. *J Med Chem* **2017**, *60* (16), 7084-7098.

175. Vetter, A. C.; Nikitin, K.; Gilheany, D. G., Long sought synthesis of quaternary phosphonium salts from phosphine oxides: inverse reactivity approach. *Chem Commun (Camb)* **2018**, *54* (46), 5843-5846.

176. Batesky, D. C.; Goldfogel, M. J.; Weix, D. J., Removal of Triphenylphosphine Oxide by Precipitation with Zinc Chloride in Polar Solvents. *J Org Chem* **2017**, *82* (19), 9931-9936.

177. Burwell, L. S.; Nadtochiy, S. M.; Tompkins, A. J.; Young, S.; Brookes, P. S., Direct evidence for S-nitrosation of mitochondrial complex I. *Biochem J* **2006**, 394 (Pt 3), 627-34.
178. Nadtochiy, S. M.; Tompkins, A. J.; Brookes, P. S., Different mechanisms of mitochondrial proton leak in ischaemia/reperfusion injury and preconditioning: implications for pathology and cardioprotection. *Biochem J* **2006**, 395 (3), 611-8.
179. Leeson, P. D.; Springthorpe, B., The influence of drug-like concepts on decision-making in medicinal chemistry. *Nat Rev Drug Discov* **2007**, 6 (11), 881-90.
180. Horton, K. L.; Stewart, K. M.; Fonseca, S. B.; Guo, Q.; Kelley, S. O., Mitochondria-penetrating peptides. *Chem Biol* **2008**, 15 (4), 375-82.
181. Reulecke, I.; Lange, G.; Albrecht, J.; Klein, R.; Rarey, M., Towards an integrated description of hydrogen bonding and dehydration: decreasing false positives in virtual screening with the HYDE scoring function. *ChemMedChem* **2008**, 3 (6), 885-97.
182. Pulukuri, S. M.; Gondi, C. S.; Lakka, S. S.; Jutla, A.; Estes, N.; Gujrati, M.; Rao, J. S., RNA interference-directed knockdown of urokinase plasminogen activator and urokinase plasminogen activator receptor inhibits prostate cancer cell invasion, survival, and tumorigenicity in vivo. *J Biol Chem* **2005**, 280 (43), 36529-40.
183. Li, Y.; Chan, S. C.; Brand, L. J.; Hwang, T. H.; Silverstein, K. A.; Dehm, S. M., Androgen receptor splice variants mediate enzalutamide resistance in castration-resistant prostate cancer cell lines. *Cancer Res* **2013**, 73 (2), 483-9.
184. Webber, M. M.; Trakul, N.; Thraves, P. S.; Bello-DeOcampo, D.; Chu, W. W.; Storto, P. D.; Huard, T. K.; Rhim, J. S.; Williams, D. E., A human prostatic stromal myofibroblast cell line WPMY-1: a model for stromal-epithelial interactions in prostatic neoplasia. *Carcinogenesis* **1999**, 20 (7), 1185-92.
185. Wenzel, C.; Riefke, B.; Grundemann, S.; Krebs, A.; Christian, S.; Prinz, F.; Osterland, M.; Golfier, S.; Rase, S.; Ansari, N.; Esner, M.; Bickle, M.; Pampaloni, F.;

Mattheyer, C.; Stelzer, E. H.; Parczyk, K.; Prechtel, S.; Steigemann, P., 3D high-content screening for the identification of compounds that target cells in dormant tumor spheroid regions. *Exp Cell Res* **2014**, *323* (1), 131-43.

186. Quesnel, B., Tumor dormancy: long-term survival in a hostile environment. *Adv Exp Med Biol* **2013**, *734*, 181-200.

187. Kyle, A. H.; Baker, J. H.; Minchinton, A. I., Targeting quiescent tumor cells via oxygen and IGF-I supplementation. *Cancer Res* **2012**, *72* (3), 801-9.

188. Khanal, G.; Hiemstra, S.; Pappas, D., Probing hypoxia-induced staurosporine resistance in prostate cancer cells with a microfluidic culture system. *Analyst* **2014**, *139* (13), 3274-80.

189. Maxwell, P. J.; Gallagher, R.; Seaton, A.; Wilson, C.; Scullin, P.; Pettigrew, J.; Stratford, I. J.; Williams, K. J.; Johnston, P. G.; Waugh, D. J., HIF-1 and NF-kappaB-mediated upregulation of CXCR1 and CXCR2 expression promotes cell survival in hypoxic prostate cancer cells. *Oncogene* **2007**, *26* (52), 7333-45.

190. Sun, W.; Chen, Y.; Wang, Y.; Luo, P.; Zhang, M.; Zhang, H.; Hu, P., Interaction study of cancer cells and fibroblasts on a spatially confined oxygen gradient microfluidic chip to investigate the tumor microenvironment. *Analyst* **2018**, *143* (22), 5431-5437.

191. Tompkins, A. J.; Burwell, L. S.; Digerness, S. B.; Zaragoza, C.; Holman, W. L.; Brookes, P. S., Mitochondrial dysfunction in cardiac ischemia-reperfusion injury: ROS from complex I, without inhibition. *Biochimica et biophysica acta* **2006**, *1762* (2), 223-31.

192. Kirby, D. M.; Thorburn, D. R.; Turnbull, D. M.; Taylor, R. W., Biochemical Assays of Respiratory Chain Complex Activity. In *Mitochondria, 2nd Edition*, 2007; pp 93-119.

193. Nicholls, D. G.; Darley-USmar, V. M.; Wu, M.; Jensen, P. B.; Rogers, G. W.; Ferrick, D. A., Bioenergetic profile experiment using C2C12 myoblast cells. *J Vis Exp* **2010**, (46).

194. Pirotte, B.; Ouedraogo, R.; de Tullio, P.; Khelili, S.; Somers, F.; Boverie, S.; Dupont, L.; Fontaine, J.; Damas, J.; Lebrun, P., 3-Alkylamino-4H-pyrido[2,3-e]-1,2,4-thiadiazine 1,1-dioxides structurally related to diazoxide and pinacidil as potassium channel openers acting on vascular smooth muscle cells: design, synthesis, and pharmacological evaluation. *J Med Chem* **2000**, *43* (8), 1456-66.
195. Ma, X.; Wei, J.; Wang, C.; Gu, D.; Hu, Y.; Sheng, R., Design, synthesis and biological evaluation of novel benzothiadiazine derivatives as potent PI3Kdelta-selective inhibitors for treating B-cell-mediated malignancies. *Eur J Med Chem* **2019**, *170*, 112-125.
196. Huwaimel, B. I.; Bhakta, M.; Kulkarni, C. A.; Milliken, A. S.; Wang, F.; Peng, A.; Brookes, P. S.; Trippier, P. C., Discovery of Halogenated Benzothiadiazine Derivatives with Anticancer Activity. *ChemMedChem* **2020**.
197. de Tullio, P.; Becker, B.; Boverie, S.; Dabrowski, M.; Wahl, P.; Antoine, M. H.; Somers, F.; Seville, S.; Ouedraogo, R.; Hansen, J. B.; Lebrun, P.; Pirotte, B., Toward tissue-selective pancreatic B-cells KATP channel openers belonging to 3-alkylamino-7-halo-4H-1,2,4-benzothiadiazine 1,1-dioxides. *J Med Chem* **2003**, *46* (15), 3342-53.
198. Pirotte, B.; de Tullio, P.; Boverie, S.; Michaux, C.; Lebrun, P., Impact of the nature of the substituent at the 3-position of 4H-1,2,4-benzothiadiazine 1,1-dioxides on their opening activity toward ATP-sensitive potassium channels. *J Med Chem* **2011**, *54* (9), 3188-99.
199. Nielsen, F. E.; Ebdrup, S.; Jensen, A. F.; Ynddal, L.; Bodvarsdottir, T. B.; Stidsen, C.; Worsaae, A.; Boonen, H. C.; Arkhammar, P. O.; Fremming, T.; Wahl, P.; Korno, H. T.; Hansen, J. B., New 3-alkylamino-4H-thieno-1,2,4-thiadiazine 1,1-dioxide derivatives activate ATP-sensitive potassium channels of pancreatic beta cells. *J Med Chem* **2006**, *49* (14), 4127-39.
200. Boverie, S.; Antoine, M. H.; de Tullio, P.; Somers, F.; Becker, B.; Seville, S.; Lebrun, P.; Pirotte, B., Effect on insulin release of compounds structurally related to the

potassium-channel opener 7-chloro-3-isopropylamino-4H-1,2,4-benzothiadiazine 1,1-dioxide (BPDZ 73): introduction of heteroatoms on the 3-alkylamino side chain of the benzothiadiazine 1,1-dioxide ring. *J Pharm Pharmacol* **2001**, 53 (7), 973-80.

201. de Tullio, P.; Boverie, S.; Becker, B.; Antoine, M. H.; Nguyen, Q. A.; Francotte, P.; Counerotte, S.; Sebille, S.; Pirotte, B.; Lebrun, P., 3-Alkylamino-4H-1,2,4-benzothiadiazine 1,1-dioxides as ATP-sensitive potassium channel openers: effect of 6,7-disubstitution on potency and tissue selectivity. *J Med Chem* **2005**, 48 (15), 4990-5000.

202. Kornahrens, A. F.; Cognetta, A. B., 3rd; Brody, D. M.; Matthews, M. L.; Cravatt, B. F.; Boger, D. L., Design of Benzoxathiazin-3-one 1,1-Dioxides as a New Class of Irreversible Serine Hydrolase Inhibitors: Discovery of a Uniquely Selective PNPLA4 Inhibitor. *J Am Chem Soc* **2017**, 139 (20), 7052-7061.

203. Hoffman, D. L.; Salter, J. D.; Brookes, P. S., Response of mitochondrial reactive oxygen species generation to steady-state oxygen tension: implications for hypoxic cell signaling. *Am J Physiol Heart Circ Physiol* **2007**, 292 (1), H101-8.

204. Baell, J. B.; Holloway, G. A., New substructure filters for removal of pan assay interference compounds (PAINS) from screening libraries and for their exclusion in bioassays. *J Med Chem* **2010**, 53 (7), 2719-40.

205. Verma, K.; Gupta, N.; Zang, T.; Wangtrakuldee, P.; Srivastava, S. K.; Penning, T. M.; Trippier, P. C., AKR1C3 Inhibitor KV-37 Exhibits Antineoplastic Effects and Potentiates Enzalutamide in Combination Therapy in Prostate Adenocarcinoma Cells. *Mol Cancer Ther* **2018**, 17 (9), 1833-1845.

206. Morsy, A.; Trippier, P. C., Reversal of Apalutamide and Darolutamide Aldo-Keto Reductase 1C3-Mediated Resistance by a Small Molecule Inhibitor. *ACS Chem Biol* **2020**, 15 (3), 646-650.

207. Berger, M. R.; Fink, M.; Feichter, G. E.; Janetschek, P., Effects of diazoxide-induced reversible diabetes on chemically induced autochthonous mammary carcinomas in Sprague-Dawley rats. *Int J Cancer* **1985**, 35 (3), 395-401.
208. Fink, M. K.; Klement, R. J., Diazoxide for Lowering Insulin Levels in Breast Cancer Patients. *Oncologist* **2017**, 22 (4), 491.
209. Kim, K. Y.; Shin, Y. W.; Kim, S. O.; Lim, H.; Yoo, S. E.; Hong, K. W., Antiangiogenic effect of KR-31372 by apoptosis via mediation of mitochondrial KATP channel opening and the phosphatase and tensin homolog deleted from chromosome 10 phosphorylation. *J Pharmacol Exp Ther* **2003**, 305 (3), 1142-9.
210. Hanahan, D.; Folkman, J., Patterns and emerging mechanisms of the angiogenic switch during tumorigenesis. *Cell* **1996**, 86 (3), 353-64.
211. Gerber, H. P.; Vu, T. H.; Ryan, A. M.; Kowalski, J.; Werb, Z.; Ferrara, N., VEGF couples hypertrophic cartilage remodeling, ossification and angiogenesis during endochondral bone formation. *Nat Med* **1999**, 5 (6), 623-8.
212. Reichardt, L. F.; Tomaselli, K. J., Extracellular matrix molecules and their receptors: functions in neural development. *Annu Rev Neurosci* **1991**, 14, 531-70.
213. Gupta, K.; Kshirsagar, S.; Li, W.; Gui, L.; Ramakrishnan, S.; Gupta, P.; Law, P. Y.; Hebbel, R. P., VEGF prevents apoptosis of human microvascular endothelial cells via opposing effects on MAPK/ERK and SAPK/JNK signaling. *Exp Cell Res* **1999**, 247 (2), 495-504.
214. Maharaj, A. S.; D'Amore, P. A., Roles for VEGF in the adult. *Microvasc Res* **2007**, 74 (2-3), 100-13.
215. Maj, E.; Papiernik, D.; Wietrzyk, J., Antiangiogenic cancer treatment: The great discovery and greater complexity (Review). *Int J Oncol* **2016**, 49 (5), 1773-1784.
216. Batchelor, T. T.; Sorensen, A. G.; di Tomaso, E.; Zhang, W. T.; Duda, D. G.; Cohen, K. S.; Kozak, K. R.; Cahill, D. P.; Chen, P. J.; Zhu, M.; Ancukiewicz, M.;

- Mrugala, M. M.; Plotkin, S.; Drappatz, J.; Louis, D. N.; Ivy, P.; Scadden, D. T.; Benner, T.; Loeffler, J. S.; Wen, P. Y.; Jain, R. K., AZD2171, a pan-VEGF receptor tyrosine kinase inhibitor, normalizes tumor vasculature and alleviates edema in glioblastoma patients. *Cancer Cell* **2007**, *11* (1), 83-95.
217. Diez-Cecilia, E.; Kelly, B.; Perez, C.; Zisterer, D. M.; Nevin, D. K.; Lloyd, D. G.; Rozas, I., Guanidinium-based derivatives: searching for new kinase inhibitors. *Eur J Med Chem* **2014**, *81*, 427-41.
218. Cho, S. M.; Lee, H. K.; Liu, Q.; Wang, M. W.; Kwon, H. J., A Guanidine-Based Synthetic Compound Suppresses Angiogenesis via Inhibition of Acid Ceramidase. *ACS Chem Biol* **2019**, *14* (1), 11-19.
219. Wu, C.; Wang, M.; Tang, Q.; Luo, R.; Chen, L.; Zheng, P.; Zhu, W., Design, Synthesis, Activity and Docking Study of Sorafenib Analogs Bearing Sulfonylurea Unit. *Molecules* **2015**, *20* (10), 19361-71.
220. Phowichit, S.; Kobayashi, M.; Fujinoya, Y.; Sato, Y.; Sanphanya, K.; Vajragupta, O.; Chularojmontri, L.; Wattanapitayakul, S. K., Antiangiogenic Effects of VH02, a Novel Urea Derivative: In Vitro and in Vivo Studies. *Molecules* **2016**, *21* (9).
221. Maren, T. H.; Sanyal, G., The activity of sulfonamides and anions against the carbonic anhydrases of animals, plants, and bacteria. *Annu Rev Pharmacol Toxicol* **1983**, *23*, 439-59.
222. Famaey, J. P., In vitro and in vivo pharmacological evidence of selective cyclooxygenase-2 inhibition by nimesulide: an overview. *Inflamm Res* **1997**, *46* (11), 437-46.
223. Yoshino, H.; Ueda, N.; Nijima, J.; Sugumi, H.; Kotake, Y.; Koyanagi, N.; Yoshimatsu, K.; Asada, M.; Watanabe, T.; Nagasu, T.; et al., Novel sulfonamides as potential, systemically active antitumor agents. *J Med Chem* **1992**, *35* (13), 2496-7.

224. Wang, M.; Xu, S.; Wu, C.; Liu, X.; Tao, H.; Huang, Y.; Liu, Y.; Zheng, P.; Zhu, W., Design, synthesis and activity of novel sorafenib analogues bearing chalcone unit. *Bioorg Med Chem Lett* **2016**, *26* (22), 5450-5454.
225. Hatcher, J. M.; Wu, G.; Zeng, C.; Zhu, J.; Meng, F.; Patel, S.; Wang, W.; Ficarro, S. B.; Leggett, A. L.; Powell, C. E.; Marto, J. A.; Zhang, K.; Ki Ngo, J. C.; Fu, X. D.; Zhang, T.; Gray, N. S., SRPKIN-1: A Covalent SRPK1/2 Inhibitor that Potently Converts VEGF from Pro-angiogenic to Anti-angiogenic Isoform. *Cell Chem Biol* **2018**, *25* (4), 460-470 e6.
226. Hughes, T. V.; Emanuel, S. L.; Beck, A. K.; Wetter, S. K.; Connolly, P. J.; Karnachi, P.; Reuman, M.; Seraj, J.; Fuentes-Pesquera, A. R.; Gruninger, R. H.; Middleton, S. A.; Lin, R.; Davis, J. M.; Moffat, D. F., 4-Aryl-5-cyano-2-aminopyrimidines as VEGF-R2 inhibitors: synthesis and biological evaluation. *Bioorg Med Chem Lett* **2007**, *17* (12), 3266-70.
227. Boverie, S.; Antoine, M. H.; Somers, F.; Becker, B.; Sebillé, S.; Ouedraogo, R.; Counerotte, S.; Pirotte, B.; Lebrun, P.; de Tullio, P., Effect on K(ATP) channel activation properties and tissue selectivity of the nature of the substituent in the 7- and the 3-position of 4H-1,2,4-benzothiadiazine 1,1-dioxides. *J Med Chem* **2005**, *48* (10), 3492-503.
228. Zahra, F. T.; Sajib, M. S.; Ichiyama, Y.; Akwii, R. G.; Tullar, P. E.; Cobos, C.; Minchew, S. A.; Doci, C. L.; Zheng, Y.; Kubota, Y.; Gutkind, J. S.; Mikelis, C. M., Endothelial RhoA GTPase is essential for in vitro endothelial functions but dispensable for physiological in vivo angiogenesis. *Sci Rep* **2019**, *9* (1), 11666.
229. Kokolakis, G.; Mikelis, C.; Papadimitriou, E.; Courty, J.; Karetsou, E.; Katsoris, P., Effect of heparin affin regulatory peptide on the expression of vascular endothelial growth factor receptors in endothelial cells. *In Vivo* **2006**, *20* (5), 629-35.

230. Maresca, A.; Temperini, C.; Pochet, L.; Masereel, B.; Scozzafava, A.; Supuran, C. T., Deciphering the mechanism of carbonic anhydrase inhibition with coumarins and thiocoumarins. *J Med Chem* **2010**, *53* (1), 335-44.
231. Williams, K. J.; Gieling, R. G., Preclinical Evaluation of Ureidosulfamate Carbonic Anhydrase IX/XII Inhibitors in the Treatment of Cancers. *Int J Mol Sci* **2019**, *20* (23).
232. He, X.; Chen, Y. Y.; Shi, J. B.; Tang, W. J.; Pan, Z. X.; Dong, Z. Q.; Song, B. A.; Li, J.; Liu, X. H., New coumarin derivatives: design, synthesis and use as inhibitors of hMAO. *Bioorg Med Chem* **2014**, *22* (14), 3732-8.
233. Chimenti, F.; Secci, D.; Bolasco, A.; Chimenti, P.; Bizzarri, B.; Granese, A.; Carradori, S.; Yanez, M.; Orallo, F.; Ortuso, F.; Alcaro, S., Synthesis, molecular modeling, and selective inhibitory activity against human monoamine oxidases of 3-carboxamido-7-substituted coumarins. *J Med Chem* **2009**, *52* (7), 1935-42.
234. Yang, F.; Zhao, N.; Song, J.; Zhu, K.; Jiang, C. S.; Shan, P.; Zhang, H., Design, Synthesis and Biological Evaluation of Novel Coumarin-Based Hydroxamate Derivatives as Histone Deacetylase (Hdac) Inhibitors with Antitumor Activities. *Molecules* **2019**, *24* (14).
235. Saglik, B. N.; Cevik, U. A.; Osmaniye, D.; Levent, S.; Cavusoglu, B. K.; Demir, Y.; Ilgin, S.; Ozkay, Y.; Koparal, A. S.; Beydemir, S.; Kaplancikli, Z. A., Synthesis, molecular docking analysis and carbonic anhydrase I-II inhibitory evaluation of new sulfonamide derivatives. *Bioorg Chem* **2019**, *91*, 103153.
236. Ahmed, A.; Channar, P. A.; Saeed, A.; Kalesse, M.; Kazi, M. A.; Larik, F. A.; Abbas, Q.; Hassan, M.; Raza, H.; Seo, S. Y., Synthesis of sulfonamide, amide and amine hybrid pharmacophore, an entry of new class of carbonic anhydrase II inhibitors and evaluation of chemo-informatics and binding analysis. *Bioorg Chem* **2019**, *86*, 624-630.
237. Angeli, A.; Di Cesare Mannelli, L.; Ghelardini, C.; Peat, T. S.; Bartolucci, G.; Menicatti, M.; Carta, F.; Supuran, C. T., Benzensulfonamides bearing spirohydantoin

moieties act as potent inhibitors of human carbonic anhydrases II and VII and show neuropathic pain attenuating effects. *Eur J Med Chem* **2019**, *177*, 188-197.

238. Nishikawa, Y.; Miki, T.; Awa, M.; Kuwata, K.; Tamura, T.; Hamachi, I., Development of a Nitric Oxide-Responsive Labeling Reagent for Proteome Analysis of Live Cells. *ACS Chem Biol* **2019**, *14* (3), 397-404.

239. Mincione, F.; Starnotti, M.; Menabuoni, L.; Scozzafava, A.; Casini, A.; Supuran, C. T., Carbonic anhydrase inhibitors: 4-sulfamoyl-benzenecarboxamides and 4-chloro-3-sulfamoyl-benzenecarboxamides with strong topical antiglaucoma properties. *Bioorg Med Chem Lett* **2001**, *11* (13), 1787-91.

240. Endo, S.; Xia, S.; Suyama, M.; Morikawa, Y.; Oguri, H.; Hu, D.; Ao, Y.; Takahara, S.; Horino, Y.; Hayakawa, Y.; Watanabe, Y.; Gouda, H.; Hara, A.; Kuwata, K.; Toyooka, N.; Matsunaga, T.; Ikari, A., Synthesis of Potent and Selective Inhibitors of Aldo-Keto Reductase 1B10 and Their Efficacy against Proliferation, Metastasis, and Cisplatin Resistance of Lung Cancer Cells. *J Med Chem* **2017**, *60* (20), 8441-8455.

241. Robert, S.; Bertolla, C.; Masereel, B.; Dogne, J. M.; Pochet, L., Novel 3-carboxamide-coumarins as potent and selective FXIIa inhibitors. *J Med Chem* **2008**, *51* (11), 3077-80.

242. Emami, S.; Dadashpour, S., Current developments of coumarin-based anti-cancer agents in medicinal chemistry. *Eur J Med Chem* **2015**, *102*, 611-30.

243. Chen, Z.; Ai, L.; Mboge, M. Y.; Tu, C.; McKenna, R.; Brown, K. D.; Heldermon, C. D.; Frost, S. C., Differential expression and function of CAIX and CAXII in breast cancer: A comparison between tumorgraft models and cells. *PLoS One* **2018**, *13* (7), e0199476.

244. Hedlund, E. E.; McDonald, P. C.; Nemirovsky, O.; Awrey, S.; Jensen, L. D. E.; Dedhar, S., Harnessing Induced Essentiality: Targeting Carbonic Anhydrase IX and Angiogenesis Reduces Lung Metastasis of Triple Negative Breast Cancer Xenografts. *Cancers (Basel)* **2019**, *11* (7).

245. Tatiparti, K.; Rauf, M. A.; Sau, S.; Iyer, A. K., Carbonic Anhydrase-IX Guided Albumin Nanoparticles for Hypoxia-mediated Triple-Negative Breast Cancer Cell Killing and Imaging of Patient-derived Tumor. *Molecules* **2020**, 25 (10).